DOT/FAA/TC-24/40

Federal Aviation Administration
William J. Hughes Technical Center
Aviation Research Division
Atlantic City International Airport
New Jersey 08405

Design, Analysis, and Test Development of Full-Scale Fuselage Test Panels to Assess Emerging Metallic Structures Technologies

November 2024

Final report

U.S. Department of Transportation
Federal Aviation Administration

NOTICE

This document is disseminated under the sponsorship of the U.S. Department of Transportation in the interest of information exchange. The U.S. Government assumes no liability for the contents or use thereof. The U.S. Government does not endorse products or manufacturers. Trade or manufacturers' names appear herein solely because they are considered essential to the objective of this report. The findings and conclusions in this report are those of the author(s) and do not necessarily represent the views of the funding agency. This document does not constitute FAA policy. Consult the FAA sponsoring organization listed on the Technical Documentation page as to its use.

This report is available at the Federal Aviation Administration William J. Hughes Technical Center's Full-Text Technical Reports page: actlibrary.tc.faa.gov in Adobe Acrobat portable document format (PDF).

Technical Report Documentation Page

Form DOT F 1700.7 (8-72) Reproduction of completed page authorized

1. Report No.	2. Government Accession No.	3. Recipient's Catalog No.
DOT/FAA/TC-24/40		

4. Title and Subtitle	5. Report Date
Design, Analysis, and Test Development of Full-Scale Fuselage Test Panels to Assess Emerging Metallic Structures Technologies	November 2024
7. Author(s)	6. Performing Organization Code
Authors Michael Kulak, John G. Bakuckas, Jr., Yongzhe Tian, David Stanley, Po -Yu Chang, Henry Sklyut	8. Performing Organization Report No.
9. Performing Organization Name and Address US Department of Transportation William J. Hughes Technical Center Aviation Research Division Atlantic City International Airport, NJ 08405	10. Work Unit No. (TRAIS) 11. Contract or Grant No.
12. Sponsoring Agency Name and Address	13. Type of Report and Period Covered 14. Sponsoring Agency Code

15. Supplementary Notes

16. Abstract

The aircraft industry is striving to improve structural performance and reduce costs in fabrication, operation, and maintenance by introducing advanced designs/materials in conjunction with advanced manufacturing/assembly technologies. Collectively these technologies are referred to as Emerging Metallic Structures Technologies (EMST). Prior tests by Arconic on large scale flat panels have demonstrated the potential for durable and damage tolerant fuselage concepts utilizing EMST. However, full-scale fuselage curved panel testing was needed under representative pressure and bending loads to fully demonstrate the improved damage tolerance and residual strength at the aircraft structural level. A collaborative effort between Arconic, Embraer, NIAR and FAA was established to design, build, and test full-scale panels representing EMST concepts. Technologies being considered include advanced metallic skin alloys 2029 and 2060 Al-Li, Al-Li 2055 stringers and Al-Li 2099 integral frames, and Glass Reinforces Aluminum Laminates (GLARE) Fiber Metal Laminate (FML) strap reinforced fuselage skins. This report describes the sizing and loading methodologies used to design baseline Panel 1 for a generic single-aisle aircraft. Crown panels were built and tested for longitudinal and circumferential repeat inspection damage scenarios in the FAA's Full-Scale Aircraft Structural Test and Evaluation (FASTER) facility, which was developed for full-scale testing of fuselage structures under simulated flight loading conditions. Panel 1 is representative of the current design and construction (2524-T3 skin with 7150-T77511 stringers and 7075-T62 shear tied frames) of transport category airplane structure. The panel was sized, and the FASTER test fixture loading was developed to represent fuselage structure located at the crown of the airplane, and forward of the wing where damage tolerance was determined to be the key sizing criterion in both the longitudinal and circumferential direction. Manufacturing differences in skin pocket thickness were accounted for by testing Panels 1 – 3 to the same stress intensity factors based on finite element (FE) analysis. A mesh convergence study was conducted. Final stress intensity solutions were provided for both the longitudinal and circumferential crack growth directions. The Panel 1 circumferential crack growth constant amplitude loading was developed using K-control Middle tension ((M(T)) testing by equating the spectrum K-control results to those of an "equivalent" constant amplitude K-control load.

17. Key Words	18. Distribution Statement
Fuselage Panel Testing, Fuselage Panel Stress Intensity Factors, Crack Growth, Inspection Intervals, Fuselage Trade Studies, Fuselage Test Panel Design, Emerging Material Structures Technology (EMST), K-control Testing, K-control Spectrum Testing, Spectrum Development	This document is available to the U.S. public through the National Technical Information Service (NTIS), Springfield, Virginia 22161. This document is also available from the Federal Aviation Administration William J. Hughes Technical Center at actlibrary.tc.faa.gov.

19. Security Classif. (of this report)	20. Security Classif. (of this page)	21. No. of Pages	22. Price
Unclassified	Unclassified	249	

Contents

1 Introduction 1

2 Panel 1 design approach 5

2.1 Overview of Panel 1 sizing approach 5

2.2 Detailed description of Panel 1 sizing approach 25

2.2.1 Crown static strength design goals—bending and pressure loading 33

2.2.2 Crown compression buckling failure criterion at negative 1.5G 34

2.2.3 Sizing methods for fatigue, initial inspection, and repeat inspection 36

2.2.4 The repeat inspection goal 41

2.2.5 Commentary on the use of spectrum retardation for the circumferential repeat inspection approach used in this study 44

2.2.6 The two-bay crack goal for the circumferential crack 46

2.2.7 The two-bay crack goal for a longitudinal crack 49

2.2.8 Design goals for side panels 53

2.3 Design goals for belly panel 54

3 Results of sizing approach for Panel 1 55

3.1 Impact of 74 in. versus 78 in. fuselage radius 59

4 Finite element modeling to support testing of panel 1 60

4.1 Use of the quarter symmetry model, Qsymm1, to determine loads for test panel 1 60

4.2 Qsymm1 FE model geometry for the as-Designed Panel 1 65

4.3 Qsymm1 results for as-designed Panel 1 (2524-T3, 0.55 in. (1.4mm) skin) for 9.9 psi (0.068 MPa) pressure differential 69

4.4 Qsymm1 circumferential stress intensity factors for as-designed Panel 1 73

4.5 Qsymm1 longitudinal stress intensity factors for the as-designed Panel 1 (0.055 in. (1.4 mm) skin in pockets) 79

4.6 Qsymm1 elastic-plastic two-bay longitudinal crack stress intensity factors 82

5 The use of K-control testing of M(T) specimens as a surrogate circumferential fatigue crack growth test for the full-scale Panel 1 83

5.1 Relation between K-control table and Qsymm1 undamaged fuselage skin stress for a given bending and pressure condition 86
5.2 Description of K-control spectrum used in this program 89
5.3 K-control constant amplitude test for the circumferential crack 94
5.4 K-control spectrum test for the circumferential crack 96
5.5 Testing to determine the equivalent constant amplitude circumferential stress 104
5.6 Comparison of K-control tests with the FASTER Panel 1 test 109
5.7 Final comments on circumferential crack growth spectrum testing approach 120
6 Finite element modeling of Panel 1 121
6.1 Original 2016-2017 as-designed Panel 1 FE modeling 121
6.2 Panel 1 loads 128
6.3 Adjustments for FASTER axial arm loads developed for the as-built Panel 1 130
6.4 Effect of skin thickness discretization on Panel 1 solutions 135
6.5 Panel 1 circumferential crack growth modeling 138
6.6 Panel 1 circumferential two-bay crack at limit load 142
6.7 Panel 1 stresses at 9.9 psi pressure load after repair 145
6.8 Panel 1 crack #2 — testing of crack turning scenario 148
6.8.1 Prediction of crack growth life and trajectory 157
6.9 Analysis of phase 2, crack #2 repair 163
6.10 Panel-1 two-bay longitudinal fatigue crack growth modeling at 9.9 psi pressure ... 165
6.11 Longitudinal two-bay crack residual strength 170
7 Repeat inspection and limit loads for Panel 2 178
8 Conclusions 191
9 References 193
A Panel 1 design drawings A-1
B Characterization B-1
C Spectrum development C-1

Figures

Figure 1. Comparison of current testing program with Mosinyi 6
Figure 2. Description of generic single-aisle aircraft 7
Figure 3. FAA FASTER facility 7
Figure 4. Panel 1 design 8
Figure 5. Detail showing skin pocketing between stringers and frames 9
Figure 6. Information used to size Panel 1 for the generic aircraft 13
Figure 7. Flow of simplified fuselage sizing/trade study approach 14
Figure 8. Smeared stiffened cylinder solutions with a variable skin, stiffener, and frame elastic modulus 15
Figure 9. Pressure loading decomposed into hoop effect and axial load effect 16
Figure 10. Comparison of Flugge smeared stiffness and discrete frame solution to FEM results for pressure loading of 9.9 psi (0.068 MPa) 20
Figure 11. Elements of the fuselage bending model used in the sizing approach 23
Figure 12. Load intensity results from the generic aircraft bending model 24
Figure 13. Moment of inertia of fuselage cross-section with smeared stringers 26
Figure 14. Bending stresses and stress intensity at top and bottom of the fuselage in Loop 1 27
Figure 15. Axial load intensity comparison between Loop 1 and Loop 2 29
Figure 16. Goals for crown section used in this study 31
Figure 17. Potential goals to consider for bottom section of the fuselage 32
Figure 18. Potential goals to consider for side sections of the fuselage 32
Figure 19. Design goals in the crown section 33
Figure 20. Static strength of fastened stiffened panel detail estimated by the strain-to-failure approach proposed by Mohaghegh 34
Figure 21. Hypothetical example using ASPAN-CO Arconic compression optimization code for curved or flat stiffened panels in compression and shear 35
Figure 22. Comparison of bending moments from landing versus the -1.5G maneuver bending moment 36
Figure 23. Comparison of some methods for inspection and S/N fatigue helpful in simplified trade studies 38
Figure 24. Damage tolerance scenarios for estimating initial and repeat inspections in simple trade study approach 39
Figure 25. Simplified method to establish the working stress target to meet the initial (threshold) inspection interval goal 40

Figure 26. Analysis cases for the “same hole” primary/secondary flaw initial inspection approach 41
Figure 27. Repeat inspection scenario used in this study 42
Figure 28. FEM modeling to develop SIFs for crack growth in the circumferential direction with a broken stringer 43
Figure 29. Spectrum and constant amplitude results with and without K-control for Panel 1 2524-T3 M(T) specimens 44
Figure 30. Two-bay crack scenario 47
Figure 31. Circumferential two-bay crack analysis for Panel 1 49
Figure 32. ABAQUS elastic/plastic analysis SIF results for a longitudinal crack with a broken frame 51
Figure 33. Crack growth da/dN versus delta-K for 2524-T3 52
Figure 34. Trade study design goals for side panels 53
Figure 35. Design goals for belly section 54
Figure 36. Bending scenarios, including ultimate, limit, gust, and maneuver loads 54
Figure 37. Simple variable radius cylinder model to estimate bending and shear loads 55
Figure 38. Panel 1 crown load intensities and bending moments 56
Figure 39. Sizing results for an STA 38 crown 57
Figure 40. Sizing results for STA 38 middle side 58
Figure 41. Sizing results for STA 38 bottom 58
Figure 42. Comparison of pressure and bending stresses for 78-in. fuselage radius versus a 74-in. radius 59
Figure 43. Schematic of FASTER actuator load development using the Qsymm1 quarter symmetry FE model in conjunction with the panel 1 FE model 60
Figure 44. FASTER hoop loading, frame loading, and axial skin loading actuators 61
Figure 45. Edge doublers used to transfer load into the test Panel 1 62
Figure 46. ABAQUS Qsymm1 fuselage FE model for the as-designed Panel 1 with 0.055 in. skin thickness in the pocketed regions 66
Figure 47. The assembly of frames (left) and the cross-section of the frame/shear tie (right) 67
Figure 48. 7150-T77511 stringers in the FEM model of Panel 1 67
Figure 49. Pocketing of Panel 1 skin 68
Figure 50. ABAQUS Qsymm1 pocketed quarter symmetry fuselage FE model 69
Figure 51. Comparison of ABAQUS panel 1 9.9 psi (0.068 MPa) pressure results with Flugge smeared stringer/smeared frame and discrete frame solutions 70
Figure 52. Qsymm1 axial and hoop stress results for 1G + 9.9 psi (0.068 MPa) 71
Figure 53. Qsymm1 axial and hoop stresses for 1.04G + pressure along a longitudinal path 72

Figure 54. Qsymm1 axial and hoop stresses for 1.04G + 9.9 psi along a circumferential path ... 73
Figure 55. Definition of rivet locations and contact surfaces for the ABAQUS Panel 1 circumferential crack growth in the skin with a broken stringer ... 75
Figure 56. Qsymm1 results for circumferential crack growth with a broken stringer ... 75
Figure 57. SIFs, Ktotal, for Qsymm1 in the circumferential skin crack under a broken stringer 76
Figure 58. SIFs for a circumferential crack under a broken stringer ... 77
Figure 59. SIFs for a circumferential crack under a broken stringer ... 78
Figure 60. Measured R-curves from 2524-T3 sheet used in Panel 1 and published data from wider 2524-T3 test panels ... 79
Figure 61. Results for the quarter symmetry model for 150mm (5.9 in.) half-crack length in the longitudinal direction with a broken frame ... 81
Figure 62. Longitudinal crack SIFs, Ktotal, for Qsymm1 representing the as-designed panel 1 geometry at 9.9 psi pressure ... 82
Figure 63. Longitudinal SIFs at limit load (11.4 psi pressure) ... 83
Figure 64. M(T) specimen testing to determine the equivalent constant amplitude axial load for circumferential crack growth ... 85
Figure 65. Qsymm1 results for 1.04G + 9.9 psi pressure ... 88
Figure 66. Use of the Flugge smeared stiffness skin stress for the K-control characteristic stress ... 88
Figure 67. Comparison of the modified mini-TWIST Spectrum to B727 & B737 flight load data from Steadman ... 89
Figure 68. Comparison of modified mini-TWIST to mini-TWIST ... 90
Figure 69. Modified mini-TWIST spectrum inputs and outputs for Panel 1 ... 91
Figure 70. Idealized K-control approach for constant amplitude loading ... 95
Figure 71. Inputs and results from a simplified hypothetic spectrum K-control example ... 98
Figure 72. K-control approach for spectrum loading ... 103
Figure 73. M(T) FCG specimen used in K-control testing program ... 105
Figure 74. Arconic M(T) crack growth test setup developed to prevent buckling due to spectrum landing loads ... 106
Figure 75. Constant amplitude and spectrum test results with and without K-control ... 107
Figure 76. Additional results of Ktotal-control testing for modified mini-TWIST spectrum ... 108
Figure 77. Results of the FASTER test Panel 1 versus the original K-control M(T) testing ... 112
Figure 78. Corrections to convert the Aeffective crack K-control table to an Aphysical K-control table ... 115
Figure 79 .Results of FASTER test Panel 1 compared with modified K1-control M(T) testing with plasticity correction ... 118

Figure 80. As-built Panel 1 stress intensity solutions vs. new as-designed Panel 1 solution for axial load arm displacement = -1.0 mm and radial link displacement = 0.0 mm 120
Figure 81. ABAQUS FEM model of Panel 1 (note that mesh is not shown) 123
Figure 82. Edge doublers used in Panel 1 FE model 124
Figure 83. Cylindrical symmetry conditions applied at actuator load points 125
Figure 84. Detail of a radial link in the FASTER fixture 126
Figure 85. Panel 1 FE model showing the elastomeric seal (dark blue edge) 127
Figure 86. Comparison of Panel 1 FEM stresses to Qsymm1 at 9.9 psi pressure 127
Figure 87. Panel 1 axial stress comparison with Qsymm1 model at 9.9 psi+1G 128
Figure 88. Panel 1 hoop stress comparison with Qsymm1 model at 9.9 psi+1G 128
Figure 89. Panel 1 actuator loads for 2.5G bending with no pressure 129
Figure 90. Panel 1 actuator loads for 9.9 psi pressure only 130
Figure 91. Comparison of superposition of SIFs using Qsymm1 results versus Qsymm1 130
Figure 92. Panel 1 showing axial load arms, the centroid of the cross-section, and LVDT 131
Figure 93. Comparison of axial strain gage measurements with Panel 1 FE analyses assuming various displacement BCs at axial loader arms 132
Figure 94. Comparison of hoop strain gage measurements with Panel 1 FE analyses for various displacement BCs at axial loader arms 133
Figure 95. Results showing final as-built Panel 1 SIFs to be similar to the two-skin element as-designed Panel 1 SIFs 134
Figure 96. Meshes used to study skin through-the-thickness mesh discretization 136
Figure 97. Full Qsymm1 FE model Ktotal versus number of skin elements through-the-thickness for a 35 mm crack half-length 137
Figure 98. Panel 1 results for 1.0 and 2.0 mm in-plane mesh size for two- and eight-element meshes through-the-thickness of the skin 138
Figure 99. Stress intensity Ktotal versus number of skin elements through-thickness 138
Figure 100. Panel 1 actuator loads for 1.04G bending with pressure 139
Figure 101. Starting notch for a circumferential crack at the mid-bay stringer to skin fastener 140
Figure 102. Circumferential crack Panel 1 final Ktotal solution compared to various solutions from 2016 142
Figure 103. Elastic/plastic property inputs for 2524-T3 sheet, 7075-T62 formed sheet, and 7150-T7751 extrusion stringer 143
Figure 104. Actuator loads for the circumferential crack at limit load (2.5G + 9.9 psi) 144
Figure 105. Panel 1 skin and stringer yield areas at 3.4G + 9.9 psi 144
Figure 106. Ktotal at limit load compared to 1G + 9.9 psi load 145
Figure 107. Panel 1 results at 3.4G + 9.9 psi (0.068 MPa) pressure 145

Figure 108. ABAQUS Panel 1 model and repair detail of the circumferential crack 146
Figure 109. Panel 1 FE model after repair of Panel 1 (0.055 in. (1.4 mm) skin) 147
Figure 110. Skin stresses with repair of circumferential crack and broken stringer..... 148
Figure 111. Panel 1 longitudinal crack turning scenario 149
Figure 112. Location of longitudinal crack #2..... 149
Figure 113. Pre-cracking loads for longitudinal crack #2 turning scenario at 70% pressure 150
Figure 114. Loads for Panel 1 longitudinal crack #2 and crack #3 at 9.9 psi (0.068 MPa)..... 150
Figure 115. ABAQUS FEM model for T-stresses in a bi-axially loaded plate 151
Figure 116. FEM results for T-Stress in bi-axially loaded plate..... 152
Figure 117. As-designed Panel 1 crack turning FE model for a 12.0in. (305 mm) starting crack total length 152
Figure 118. Sub-structure model used for the as-designed Panel 1 cack turning analysis 153
Figure 119. FE model of the as-designed Panel 1 showing the sub-structure detail 153
Figure 120. FEM Von Mises stress contour plots for various crack lengths along the stringer (internal view)..... 154
Figure 121. FEM Von Mises stress contours for various crack lengths along the stringer (external view) 154
Figure 122. As-designed Panel 1 sub-model Von Mises stresses for various crack lengths along the stringer 155
Figure 123. Direction of crack turning for positive K2 in ABAQUS model..... 156
Figure 124. Results for K1 and K2 for various crack lengths along the stringer mill line 156
Figure 125. Calculation of T-stress for a 6.0-inch total crack length 157
Figure 126. ABAQUS FE model after the first crack turning segment..... 159
Figure 127. At 6 in. total length, the crack is assumed to grow at 22° for 10 mm 160
Figure 128. Crack growth rate, da/dN, for 2524-T3 in T-L direction 161
Figure 129. ABAQUS FE model coordinate system for K1, K2 calculations after the first crack turning segment..... 162
Figure 130. Calculated angle for second crack turning segment 162
Figure 131. Summary of the four-step prediction of crack turning life..... 163
Figure 132. External view of Panel 1, Phase 2 crack repair and FEM model 164
Figure 133. Axial and hoop stresses after repair of Phase 2 crack at 1G+9.9 psi..... 165
Figure 134. Location of the longitudinal two-bay crack..... 166
Figure 135. Von Mises stresses for various as-designed Panel 1, Phase 3 longitudinal cracks . 167
Figure 136. Comparison of the 2016 Panel 1 as-designed SIF solutions to the 2020 as-built longitudinal crack solutions 168
Figure 137. Detail of the 2016 Panel 1 as-designed stress intensity..... 169

Figure 138. Frame differential displacement and rotation due to non-symmetric Panel 1 longitudinal crack placement 170
Figure 139. Comparison of as-designed, 0.055 in. skin thickness Panel 1 Ktotal for the longitudinal two-bay crack at 1.15 x pressure limit load with results at 9.9 psi..... 171
Figure 140. Analysis of Panel 1 longitudinal two-bay crack at limit pressure of 1.15 x pressure, or 11.385 psi (0.0785 MPa) 172
Figure 141. R-Curve for same lot 2524-T3 used in Panel 1 and wide panel data from Bucci, et al., used to estimate Aphysical based R-Curve..... 173
Figure 142. FE model (mesh not shown) of test Panel 1 showing a crack grown in the skin from the central broken frame 175
Figure 143. FEM approach for two-bay longitudinal crack elastic/plastic R-Curve analysis 176
Figure 144. First three iteration steps in Panel 1 longitudinal two-bay crack analysis 177
Figure 145. Location in fuselage of as-designed Panel 1 versus as-built Panel 1 182
Figure 146. FASTER actuator loads for the Panel 2 Phase 1 fatigue test 184
Figure 147. Location of Panel 2 for various sizing studies..... 186
Figure 148. FASTER fixture actuator loads for Phase 1 limit load..... 191

Tables

Table 1. Stresses for a 74in. (1.88 m) fuselage radius and a 78 in. (1.98 m) radius 17
Table 2. Fastener nonlinear load displacement for NAS1097KE5 rivet (5/32 in. [3.97 mm] diameter, 100 degrees countersunk, 7050-T73) and NAS1097KE6 rivet 74
Table 3. Bending and pressure stresses for a 74 in. (1.88 m) and 78 in. (1.98 m) radius fuselage 92
Table 4. As-designed Panel 1 FE model results — one C3D20 element versus two elements .. 111
Table 5. Comparison of panel 1 FE model Ktotal with K1 113
Table 6. Comparison of original K-control (2016) to K1-Control (2020) with skin mesh refinement and use of K1 with plastic zone correction..... 116

Acronyms

Acronym	Definition
σ_{ys}	yield stress
α	Axial landing compressive stress divided by the axial bending stress at 1G
$A_{effective}$	Effective crack length which includes the plastic zone compliance
A_{fr}/B_t	Area of frame divided by average area of skin over the frame bay
$A_{physical}$	Physical crack length
A_s/B_t	Area of stringer divided by the average area of skin over the stringer bay
β	beta
BC	Boundary condition
COD	Crack opening displacement
CTOA	Crack tip opening angle
DT	Damage tolerance
E	Modulus of elasticity
EIFS	Equivalent initial effective flaw size
EMST	Emerging metallic structures technologies
FAA	Federal Aviation Administration
FASTER	Full-scale aircraft structure test evaluation and research
FCG	Fatigue crack growth
FE	Finite element
FEM	Finite element modeling
FML	Fiber metal laminate
GLARE	Glass fiber reinforced fiber metal laminates
I_{xx}	The fuselage cross-section moment of inertia at the mid-point of the test panel
ISP	Inspection start points
J	J-integral
Kcirc(a)	Stress intensity factor for the circumferential crack at max stress as a function of the crack half-length
Ki	Stress intensity factors K1, K2, K3
K_{phys}	Stress intensity factor from elastic/plastic analysis where the crack is the “physical” crack length
Ktotal	Total stress intensity factor
MTOW	Maximum takeoff weight
LOV	Limit of validity

LVDT	Linear variable differential transformer
M_f	Fuselage shell bending moment along the length of the fuselage
Mfs	Mean flight stress
MSD	Multiple site damage
MED	Middle takeoff weight
M(T)	Middle tension
NDI	Non-destructive inspection
NIAR	National Institutes for Aviation Research
NLG	Non-linear geometry displacement corrections applied to the ABAQUS FEM model
Nθ	Fuselage hoop load intensity
Nx	Fuselage axial load intensity
OEM	Original equipment manufacturer
Qsymm1	Quarter symmetry finite element model simulating the top section of the fuselage at the Panel 1 location in the crown
ry	Irwin first order estimate of the plastic zone
SHM	Structural health monitoring
SIF	Stress intensity factor
SMP	Structural modification points
STA	Station number of fuselage measured in feet
S/N	Fatigue limit
3D	Three-dimensional
Vf	Fuselage shell shear force along the length of the fuselage

Glossary

Term	Definition
δ	In the discrete frame Flugge solution, δ, represents an effective width of skin used with the stringer to determine the axial direction bending stiffness of the curved stringer/skin detail in response to a local bending moment load intensity per unit circumferential length.
Beta (β)	The stress intensity from FEM fuselage model normalized by s*sqrt[π*a]
EIFS	Equivalent initial effective flaw size that provides the same life in a damage tolerance calculation as that resulting from a S/N fatigue test
Eluent	The liquid solvent in ion chromatography that transports the analytes through the separator columns and detectors of the ion chromatograph.
Mfs	1G + pressure stresses for this program
Fuselage hoop load intensity (Nθ)	pressure ∗ radius for pressure only loading
Fuselage axial load intensity (Nx)	bending axial load intensity + pressure ∗ radius/2
Fatigue limit (S/N)	Relationship between cyclic stress amplitude (S) and cycles to failure (N)

Executive summary

A collaborative effort was established among Arconic, Embraer, National Institute for Aviation Research (NIAR) and the Federal Aviation Administration (FAA) (hereinafter referred to as the "team") to design, build, and test full-scale fuselage panels that include emerging metallic structures technologies (EMST) that represent improvements in materials, structural design, and manufacturing approaches.

The EMST being considered include advanced metallic skin alloys 2029 and 2060 Al-Li, Al-Li 2055 stringers, Al-Li 2099 integral frames, and glass reinforced aluminum laminates (GLARE) fiber metal laminate (FML) strap reinforced fuselage skins. Altogether, five fuselage panels incorporating varying EMST are planned to be tested as part of this program: Baseline Panel 1 was built using conventional materials and processes: 2524-T3 for the skin and 7000-series aluminum frame/shear ties and stringers assembled by riveting. Panel 2 used 2060-T8 Al-Li skin stiffened with integral frames made of 2099-T83 and stringers made of 2055-T84 Al-Li. Panel 3 was constructed from advanced aluminum clad alloy and 2029-T3 skins stiffened with the same substructure materials as Panel 2. Panels 4 and 5 will be comprised of the same baseline construction as Panel 1 with FML straps bonded to the skins under the stringers and frame/shear ties to improve the damage tolerance. The frame/shear ties and stringers are riveted to the bonded skin/FML straps.

The design goals currently defined for this program include:

- Demonstrating longer repeat inspection intervals for circumferential and longitudinal crack growth and improved two bay crack limit load capability at an operating differential pressure of 9.9 psi (0.0683 MPa), which is higher than current metallic transport airplanes are typically designed to.
- Demonstrating the improvements in repeat inspection and two bay crack residual strength scenarios for FML strap reinforcement under stringers and frame/shear ties at a higher operating pressure of 9.9 psi (0.0683 MPa).
- Demonstrating the damage tolerance capability of integral extruded frames using new aluminum lithium extrusions at a higher operating pressure of 9.9 psi (0.0683 MPa).
- Identifying and evaluating applicable nondestructive inspections (NDIs) and structural health monitoring (SHM) technologies.

Material characterization testing and middle tension (M(T)) crack growth testing will be conducted to supplement the full-scale panel testing. Also, supplemental tests will be conducted on smaller-scale stiffened coupons with smaller initial cracks to supplement the large-scale testing, including constant amplitude and spectrum testing. Fatigue limit (S/N) testing will be conducted to compare the fatigue performance of the new aluminum skin alloys. Finally, wide flat multicolumn lap joints will be tested for multiple site damage (MSD) scenarios, as well as wide curved lap joints for MSD scenarios under pressure loading. These results will be published in subsequent reports.

In this program, EMST test panels represent a generic single-aisle fuselage of a transport category airplane. The assumptions used in this study simplified performance, life, and inspection goals. Simple loading and design methodologies were used to ensure the team-defined static strength, buckling, and damage tolerance requirements were met. Objectives of this program include designing, building, and testing fuselage skin panels based on representative geometry and loading conditions of an airplane fuselage location where damage tolerance was the key sizing criterion for both the longitudinal and circumferential directions. The intention was not to design test panels that met all certification design requirements, but to provide a basis for "apples to apples" crack-growth comparisons between fuselage panels that include EMST and a baseline fuselage panel built from conventional materials. Using the methodology described in this report, metallic alloy Panels 1–3 were designed for a crown location where a similar skin thickness was required to meet both longitudinal and circumferential inspection goals. The Panel 1–3 plan was designed to test crack growth performance in the circumferential and longitudinal directions. The circumferential direction is tested first, then, after repairing the crack, the longitudinal crack direction is tested. In Panel 1 only, a one-bay crack growth test is conducted for a longitudinal crack positioned midway between frames along the pocket mil-line to evaluate crack turning. After repair, another longitudinal crack is grown from under a broken frame/shear tie at a location midway between the stringers. The program testing was initially defined to test all panels to the same cross-sectional area and to the same loads. However, because the panel skins were thin, small manufacturing tolerance differences in the chemically milled pocket thickness, as identified by the dimensional tolerances for the design, would have resulted in significant crack-growth life differences. Thus, manufacturing differences in the "as-built" panel skin pocket thickness were accounted for by testing all panels to the same stress intensity factors (SIFs) versus crack size based on finite element (FE) analysis.

This report describes the sizing and loading methodology of Panel 1. The fuselage test panel was developed to represent a generic single-aisle aircraft of comparable size and performance characteristics to existing in-service Title 14, Code of Federal Regulations (CFR) Part 25

transport category airplanes. This generic methodology was used to develop a program to test Panels 1–3 with longitudinal and circumferential damage scenarios and repetitively inspect the panels using conventional NDI and SHM methods. The tests and inspections occurred at the FAA Full-Scale Aircraft Structure Test Evaluation and Research (FASTER) Test Facility located at the FAA Technical Center. The FASTER fixture was developed for full-scale testing of fuselage structures under simulated flight loading conditions (Tian & Bakuckas, 2019).

1 Introduction

The aircraft industry is striving to improve structural performance and reduce costs in fabrication, operation, and maintenance by introducing advanced designs and materials in conjunction with advanced manufacturing and assembly technologies. In response to increasing competition from composite materials, the aluminum industry has made significant advancements over the past decade developing new lightweight alloys and product forms, improved structural concepts, and manufacturing processes aimed at competing with composite materials in manufacturing cost and performance. These technologies are referred to as emerging metallic structures technologies (EMST) in this report. Original equipment manufacturers (OEMs) are evaluating new applications for using EMST in safety-critical aircraft structures, such as fuselage structures. These applications have very limited or no prior in-service and certification experience. The primary technologies under consideration include aluminum–lithium (Al-Li) , aluminum clad alloys (Prasad, Gokhale, & Wanhill, 2014), bonding and joining methods (Bertoni, Fernandez, & Miyazaki, 2014; Chaves, 2017; Kok, Poston, & Moore, 2011; Schmidt, 2005), and hybrid construction using fiber metal laminate (FML) reinforcement (Bertoni, Fernandez, & Miyazaki, 2014; Beumler, 2014; Heinimann & et al., 2007; Schmidt, 2005; Silva & al., 2017). Industry is interested in the use of these material systems due to the following benefits:

- In comparison to conventional alloys:
    - Weight savings due to higher strength-to-weight ratios
    - Improvements in other properties (e.g. fatigue and damage tolerance capabilities) resulting in reduced inspection burden and more efficient design
    - Improvements in corrosion resistance
- In comparison to composites:
    - Reduced supply chain challenges (e.g., flexibility and lead time) and fabrication cost

Prior testing by Arconic (Heinimann, et al., 2007) on large-scale, flat-panel test articles have demonstrated the potential to design, build, and test improved damage tolerant fuselage concepts that use EMST. Because these large-scale fuselage tests were conducted using flat panels, full-scale fuselage curved panel testing was needed using representative pressure and bending loading to demonstrate the improved damage tolerance and residual strength at the structural

level. A collaborative effort with Arconic, Embraer, National Institute for Aviation Research (NIAR) and the Federal Aviation Administration (FAA) (hereinafter referred to as the "team") was initiated to design, build, and test full-scale fuselage panels representing EMST concepts to determine if structural integrity and airframe safety is as good or better than fuselage panels built from conventional materials. This program is evaluating new, stronger, and lighter materials, improvements in structural designs, and manufacturing approaches.

The EMST being considered include advanced metallic skin alloys 2029 and 2060 Al-Li, Al-Li 2055 stringers, Al-Li 2099 integral frames, and glass reinforced aluminum laminates (GLARE) fiber metal laminate (FML) strap reinforced fuselage skins. Altogether, five fuselage panels incorporating varying EMST will be tested as part of this program: Baseline Panel 1 was built with conventional materials and processes; Panels 2 and 3 incorporated advanced aluminum alloys; and Panels 4 and 5 included hybrid FML reinforcement straps.

The design goals currently defined for this program include:

- Demonstrating longer repeat inspection intervals with a central broken stringer for circumferential crack growth at an operating pressure of 9.9 psi (0.0683 MPa), which is higher than transport airplanes are typically designed to.
- Demonstration of limit load capability for a two-bay circumferential crack scenario.
- Demonstrating longer repeat inspection intervals with a central broken frame for longitudinal crack growth at an operating pressure of 9.9 psi (0.0683 MPa).
- Demonstrating limit load capability and residual strength for a two-bay longitudinal crack scenario.
- Demonstrating the improvements in repeat inspection and two bay crack residual strength scenarios for FML strap reinforcement under stringers and/or frames at an operating pressure of 9.9 psi (0.0683 MPa).
- Identifying and evaluating applicable nondestructive inspection (NDI) and structural health monitoring (SHM) technologies.

Various supplemental testing programs are being conducted to support the goals of the full-scale panel testing program. Smaller specially designed flat stiffened specimens will be tested for growth testing to supplement the full-scale panel testing results as well as additional K-controlled M(T) coupon testing. Testing will also be done on both medium size flat panels lap joints and curved panels (under pressure) lap joints to demonstrate the improved performance (longer crack growth lives and higher residual strength) of the new aluminum alloys under

multiple site damage (MSD) conditions. Also, S/N testing will be conducted to compare the fatigue performance of the new aluminum skin alloys. These results will be published in subsequent reports.

The approach for the panel testing was to conduct "apples-to-apples" testing under the same conditions at a key location in the crown of a generic single aisle commercial aircraft. The first step was to locate and design a baseline panel to "representative" performance goals. The panel sizing for a single aisle aircraft by the original equipment manufacturer (OEM) is complex, even when next-generation design goals are not considered which include higher performance at a lower cost. The panel sizing at any location depends, among other things, on performance goals, including flight performance, service life, maintenance, and flight safety inspection goals. Various loading conditions must be considered by the OEM for a wide range of flight conditions.

The goal of this program was to define a generic, OEM-independent, single-aisle aircraft and select a key location in the crown to design and test EMST panels in an "apples-to-apples" manner. The intention was not to design panels that met all certification design requirements or provide a simple approach to do this. Since there is no unique definition of a generic single-aisle aircraft that covers all potential future usage scenarios, the generic aircraft constructed for this study assumed simplified performance, life, and inspection goals. Also, simplified loading and design methodologies were used to ensure static strength, buckling, fatigue, and damage tolerance goals defined by the team were met. The goal was to generate representative geometry and loading for a crown panel location where damage tolerance is the key sizing criterion for both the longitudinal and circumferential direction. The results of design trade studies described in this report indicated a large area of the crown forward and rear of the center wing was sized to meet damage tolerance requirements (when considering the goals of both a cost-effective inspection interval and a higher operating pressure of 9.9 psi (0.068 MPa) used in this study). Using the methodology described in this report, the baseline Panel 1 (2524-T3 skin with 7150-T77511 stringers and 7075-T62 shear tied frames) as well as Panels 2 and 3 were designed at a key crown location where a similar skin thickness was required to meet both longitudinal and circumferential inspection goals. Thus, Panels 1–3 were used to test crack growth performance in the circumferential direction, repaired, and then tested in the longitudinal direction. It is realized that the simplified sizing approach will result in geometry and loading that will not reflect an OEM design; however, the key for this program was to develop a realistic geometry and loading conditions to compare the various EMST panel concepts in an "apples-to-apples" damage tolerance testing plan. The program was initially defined to test panels for the same cross-sectional areas to the same loads (referred to in this report as the *as-designed* panels). However, because the panel skins are thin, small manufacturing differences in chem-milling the pockets

between Panels 1, 2, and 3 resulted in significant pocket thickness differences. This required a change of plan in the testing. Thus, these differences in skin pocket thickness for the various as-built panels were accounted for in an "apples-to-apples" manner by testing all panels to the same SIFs versus crack size based on finite element (FE) analyses of Panels 1, 2, and 3.

This report describes the methodology used for sizing and developing the loads that were applied to Panel 1, which were initially intended to be applied to Panels 2 and 3. The goal for Panels 2 and 3 was to build and test the panels with the same geometry and loading as Panel 1. Testing was completed on Panels 1, 2 and 3 in 2019, 2021, and 2024, respectively and reported in Tian & Bakuckas (2019), Tian, Stanley, & Bakuckas (2021), and Tian, et al. (2023). The FASTER fixture was developed for full-scale testing of fuselage structures under simulated flight loading conditions.

This report is organized as follows. Section 2 describes the sizing goals and methods used for Panel 1. Section 3 provides the results of the sizing approach for Panel 1. Section 4 describes the FE approach, which links the global generic fuselage to the curved fuselage test panel used in the FASTER test fixture. This approach was necessary to develop loads for the test Panel 1, which is heavily reinforced around the edges for load introduction by metallic doublers. A quarter symmetry stiffened cylindrical FE model, Qsymm1, was used to generate SIF targets for Panel 1 to develop the FASTER actuator loads. Section 5 describes the "equivalent" constant amplitude axial loading for Panel 1, which was developed for the circumferential crack based on K-control testing. In this approach, the circumferential SIF versus crack size solutions generated from the Qsymm1 FE model were used to grow cracks in a M(T) specimen. The "equivalent" constant amplitude stress was determined as the constant amplitude K-control M(T) stress, which produced the same life as the spectrum K-control M(T) test. The K-control method and the spectrum used are described in Section 5. The Panel 1 FE model, the loads/boundary conditions (BCs), and SIFs are described in Section 6 for both circumferential and longitudinal cracks. Predictions of the as-designed, 0.055 in. (1.4 mm) skin pocket Panel 1 and Phase 2 crack turning test are presented in Section 6 as well as the residual strength predictions for the as designed Panel 1. Section 7 describes the repeat inspection methods and results, as well as limit loads for the as built Panels 2 and 3. Finally, Section 8 contains the conclusions.

2 Panel 1 design approach

2.1 Overview of Panel 1 sizing approach

This report outlines the approach used to size the baseline FASTER Test Panel 1. The goal for Panels 2 and 3 was to build and test the panels with the same geometry and loading as Panel 1. The team used a simplified, generic approach to design and size the curved fuselage test panel, and to establish the loads to apply to the test article. They did not consider any specific OEM design approach or OEM load development approach when developing this generic approach. The simplified test panel sizing and loading approach developed for this program was based on methods available in literature. It should be emphasized that any discussion in this report regarding the simplified sizing or analysis approaches used to design the test panels in this program is limited to the objective of developing a simplified approach for developing panels that are reasonably representative of the fuselage panel location being considered on transport category airplane. Using these simplified methods does not necessarily result in designs which are in compliance with all regulations, including, but not limited to, regulations related to MSD, multiple element damage (MED), and limit of validity (LOV). In summary, these simplified methods are not intended for use in the actual design of a structure.

Measured flight loads on commercial single aisle aircraft were used for circumferential spectrum loading. Primary differences between this panel testing program and a similar OEM-driven effort are compared in Figure 1 (Mosinyi, Bakuckas, & Steadman, 2007).

The goal was to design the crown panels to be tested in the FASTER facility in a reasonable manner consistent with industry practices and tested in a manner to produce a direct “apples-to-apples” performance comparison of the EMST panels for the primary damage tolerance design driver for the crown location selected. A reference aircraft was developed to represent a generic single-aisle aircraft of similar size and performance characteristics to existing single-aisle aircraft (Figure 2). Panel 1 was tested for longitudinal and circumferential damage scenarios representing repeat inspection scenarios in the FASTER Facility located at the FAA William J. Hughes Technical Center. The FASTER fixture (Tian & Bakuckas, 2019), shown in Figure 3 was developed for full-scale testing of fuselage structures under simulated flight conditions.

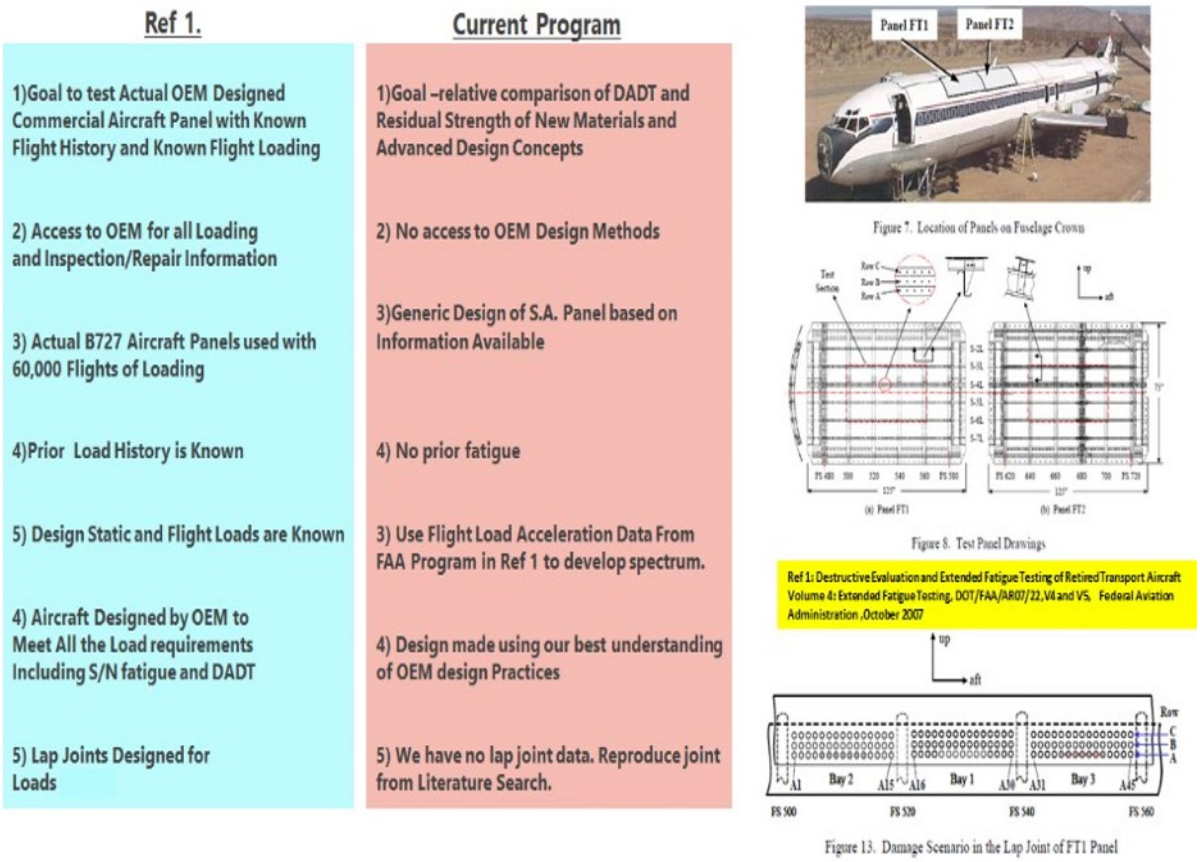

Figure 1. Comparison of current testing program with Mosinyi

The Panel 1 test article is shown in Figure 4. A full set of engineering drawings is included in Appendix A. The methodology used to locate and size the panel in the generic single aisle aircraft is described in this section. The results of the sizing study are presented in Section 3. The skin radius is 74 in. (1879.6 mm). A pocketed skin construction was used (Figure 5) in the as-designed Panel 1 with a 2524-T3 skin thickness of 0.063 in. (1.6 mm) in the pad-up areas and a thickness of 0.055 in. (1.4 mm) in the pocketed regions. The two-piece frame/shear tie was comprised of 7075-T62 extruded frames and 7075-T62 sheet hydroformed shear ties and the stringers were 7150-T77511 extrusions. The frame and shear ties were formed in the O temper and then quenched/aged to the T6 condition. The rivets fastening the stringers/frames to the skin were NAS1097KE5 (5/32 in. (3.97 mm) diameter, 100 deg. countersunk, 7050-T73). Properties for materials used in this program are included in Appendix B.

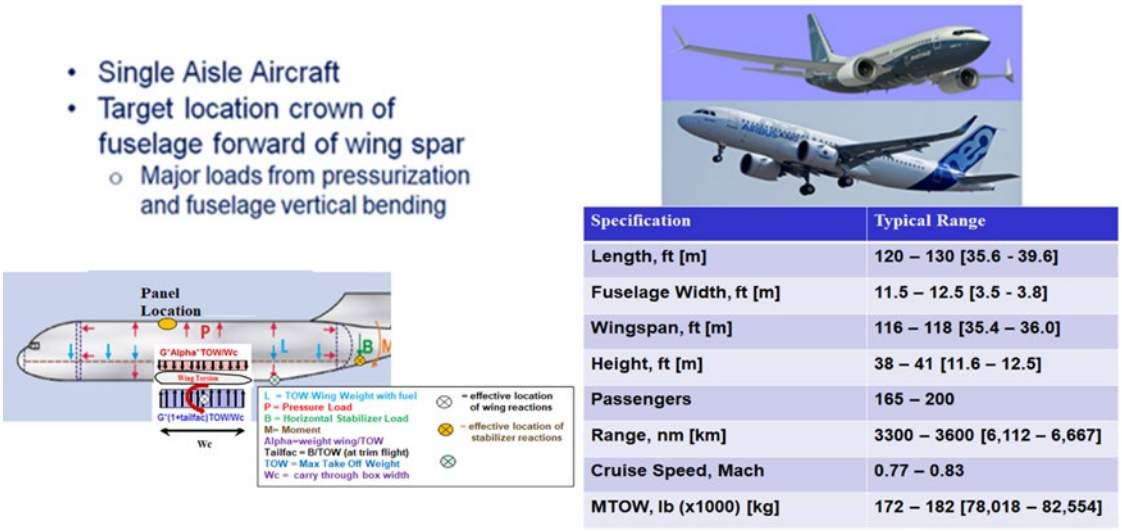

Specification	Typical Range
Length, ft [m]	120 – 130 [35.6 - 39.6]
Fuselage Width, ft [m]	11.5 – 12.5 [3.5 - 3.8]
Wingspan, ft [m]	116 – 118 [35.4 – 36.0]
Height, ft [m]	38 – 41 [11.6 – 12.5]
Passengers	165 – 200
Range, nm [km]	3300 – 3600 [6,112 – 6,667]
Cruise Speed, Mach	0.77 – 0.83
MTOW, lb (x1000) [kg]	172 – 182 [78,018 – 82,554]

Figure 2. Description of generic single-aisle aircraft

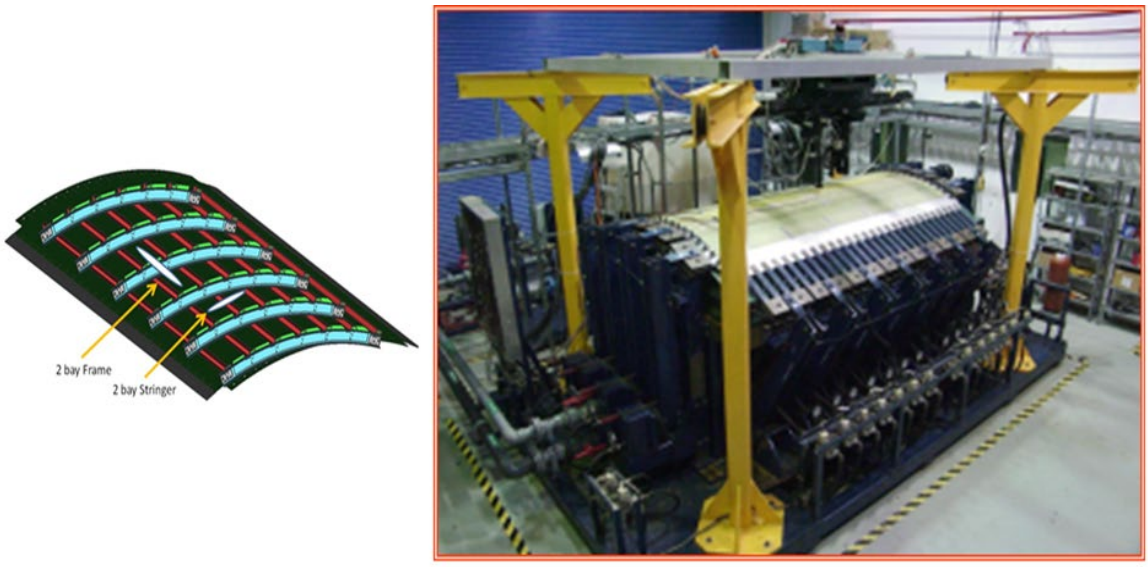

FAA FASTER Fixture Showing Hoop and Edge Actuators (each delivering 4 equal loads via a wiffle setup)

Figure 3. FAA FASTER facility

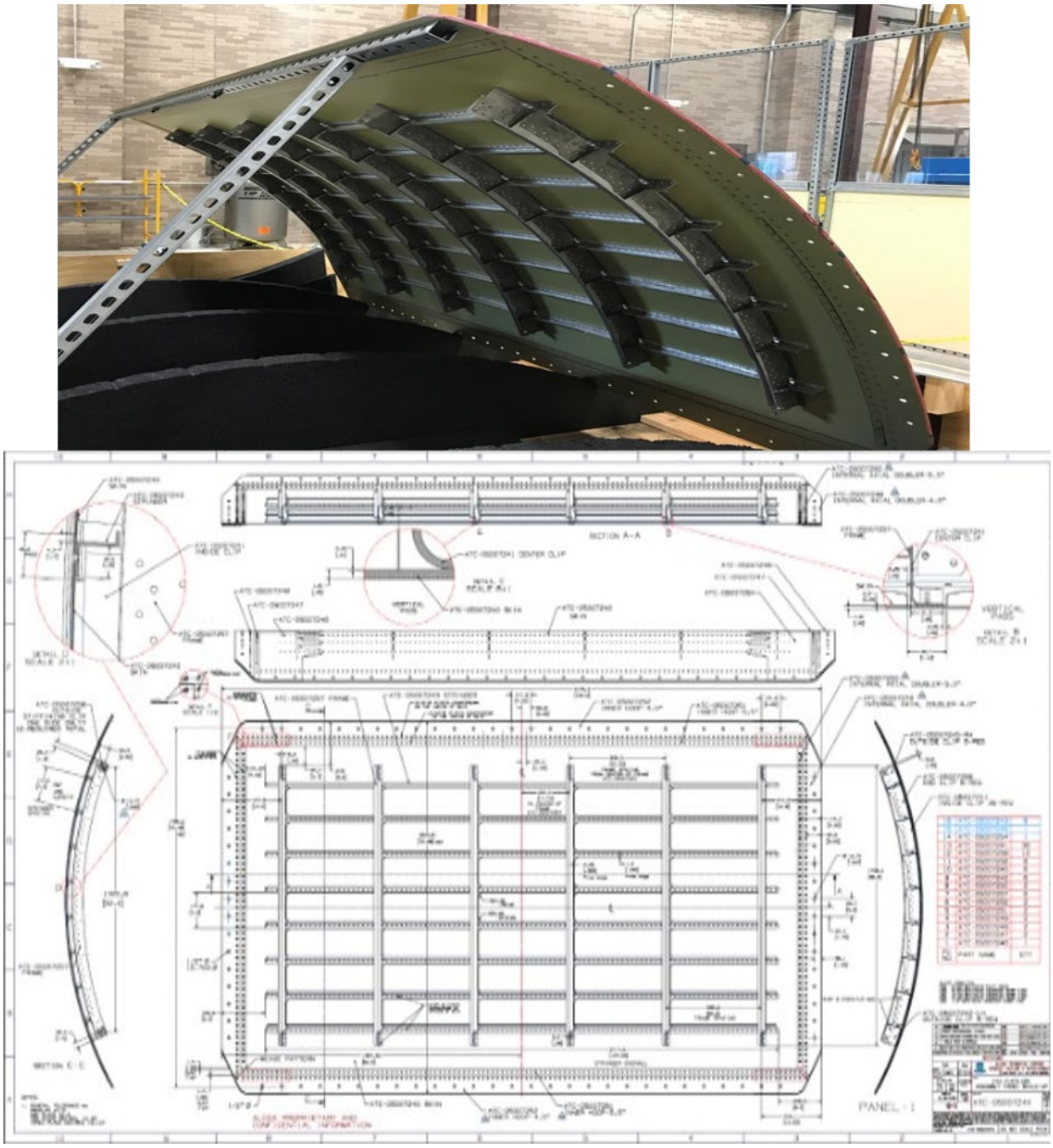

Figure 4. Panel 1 design

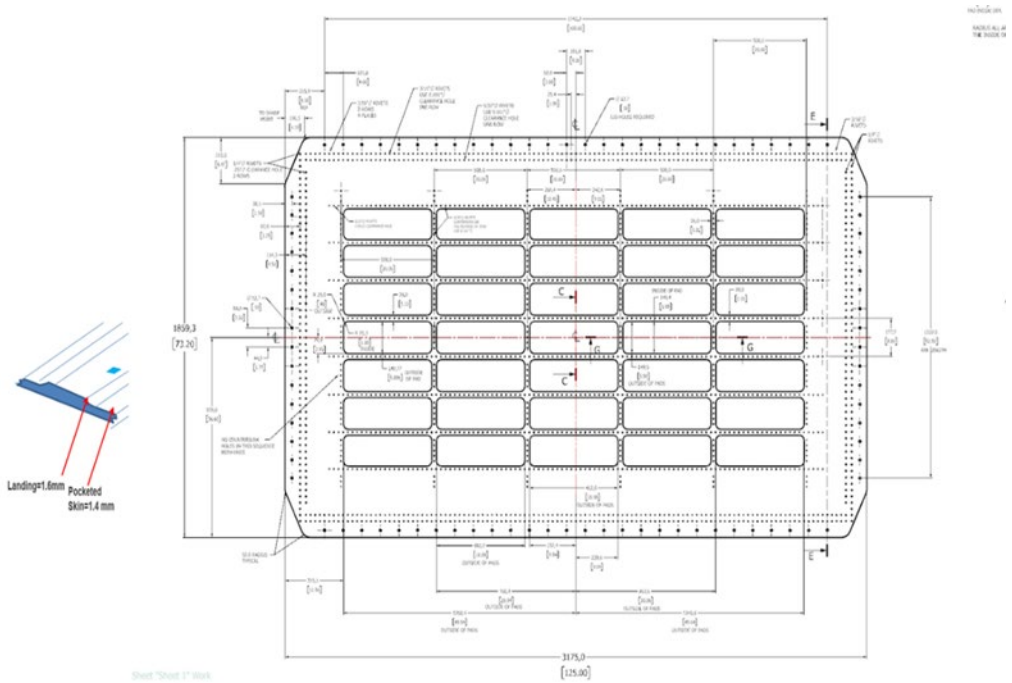

Figure 5. Detail showing skin pocketing between stringers and frames

Panel 1 was built to a tolerance of ±0.005in. (0.13 mm), and after the full-scale testing was completed, the skin thickness in the pocket regions was discovered to be an average of 0.004 in. (0.10 mm) thicker in the pocket region than the as-designed thickness of 0.055 in. (1.4 mm). The original goal for panel testing was to keep the cross-sectional areas and loads the same for the various EMST panels. The Panel 2 skin thickness was measured to be an average of 0.05 in. (1.27mm) or 10% below the as-designed thickness of 0.055 in. (1.4mm). It was realized that these pocket thickness deviations of +7.3% to -10.0% from the as-designed skin pocket thickness of 0.055 in. (1.4 mm) were significant enough to negate the original plan of applying the same loads to the same geometry panels in order to apply the same SIFs to all the EMST panels. As a result, the team needed to develop a new approach to appropriately compare the panels.

It was decided that Panels 2 and 3 would be tested to the same SIFs versus crack length as the as-built Panel 1 by adjusting the FASTER loads. This new approach is consistent with the original plan in keeping the SIFs the same for Panels 1, 2, and 3. Also, since the critical design driver for the location chosen was to meet the repeat inspection interval goal, the team decided that maintaining an equal SIF would help with the post-testing comparison of panel-to-panel results. It is assumed that there are about four flights per day for a typical single-aisle aircraft. Assuming a two-year C-check goal, this results in approximately 3,000 flights between C-checks. We set a goal of 6,000 flights (equivalent to two C-check intervals) as a challenge target for EMST

structural concepts. Using a safety factor of 2 for the repeat inspection, the goal for the repeat inspection to size the panel in the trade study was set at 12,000 flights. Note that the stringers and frames were extruded and maintained tight tolerances for Panels 1–3. Therefore, no stringer or frame corrections were needed in the subsequent FEM modeling used to obtain the new loads needed to develop SIFs for the as-built Panel 1, as well as Panels 2 and 3.

The team developed a simplified trade study/panel sizing methodology to size Panel 1 using the following objectives:

- The panel sizing/loading approach should be rapid and flexible to capture differences in aircraft fuselage sizes, design goals, design principle methods for establishing working stress targets, loading conditions, material/product forms, and geometry of the skin stiffening elements. As discussed later, S/N fatigue, MSD, and MED were not considered in the panel sizing studies.
- Reproducing OEM detail level design panels was not the goal for this program or for this simplified method. The goal was to establish a panel geometry and loading that is representative of the main design drivers (damage tolerance and residual strength) for the single-aisle crown location chosen. As discussed, the original plan was for each panel to be tested to similar stringer/frame/skin geometry and loading conditions. The revised plan (see Section 6) was to test the various EMST panels to the same crack-driving SIFs.
- The method should capture aircraft fuselage panel dimensional differences from front to back and internal variations in stringer, frame, and skin along the fuselage length and between the top, middle, and bottom sections of the fuselage.
- The method should capture the major inertia loading conditions (in this case only vertical loading conditions were considered) to provide a reasonable panel geometry in the crown.
- The method allows for flexibility in the definition of multiple design goals separately for the crown, middle, and fuselage bottom. Currently this sizing takes place only along three lines running from the front of the aircraft to the back. That is, sizing solutions are developed along the top line of the fuselage from front to back, the midline of the fuselage along the length (windows, floors, lap and butt joints, and wing cutout reinforced regions are not modeled), and the fuselage bottom line. In the future, this method can be refined to include additional solutions along lines parallel to the three described above between the crown and belly.

- The method currently captures differences in material modulus separately for the crown, the side panel, and the belly along the fuselage length, but it can easily be adapted to vary along the fuselage. The method captures material properties as they affect the working stress targets required to meet each design goal independently in the crown, side, and belly. Working stress targets are dependent on the location in the fuselage. Damage tolerance sizing targets were determined for the as-designed Panel 1, STA 38 location (38 ft or 11.58 m from the front) and were assumed not to change along the fuselage length for the Panel 1 sizing study. Fuselage geometry changes, such as diameter taper near the empennage, are captured in the cross-sectional moment of inertia calculation.
- Skin working stress targets are defined for each goal as the maximum stress (or stress intensity) in a given direction, which will still meet the specific design goal. These are generated for each design goal. Since stringers and frame/shear ties are related to the skin thickness through the Axx/Bt ratios, design goals based on these can be rewritten into skin working stress targets. The skin working stress target may be a function of the tension, compression, and shear stresses in the other directions, the thickness, the R-ratio, the spectrum, etc., depending on whether the goal is strength-based, fracture mechanics-based, or stability-based. The method may use as many design goals as needed to define the structural requirements of the aircraft. The working stress target for each design goal was calculated separately using design principles available in the literature, or in some cases by testing, and these values were entered into the trade study model.
    - For example, the skin working stresses targets for repeat inspection intervals were developed using K-control testing (both spectrum and constant amplitude). Finite element modeling (FEM) of Panel 1 was used to generate SIF solutions (including bulging) as a function of crack length used to drive the K-control testing.
    - In another example, the skin working stress targets for stiffened, curved fuselage skins were generated using the Alcoa (Arconic) compression optimization code ASPAN-CO (Kulak, et al., 1995) that includes multiple stiffened panel failure modes and multiple solution constraint conditions. These compression/shear skin working stress targets were entered into the panel sizing tool as either a constant or as a table of working stress targets as a function of a solution variable (geometry, solution stress/strain, running loads, etc.).

Key information for the generic aircraft used to size the crown Panel 1 is shown in Figure 6. For the sizing approach, the equations for a pressure loaded stiffened cylinder model (Flugge, 1952) were modified to include variable moduli in the skin, frames, and stringers to estimate pressure stresses. For bending stresses, a simplified cylindrical beam bending model was developed by Kulak (2018) to estimate shear and vertical bending in the fuselage, as shown in Figure 7.

The next section describes in detail the loading approach and the methodology used to set design goals and how these design goals were used to generate working stress targets to size the skin thickness, stringer area, and frame area along the length of the fuselage. As shown in Figure 7, there were three primary sources of fuselage loading considered in this simplified approach: fuselage vertical bending generating axial load intensities, fuselage shear load intensities, and internal pressure differential load intensities in the axial and hoop directions. To be competitive with future graphite/epoxy composite fuselage designs, the cabin pressure differential was increased to 9.9 psi (0.0683 MPa) for this study.

For pressure differential loading (shortened to pressure loading in this report) a modified stiffened cylinder solution (Flugge, 1952) was used to estimate skin, stringer, and frame stresses. Using the original Flugge approach, the equations for skin hoop and axial stress, frame, and stringer stresses were modified using Mathcad (PTC, s.l., & s.n., 2019) to allow an independent modulus of elasticity (E) for the frame, stringer, and skin. Equations for skin stress, stringer stress, and frame stress for a given Nθ hoop load intensity, Nx axial loading intensity (combination of pressure axial component + bending axial load intensity) are provided in Figure 8. In this report, these simplified Flugge solutions in Figure 8 are referred to as the *smeared stress* solutions. In the same paper, Flugge also presents a *discrete frame solution*, which includes variations in hoop stresses between frames. The stresses in the as-designed, 0.055in. (1.4 mm) skin pocket crown panel at 9.9 psi (0.068 MPa) pressure loading using the Flugge smeared stiffness solutions are shown in Figure 9. For this example, the same modulus was used for skin, stiffener, frame. The Nθ (hoop load intensity) and Nx (axial load intensity) components of the pressure stress are decomposed to illustrate the pressure-only solution for an axially unconstrained stiffened cylinder and that of only an axial load on a stiffened cylinder. Note the axial load produces nearly an equal axial stress change in the skin and stiffener for the Flugge smeared stiffness solution. However, for a positive axial load, the solution indicates a small tensile hoop skin stress is produced in the skin balanced by a small compressive stress in the frame. These Flugge smeared stiffness solutions reflect the simplified assumptions used. In the case when axial-only loads are applied, the skin and frame hoop stresses from the Flugge smeared stiffness solution were larger than those observed using the three-dimensional (3D) FEM cylindrical model (Qsymm1).

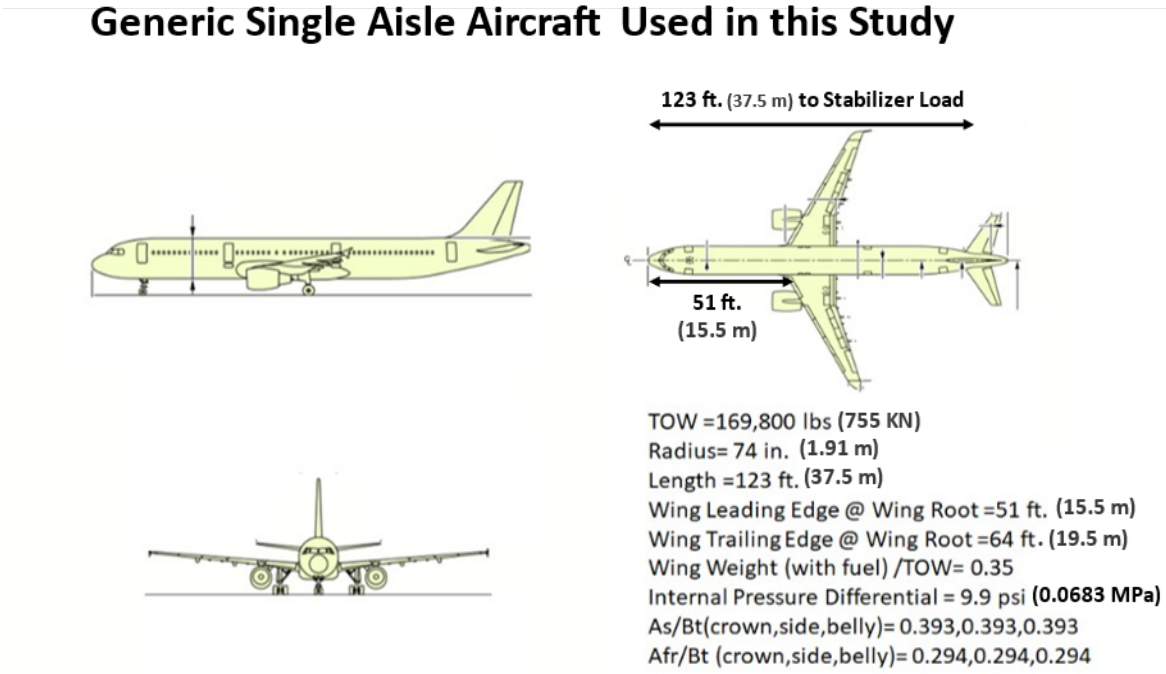

Figure 6. Information used to size Panel 1 for the generic aircraft

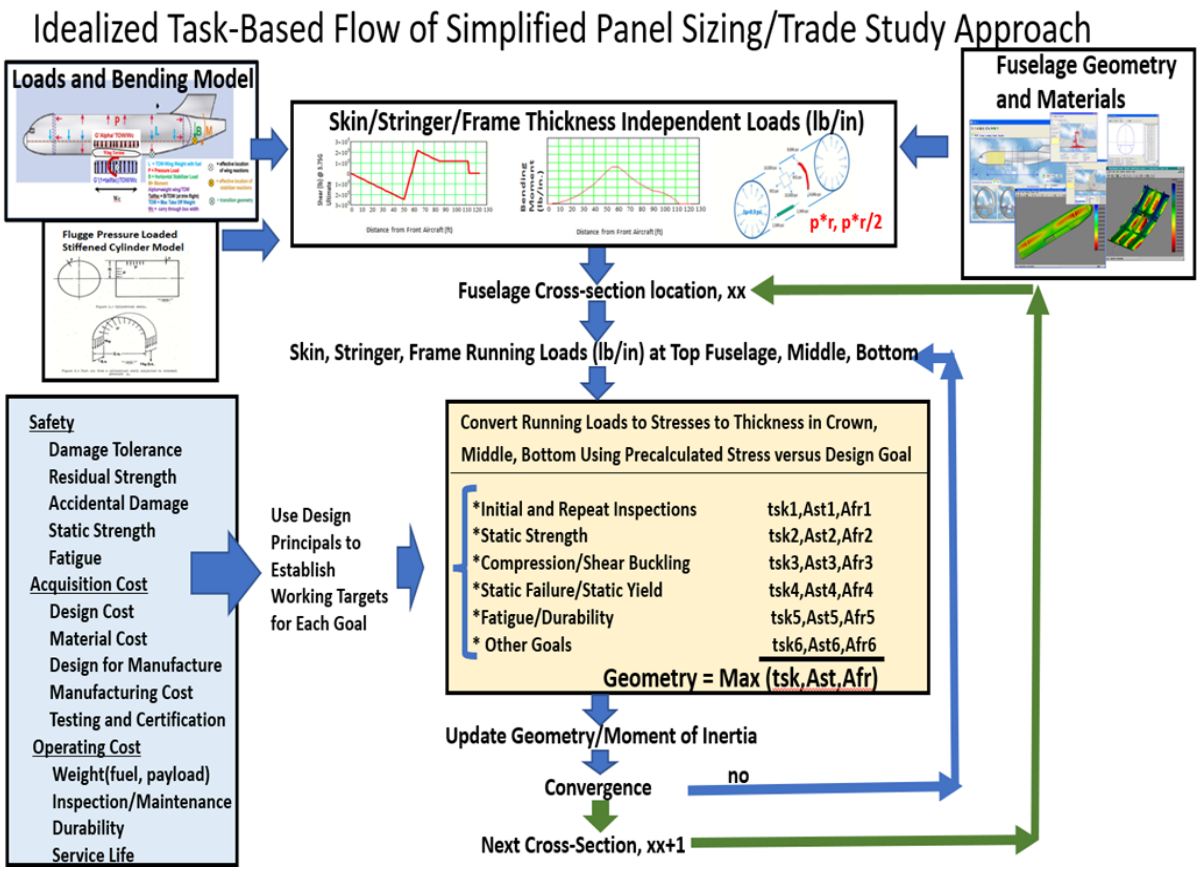

Figure 7. Flow of simplified fuselage sizing/trade study approach

Flugge smeared stiffness calculations for the current as-designed 0.055 in. (1.4 mm) pocketed skin Panel 1 are presented in Table 1 along with results from the fuselage cylindrical beam used in the sizing study for bending for both a 74 in. (1.88 m) fuselage radius and a 78 in. (1.98 m) radius. As expected, the larger 78 in. (1.98 m) radius results in higher axial and hoop stress intensities from pressure. On the other hand, the larger 78 in. (1.98 m) cross-sectional moment of inertia results in a lower bending load intensity for the 78 in. (1.98 m) radius fuselage.

Pressure and Axial Load

Nx = Nx axial + press*radius/2 N0 = press*rad

Skin Hoop Stress

$$\frac{Eskin\cdot(Al\cdot Est\cdot L\cdot N0 + Ar\cdot Eframe\cdot Nx\cdot Sp\cdot new + Eskin\cdot L\cdot N0\cdot Sp\cdot t)}{Eskin^2\cdot L\cdot Sp\cdot t^2 + Al\cdot Ar\cdot Est\cdot Eframe + Al\cdot Est\cdot Eskin\cdot L\cdot t + Ar\cdot Eskin\cdot Eframe\cdot Sp\cdot t - Al\cdot Ar\cdot Est\cdot Eframe\cdot new^2}$$

Skin Axial Stress

$$\frac{Eskin\cdot(Ar\cdot Eframe\cdot Nx\cdot Sp + Al\cdot Est\cdot L\cdot N0\cdot new + Eskin\cdot L\cdot Nx\cdot Sp\cdot t)}{Eskin^2\cdot L\cdot Sp\cdot t^2 + Al\cdot Ar\cdot Est\cdot Eframe + Al\cdot Est\cdot Eskin\cdot L\cdot t + Ar\cdot Eskin\cdot Eframe\cdot Sp\cdot t - Al\cdot Ar\cdot Est\cdot Eframe\cdot new^2}$$

Frame Stress

$$\frac{Est\cdot Sp\cdot\left(Ar\cdot Eframe\cdot Nx - Eskin\cdot L\cdot N0\cdot t\cdot new - Ar\cdot Eframe\cdot Nx\cdot new^2 + Eskin\cdot L\cdot Nx\cdot t\right)}{Eskin^2\cdot L\cdot Sp\cdot t^2 + Al\cdot Ar\cdot Est\cdot Eframe + Al\cdot Est\cdot Eskin\cdot L\cdot t + Ar\cdot Eskin\cdot Eframe\cdot Sp\cdot t - Al\cdot Ar\cdot Est\cdot Eframe\cdot new^2}$$

Stringer Stress

$$\frac{Eframe\cdot L\cdot\left(Al\cdot Est\cdot N0 - Eskin\cdot Nx\cdot Sp\cdot t\cdot new - Al\cdot Est\cdot N0\cdot new^2 + Eskin\cdot N0\cdot Sp\cdot t\right)}{Eskin^2\cdot L\cdot Sp\cdot t^2 + Al\cdot Ar\cdot Est\cdot Eframe + Al\cdot Est\cdot Eskin\cdot L\cdot t + Ar\cdot Eskin\cdot Eframe\cdot Sp\cdot t - Al\cdot Ar\cdot Est\cdot Eframe\cdot new^2}$$

new = Poisson ratio
Ar= frame area (including shear tie)
Al= longeron area
N0= pressure* radius

Nx= bending axial load intensity +pressure* radius/2
L=frame spacing
Sp= stringer spacing
t=skin thick averaged pocket with landing

Figure 8. Smeared stiffened cylinder solutions with a variable skin, stiffener, and frame elastic modulus

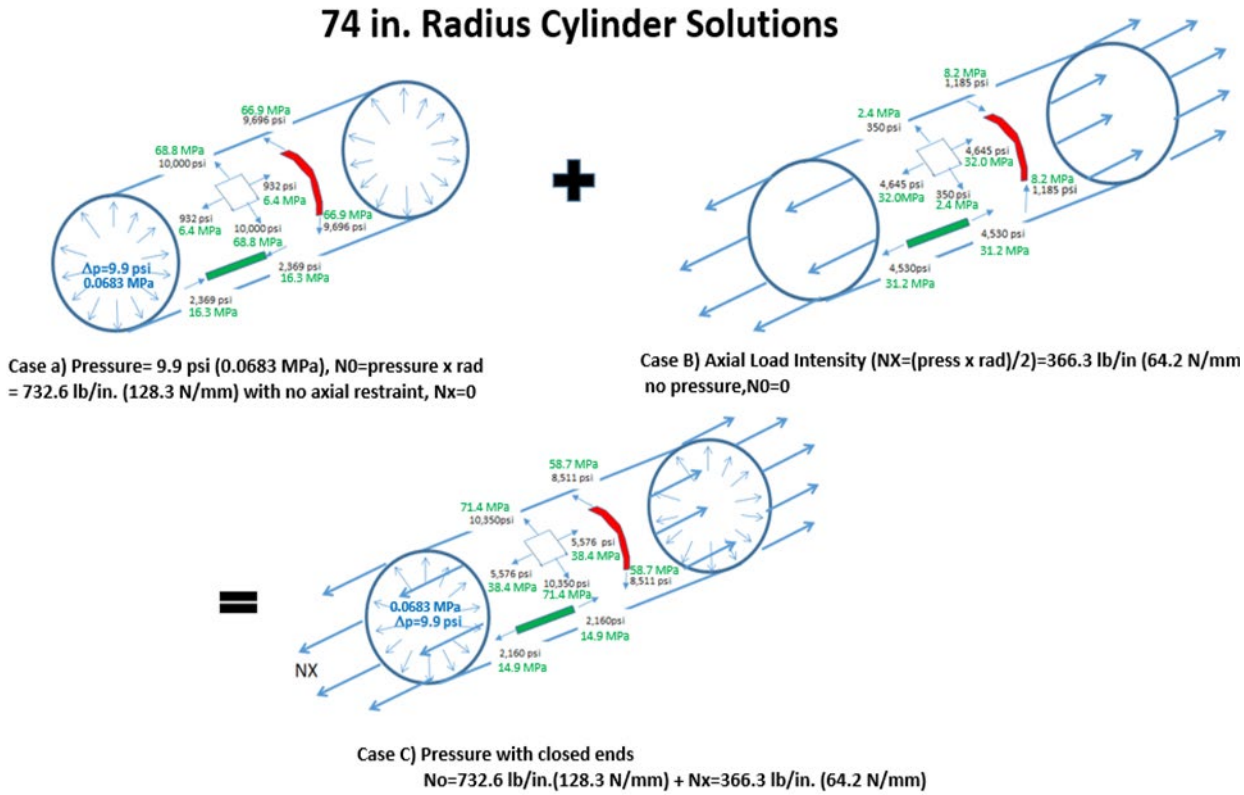

Figure 9. Pressure loading decomposed into hoop effect and axial load effect

Table 1. Stresses for a 74in. (1.88 m) fuselage radius and a 78 in. (1.98 m) radius

English Units								
	74" radius 9.9 psi pressure	**78" radius 9.9 psi pressure**	**74" radius, 1G+ 9.9 psi pressure**	**74" radius ΔStress Bending**	**78" radius. 1G+ 9.9 psi pressure**	**78" radius ΔStress Bending**	**74" radius, 2.5G +9.9 psi pressure**	**78" radius 2.5G +9.9 psi pressure**
No, press (lb/in.)	733	772	733		772		733	722
Nx, press (lb/in.)	366	386	366		386		366	386
Nx, bend (lb/in.)	0	0	562		541		1,406	1,340
No/to (psi)	9927	10,463	9,927		10,463		9,927	10,463
Nx, press/tx (psi)	4,613	4,861	4,613		4,861		4,613	4,861
Nx, bend/ tx (psi)	0	0	7,082		6,817		17,708	16,877
skin hoops stress (psi)	10,350	10,991	10,866	536	11,426	435	11,687	12,197
skin axial stress (psi)	5,576	5,907	12,706	7,130	12,742	6,835	23,401	23,037
stringer stress (psi)	2,160	2,277	9,114	6,954	8,971	6,694	19,544	19,012
frame stress (psi)	8,511	8,971	6,693	-1,818	7,221	-1,750	3,956	4,595

SI Units								
	1.88 m radius 9.9 psi pressure	**1.98 m radius 9.9 psi pressure**	**1.88 m radius, 1G + 9.9 psi pressure**	**1.88m radius ΔStress Bending**	**1.98 m radius, 1G +9.9 psi pressure**	**1.98 m radius ΔStress Bending**	**1.88 m radius, 2.5G +9.9 psi pressure**	**1.98 m radius, 2.5G +9.9 psi pressure**
No, press(N/mm)	128	135	128		135		128	135
Nx, press(N/mm)	64	68	64		68		64	68
Nx, bend (N/mm)	0	0	98		95		246	235
No//to (MPa)	68	72	68		72		68	72
Nx, press/tx (MPa)	32	34	32		34		32	34
Nx, bend/ tx(MPA)	0	0	49		47		122	116
skin hoop stress (MPa)	71	76	75	3.7	79	3.0	81	84
Skin axial stress (MPa)	38	41	88	49	88	47	161	159
stringer stress (MPa)	15	16	63	48	62	46	135	131
frame stress (MPa)	59	62	46	-13	50	-12	27	32

The modified smeared stiffness Flugge solution and the discrete frame Flugge solution for the as-designed Panel 1 (0.055 in. (1.4 mm) pocketed skin, 74 in. (1.88 m) radius fuselage) loaded to 9.9 psi (0.0683 MPa) pressure shows good agreement with both the ABAQUS Panel 1 Qsymm1 FE model (multiple bay, constant spaced frame and stringer cylindrical model loaded by internal pressure plus the axial component of pressure loads) and the ABAQUS Panel 1 FE model shown in Figure 10a. Figure 10b shows the axial stress variation in the longitudinal direction (for 1.04G+pressure). Figure 10 results are for the undamaged (no crack) case.

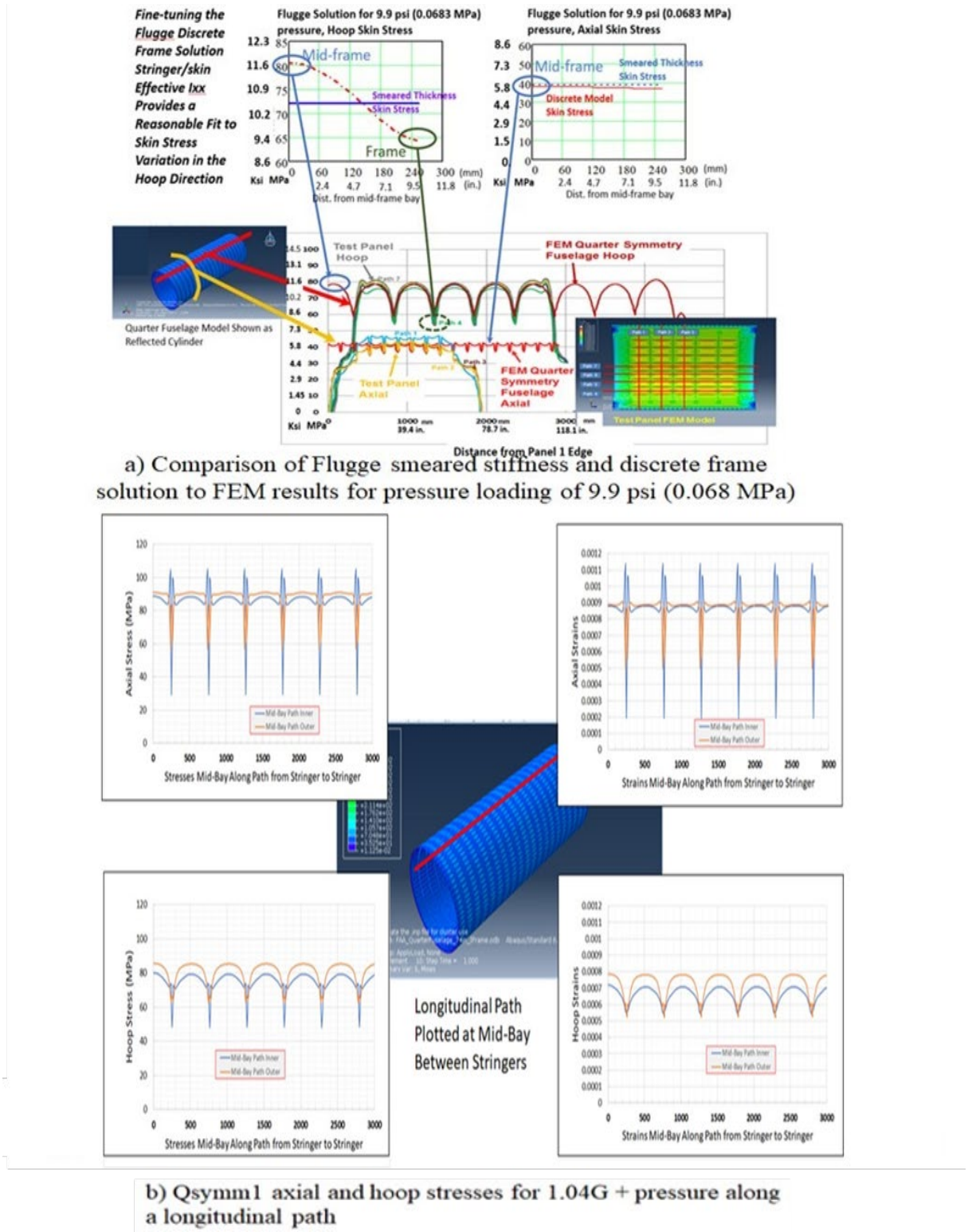

Figure 10. Comparison of Flugge smeared stiffness and discrete frame solution to FEM results for pressure loading of 9.9 psi (0.068 MPa)

As shown in Figure 10a, for a given axial load intensity (in this case zero from bending, plus axial component of the pressure, $\frac{pressure \times radius}{2}$, load intensity) and pressure hoop load intensity, the FE stress results show the fuselage skin axial and hoop stress varies along the center of the bay (a bay defined by one stiffening element to the adjacent stiffening element). This is especially true for the hoop stress which varies in a sinusoidal fashion due to pillowing. However, for a given pressure and axial load (due to bending) it is convenient to label the varying undamaged fuselage skin stresses results by a point stress (axial, hoop, shear). For example, longitudinal crack growth testing of flat skin coupons driven by hoop loads would be influenced by the undamaged sinusoidal hoop stress distribution shown in Figure 10. As another example, the spectrum used in this report is defined by a single mean flight stress and the flight excursion stress (+/- 0.8 G stress), although there is some dependency of axial stress at the mid bay from stringer to stringer, as shown in Figure 10. The Flugge stress is used in this paper when referring to a single fuselage skin characteristic stress with the following clarifications:

1. It is recognized that the FE fuselage model using solid elements for skins and stiffening elements captures 3D structural effects that the simplified Flugge model does not. It is assumed that if the Flugge model were able to capture these effects that the results would show that the *characteristic hoop stress* along the mid bay line is very close to the average hoop stress (i.e. the area under the sinusoidal stress curve divided by the length) and the Flugge *characteristic axial stress* can be similarly considered as the average of the axial stresses.

2. The Flugge characteristic hoop stress occurs at approximately 25% of the distance from the frame rivet midway between stringers (note this is more like 28% in Figure 10, but it is assumed that the main difference is due to the 3D FE solution as opposed to the Flugge solution). This distance is considered the *characteristic Flugge location*.

3. For axial stress variation, it appears that the same 25% distance from the stiffening element for the characteristic hoop stress is a reasonable assumption, as shown in Figure 10a for the variation in axial stress in the circumferential direction and Figure 10b for the variation in axial stress in the longitudinal direction.

4. The use of the Flugge stress for static purposes (comparing Flugge stresses to working target stresses for different design goals) or for fracture mechanics (for crack growth life or residual strength) implies the use of the same distribution of axial and hoop stresses that exist in the FE model (Qsymm) of the fuselage when the characteristic Flugge axial and hoop stresses are the same as the FE model results at the *Flugge characteristic*

location (25% of the distance from the stiffening element). In this case, the Flugge model and FE models must represent the same geometry, materials, and loading conditions.

5. As an example, consider the K-control testing used to determine the *equivalent constant amplitude axial stress*, which matches the spectrum K-control circumferential crack life results. For this testing, a vector of SIF versus crack length is generated using the Qsymm FE models, which includes the stress variations across the bay defined by the stiffening elements. The contributions from the axial component of pressure and axial components due to bending can be separated from these FE elastic analyses for superposition. We associate this vector of FE SIF results to a single *Flugge characteristic axial stress* as defined in point 4 above to be the axial stresses in the FE model at the 25% distance from stringer to stringer at the crown.
    - In this example, for a fixed radius and fixed pressure, the axial component of the pressure load intensity defined as pressure x radius /2 is constant.
    - Therefore, any change the characteristic axial stress in the constant amplitude K-control testing needed to match the spectrum life is interpreted as a change in cross-sectional area, which does not change the axial component of load intensity due to pressure, which is constant, but does change the axial load intensity due to fuselage down-bending (change in moment of inertia).
    - Thus, the Flugge characteristic axial stress of 13 ksi (89.6 MPa) is reported as the Flugge stress at 1.04 G + pressure where the axial stress component of pressure is constant, and the bending component has increases by 0.04 times the 1G bending stress.

It should be noted that for the results in Figure 10, the Flugge discrete frame solution (Flugge, 1952) requires the user to enter a factor, δ, which represents an effective width of skin used with the stringer to determine the bending stiffness (in the axial direction) of the curved stringer/skin detail in response to a local bending moment load intensity per unit circumferential length. This factor had been previously fit (Kulak, 2015) using FEM models for a different-but-similar single-aisle construction and used in Figure 10.

Elements of a simplified fuselage bending model used in this study are shown in Figure 11. The model considers aircraft weight plus cargo and passenger loads and flight maneuver vertical acceleration factors. For ultimate and limit-bending conditions, the simplified fuselage bending model uses the maximum takeoff weight (MTOW) and assumes these loads are uniformly distributed. These loads were used to determine the skin working *mean flight stress* (Mfs)

(defined as 1G bending stress + pressure stresses for this program) that meets the circumferential crack repeat inspection goal (12,000 flights with a safety factor of 2) used in this study. For the repeat inspection, a goal of two C-Check intervals, or 4 years, was chosen for the EMST panels, assuming a usage of 4 flights per day. This amounts to about 6,000 flights (rounded) and considering a safety factor of two, a final goal of 12,000 flights was set for the repeat inspection.

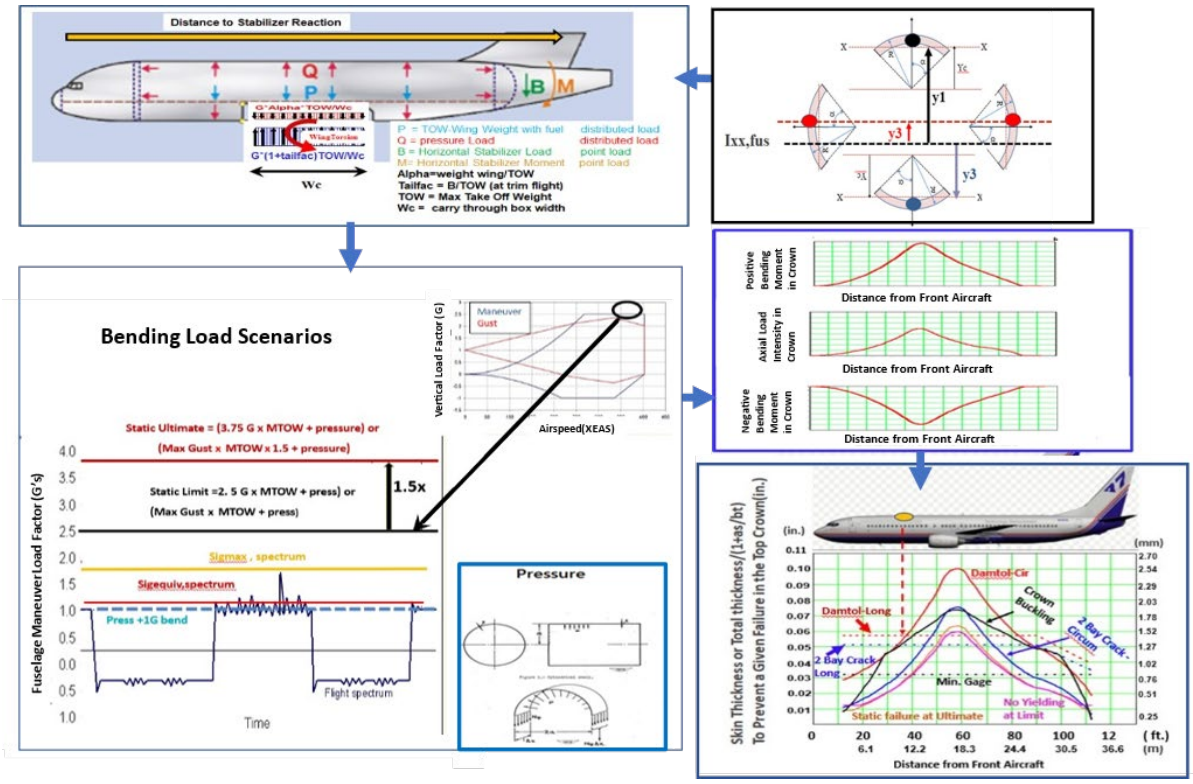

Figure 11. Elements of the fuselage bending model used in the sizing approach

Results for bending moments, shear, shear intensity, and axial load intensity for various maneuver conditions for the single aisle aircraft defined in Figure 6 are shown in Figure 12. The bending moment, M, at the stabilizer (see upper left plot in Figure 11) was set as zero, assuming an effective vertical tail balancing load of 18% of the wing load captured both moment and vertical load effects in the fuselage crown area of interest forward of the wing.

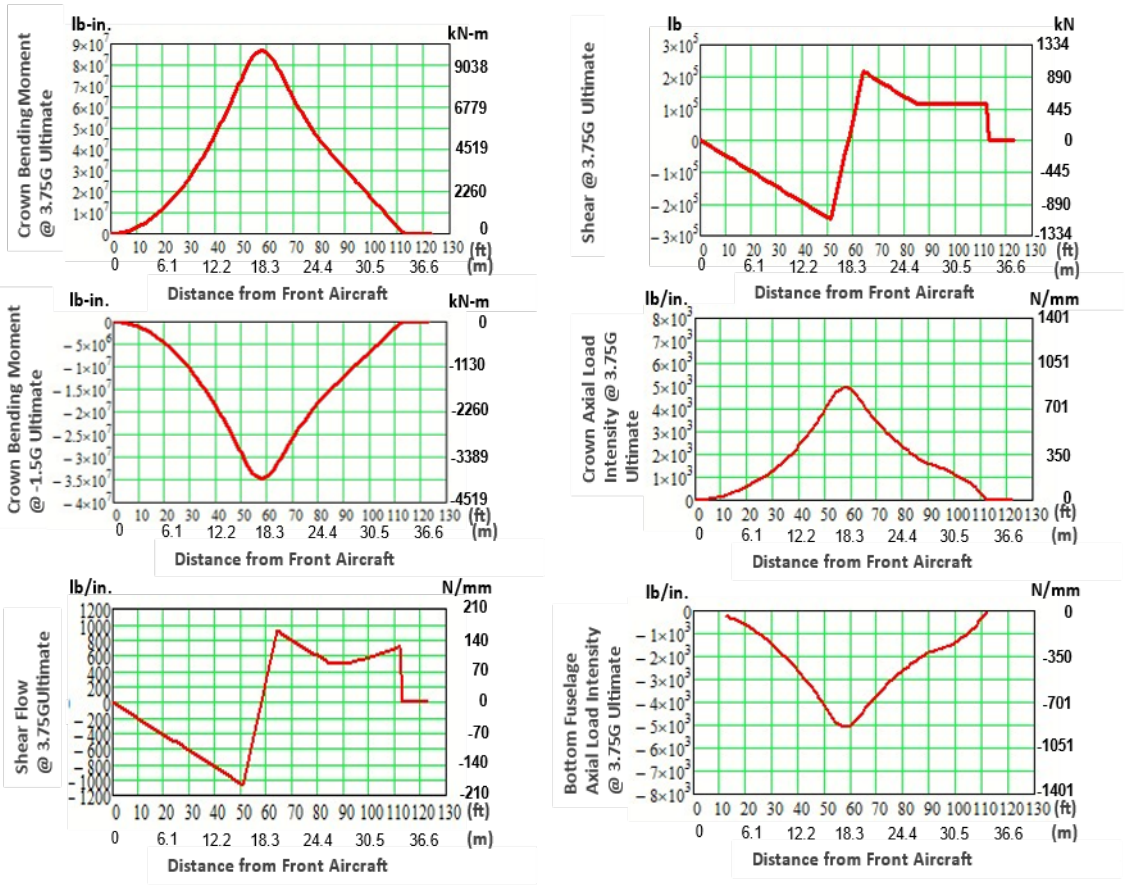

Figure 12. Load intensity results from the generic aircraft bending model

Currently the Mathcad-based panel sizing model (PTC, 2019) is set up to use two iterative loops to size the fuselage stiffened shell. In Loop 1, a constant cylindrical cross-section is used (detail to follow) to calculate the bending load intensities. Starting from the fuselage front, this calculation is repeated in 1 ft. (0.31 m) increments, because the bending moment and pressure load intensities change along the fuselage length. This Loop 1 solution for load intensities around the fuselage cross-section is used to calculate the skin thickness and stringer and frame/shear tie load intensities change along the fuselage length and meet all design goals. This information is then used to calculate the new moment of inertia at each cross-section for Loop 2 using the model shown in Figure 13. Then using the loads and design goals new skin thicknesses are established (one effective skin thickness for the crown, one effective skin thickness for the side panel, and one for the belly) which vary along the fuselage cross-section and length. These thicknesses were calculated at 1 ft. (0.305 m) increments along the fuselage length to satisfy all the multiple set of goals in the crown, side, and belly panels. Given these new skin thickness

solutions from Loop 2, the stringer cross-section area (As) and frame cross-section area (Afr) along the fuselage length were calculated using the input As/Bts and Afr/Btf ratios where Bts is the average area of skin in the stringer bay direction and Btf is the average area of skin over the frame bay direction.

Ideally, many looping increments would be used, but time did not permit the coding of additional loops into the sizing module. As shown later in the following subsection, the use of two loops provided a reasonable solution for our purpose of "apples-to-apples" studies.

For the sizing model, a simplifying assumption was made regarding the relationship between the axial stresses due to bending in the fuselage and the axial loads in Panel 1. Due to curvature, the axial stress in the fuselage curved crown at the Panel 1 location at STA 38 varies along the leading and trailing edge of Panel 1 in proportion to the vertical distance from the neutral bending axis of the fuselage cross-section. Also, the bending moment changes between the Panel 1 leading and trailing edges, so the axial stress intensity varies from leading to trailing edges as well. To simplify this axial loading due to bending, it was assumed the axial load intensity was constant along the Panel 1 circular leading and trailing edges. Also, it was assumed this constant axial load intensity did not vary between Panel 1 leading and trailing edges. The Panel 1 midpoint axial load intensity solution from the simplified fuselage bending model (mid-point at top of crown) was used as the representative axial load intensity for bending for Panel 1. This axial load intensity was applied as a constant load intensity at the leading and trailing edges of Panel 1. This axial load intensity due to bending when applied to the Panel 1 FE models results in the same stress distribution in all interior bays similarly to the axial component of pressure.

This set of assumptions for axial load intensity allowed the superposition of load intensity from bending with the axial load intensity from pressure. Superposition can also be used for the hoop load intensities with the axial load intensities assuming these load intensities are consistently developed using either exclusively FEM results or exclusively Flugge solution results (recall that the axial to hoop coupling effects are slightly different comparing the 3D FE solutions to the Flugge solutions).

2.2 Detailed description of Panel 1 sizing approach

The fuselage is divided along the length into 1 ft wide (0.305 m) sections represented by the cross-section at the middle of the section. A set of calculations is done for each cross-section independent of the other cross-sections. This approach assumes plane sections remain plane in the simple cylindrical beam model and the bending moment is statically determinate, so it does not change with skin, stringer, or frame geometry changes. The pressure stresses are assumed to

be only dependent on the cross-sectional area at the specific location. It is recognized smaller divisions of cross-section spacing may produce a more refined solution. At each cross-section, the fuselage is divided into three distinct working areas: crown section, side sections, and a belly section, as shown in Figure 13. The focus of this study is the crown section of the aircraft. Since the moment of inertia influences the crown solution, an attempt was made to develop a solution for the side panels and the belly. The floor structural contribution to the bending stiffness was not considered. The skin, frame, and stringer sizing assumed no widow cutouts/reinforcement and therefore the side panel sizing results are considered a lower bound of material usage.

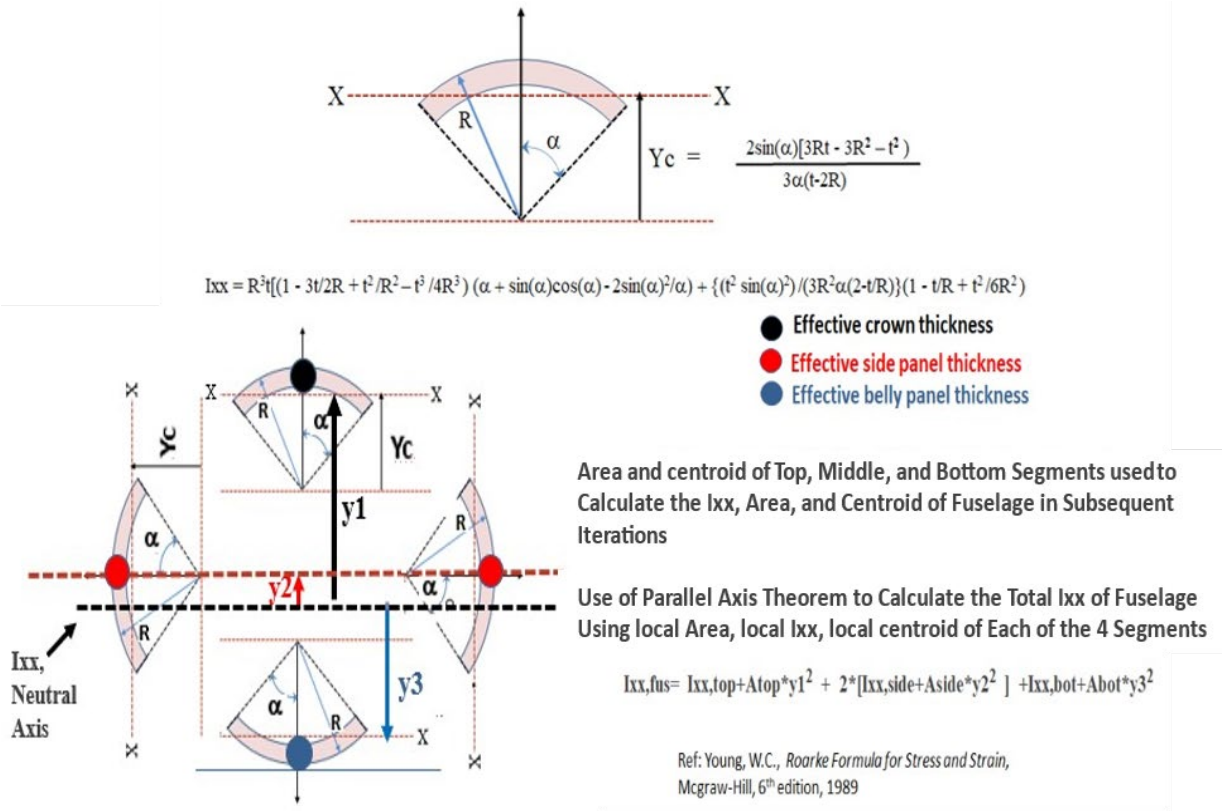

Figure 13. Moment of inertia of fuselage cross-section with smeared stringers

The following approach is used:

- For each of the 3 fuselage sections (crown, or side panel, or belly) an As/Bt and Afr/Bt ratio is entered for that section (ratio of the area of the stringer or frame to the area of the skin). In the current Panel 1 sizing model these three input As/Bt and three Afr/Bt ratios were constant along the fuselage length since we were interested in the Panel 1 location. However, in the future this approach can be modified to have As/Bt and Afr/Bt vary along the length along the fuselage.

- The sizing process involves a sequence of looping steps. The objective at the end of Loop 1 is to construct an approximate sizing for the skin, stringer, and frame for use in Loop 2. In Loop 1, a simplifying assumption is made that the entire fuselage cross-section has the same smeared skin/stringer thickness.
    - This smeared thickness cross-section changes along the fuselage length depending on the bending moment and pressure.
    - In this case, the thin ring solution shown in Figure 14 was used for the Loop 1 calculation of the bending moment of inertia and bending load intensities. This assumed that the fuselage radius is much larger than the depth of the stringer or frame and these stiffening elements can be smeared in the skin.
    - The axial pressure load intensity was calculated using the closed cylinder solution ($press \times radius$).

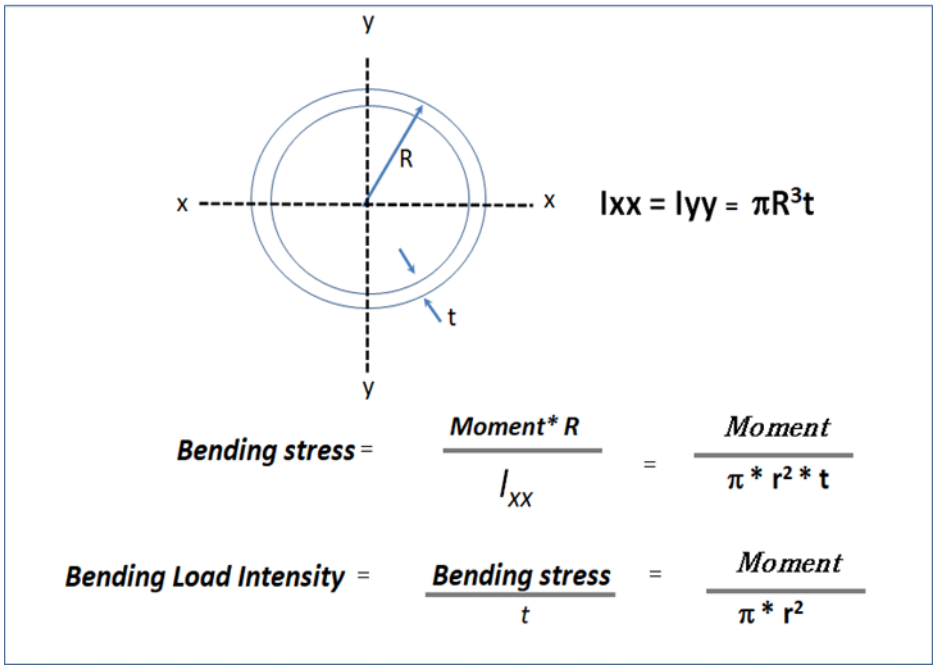

Figure 14. Bending stresses and stress intensity at top and bottom of the fuselage in Loop 1

- The bending model for the fuselage shown Figure 11 was used to calculate the bending moment, Mf, and the cross-sectional shear force, Vf, along the length of the fuselage.
    - The bending moment and shear distributions for a cylindrical beam are converted into an axial load intensity distribution along the top crown line, a shear load intensity distribution in the midsection, and an axial load intensity distribution on the bottom of the belly section.

- Given these quantities, the skin thickness which meets all the design goals can be determined along a line running front to back along the crown, a line front to back along the side of the fuselage, and a line along the bottom.
- Stringer and frame shear tie areas along those three lines can be calculated from the input As/Bts.

- In Loop 2, the moment of inertia model shown in Figure 13 was used with the resulting Loop 1 results for the three lines representing the top, mid, and bottom sections.
  - Using the new moments of inertia at each section, bending moments, shear loads, and new load intensities are calculated for Loop 2.
  - Since the change in the cross-sectional moment of inertia in Loop 2 reflects an integrated effect of the different changes in skin/stringer/frame/shear tie thickness in the top, mid, and bottom sections, the change in the cross-sectional moment of inertia for Loop 2 was small as shown in Figure 15 for the Panel 1 location. Therefore, no additional loop steps were added to the sizing model for this study.
- Once the loading intensities are determined in any Loop step, the crown, side panel, and belly sections are sized for each individual design goal in that section.
  - At each fuselage station the goal is to find the skin thickness that meets all the design goals defined by the user.
  - Even though the skin thickness is used as the key variable, the skin thickness is coupled to stringer and frame stresses through the input As/Bt and Afr/Bt ratios. As such, any working stress target goals for stringer or frame could be defined in terms of skin thickness needed to achieve that working stress goal. Therefore, the working stress targets could be defined in terms of skin, stringer, or frame goals or some combination of these.
  - Using the load intensity plus a trial thickness for the skin, the skin, frame/shear tie, or stringer stresses can be determined and compared to the input working stress target for each design goal being evaluated (this working stress target is determined prior to conducting this sizing study and described later in this section). This trial thickness is adjusted until that design goal is met. This process is repeated for each design goal.

- The *critical design driver* is identified as the goal which requires the maximum skin thickness. The difference between this design goal skin thickness and the next critical design goal skin thickness represents a type of *margin of safety* between these design goals.

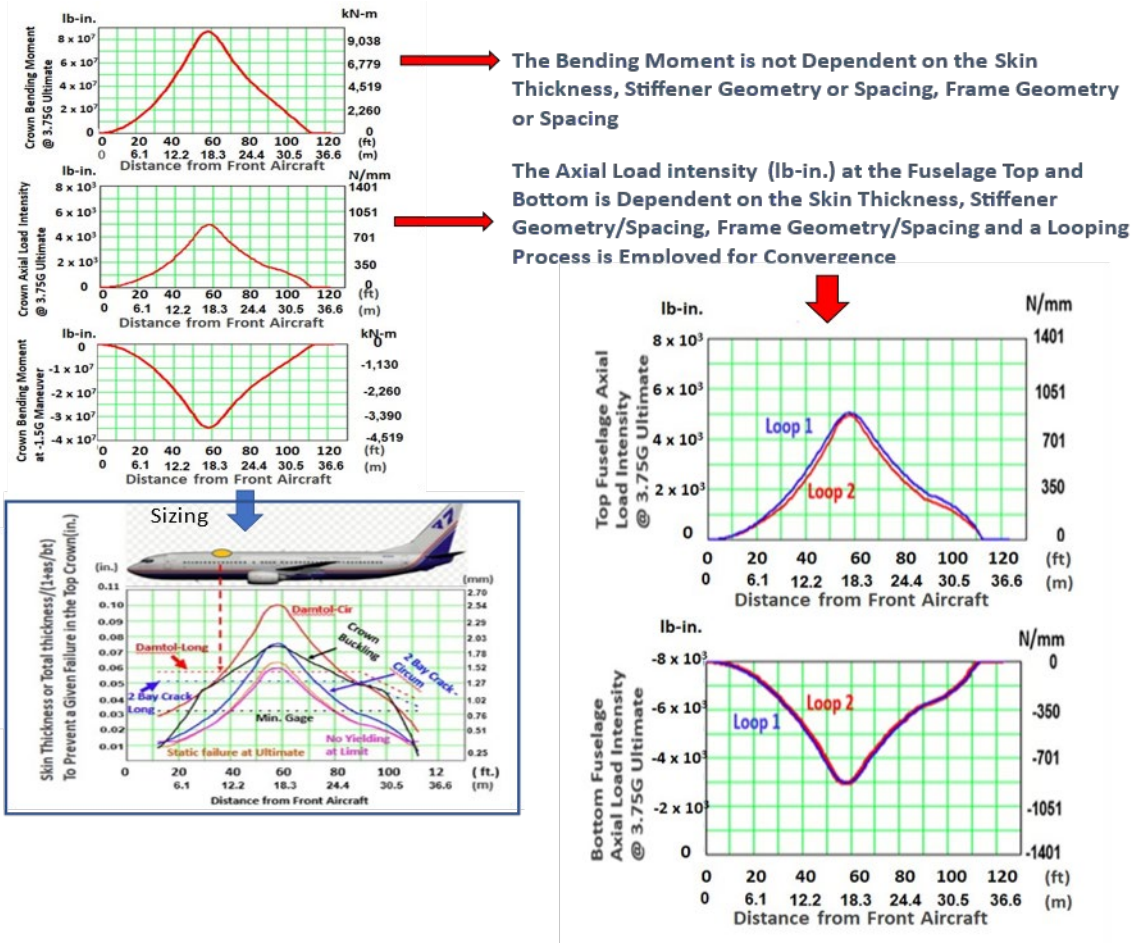

Figure 15. Axial load intensity comparison between Loop 1 and Loop 2

Design goals used in this study to size Panel 1 are shown in Figure 16, Figure 17, and Figure 18.

Each design goal is usually, but not necessarily, related to a stress representing a flight maneuver and/or internal cabin pressure.

As an example, for static strength, loaded by axial bending and the axial component of pressure, the working stress target was defined to prevent panel failure in tension at ultimate load (stresses at 3.75G maneuver acceleration + pressure).

As another example, a working stress was developed to meet the crown damage tolerance repeat inspection goal in the circumferential direction. For this goal, an "equivalent" constant amplitude skin target stress at 1G bending + pressure loading was determined experimentally by equating the life of the spectrum loaded K-control M(T) specimen to the life of an M(T) specimen-loaded under constant amplitude K-control (as described later in this report).

As another example, for the side panels, the initial shear/compression buckling depends on the shear stress.

As a final example, the bottom of the fuselage the buckling was dependent on the axial load intensity (shear was not considered in the bottom section). The working target stresses for panel-level shear and compression load intensities which met the design goals were developed using the ASPAN-CO compression optimization tool (Kulak, et al., 1995). The stability-related working target stresses were inputted into the sizing module as a table of stress targets versus axial load intensity and stiffener spacing.

Some design goals include other parameters. For example, the skin minimum gage cutoff uses skin thickness as the parameter.

As can be seen from these examples, the goals definitions are flexible as long as they can be related to the variables used in the sizing module. The goals considered for this study and the methodology to establish working stress targets are discussed in more detail later in this section.

At the end of Loop 2, the skin thickness required to meet every goal in the crown was determined, and the same for the side panels and the belly. Upon finishing this loop, the skin thickness required to meet separate design goals was plotted along the crown, the bottom section, and the side section (Figure 16, Figure 17, and Figure 18). These plots display a visual mapping of the skin thickness required to meet each design goal. The plots show the margins of safety over the other design goals at each cross-section of the fuselage.

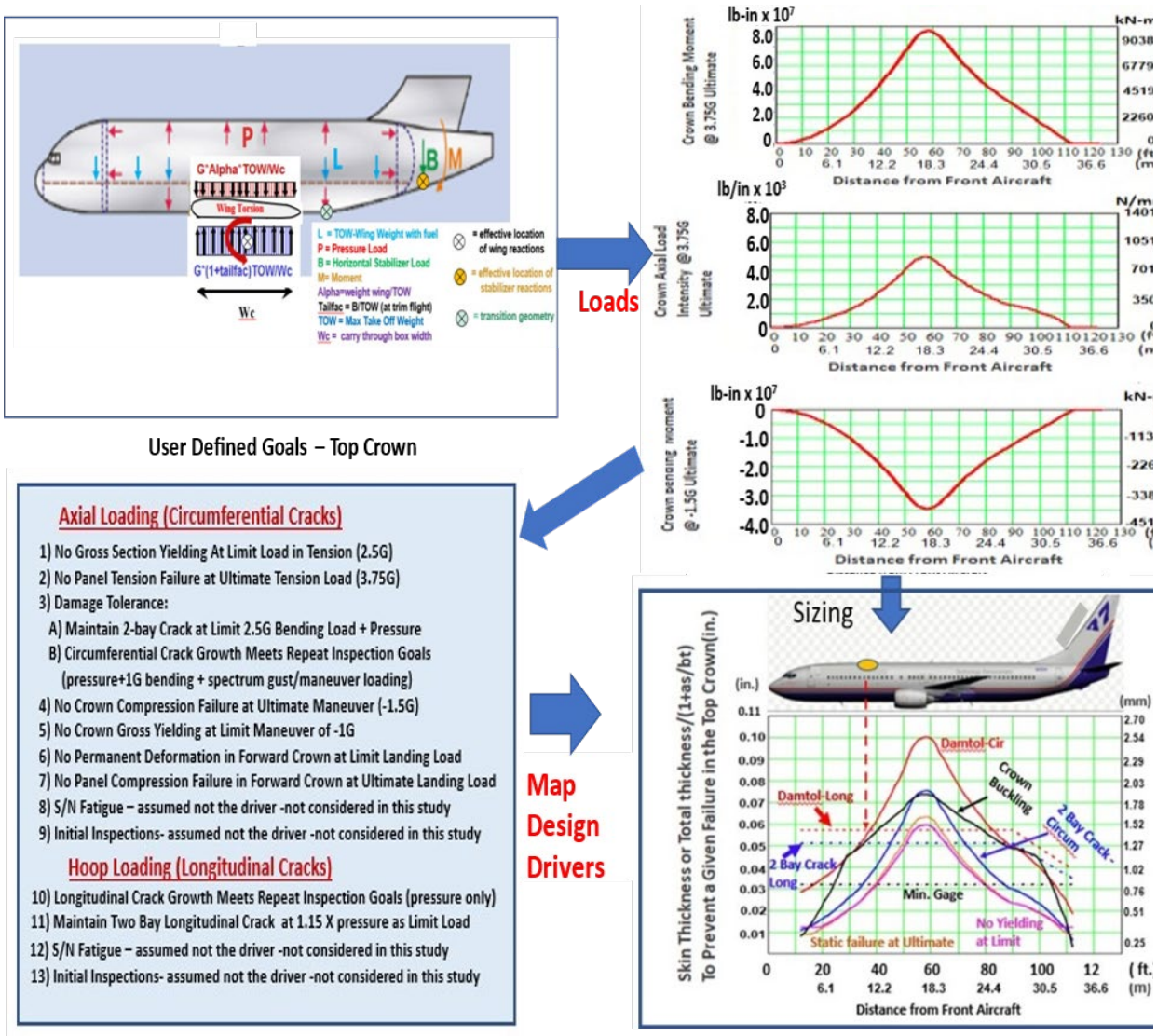

Figure 16. Goals for crown section used in this study

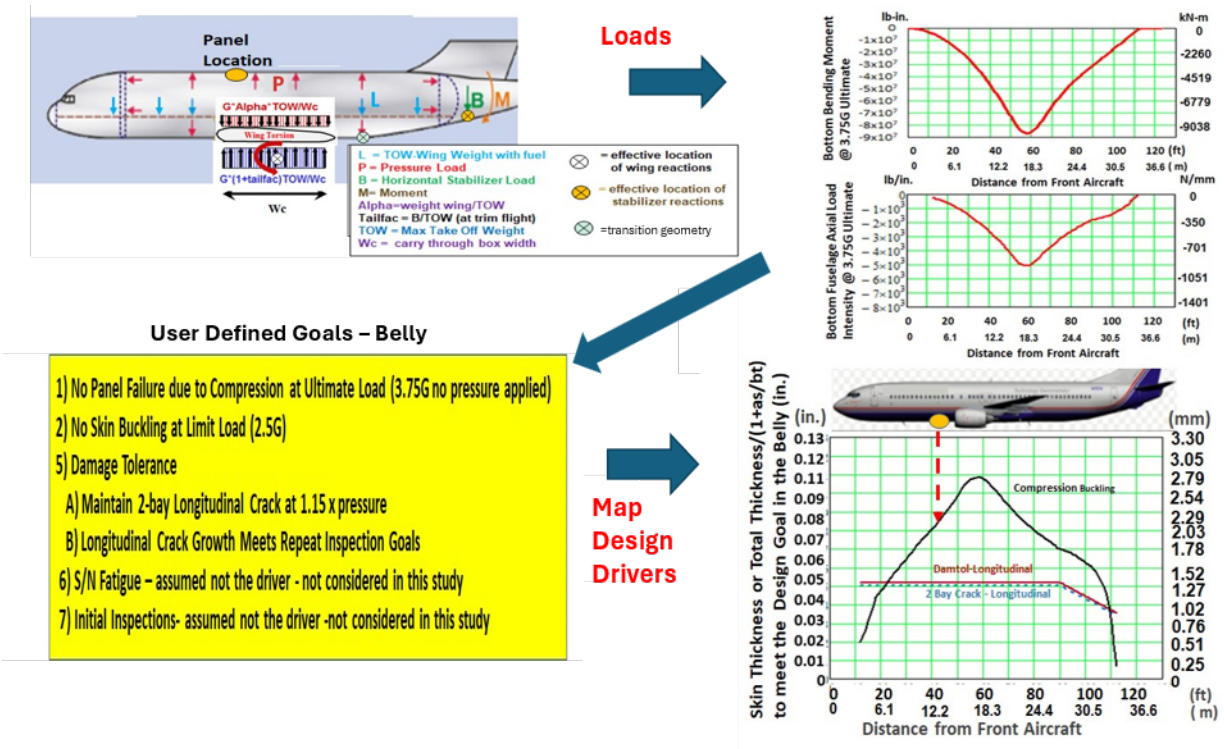

Figure 17. Potential goals to consider for bottom section of the fuselage

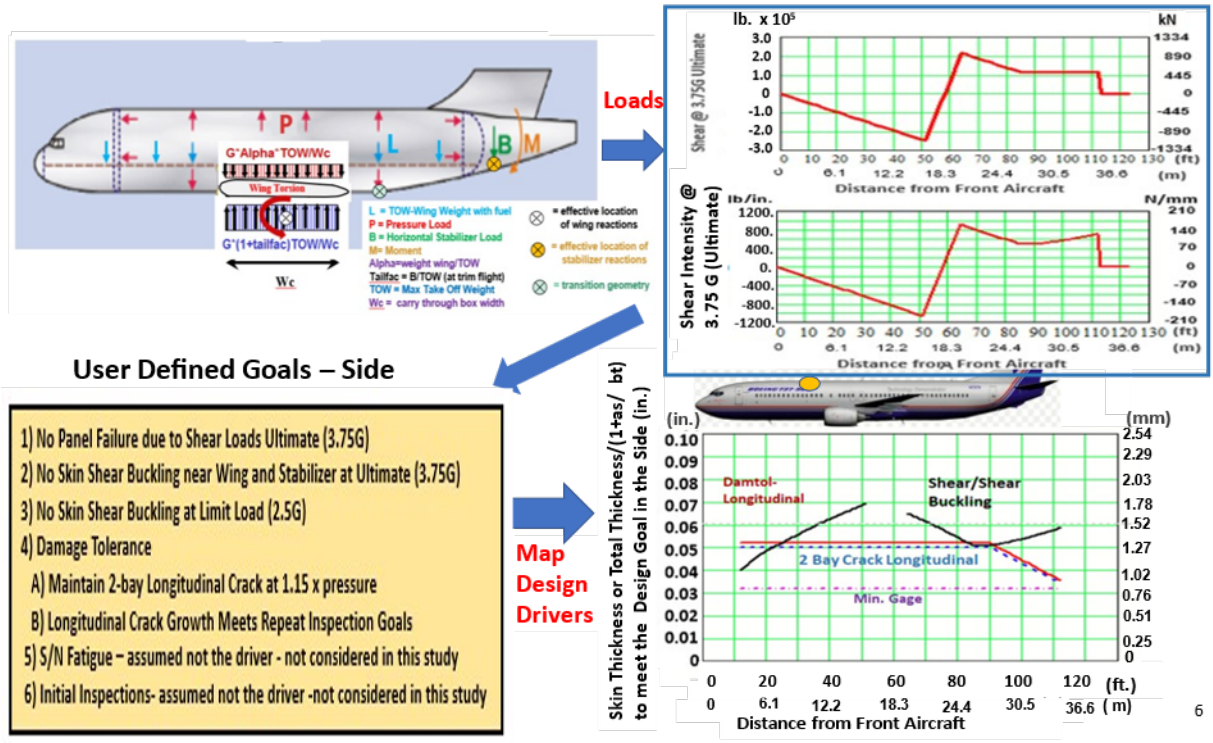

Figure 18. Potential goals to consider for side sections of the fuselage

2.2.1 Crown static strength design goals—bending and pressure loading

The design goals used in the crown to size Panel 1 are summarized in Figure 19, and the approaches to develop working stress targets for each goal are described in this section.

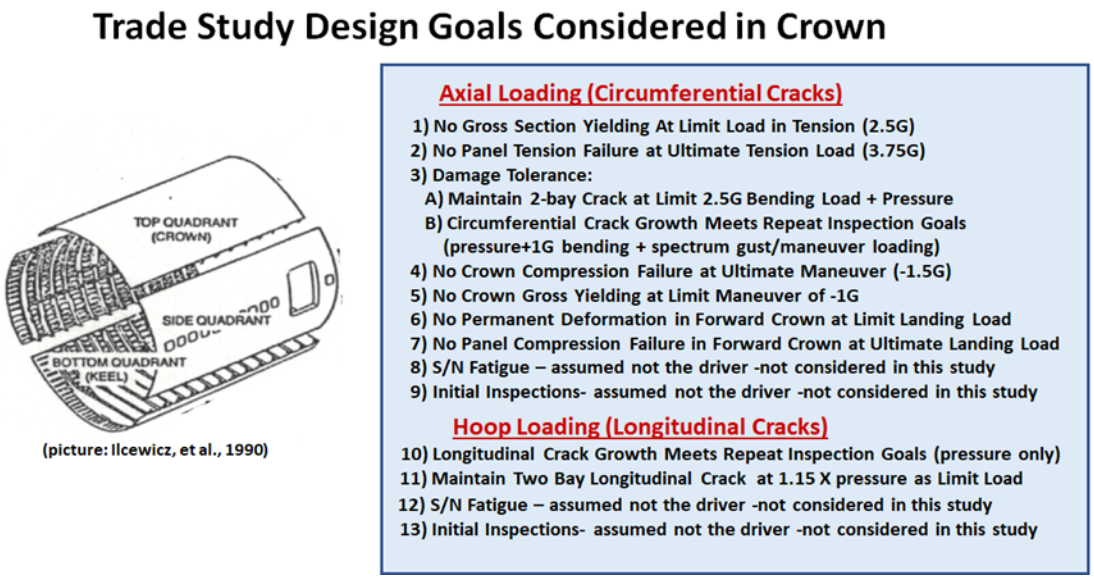

Figure 19. Design goals in the crown section

2.2.1.1 Working stress targets for no gross panel yielding at limit load in tension

One goal for the crown section in Panel 1 was to prevent axial gross yielding at the limit 2.5G plus pressure loading condition. That is, no yielding was permitted at the limit load away from stress concentrations such as fastener holes and cutout corners. The working stress target was established using a volume fraction average of the yield strength of the skin and stiffener. B-basis yield strength values were used from MMPDS (MMPDS, 2015) and supplemental testing data.

2.2.1.2 Working stress targets for no panel failure at ultimate tension load

The static tension strength axial working stress target in this study was evaluated at 3.75G plus 9.9 psi (0.068 MPa) pressure using a strain to failure cutoff proposed by Mohaghegh (Mohaghegh, 1985) as a result of the strain concentration at the fastener holes (Figure 20). In this paper, the strain to failure was measured by testing specially designed representative stringer/skin fastened tensile specimens representing a volume fraction distribution of skin and stringer materials. MMPDS B-basis yield and ultimate values were used to construct hypothetical “B” basis stress strain curves and the skin and stringer (or frame) stresses at the strain-to-failure from the coupon testing program were averaged by volume fraction (Figure 20). This volume fraction averaged skin and stiffener stress at the failure strain was converted to gross panel stress and used as the working stress target for the axial direction static strength at

ultimate load. Ideally, tensile strain-to-failures tests should be run over the range of thicknesses to determine if there is a significant thickness effect. In the absence of test data, a gross area strain at failure of 2.5 % strain was used in this study for Panel 1. This strain was based on engineering judgement considering the previously published test data by Mohaghegh.

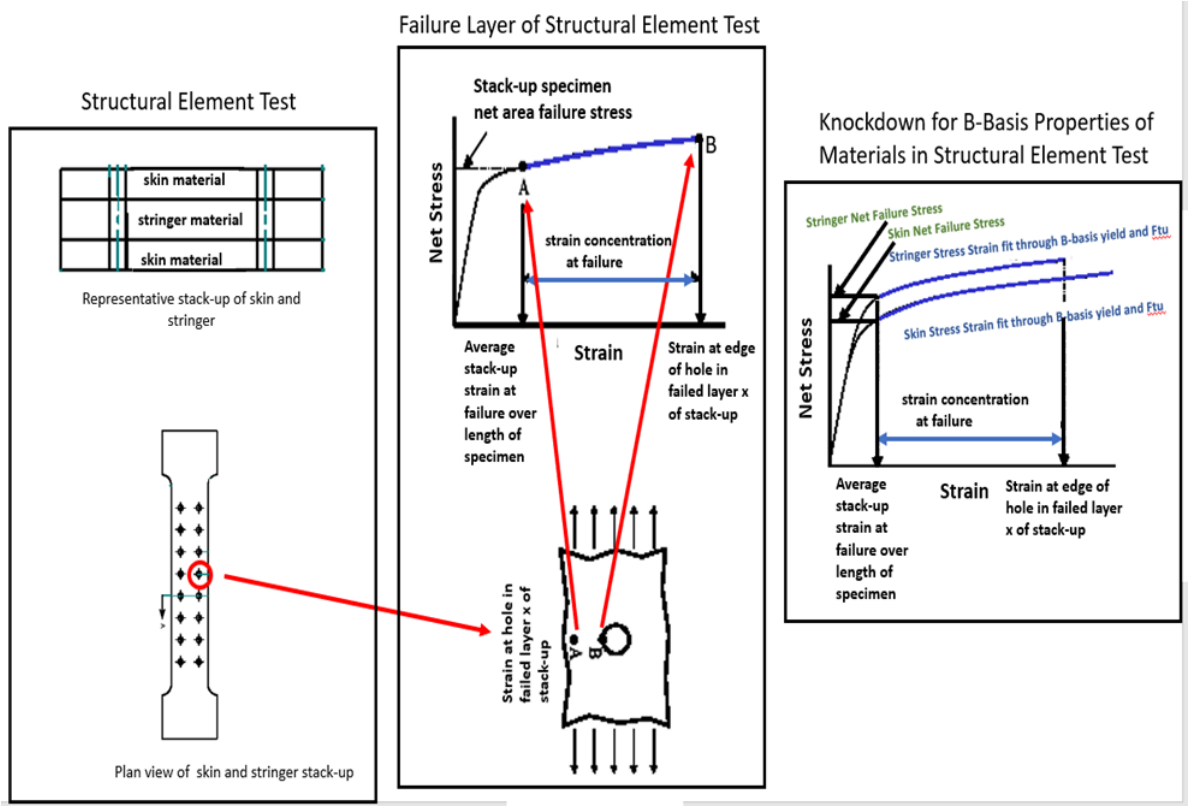

Figure 20. Static strength of fastened stiffened panel detail estimated by the strain-to-failure approach proposed by Mohaghegh

2.2.2 Crown compression buckling failure criterion at negative 1.5G

The crown panels in this study are designed to prevent failure in compression at the ultimate negative maneuver load (-1.5G from V-N diagram, Figure 11). Note that to simplify the sizing study, only compression loads due to vertical down-bending were used in this study for the top of the crown. The working stress targets for compression failure in the crown panel were evaluated using the Arconic proprietary compression-stiffened panel optimization code ASPAN-CO (Kulak, et al., 1995). A sample ASPAN-CO output for a hypothetical panel geometry is shown in Figure 21 for illustrative purposes only. The ASPAN-CO results are individually optimized at every load intensity, so the results of attainable stresses may not be achieved in production. For instance, there is no manufacturing constraint that requires all solutions from

STAxx to STAyy be smooth and continuous (i.e. machined from a single extruded stringer). For the Panel 1 sizing, a table of working stress targets was generated (keeping the As/Bt constant for the Panel 1 crown) as a function of axial compression load intensity maneuver and entered as a Table in the Mathcad (PTC, 2019) sizing module. The thickness required to prevent compression failure (skin buckling leading to stringer failure) was calculated at each crown location in 1 ft. intervals. Note, the bi-axial hoop load intensity contribution from pressure, the shear load intensity from fuselage torsion and vertical shear loading, and lateral bending or shear stresses were not included in any of the crown sizing calculations.

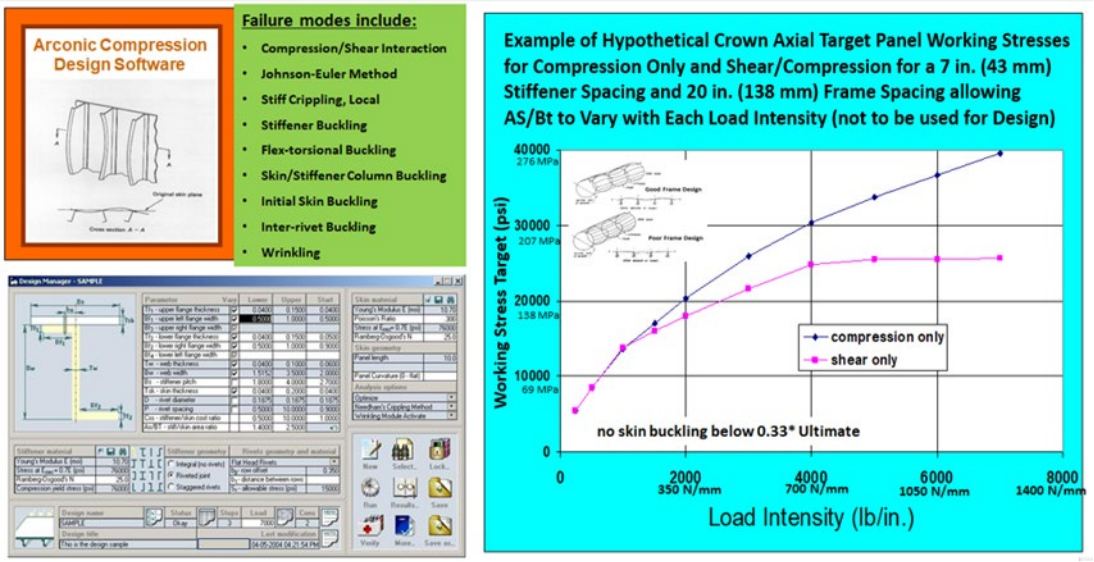

Figure 21. Hypothetical example using ASPAN-CO Arconic compression optimization code for curved or flat stiffened panels in compression and shear

An additional design goal was the compression landing load, which occurs in the crown between the main landing gear and the front landing gear. A comparison of bending moment due to a -1.5G maneuver in Figure 22 shows that, for the current assumptions, the bending due to the landing load generated by the method described by Astori, Hupperts, & van Tooren (2003) was lower than the bending moment for the -1.5G maneuver (at the target STA 38 ft. location). Therefore, the skin sized for the -1.5G maneuver was more critical than the skin sized for the typical landing load for the generic aircraft defined in this study.

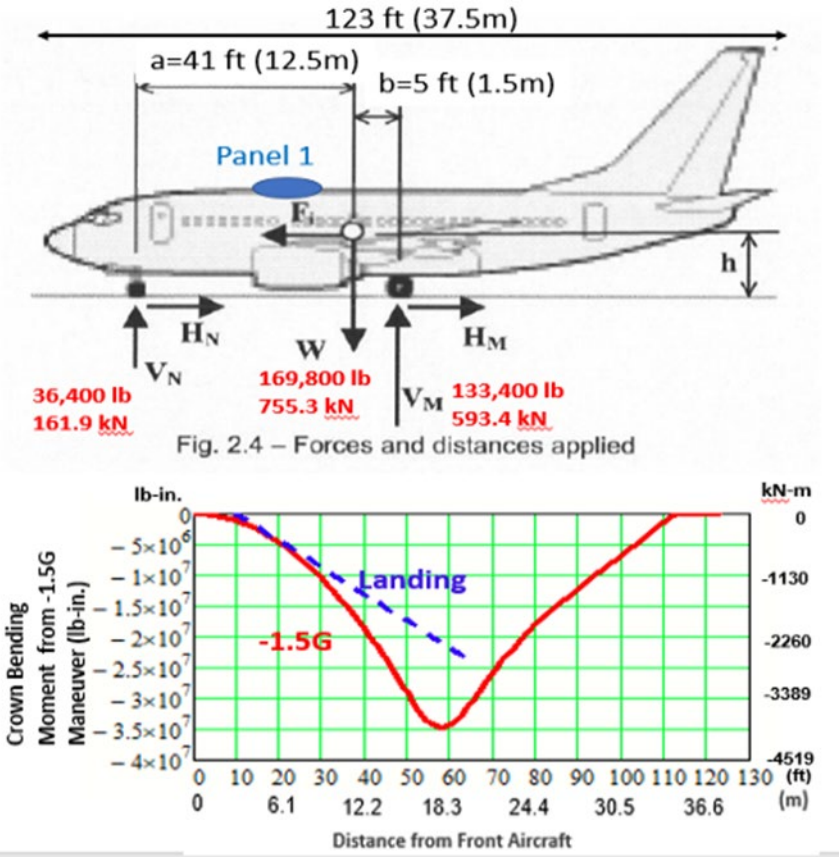

Figure 22. Comparison of bending moments from landing versus the -1.5G maneuver bending moment

2.2.3 Sizing methods for fatigue, initial inspection, and repeat inspection

Fatigue and initial inspections were not used as design goals in this study. It was assumed that S/N fatigue and initial inspections were not the critical sizing criterion for the fastened stringer and fastener frame/shear tie details in Panel 1. S/N fatigue methods calibrated by years of testing and flight experience are considered a proprietary technology by OEMs. The inclusion of S/N in sizing studies requires generating working stress targets, which would depend on the specific OEM and their methods. Although S/N and initial inspection goals were not used in the sizing of Panel 1, it is worthwhile to outline some details of S/N and initial inspections to illustrate the complexities and issues involved in including these failure modes in simplified trade studies. This discussion does not include the effect on structural sizing for the critical non-inspectable structure sized by fatigue or the design considerations for fatigue critical structures involving MSD and MED in setting structural modification points (SMP), inspection start points (ISP), or subsequent repetitive inspections related to an airplane's LOV.

2.2.3.1 Further discussion on working stress targets for S/N fatigue

This section discusses the difficulties of including S/N fatigue and initial inspection goals in sizing trade studies. Sizing of a structure driven by S/N fatigue life is typically associated with fastened joints and high stress concentration details and is dependent on many variables, including the quality of the manufacturing/assembly of these details, the fasteners, sealing, fretting, corrosion, and so on.

Test articles are typically used in a building block manner to validate the S/N life goals and initial inspection design goals are met. First smaller surrogate scale fatigue test articles are used with coupon-to-structure knockdown factors as shown in Figure 23 for a skin to stringer fastened detail. However, these coupon-to-structure scale factors are also considered proprietary information at the OEMs. The performance of the S/N test article is related to quality of the design/manufacturing/assembly details and on the manufacturing practices and specifications unique to each OEM. Test articles should reproduce the manufacturing approaches used in the aircraft build, if not built by the OEM's, to avoid questions regarding differences between "research specially built" fatigue test articles and "aircraft manufacturer" build grade articles.

Testing is also conducted on full-scale fuselage production fatigue test articles by the OEM to demonstrate multiple lifetimes of loading can be achieved without exceeding a regulatory defined failure level as shown in Figure 23. These full-scale results can be used to identify and improve details in problematic fatigue areas and verify the absence of MSD and MED during multiple design service lives. As mentioned previously, the S/N sizing approach described herein does not include the design considerations involving MSD and MED in setting SMP using LOV results.

The definition of S/N working stress targets for a simplified trade study is difficult as described above. The goal of this test program was to compare the various EMST stiffened fuselage panels for damage tolerance. Stringer/frame/skin stiffened panels represent a significant percentage of the fuselage shell area. It was assumed that S/N fatigue design approaches for fuselage panel stringer, frame, and skin details have evolved to the point that the stress levels needed to achieve damage tolerance goals are more critical than those needed to meet the S/N goals and initial inspection goals. Areas of fuselage shell sensitive to meeting S/N fatigue requirements, such as lap joints between panels, butt joints between barrels, and cutouts involving high stress concentrations, are not included in this crown panel sizing study. Therefore, the weight and performance benefits estimated by this program only apply to the fuselage crown panel areas sized by damage tolerance requirements.

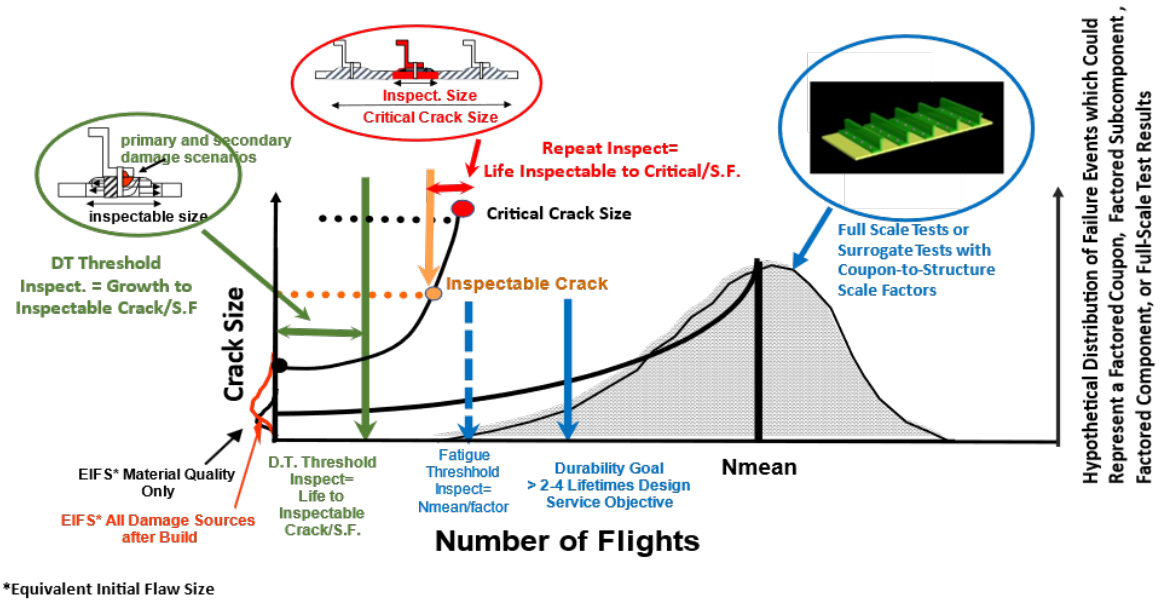

Figure 23. Comparison of some methods for inspection and S/N fatigue helpful in simplified trade studies

2.2.3.2 Methods for working stress targets to meet the initial (threshold) inspection goal

For the Panel 1 sizing approach, developing working stress targets for initial inspection goals were beyond the scope of this effort. It was assumed the sizing goal of the repeat inspection was more critical for sizing the panel. Although initial inspection goals were not used in the sizing of Panel 1, it is worthwhile to briefly discuss simplified options for including initial inspections in simplified trade studies to highlight the difficulties of including initial inspections in sizing trade studies. The approaches described below are not intended for actual design purposes and only apply to fuselage stiffened skin panels. Title 14 CFR 25.571 amendment 25-96 and later requires establishing thresholds based on crack growth analyses and/or tests, assuming an initial flaw of the maximum probable size that could exist as a result of manufacturing or service-induced damage (2023). Advisory Circular (AC) 25.571-1D provides some guidance on setting inspection thresholds (Federal Aviation Administration, 2011). The AC also provides guidance on assumptions to consider when identifying the extent of damage to consider in the damage tolerance (DT) evaluation. Industry has had to consider multiple distinct crack scenarios when establishing inspection thresholds. Figure 24 to Figure 26 are examples of possible discrete location cracking scenarios that are considered for DT evaluation in this program. These do not consider MSD or MED conditions. Each OEM will have its own design requirements for complying with Section 25.571.

Setting the target life for the initial (threshold) inspection depends on the methods chosen for detection of cracks, which influence the size of cracks that can be detected, the reliability, and the cost of inspection. Over the years, fatigue crack growth (FCG) from manufacturing and assembly quality structures have been back-calculated using crack growth data. Over time, methods have been developed involving the use of these *equivalent flaws* for use in development of initial inspection goals for skin/stiffener and skin/frame details for the damage shown in Figure 24.

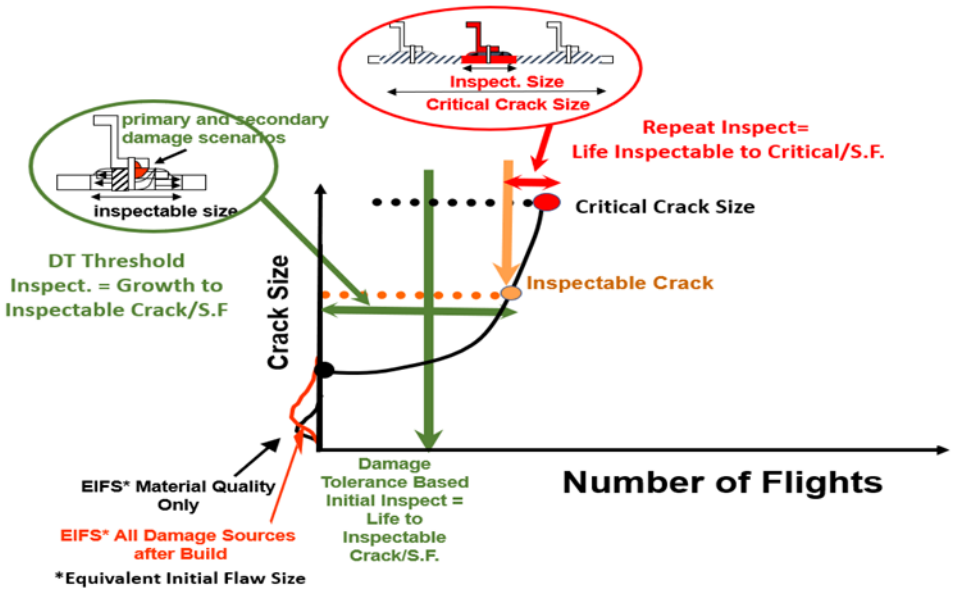

Figure 24. Damage tolerance scenarios for estimating initial and repeat inspections in simple trade study approach

In one stiffened panel approach (not used in this sizing study) to predict the initial inspection life, primary (0.05 in. (1.27 mm)) and secondary (0.005 in. (0.127 mm)) flaws are placed in strategic locations (see Figure 24) in the intact stringer attach flange fastener hole (or an intact frame fastener hole) and in the skin (at the same location or the adjacent fastener). These cracks are grown simultaneously until a predetermined (based on inspection technique) inspectable crack is reached in the skin, or in some cases a critical crack size before the two bay crack is reached, or in some cases when a two bay crack is reached. First, an analysis is conducted with the primary flaw placed in the stringer (or frame shear tie) fastener hole and a secondary crack in the skin at the fastener hole. Then the initial flaw situation is reversed and the life recalculated (Figure 25). The analysis of the primary flaw/secondary flaw analysis involves the possibility for multiple solutions paths and requires the analysis of various crack paths, as illustrated in Figure 26. The longitudinal crack is grown under constant amplitude loading, while circumferential stiffener/skin cracks could be grown under constant amplitude or spectrum loading. The

minimum life of the two primary/secondary flaw analyses would be used to compare to a design goal, which could be some percentage of the design life (50% is sometimes used).

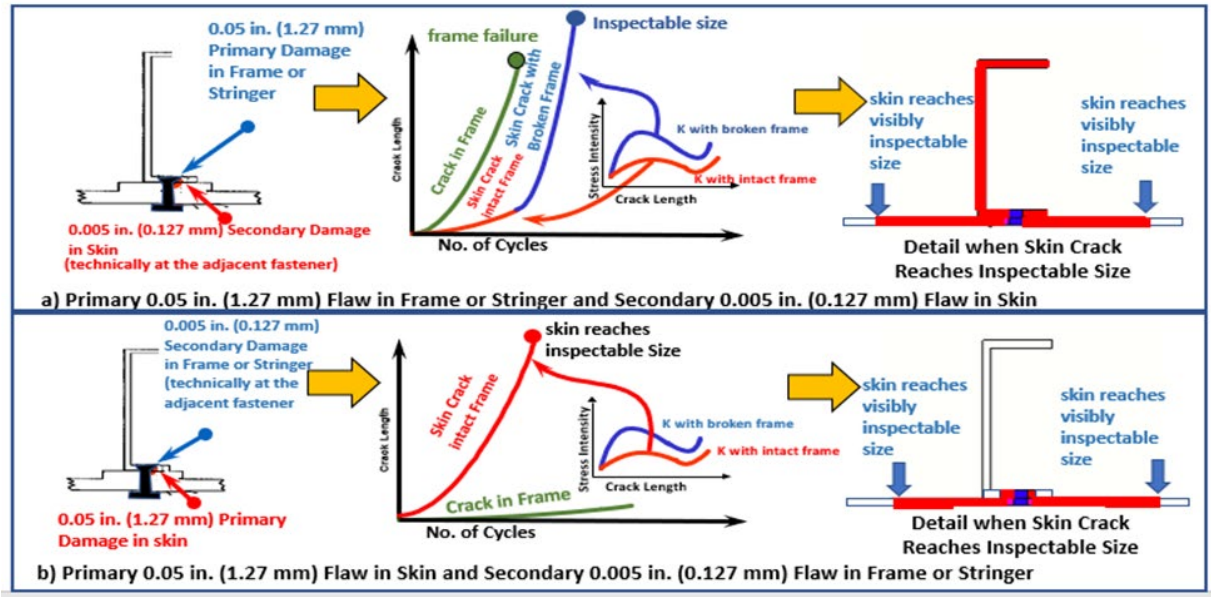

Figure 25. Simplified method to establish the working stress target to meet the initial (threshold) inspection interval goal

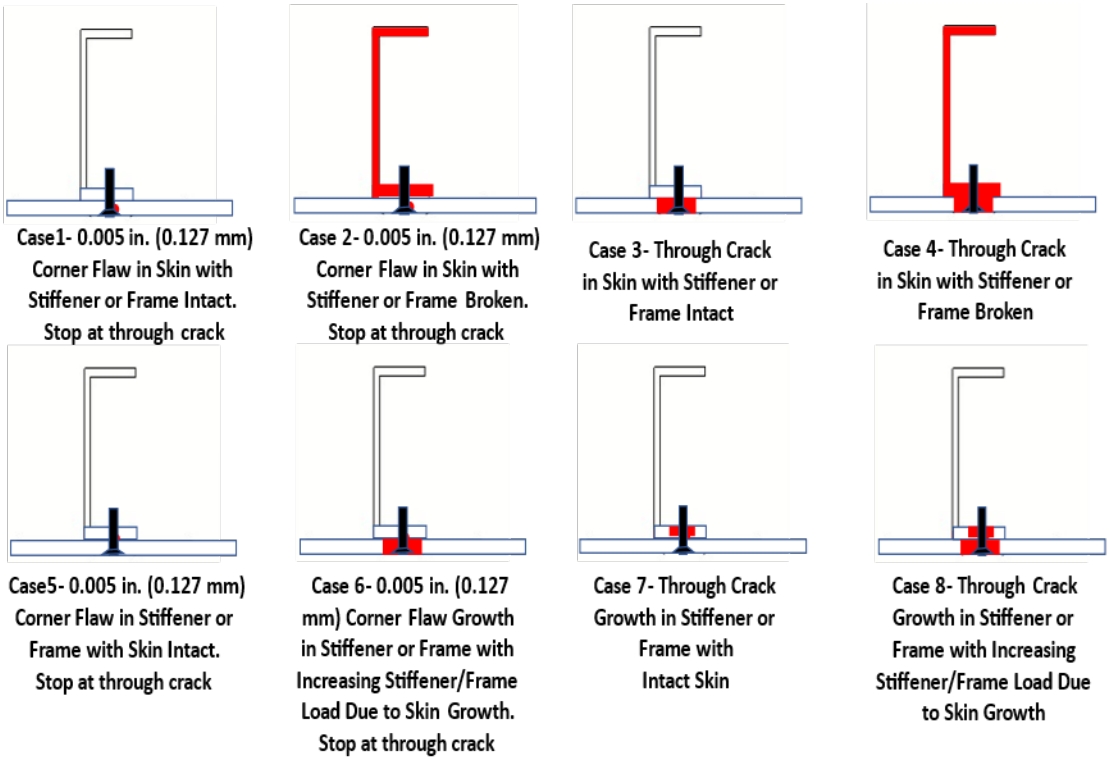

Figure 26. Analysis cases for the "same hole" primary/secondary flaw initial inspection approach

In addition to crack analysis, it is good practice to do an independent check using S/N fatigue if data is available. This S/N check could be made by factoring the total S/N fatigue life of the same stringer (or frame)/skin detail based on statistics to a level of confidence such that the same percentage of the design life goal as the crack growth is met or exceeded (labeled Fatigue Threshold Inspection in Figure 23). In practice, additional design considerations for fatigue-critical structures involving MSD and MED would be evaluated in setting ISP related to an airplane's LOV. The most conservative of the described approaches would be used. Unfortunately, establishing the S/N database and coupon to structure-based correction factors involves extensive flight and test experience and is typically considered proprietary information.

2.2.4 The repeat inspection goal

The repeat inspection interval scenario used in this study for Panel 1 assumes the externally nonvisible stringer or frame/shear tie fails first, and the crack growth in the skin (starting from under the stringer or frame at the fastener) would be found during the repeat inspection. The approach described below was used for the stiffened panels in this program and is not intended

for actual design purposes. In practice, additional design considerations for fatigue-critical structures involving MSD and MED could impact the subsequent repetitive inspections related to an airplane's LOV. This was beyond the scope of the current program.

The repeat inspection interval (see Figure 23, Figure 24, and Figure 27) was defined as the life from an initial inspectable crack size (the size depends on the inspection method) to the critical crack size (the crack size at which the panel can no longer carry the limit load or the crack has reached the adjacent stringer or frame). A detectable crack of 1.0 in. (25.4 mm) half-crack length was used in this study for both the longitudinal and circumferential cracks. For Panel 1, the repeat inspection goal for both the longitudinal and circumferential cracks was set to be 6,000 flights for skin crack growth with a safety factor of two, or 12,000 total flights total. An elevated pressure differential of 9.9 psi (0.068 MPa) was used to set an aggressive performance goal for future metallic aircraft to compete with composite fuselage shells. For the circumferential crack growth testing in Panel 1, the bending and pressure loads were used to develop the skin working stress target for the circumferential crack inspection. The axial stress from bending was not included in the longitudinal crack testing in Panel 1 (i.e., only the pressure hoop stress and the axial component of the pressure was used for the Panel 1 longitudinal crack testing).

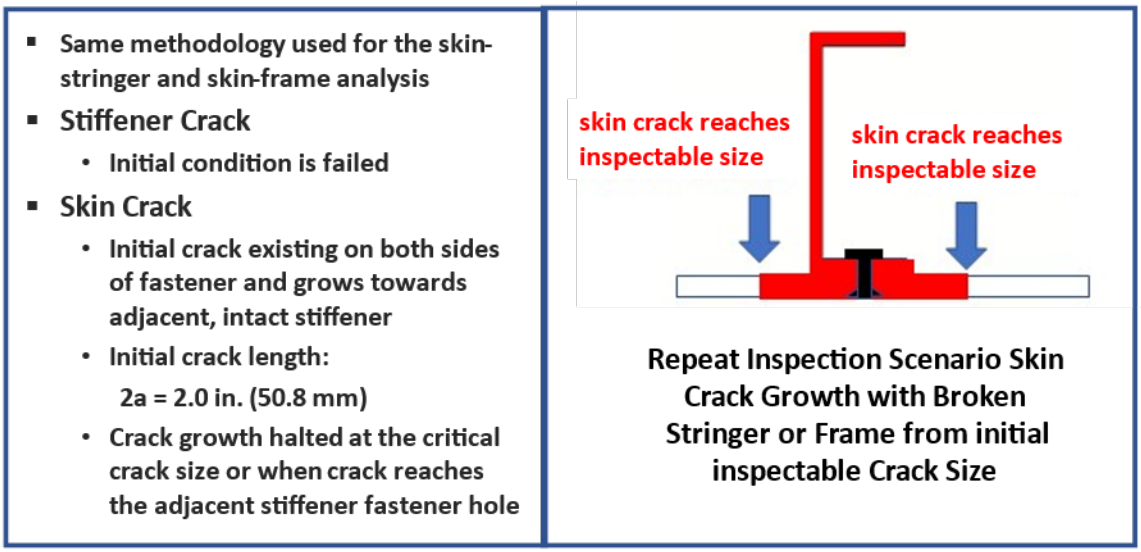

Figure 27. Repeat inspection scenario used in this study

The repeat inspection skin working stress target for the circumferential crack was determined by a stand-alone K-control testing program. M(T) specimens were first tested under spectrum K-control, and then an equivalent constant amplitude K-control loading stress was determined, which resulted in the same crack growth life as the spectrum K-control test.

K-control is a test method where the SIFs from the FEM analysis of the FASTER Panel 1 were reproduced by the test frame software to drive the M(T) specimen test (see Section 3). The Panel 1 SIFs were developed using the quarter symmetry fuselage FE model, Qsymm1 (see Figure 28), for a skin crack under broken stringer for circumferential cracks, and a skin crack under a broken frame for longitudinal cracks. The M(T) specimens were tested in K-control using the same circumferential SIF values as a function of crack length. Thus, at a given crack length, both the stress intensity magnitudes and the stress intensity gradients were the same in the K-control M(T) specimen as the FE Qsymm1 model. The loads for the FASTER Panel 1 test were developed to match the Qsymm1 FE SIFs.

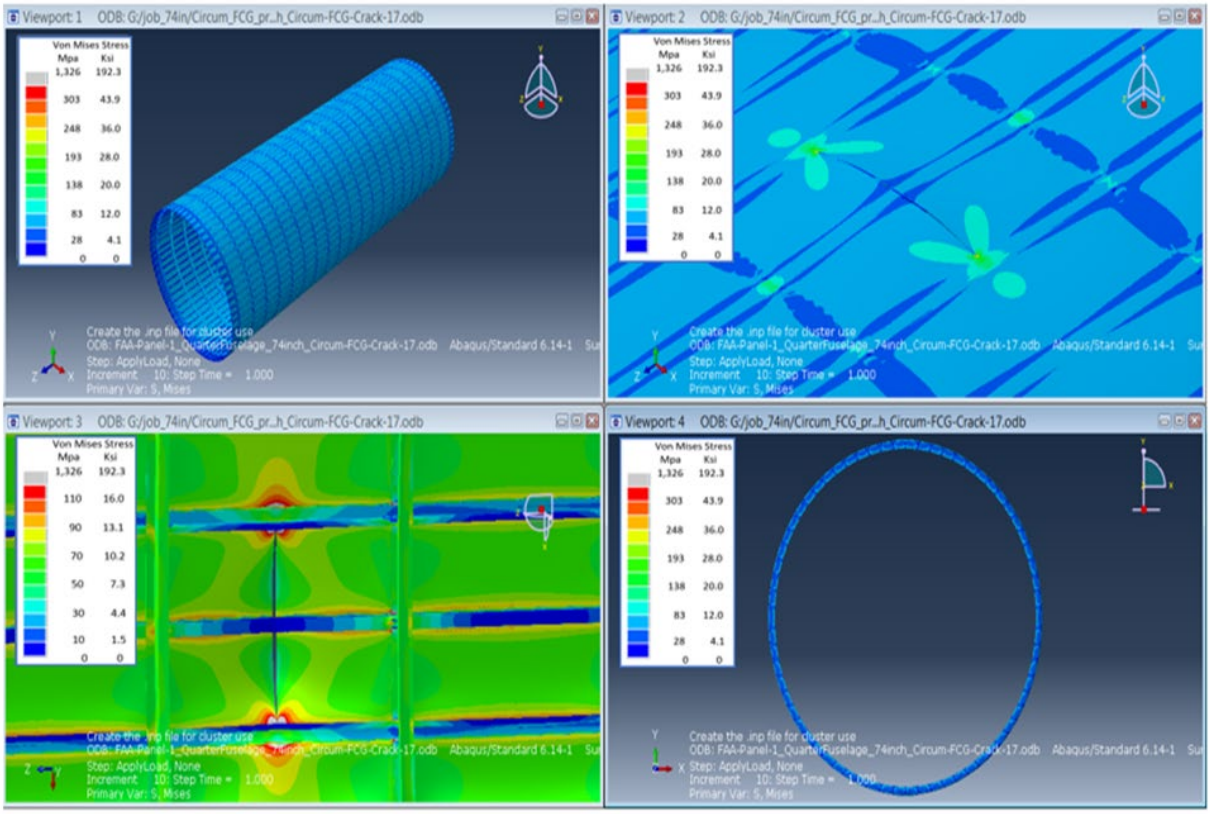

Figure 28. FEM modeling to develop SIFs for crack growth in the circumferential direction with a broken stringer

Panel 1 (2524-T3 skin) circumferential crack results from the K-control testing are shown in Figure 29 for spectrum and constant amplitude. Circumferential crack growth results are compared with and without K-control. The results indicate a life somewhat greater than 12,000 flights could be achieved at a 1G+ pressure defined Mfs, of 12.7 ksi (87.6 MPa). Since the max valid data for the specimen was about 3 in, to be conservative, the modified mini-TWIST spectrum Mfs was assumed to be 12.7 ksi for Panel 1, for the 6,000-flight repeat inspection goal with a safety factor of two, or 12,000 flights total. Mfs was defined in this study as the Flugge

characteristic stress at 1G + 9.9 psi (0.0683 MPa pressure differential). Also, to be conservative, the 1G bending stresses were calculated using 100% of the MTOW. The constant amplitude K-control test was conducted at R=0.05 to match the FASTER Panel axial loading as a constant amplitude test at R=0.05. As shown in Figure 29, a maximum stress of 13.0 ksi (89.6 MPa) at an R=0.05 was estimated to have the same life as the spectrum K-control test at a MFS of 12.7 ksi (87.6 MPa). It was surprising the 13.0 ksi equivalent stress was so close to the spectrum Mfs. Some possible differences include a 50% reduced excursion envelope for the modified mini-TWIST spectrum and matching the non K-control spectrum results would have resulted in a larger constant amplitude equivalent stress. K-control testing is described in Section 3.

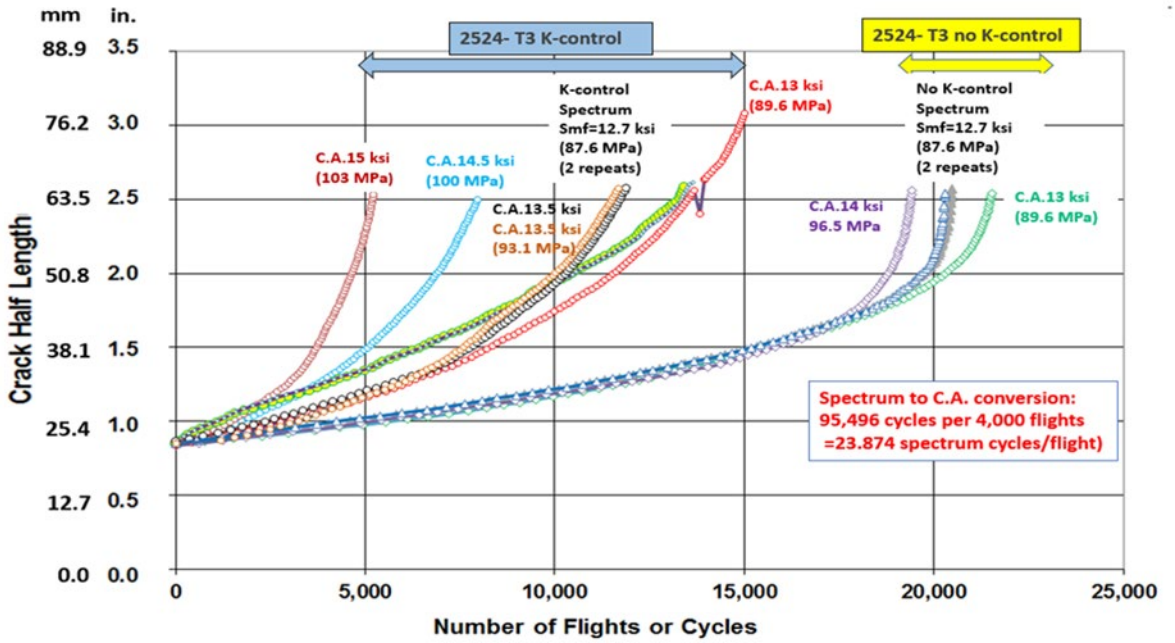

Figure 29. Spectrum and constant amplitude results with and without K-control for Panel 1 2524-T3 M(T) specimens

2.2.5 Commentary on the use of spectrum retardation for the circumferential repeat inspection approach used in this study

Sizing trade studies conducted using spectrum loading in the early aircraft design phase require test data to understand the material crack growth behavior. The M(T) K-control spectrum testing results reflect crack retardation effects which increase the life of the test when compared to constant amplitude, R=-0.5 or linear, elastic software predictions using a spectrum crack growth analysis code without crack retardation. Using crack retardation test data to establish circumferential skin working stress targets may not be conservative for some flight cases.

K-control spectrum loading assumes every aircraft is subject to the same flight spectrum. However, when considering a fleet of aircraft with different usage flight types, there may be cases where the spectrum crack retardation approach used herein (based on K-control spectrum testing) may not be conservative. For example, consider an aircraft that is primarily used for one route where the high-load portions of the spectrum are much lower than the +/- 0.8G range used in this study. This was the case for modified mini-TWIST spectrum where every flight excursion load was clipped by a factor of 2. In this case, retardation effects may be significantly smaller, as demonstrated by J.C. Newman, Jr (1992) in tests where the TWIST spectrum was systematically clipped. The results showed a shorter life with clipping, and with each successive clipping level, the life (life from 20mm to critical crack size) becomes successively less.

For extreme clipping, it is speculated the Newman results approach an asymptote in total life. This total life appears to approach the life from constant amplitude loading for the ground-air-ground loading cycle. Mfs is close the max stress in this clipped spectrum since the larger the clipping the closer the flight loads excursions (not including the landing) cycle about the Mfs. This suggests that constant amplitude tests at R=-0.5 may represent a highly clipped spectrum. In this program the modified Mini-TWIST spectrum excursions have been reduced by 50% to match flight load data showing significant flight alleviation improvements over the years the mini-TWIST has been developed.

Running the FASTER panel test at a negative axial loading R-ratio was not an option for this program. The FASTER panel test was run at a positive R-ratio of 0.05; therefore, to be consistent, the constant amplitude K-control testing was run at an R-Ratio of 0.05 also. During the test evaluation phase, this life will be interpreted as being longer than the ground-MFS-ground loading.

As shown in Figure 29, a maximum stress of 13.0 ksi (89.6 MPa) at an R=0.05 was estimated to have the same life as the spectrum K-control test at an Mfs of 12.7 ksi. (87.6 MPa) for the modified mini-TWIST spectrum. However, there were no landing loads in the constant amplitude testing at R=0.05, and it was expected that constant amplitude results for the R=-0.5 would establish a sigmax equivalent constant amplitude stress lower than 13.0 ksi. This discussion above does not include roughness, corrosion, and other effects which impact crack closure.

Finally, to be conservative, the effect of including the axial tensile bending stress on the longitudinal crack growth in Panel 1 was not included in either the sizing approach or in the FASTER Panel 1 longitudinal crack test. This tensile axial loading would tend to decrease the bulging component of the stress intensity.

2.2.6 The two-bay crack goal for the circumferential crack

Per FAA policy, Policy Statement PS-ANM100-1993-00047, manufacturers should continue to consider a two-bay cracking scenario when designing an airplane (Federal Avaiation Administration, 1993). Regardless of the design philosophy used by the manufacturers, they should continue the current practice of designing for a two-bay crack with a broken central frame to account for the unpredictable nature of damage that might be inflicted on the fuselage, i.e. fatigue (MSD), corrosion, and accidental damage. Tests to substantiate the ability to sustain a two-bay skin crack should include all the effects that influence this failure mode. Internal cabin pressure, skin shear due to fuselage down bending, and the effects of frame bending on the skin are some of the conditions that must be realistically accounted for in these tests. Tests conducted on pressurized barrel sections without these effects would not adequately demonstrate the ability of the skin to sustain large cracks without catastrophic results. However, the complexity of this testing was beyond the scope of this program. Therefore, a simplified approach was used in the Panel 1 sizing study for the two-bay crack calculations as described in this section.

Residual strength for this sizing study does not consider the potential effect of MSD and MED on either the panel design or residual strength. In this program, the circumferential two-bay crack skin working stress target was determined for a condition where the central frame or stringer is broken, and the crack size in both directions is defined to be at the adjacent shear tie fastener hole or stringer fastener hole. This could be a result of FCG or an accidental damage condition where the skin and stringer are severed, as shown in Figure 30 (Swift, 1974).

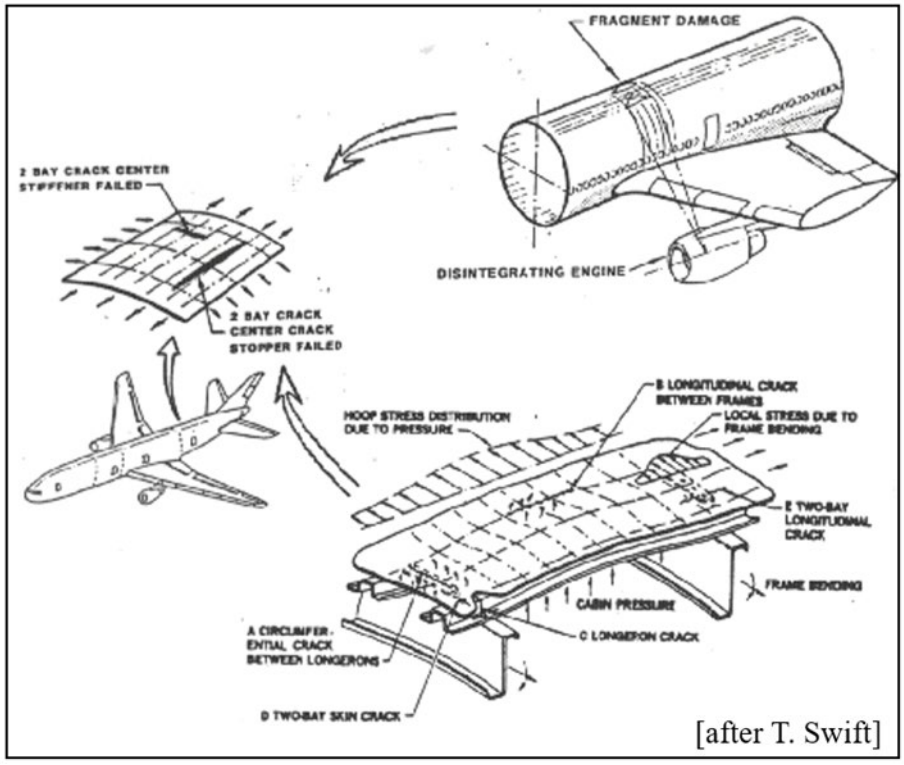

Figure 30. Two-bay crack scenario

The skin working stress target for this failure mode was determined as the panel stresses, which meets the design goal to carry limit load for damage up to a full two-bay crack (i.e. a crack extending to the rivets at the adjacent intact frames/shear ties) with a severed stringer or frame. The argument may be made that this criterion is conservative if accidental damage only is considered for the case of limit load, since a severe event involving penetration of the stringer or frame would be apparent to the pilot and result in an immediate landing of the plane as gently as possible. Therefore, the probability of an accidental damage event and the aircraft experiencing the 2.5G V/N limit load definition or a more severe gust than 2.5G occurring during this timeframe is reduced when compared to a lifetime of aircraft usage. However, for metallic aircraft fuselage panels, this two-bay crack goal ensures a layer of safety in the event of FCG, as described below.

For metallic fuselage panels, the other possibility for a two-bay scenario to develop is from FCG. Although it may be argued that cabin pressure would be hard to maintain for this crack size, it was still considered a good practice to assume this size could occur due to crack growth. The damage tolerance scenario used herein assumes the non-visible stiffening element fails first, and the crack growth in the skin is found by inspection before reaching the critical crack size. The repeat inspection interval in this study was defined as the life of the inspectable crack (depending on the inspection method) to the smaller of the critical crack size or the distance to the adjacent

stiffening element fastener hole. To determine if this criterion is met, the residual strength calculation is evaluated for all crack sizes up to the adjacent frame or stringer, whether from crack growth or accidental damage. The two-bay crack FE model should include plasticity and rivet failure and stringer (or frame/shear tie) failure. If fast fracture is prevented for all cracks up to the two-bay condition (to the adjacent frame or stringer), the difficult task of verification for fast fracture crack arrest at the adjacent frame or stringer is avoided. This fast fracture arrest condition increases the loads in the frame or stringer compared to those calculated from a static elastic/plastic FEM analysis of the two-bay crack. Because the SIFs increase rapidly in the longitudinal crack, fast fracture is more likely to occur for the longitudinal crack.

For the circumferential crack, the limit load axial stress for Panel 1 was defined in this program as the undamaged fuselage stress at 2.5G plus differential pressure. The skin stress for this condition was approximately 23.4 ksi (161.3 MPa) at the Flugge characteristic stress location, as defined in Table 1. Typically, the circumferential stress intensities in the skin at the limit condition of 2.5G plus differential operating pressure in the crown are not large enough to cause fast fracture for tough skin materials like 2524-T3. For 2524-T3 skins, the circumferential two bay crack failure is usually driven by the static failure of the stringer or rivets at the increased stringer/rivet loading due to the large crack. For example, the results of a finite element analysis of the as-designed 0.055 in. (1.4 mm) Panel 1 at a total axial load of 30 ksi (207 MPa) plus 9.9 psi (0.068 MPa) pressure is shown in Figure 31. Note that the skin R-Curve resistance is larger than the stress intensity solution, and failure is expected to occur by stringer or rivet failure.

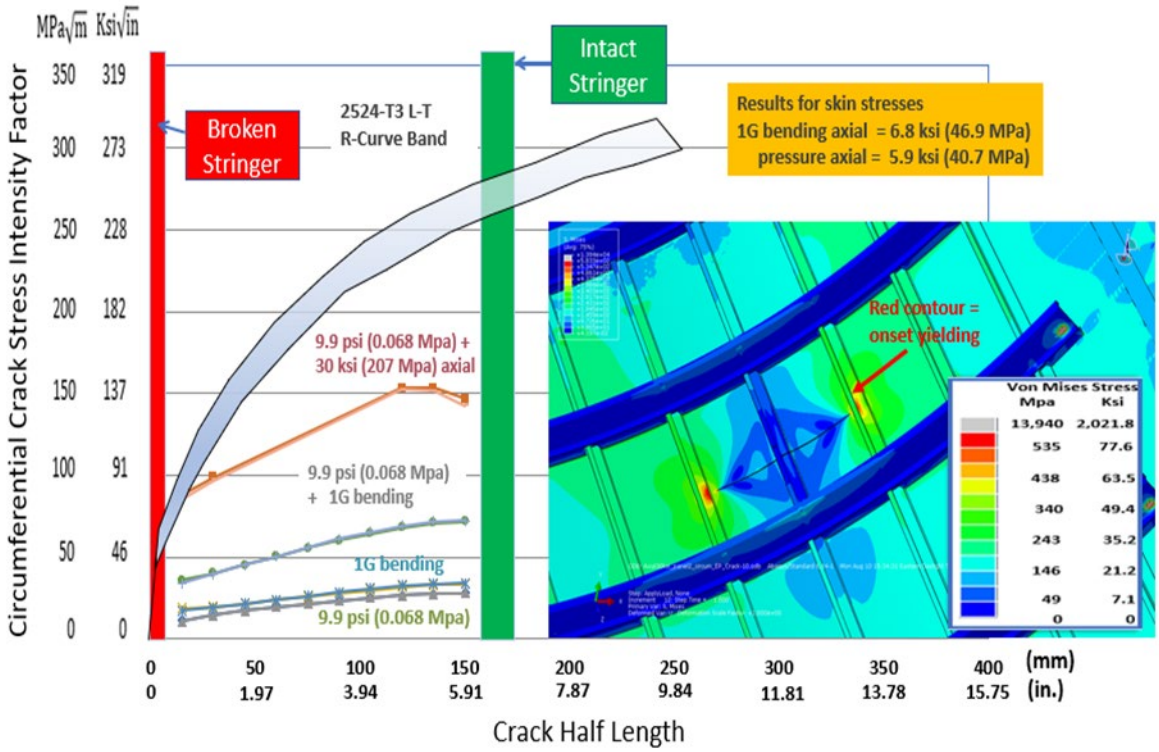

Figure 31. Circumferential two-bay crack analysis for Panel 1

Note, an *Aeffective*-based (Kr vs. DAeff) R-curve was used in Figure 31. However, because of the large amount of plasticity (especially in the skin) at the limit load, an *Aphysical* R-Curve may be more appropriate for circumferential two-bay crack skin failure prediction. The LT direction Aphysical curve for 2524-T3 was not available, but since the skin SIFs were well below the Aeffective-based R-curve at a load case 28% above limit load, skin failure was not expected. For this analysis, failure of the stringer was assumed when the average stringer strain in the flange attached to the skin reaches a critical strain to failure for a fastened skin/stiffener of 2.5% strain averaged between two fasteners. The two-bay circumferential crack working stress target used for this sizing study was the stress that results in stringer failure.

2.2.7 The two-bay crack goal for a longitudinal crack

Again, residual strength for this sizing study did not consider the potential effect of MSD and MED on the panel design or load carrying capability. The sources of longitudinal crack damage include a two-bay crack from FCG or from accidental damage, as previously shown in Figure 30. In this study, the longitudinal critical crack size was evaluated during crack growth for the condition where the frame is broken, and the skin crack grows from under the broken frame to the adjacent frame/shear tie fastener hole on both sides of the broken central frame/shear tie. As with the circumferential two-bay crack, both accidental damage and crack growth damage cases are considered.

A quick first check on fast fracture was made for the Panel 1 geometry by plotting the elastic/plastic FE model SIFs at limit load and checking if these are safely below the R-Curve crack resistance for the roughly 8 in. (203 mm) of crack growth measured on the FASTER Panel 1 test (the SIFs were too high beyond this crack size to contribute much to life). As shown in Figure 32, the SIFs represented by the orange square markers are below the R-Curve for crack sizes within the two bays. However, this analysis did not include rivet failure or shear tie failure. As mentioned in the previous section, if fast fracture is prevented for all crack sizes growing to the full two-bay condition (to the adjacent frame fastener or stringer fastener), the difficult task of verification for fast fracture crack arrest at the adjacent frame is avoided. This dynamic fast fracture arrest condition increases the loads in the frame as calculated from a static elastic/plastic FEM analysis of the two-bay crack.

The Panel 1 elastic/plastic two-bay crack analyses results with no rivet or shear tie failure considered are shown in Figure 32 (orange square markers). These results show the stress intensity decreasing as the crack approaches the adjacent frame due to the frame bridging and these results form a hypothetical lower bound to the SIF solution in Figure 32. Note that the SIFs for cracks near and beyond two bays in Figure 32 are only a hypothetical engineering estimate (dashed lines) to illustrate the conditions that could impact the SIF solutions near and beyond the adjacent frame. The upper bound curve reflects a more detailed FE analysis for the longitudinal crack SIF solutions approaching the frame/shear tie that includes skin large scale plasticity, rivet failure, frame/shear tie plasticity, or frame/shear tie failure. The hypothetical upper and lower bound of SIF solutions near the adjacent frame is defined by the solid brown region in Figure 32. If the SIFs on the hypothetical upper dashed curve result were attained because of yielding of skin and/or frame/shear tie, failure of rivets, or frame failure then it is questionable whether Panel 1 could carry the limit load.

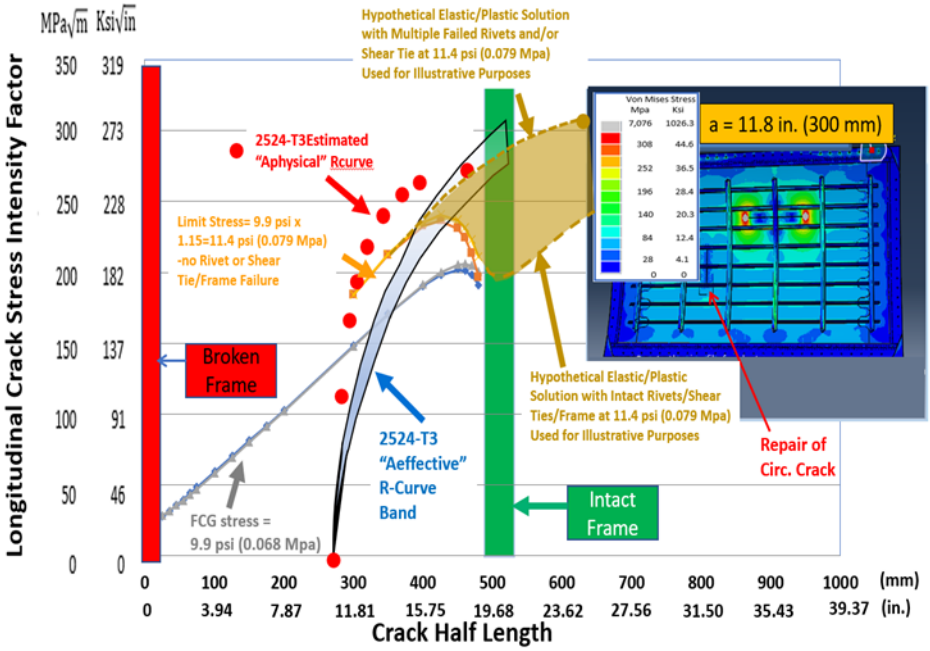

Figure 32. ABAQUS elastic/plastic analysis SIF results for a longitudinal crack with a broken frame

A full two bay crack analysis represents an accidental damage scenario. However, the effective Panel 1 loads in this accidental damage analysis may have to be increased to cover impact loads from the accidental damage event. The results of a detailed frame-to-frame two-bay crack analysis from crack growth in Panel 1 is discussed in Section 6.1. The analysis did not include increased loads for impact. For Panel 1, the two-bay longitudinal crack working stress was determined using a limit load pressure of 1.15 x 9.9 psi = 11.385 psi (0.078 MPa). The skin hoop stress is about 12 ksi (82.7 MPa) for this limit load definition (see Table 1).

As shown in Figure 32, the ABAQUS elastic/plastic analysis SIF results for a longitudinal crack with a broken frame are very high in the fuselage when the half-crack length is 6 in. (153 mm) and crack growth is rapid (about 0.004 in/cycle (0.1mm/cycle) as shown in Figure 33). In this case, most of the repeat inspection crack growth life for Panel 1 occurs between the 1.0 in. (25.4 mm) half-crack length assumed in this study as the initial inspection crack size and approximately 6.0 in. (152.4 mm) in half-length.

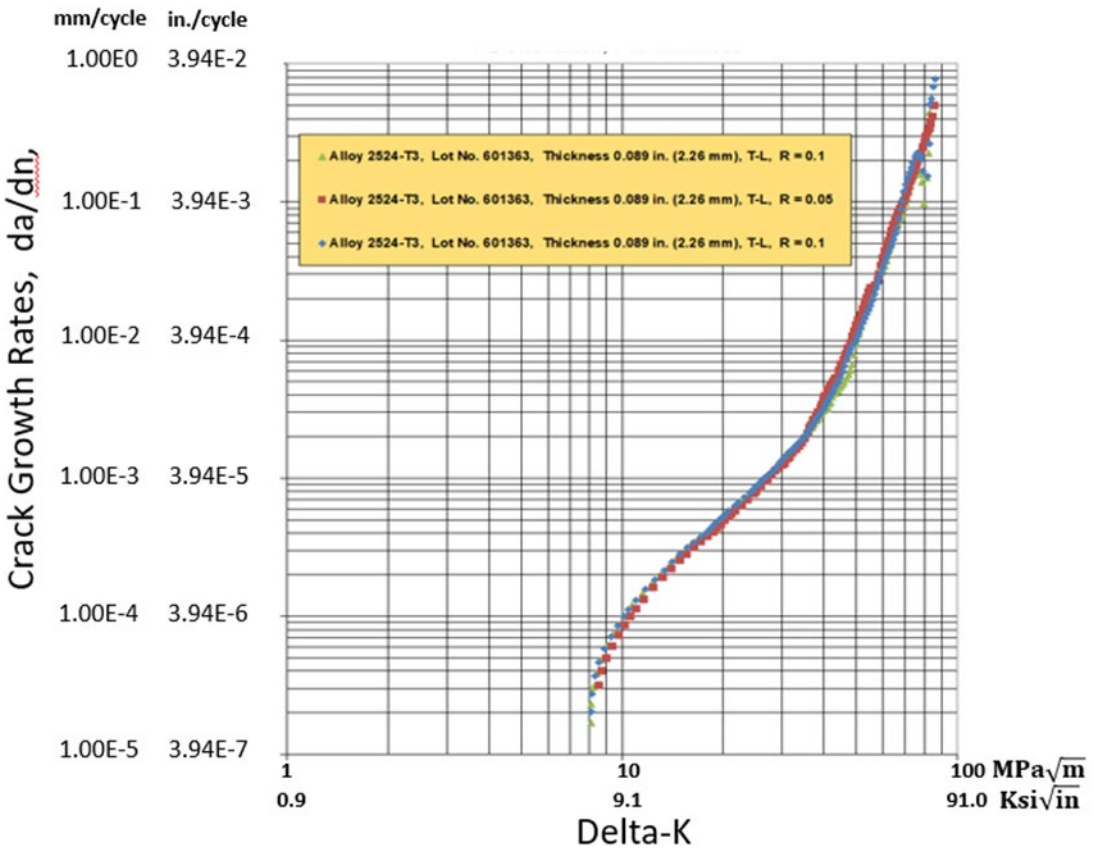

Figure 33. Crack growth da/dN versus delta-K for 2524-T3

There are limitations using the R-curve for estimating skin failure, as described below:

It should be noted that in Figure 32 the SIFs from the FE elastic/plastic two-bay crack analysis were interpreted as Aphysical-based SIFs. A wide panel Aphysical-based R-Curve was not available. The Aphysical-based R-Curve in Figure 32 was estimated using the Aeffective R-Curve (Bucci, et al., 2000), COD, and test specimen loading information. This was done using an elastic/plastic FEM model of a 40 in. (1,016 mm) wide M(T) panel and an elastic model of the same 40 in. wide panel. FE analyses were conducted for various size crack lengths where the goal was finding the Aphysical crack size that produced the same crack opening displacement (COD) as the elastic analysis for the same crack/load combination as measured in the Aeffective-based R-Curve test.

Considering the difficulties described below in employing the R-Curve approach for two-bay cracks, crack tip opening angle (CTOA) and delta-5 may be more appropriate for two-bay crack residual strength analysis.

- An elastic plastic analysis requires an Aphysical-based R-Curve from a very wide panel (40 in. or wider), which is difficult and costly to test.

- The extensive plasticity in the skin when the crack is near two bays may result in an unusual situation where the physical crack, Aphysical, is approaching the frame while the effective crack, Aeffective, could be beyond the frame.
- Complex finite element models are needed to capture a) rivet failures, b) the rivet reactions at the frame/shear ties, which may be partially or fully yielded when there is a large plastic zone in the skin which extends beyond the frame, and c) shear tie failures, especially at the mousehole.

2.2.8 Design goals for side panels

Design goals used in this program for the side sections are shown in Figure 34. The skin, frame, and stringer sizing assumed no widow cutouts/window reinforcement and therefore the sizing results are considered a lower bound of weight. The repeat inspection for the longitudinal crack approach was determined as described for the crown. In this case, only pressure-related loads were considered (no axial loads from bending or shear loading). The shear failure goals included no panel shear buckling failure at ultimate load and no skin shear buckling at limit load.

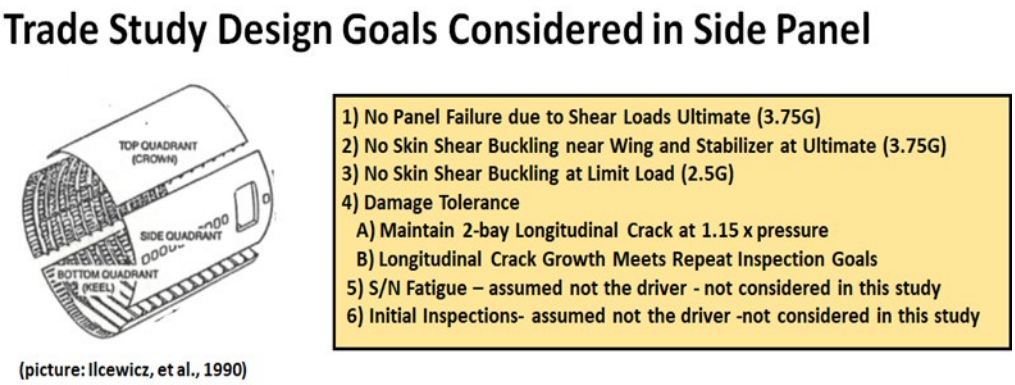

Figure 34. Trade study design goals for side panels

The Arconic compression optimization tool ASPAN-CO (Kulak, et al., 1995) was used to develop working stress targets required to meet the shear buckling goals. The methodology used in ASPAN-CO can optimize panels to include a separate criterion for skin buckling as a fraction of collapse load as well as meeting a target load to prevent total panel shear failure.

The longitudinal crack inspection and residual strength approaches were similar to those used for the crown (shear effects were not considered for crack growth or residual strength).

2.3 Design goals for belly panel

The design goals used in this study for the belly panel are shown in Figure 35. Compression goals include no panel buckling failure at the ultimate load and no skin buckling at limit load. Shear load was not included in the buckling calculations. The Arconic compression optimization tool ASPAN-CO (Kulak, et al., 1995) was used to develop working stress targets required for the compression buckling goals.

The repeat inspection goal and the longitudinal two-bay crack approaches are similar to the crown and side panel approaches already discussed. The effect of including the axial compression bending load on the longitudinal crack growth or two-bay crack was not included.

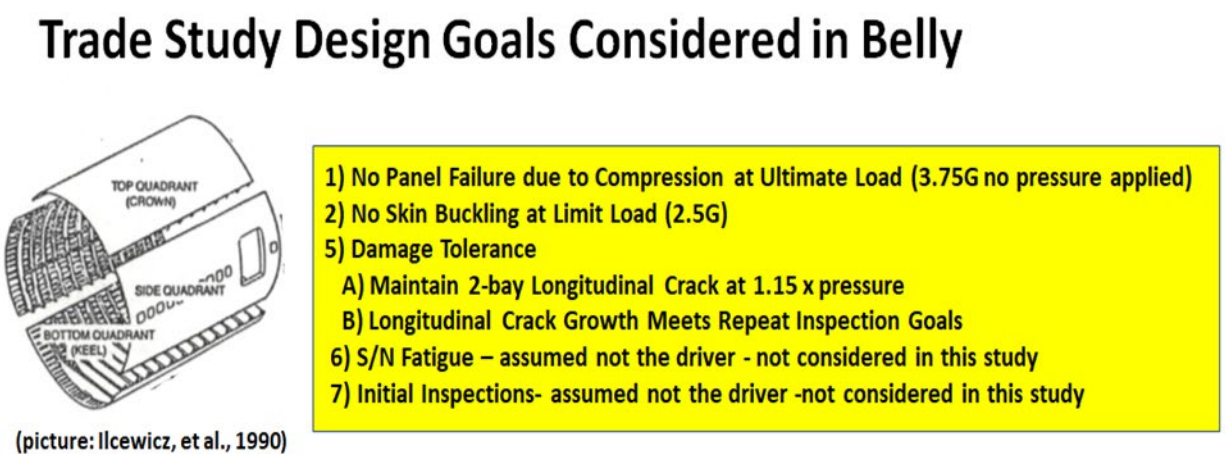

Figure 35. Design goals for belly section

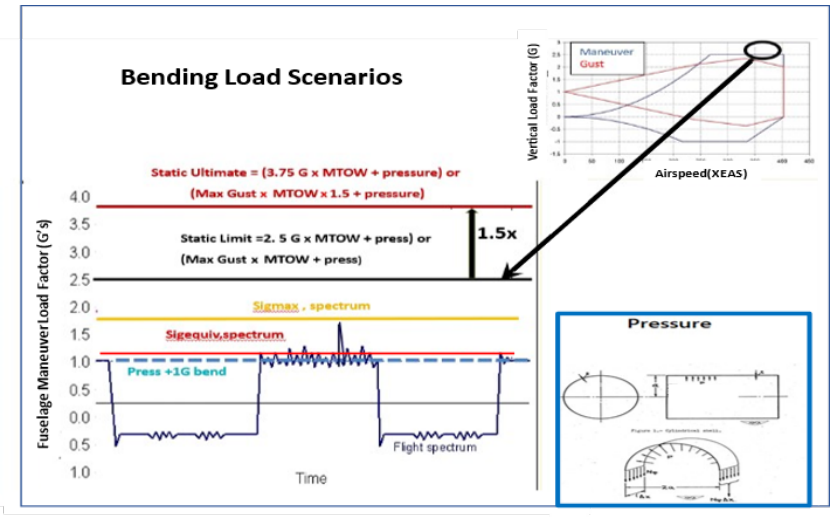

Figure 36. Bending scenarios, including ultimate, limit, gust, and maneuver loads

3 Results of sizing approach for Panel 1

The reference aircraft developed for use in this program to represent a generic single aisle aircraft was shown in Figure 6. The sizing approach was described in Section 2. This section describes the results of the sizing study for the crown Panel 1 tested in the FASTER fixture for longitudinal and circumferential damage scenarios representing repeat inspections.

Results using the modified smeared stiffness Flugge (1952) approach and bending results for the simple 74-in. fuselage radius cylinder model were summarized in Table 1. The fuselage bending model is shown in Figure 37 and the gust/maneuver loading conditions used for bending are defined in Figure 36. As shown, 100% of MTOW was used for spectrum Mfs. Shear and moment diagrams for the fuselage bending model and load intensities are shown in Figure 38.

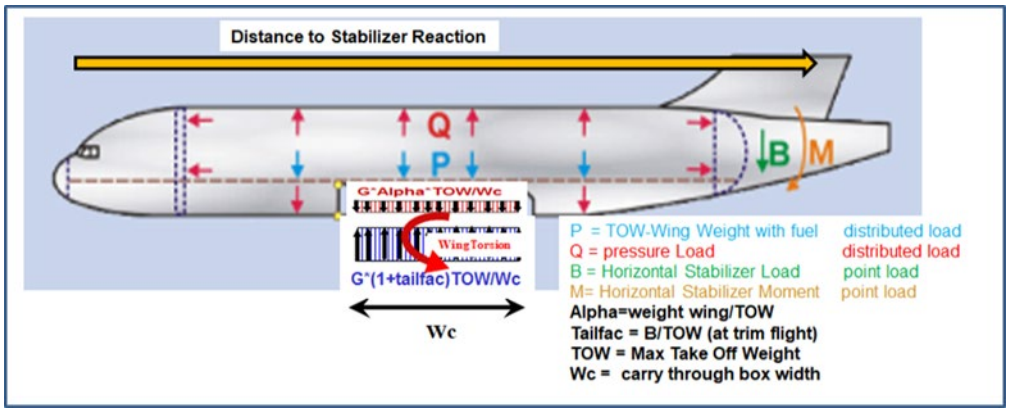

Figure 37. Simple variable radius cylinder model to estimate bending and shear loads

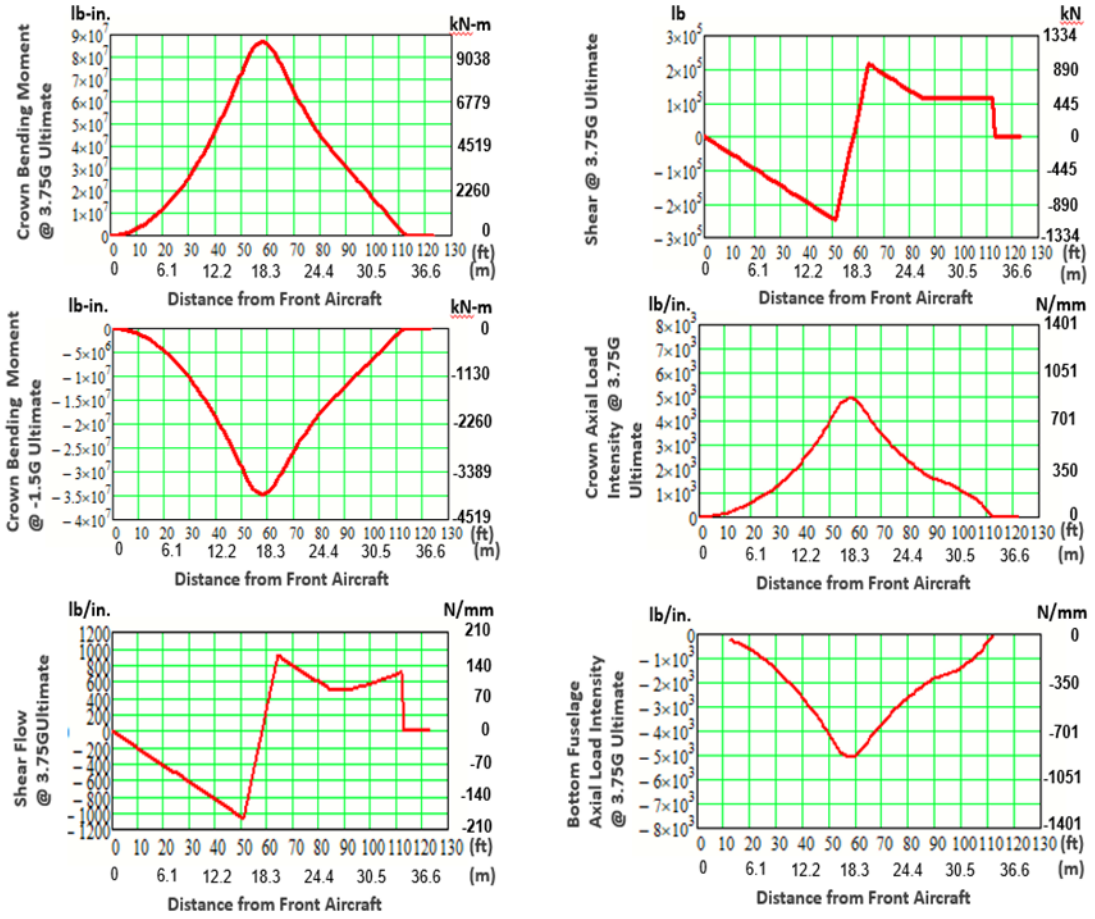

Figure 38. Panel 1 crown load intensities and bending moments

The results of the sizing study for the crown location (STA 38) are shown in Figure 39. The skin thickness required to meet each design goal is plotted from STA 0 to STA 112. The stringer and frame cross-sectional areas are determined from the skin thickness using the As/Bt and Afr/Bt stiffening ratios. Longitudinal crack growth (Damtol-long) to meet the repeat inspection interval goal was the key sizing goal from STA 12 to STA 38 (see Figure 39). Circumferential crack growth (Damtol-cir) to meet the repeat inspection interval goal was the key sizing goal from STA 38 to STA 83. Beyond STA 83, longitudinal crack growth (Damtol-long) to meet the repeat inspection interval goal was again the key sizing goal. STA 38 was chosen as a key location for Panel 1. At this location, the smeared skin thickness is about 0.057 in. (1.45 mm). This smeared thickness represents a skin pocket thickness of 0.055 in. (1.4 mm), and a pad-up skin region of 0.063 in. (1.6 mm). Panel 1 was located at STA 38 where the same skin thickness was required to meet the crack growth goals in both directions; therefore, the same panel can be used to test both key sizing goals (longitudinal and circumferential for both the circumferential crack repeat inspection and the longitudinal crack inspection and repeat inspections). Results for the side section (Figure 40) and bottom section (Figure 41) are included for completeness. For the

assumptions used in this study these areas are primarily driven by shear or compression buckling. Although panel sizing in these areas was not the goal of this program, it was still important to establish a reasonable estimate for skin thickness in the sides and belly, because the contribution to the cross-section moment of inertia influences the crown sizing.

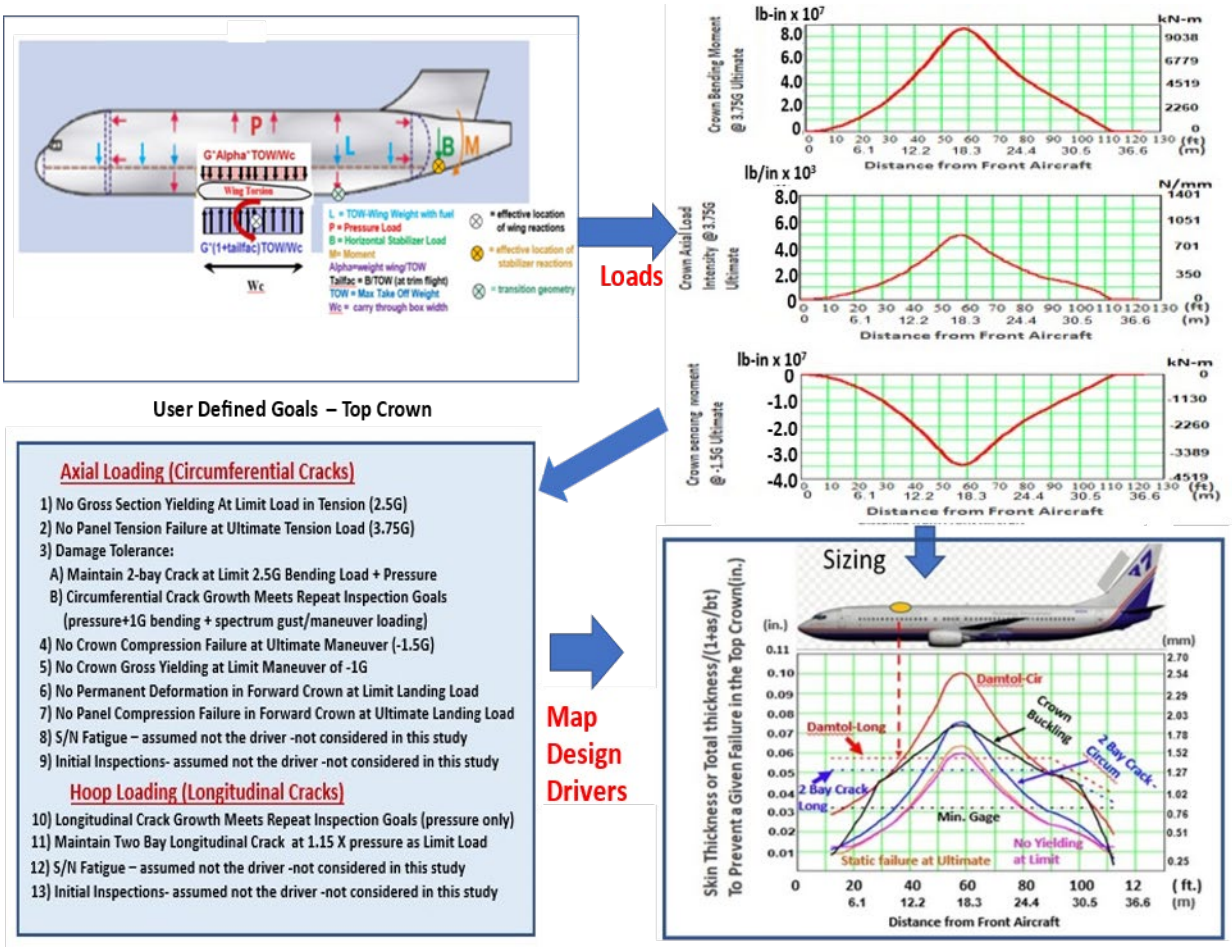

Figure 39. Sizing results for an STA 38 crown

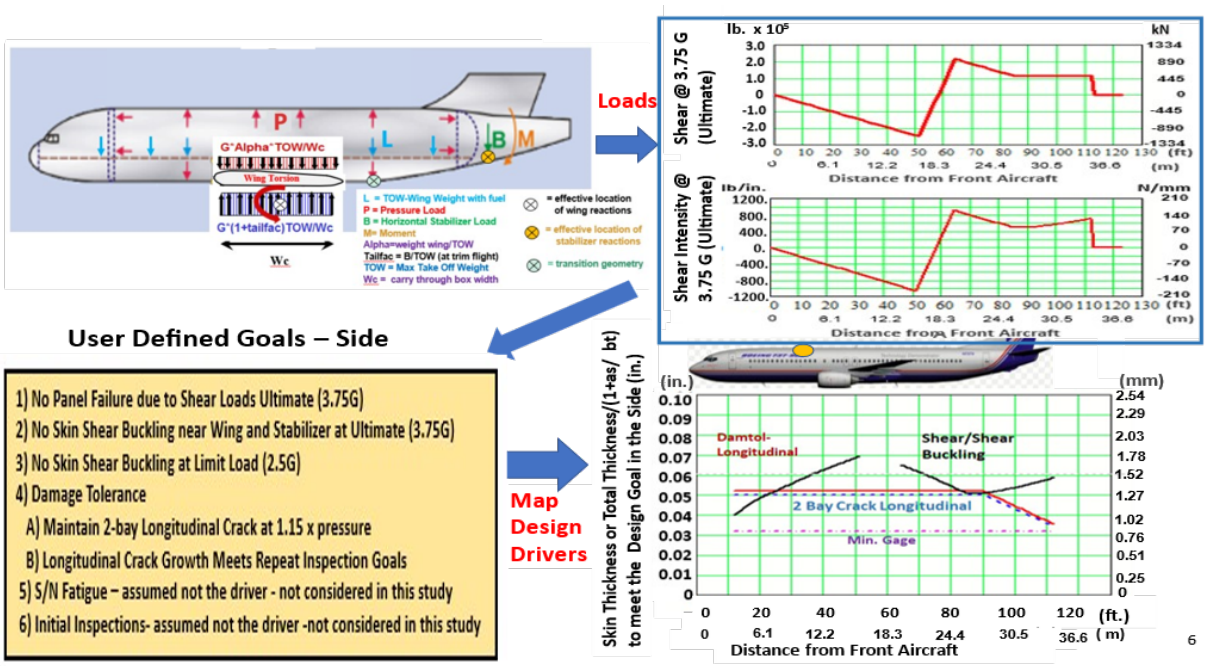

Figure 40. Sizing results for STA 38 middle side

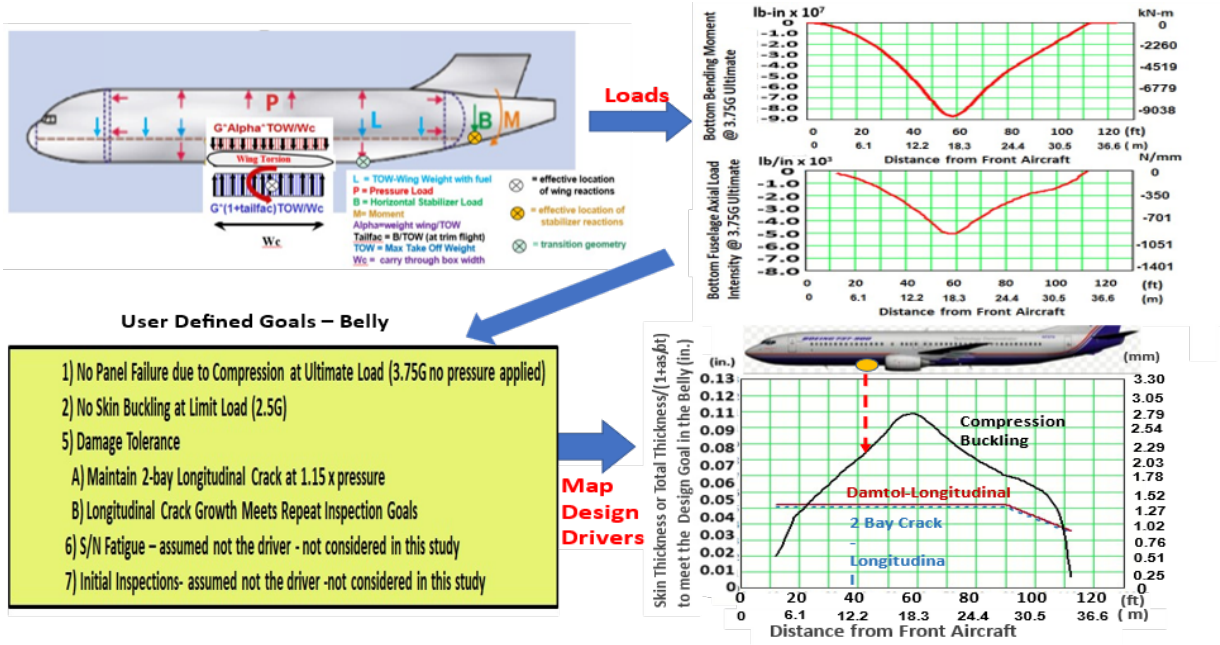

Figure 41. Sizing results for STA 38 bottom

3.1 Impact of 74 in. versus 78 in. fuselage radius

The original program goal was to design a panel for a generic aircraft with a 78-in. (1.98 m) radius fuselage. A circumferential crack growth spectrum was developed for this 78-in. (1.98 m) radius, and K-control testing was already underway before the decision was made to change the Panel 1 radius to 74 in. (1.88 m). This change simplified the FASTER setup, since the 74 in. (1.88 m) radius was already in place and validated. A comparison study of pressure and bending stresses was conducted (Figure 42) for the same aircraft weight and length to decide whether to change the spectrum and redo the significant amount of K-control M(T) testing already completed. The skin working stress target for pressure plus 1G bending for the repeat inspection goal stress was set to be 12.7 ksi (87.6 MPa) for the circumferential crack developed from K-control spectrum testing for the location of Panel 1 (STA 38). The calculations show a 4.3% difference in the range of spectrum stresses for a 74-in. (1.88 m) radius fuselage versus a 78-in. (1.98 m) at STA 38. Thus, a radius change to 74 in. (1.88 m) would result in a small change in the working target. However, since the same spectrum would be applied to all panels, this would not change the relative head-to-head results significantly. Thus, it was decided to use the 78-in. (1.98m) radius spectrum K-control testing results for the equivalent constant amplitude stress.

English Units			
	Rad=74 in.	Rad=78 in.	
	2524-T3	2524-T3	
	Station 38	Station 38	
Working Stress Mfs target for Cir. Crack @ 1G + 9.9 psi (ksi)	12.7	12.7	% Difference
Avg. Skin thickness incl. Pad-Up (in.)	0.057	0.057	0.0%
Sig 1G bending (ksi)	7.20	6.8	-5.0%
Sig @ 9.9 psi pressure (ksi)	5.50	5.9	6.7%
Sig max spectrum (ksi)	18.60	18.3	-1.6%
Sig min spectrum (ksi)	7.00	7.3	3.7%
Sig max-Sig min (ksi)	11.60	11.1	-4.3%

SI Units			
	Rad=1.88 m	Rad=1.98 m.	
	2524-T3	2524-T3	
	Station 38	Station 38	
Working Stress Mfs target for Cir. Crack @ 1G + 9.9 psi (MPa)	87.6	87.6	% Difference
Avg. Skin thickness incl. Pad-Up (in.)	1.4	1.4	0.0%
Sig 1G bending (ksi)	49.6	47.2	-5.0%
Sig @ 9.9 psi pressure (ksi)	37.9	40.5	6.7%
Sig max spectrum (ksi)	128.2	126.2	-1.6%
Sig min spectrum (ksi)	48.3	50.1	3.7%
Sig max-Sig min (ksi)	80.0	76.5	-4.3%

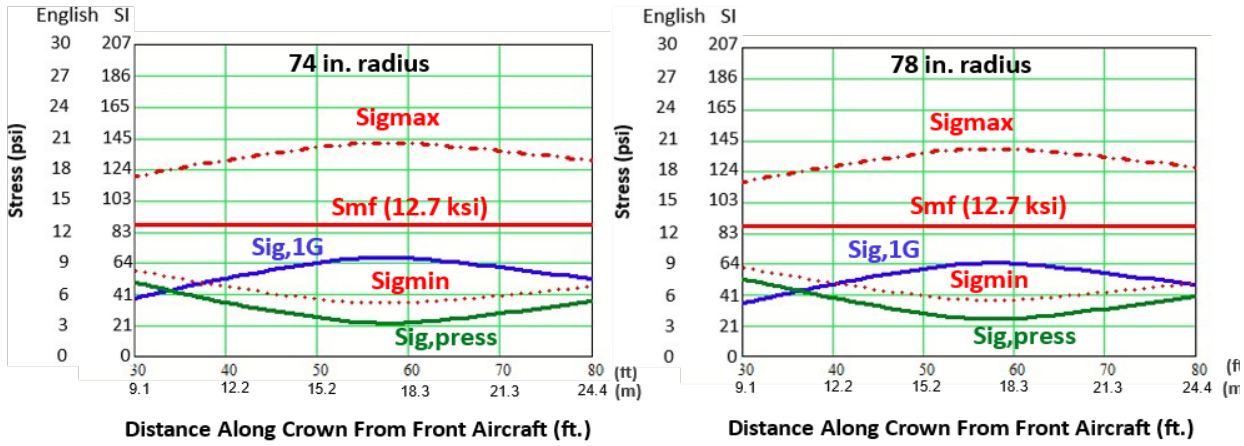

Figure 42. Comparison of pressure and bending stresses for 78-in. fuselage radius versus a 74-in. radius

4 Finite element modeling to support testing of panel 1

4.1 Use of the quarter symmetry model, Qsymm1, to determine loads for test panel 1

A schematic of the analysis approach used to develop the actuator loads for Panel 1 is shown in Figure 43. The approach uses a quarter symmetry finite element model, Qsymm1, of the

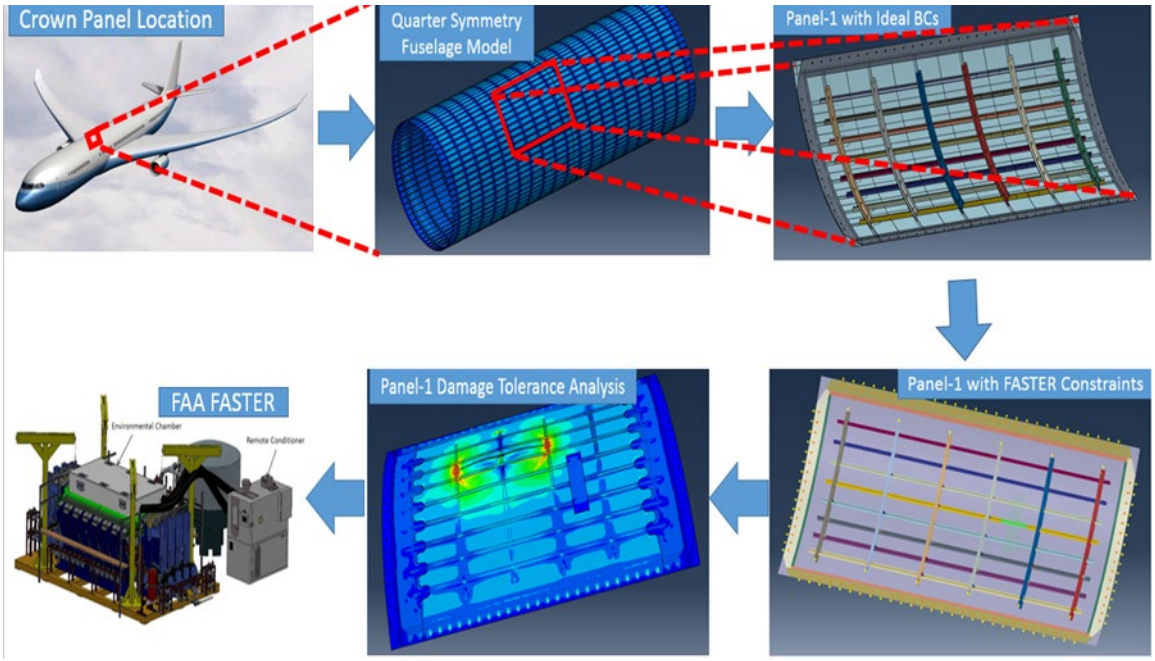

Figure 43. Schematic of FASTER actuator load development using the Qsymm1 quarter symmetry FE model in conjunction with the panel 1 FE model

generic single-aisle fuselage shell (note, a full 360 degree model is shown in Figure 43) . The inclusion of details such as the floor section, wing, window areas, and doors in the fuselage shell FE model was beyond the scope of this comparative study. Inclusion of the fuselage floor would increase the section moment of inertia but at the same time increase the distance from the neutral axis to the crown. The effect of these details on the sizing results is unknown, but it was considered that the current Qsymm1 results were adequate for comparative study purposes. Results from the Panel 1 sizing study described in Section 2 were used for the FE Panel 1 geometry to develop stresses and SIFs for various pressure-plus-bending scenarios. These FASTER Panel 1 results were then used to determine the FASTER actuator loads for the circumferential crack repeat inspection test phase, circumferential crack limit load test phase, the longitudinal crack turning phase, longitudinal crack repeat inspection test phase, and the panel longitudinal crack residual strength failure load test phase. Only fuselage down bending loads

due to maneuver and gust (during spectrum loading) and fuselage pressure loads were included in the Panel 1 FE models.

The FASTER test facility is described by Tian & Bakuckas (2019). Key aspects of the FASTER actuator load mechanisms are shown in Figure 44. The Qsymm1 to Panel 1 FEM analysis approach described in Figure 43 was necessary to determine the loads for the FASTER test fixture, because the heavy local reinforcement system around the Panel 1 edges introduced load paths in the axial and hoop directions that are not present in the fuselage. Also, the frames and stringers terminate within the test panel. All FASTER axial loads are introduced through the skin, and an edge doubler package is used to distribute the load into the stringers. Also, hoop loads are applied to the skin reinforced by edge doublers while individual actuator loads are directly applied to the frames. Thus, the load paths at the reinforced edges of Panel 1 are complex, especially at the heavily reinforced corners (see Figure 45). The doublers are a cold-bonded build-up of 7075-T6 sheets of various thicknesses.

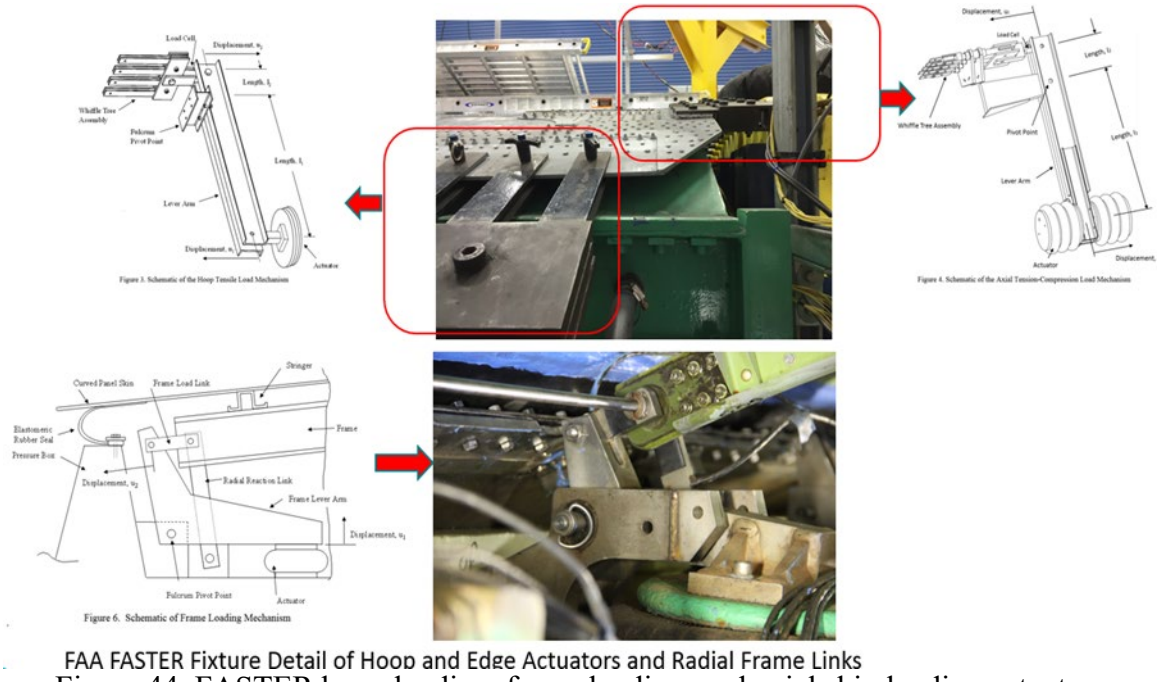

Figure 44. FASTER hoop loading, frame loading, and axial skin loading actuators

English Units

	orange area (in.)	greene area (in.)	red area (in.)	black box area (in.)	blue box area (in.)	purple box area (in.)	yellow box area (in.)	finger doubler area (in.)
outside doubler #2	0.080	no doubler	no doubler	no doubler	no doubler	no doubler	no doubler	no doubler
outside doubler #1	0.080	0.080	no doubler	no doubler	no doubler	no doubler	0.080	no doubler
finger doubler	0.050	0.050	0.050	0.050	no doubler	no doubler	0.050	0.050
skin	0.063	0.063	0.063	0.063	0.063	0.063	0.063	0.063
inside doubler #2	0.075	0.075	0.075	0.075	0.075	0.075	0.075	no doubler
inside doubler #1	0.075	no doubler	no doubler	0.075	no doubler	0.075	0.075	no doubler
total thickness for bearing(mm)	0.423	0.268	0.188	0.263	0.138	0.213	0.343	0.113
total thickness for bearing(in)	0.017	0.011	0.007	0.010	0.005	0.008	0.014	0.004

SI Units

	orange area (mm)	greene area (mm)	red area (mm)	black box area (mm)	blue box area (mm)	purple box area (mm)	yellow box area (mm)	finger doubler area (mm)
outside doubler #2	2.030	no doubler	no doubler	no doubler	no doubler	no doubler	no doubler	no doubler
outside doubler #1	2.030	2.030	no doubler	no doubler	no doubler	no doubler	2.030	no doubler
finger doubler	1.270	1.270	1.270	1.270	no doubler	no doubler	1.270	1.270
skin	1.600	1.600	1.600	1.600	1.600	1.600	1.600	1.600
inside doubler #2	1.910	1.910	1.910	1.910	1.910	1.910	1.910	no doubler
inside doubler #1	1.910	no doubler	no doubler	1.910	no doubler	1.910	1.910	no doubler
total thickness for bearing(mm)	10.750	6.810	4.780	6.690	3.510	5.420	8.720	2.870
total thickness for bearing(in)	0.423	0.268	0.188	0.263	0.138	0.213	0.343	0.113

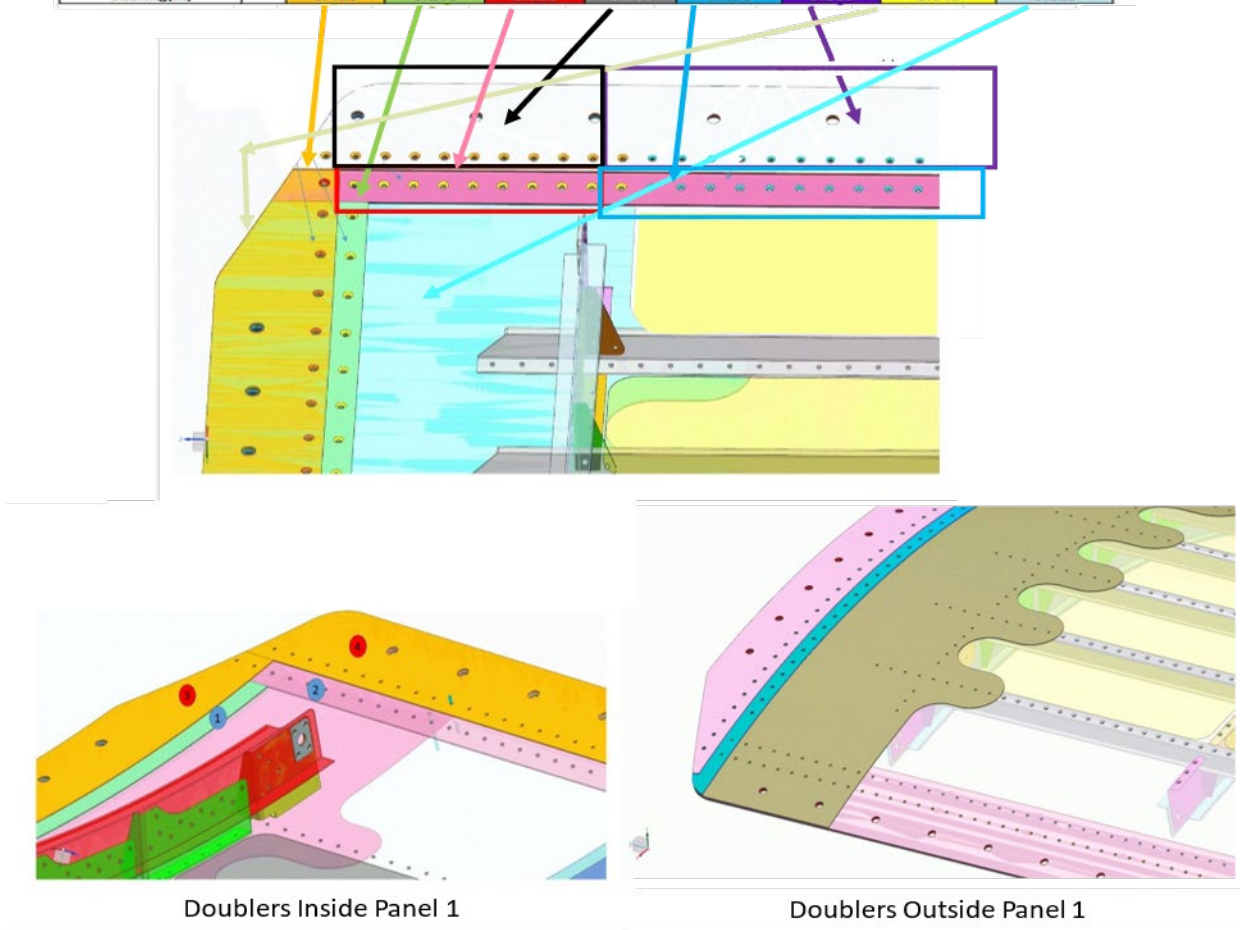

Figure 45. Edge doublers used to transfer load into the test Panel 1

The FASTER test frame applies discrete actuator loads along the axial edges, hoop edges, and frame ends. Each unidirectional skin actuator has four equally loaded arms. Actuator loads were determined by FE analysis and thus were in equilibrium with the applied pressure loading and axial loads simulating bending for the as-designed Panel 1. In the FASTER fixture, Panel 1 is

supported by radial links (see Figure 44), preventing the panel from expanding radially at the attachment points during a pressure loading cycle. This disturbs the panel stresses locally in the link attachment region. These radial links serve to tie down the panel at failure during high pressurization residual strength testing. They also pick up loads to keep the panel in equilibrium if there is an imbalance between applied actuator loads and internal pressure.

In the as-designed Panel 1 FEM models (circa 2016-2017), the actuator loader arms were assumed to apply load tangent to the skin or frames at the panel edges and provide no rotational resistance. Thus, in Panel 1, the bending moment of the axial actuator load arms about the global XX axis through the centroid of the cross-section (centroid of curved panel segment as shown by the top section in Figure 13) was balanced to be zero using the approach shown in Figure 43. That is, the Qsymm1 to Panel 1 iterative FE approach of generating loads for the as-designed 0.055 in. (1.4mm) skin pocket thickness Panel 1 resulted in a balanced loading about the Panel 1 neutral axis (axis XX of the top segment in Figure 13). However, when these loads developed for the as-designed 0.055 in. (1.4 mm) skin pocket thickness Panel 1 were (unknowingly at the time) applied to the as-built 0.059 in. (1.5 mm) skin pocket thickness Panel 1, a small bending moment about the cross-section centroid line XX was produced. Strain gage readings from Panels 1 and 2 and linear variable differential transformer (LVDT) measurements of Panel 2, along with ABAQUS panel FE analysis, confirmed this effect. To correct this loading moment for the FE analysis to better agree with measurements for the as-built Panel 1, the movement of the FE as-built Panel 1 model at all the axial actuator arm loading locations was specified in the radial direction to be +0.039 in. (1.0 mm) in the FASTER fixture coordinate system (-0.039 in. (1.0 mm)) radial movement in the ABAQUS FE model cylindrical coordinate system). New SIFs were generated to evaluate the FASTER as-built Panel 1 crack growth results for these new BCs. Also, these new SIFs for the as-built Panel 1 were used to generate loads for the as-built Panel 2 to ensure the same SIFs were used for Panel 2. The impact of the bending moment increased the circumferential SIFs at the crack tip for all crack sizes, while the increase in skin pocket thickness for the as-built Panel 1 decreased the SIFs for all crack sizes. The net effect (further discussed in Section 6) was a slight change in the SIFs for the as-built Panel 1 from the original solution for the as-designed Panel 1. However, for documentation completeness of the approach, the as-designed Panel 1 analysis results presented in this section are still relevant. Results for the as-built Panel 1 are described in Section 6.

There are four actuators in the FASTER test frame applying loads to the front edge of Panel 1 and 4 actuators applying loads to the rear edge. Each actuator has 4 equally loaded arms for a total of 32 load points (but only the 8 actuators total loads are considered independent loads). There are 7 actuators in the FASTER test frame applying loads to each hoop edge of Panel 1,

each with 4 equally loaded arms, for a total of 56 load points (but only the 14 actuators total loads are considered independent loads). Finally, there are 12 independently driven frame actuators that load the 6 frames at each end of the frame.

Using symmetry, the Qsymm1 model for the Panel 1 location represents a continuous cylinder and is loaded by a uniform axial end load intensity and an internal pressure. The uniform end loads included the axial pressure contribution for a closed cylinder as well as an effective uniform axial load intensity representing the bending condition at the top of the fuselage at the test Panel 1 location. These Qsymm1 applied load intensities at STA 38 in the crown represent the conditions that occur at the center point of Panel 1. The geometry of the skin (including pad-ups), stringer, and frames for STA 38 in the FASTER Panel 1 FE model are the same as the Qsymm1 FEM model except for the panel edge doubler reinforcements in the Panel 1 FE model. The FASTER loads for Panel 1 will not be the same as the internal reaction loads in the Qsymm1 model along the edges outlining the location of Panel 1 in the Qsymm1 model. This is because of the additional loads needed to stretch doublers in Panel 1 to conform to strains predicted by Qsymm1 at the Panel 1 location. Also, the FASTER Panel 1 has the radial links (Figure 44) constraining the frame ends from radial displacement, whereas the Qsymm1 fuselage model represents a cylinder expanding radially and stretching axially in response to the hoop pressure loads and the axial loads.

The FASTER radial links attached to frames ends to prevent the test panel frame from displacing radially locally at the frame attach points. This local radial displacement restriction does not occur in the Qsymm1 pressure loaded stiffened cylinder, since there is a uniform finite radial displacement under pressure loading around the circumference. Therefore, these FASTER radial links slightly disrupt the stresses locally in the Panel 1 test article from the ideal stiffened cylinder pressure stress state locally at the links. For these reasons described above (as -built versus as-designed geometry, load introduction edge doublers, and radial links), the FASTER loads for Panel 1 were determined using the Panel 1 FE model in an iterative approach to determine the actuator loads that provide the same SIFs versus crack size as the Qsymm1 FE model. This FASTER load development is done separately for each of the three crack phases, the circumferential two-bay crack limit load phase, and the longitudinal two-bay crack residual strength phase of the Panel 1 test.

The iterative procedure involved searching for a set of FASTER actuator loads that provide the best stress fit to the SIF versus crack size results obtained from the Qsymm1 quarter symmetry cylindrical fuselage FE model for the same pressure and effective axial load due to bending load scenarios. To apply this method in a rigorous manner, FASTER Panel 1 loads would have to be

developed for many crack sizes. However, changing the actuator loads during the test would be too complex. Fortunately, it was found that one set of loads could provide a good fit to the SIF results for the smaller cracks (where most of the life occurs), while at the larger cracks the stress intensity solutions were kept within 4% of the Qsymm1 results. Using this criterion, it was determined that adjustments to FASTER loading during crack growth testing were not necessary for any of the test phases.

4.2 Qsymm1 FE model geometry for the as-Designed Panel 1

The crown panel location used for this program was chosen to be at STA 38, which is forward of wing leading edge. At this location, a similar skin thickness was required to meet both the longitudinal and circumferential repeat inspection goals (see Figure 39). The Qsymm1 fuselage FE model (Figure 46) was developed for the as-designed skin thickness (0.055in. (1.4 mm) in the pocketed region) and stringer/frame dimensions determined in the sizing study (Figure 47 and Figure 48). The stiffened cylinder FE model, Qsymm1, was used to generate the target stress and damage tolerance stress intensity solutions for the Panel 1 FE model. These SIF solutions were used to develop FASTER loading for the Panel 1 test article. The 2524-T3 skin radius is 74 in. (1879.6 mm). A pocketed skin construction was used (see, for example, schematics in Figure 49). Details are provided in Appendix A for the as-designed Panel 1 skin thickness of 0.055 in. (1.4 mm) in the pocketed areas and 0.063 in. (1.6 mm) in the pad-up areas. There are 10 frames and 17 stringers in the Qsymm1 FE fuselage model. The two-piece 7075-T6 shear tie/frame design used for Panel 1 is shown in Figure 47. The frame spacing is 20 in. (508 mm), and the Afr/Bt ratio of frame area to skin area is 0.294. The 7150-T77511 stringer is shown in Figure 48. The stringer spacing is 7 in. (177.8 mm), and the As/Bt ratio of the stringer cross-section area to skin cross-section area is 0.393. An elastic modulus of 10.2 Msi (70.3 GPa) was used for the skin, and 10.4 Msi (71.7 GPa) was used for the stringers and frame. The rivets fastening the stringers/frames to the skin were NAS1097KE5 (5/32 in. (3.97 mm) diameter, 100° countersunk, 7050-T73). Material properties used in the FE models are included in Appendix B.

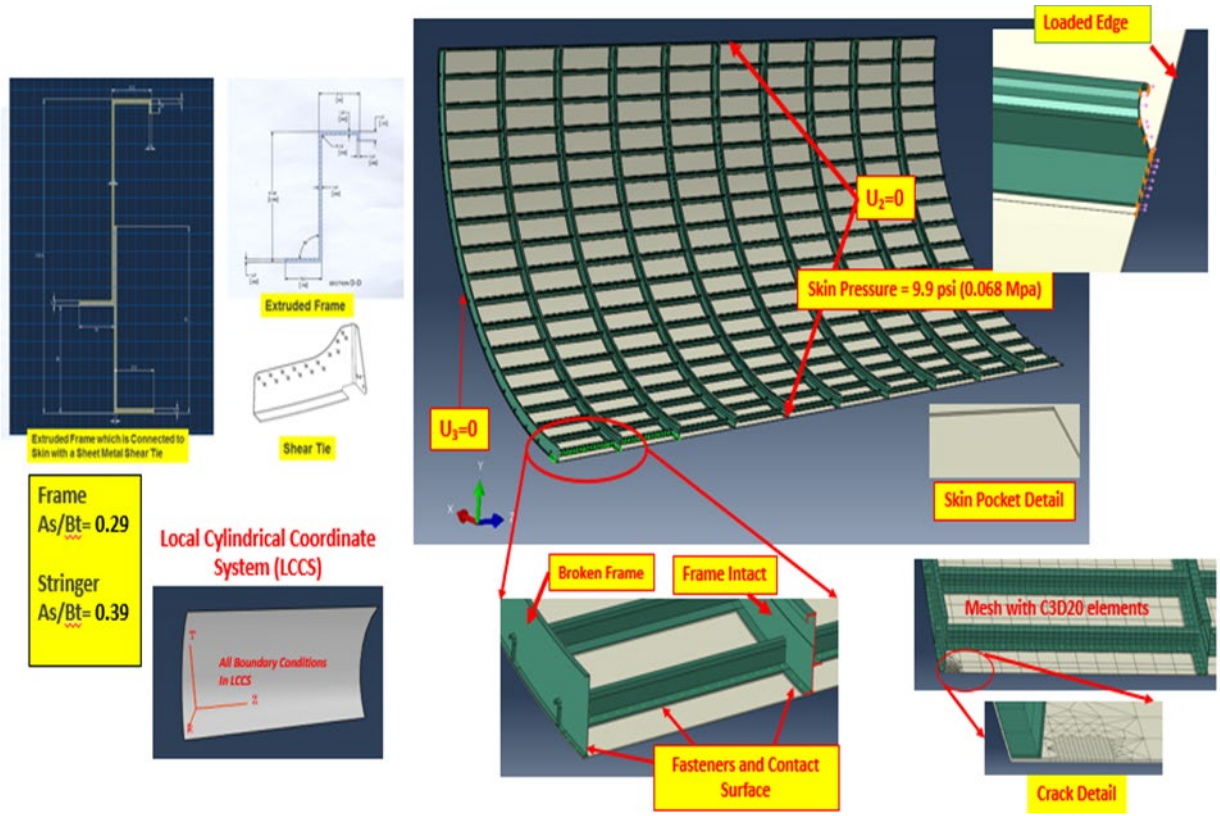

Figure 46. ABAQUS Qsymm1 fuselage FE model for the as-designed Panel 1 with 0.055 in. skin thickness in the pocketed regions

The commercial code ABAQUS (Hibbit, Karlson, & Sorenson, 2018) was used for the Qsymm1 and Panel 1 FEM analysis. To obtain more representative SIFs for crack growing in the skin panel, ABAQUS 3D solid C3D20 elements were used for all features, including skins, frames, shear ties, and stringers. The cylindrical coordinate system (U1=radial, U2=hoop, U3 = axial length direction of fuselage) was shown in Figure 46.

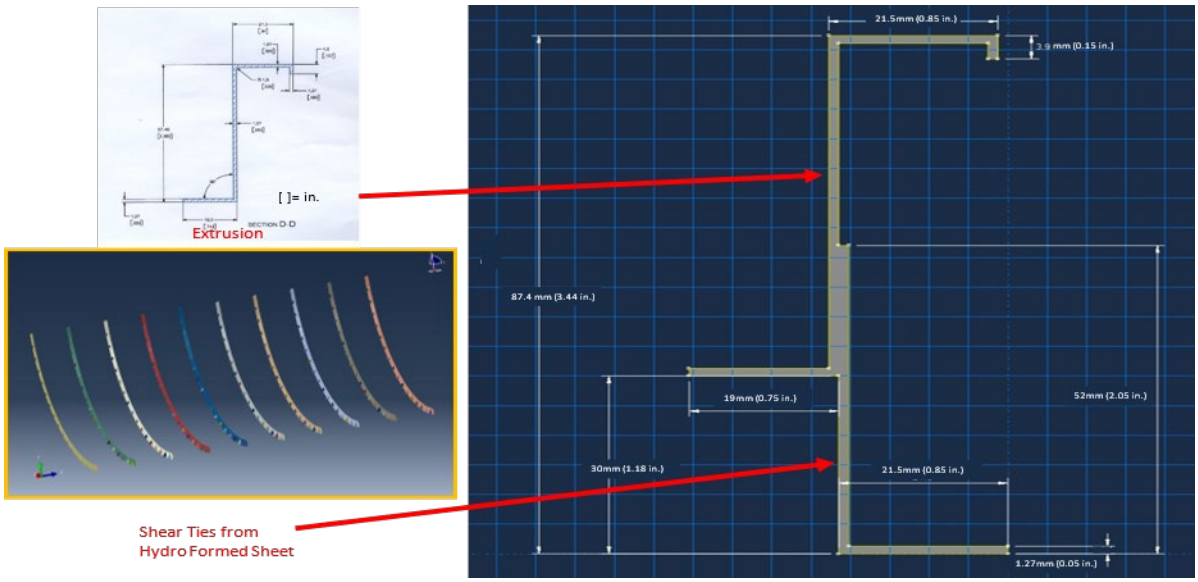

Figure 47. The assembly of frames (left) and the cross-section of the frame/shear tie (right)

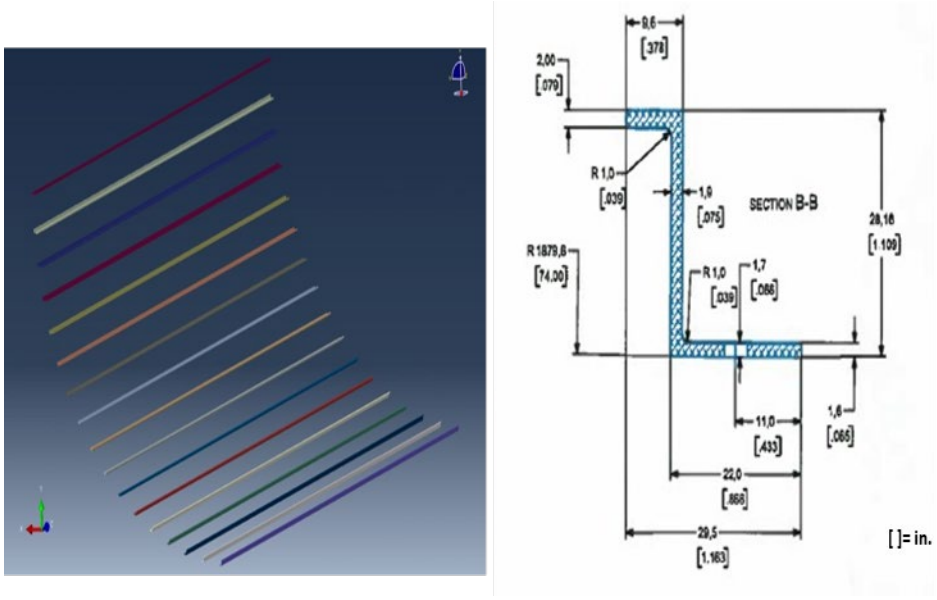

Figure 48. 7150-T77511 stringers in the FEM model of Panel 1

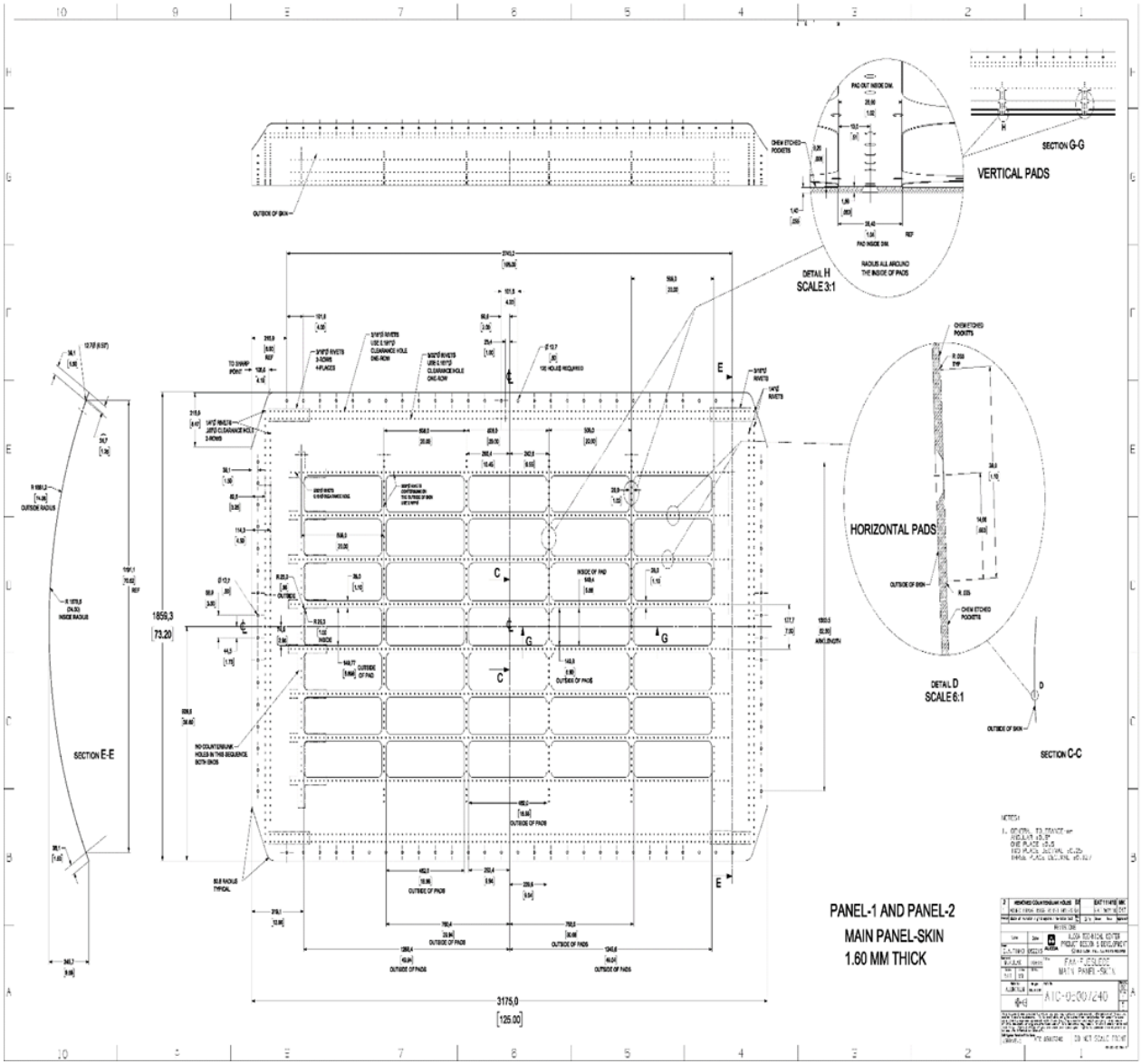

Figure 49. Pocketing of Panel 1 skin

4.3 Qsymm1 results for as-designed Panel 1 (2524-T3, 0.55 in. (1.4mm) skin) for 9.9 psi (0.068 MPa) pressure differential

An analysis was conducted using the Qsymm1 stiffened cylinder model (Figure 50) to estimate the stresses/strains in the fuselage crown with no crack damage and a differential pressure of 9.9 psi (0.068 MPa). The EMST metallic test panels were targeting an elevated cabin pressure of 9.9 psi (0.068 MPa) to compete with composite fuselage designs where the cabin differential pressure was expected to increase. A cylindrical coordinate system was used to apply cylindrical symmetry BCs. An inside pressure load of 9.9 psi was applied (0.068 MPa). The axial loads from the closed cylinder due to pressure were applied manually since the pressure bulkheads were not modeled. The Flugge solution for the 74 in. (1.88 m) radius stiffened cylinder was used to distribute the axial load intensity (press x rad/2) between skin and stringer and applied at the end of the Qsymm1 FE model opposite from the symmetry plane.

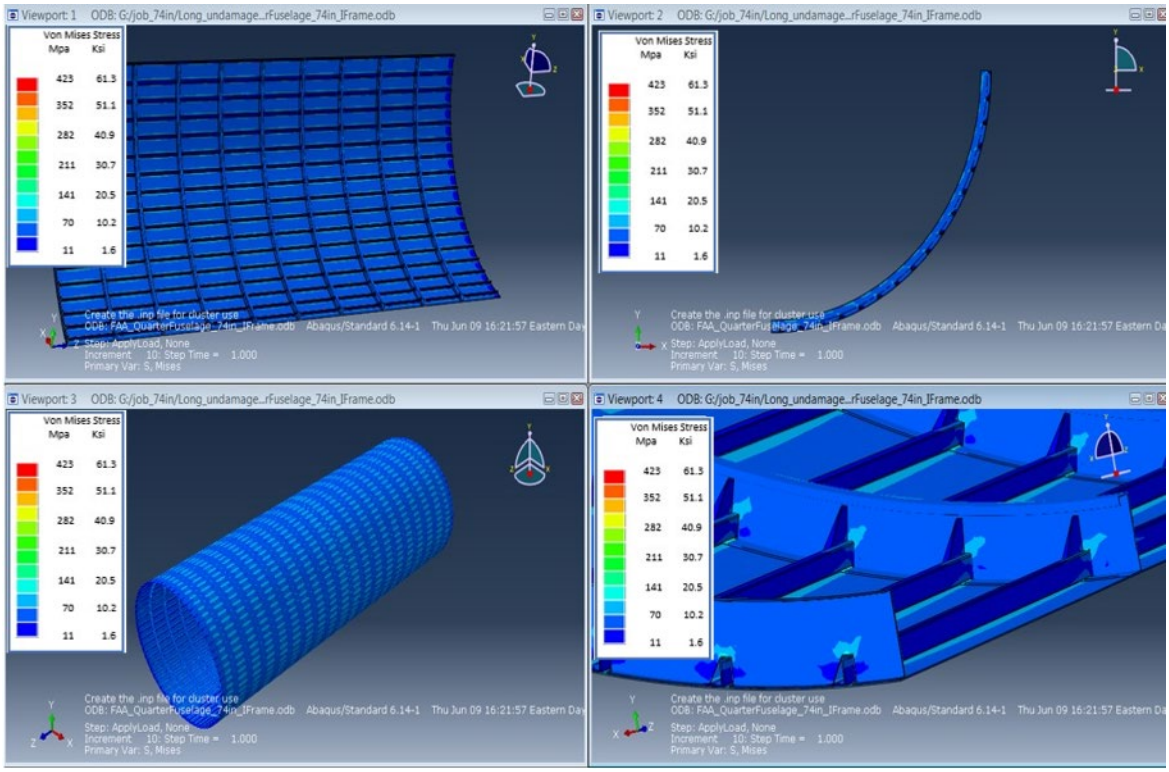

Figure 50. ABAQUS Qsymm1 pocketed quarter symmetry fuselage FE model

Since the axial load intensity is based on equilibrium, any skin to stiffener/frame difference between the Flugge distribution of skin to stringer were expected to be corrected in the FE model a short distance from the cylinder end. A geometrical non-linearity correction (NLG) was used in the ABAQUS solution to correct for large displacement movement. Also, for crack damage, the

NLG correction was used to account for pressure bulging effects on the crack and plasticity effects for the residual strength analyses. The hoop and axial stresses for the undamaged as-designed Qsymm1 case at 9.9 psi (0.068 MPa) pressure are plotted in Figure 51. The skin pillowing stress variation between frames and stringers can be seen.

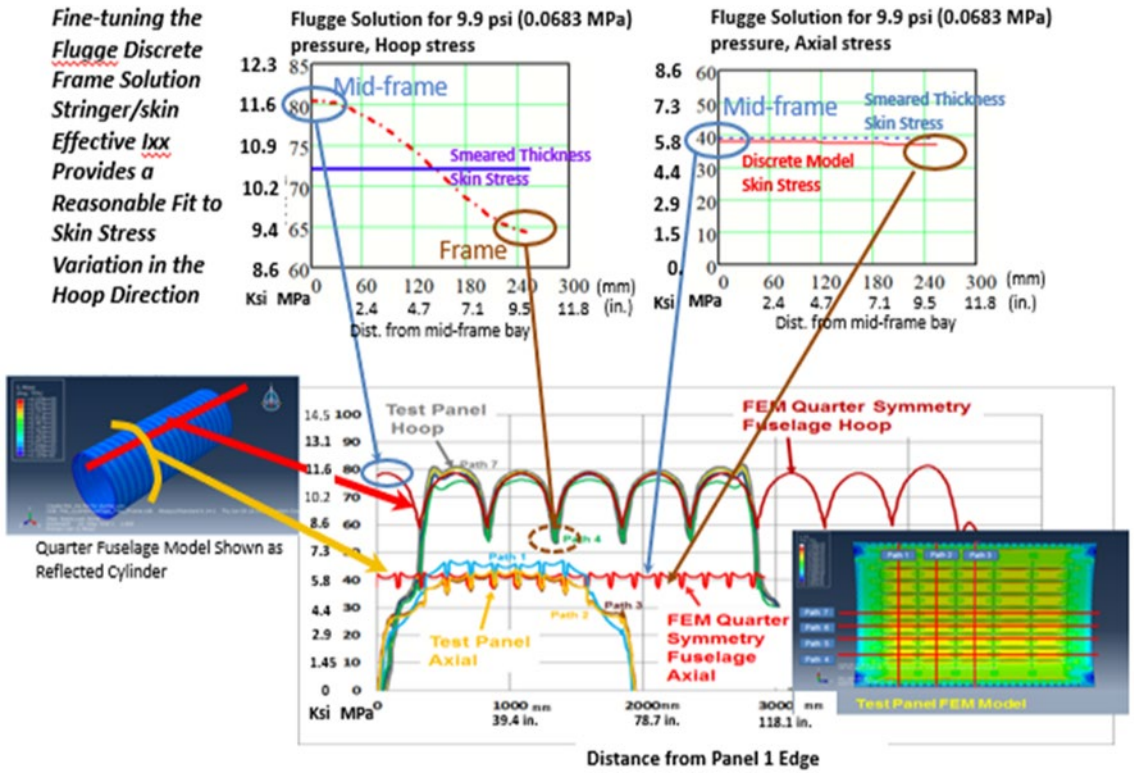

Figure 51. Comparison of ABAQUS panel 1 9.9 psi (0.068 MPa) pressure results with Flugge smeared stringer/smeared frame and discrete frame solutions

The ABAQUS FEM results are compared with the Flugge (1952) predictions in Figure 51. In this case the Flugge smeared stiffness results appear to be representative of the averaged FEM stress results. The FEM skin stresses are also compared with the Flugge *discrete frame/smeared stringer* solution in Figure 51. This Flugge discrete solution also predicts lower skin stresses at the frames and stringers similar to the Qsymm1 model as a result of the frames and stringers restricting the radial skin expansion. This results in the pillowing stress variation between stringers and frames shown in Figure 51 and Figure 52. Some differences were expected, as the discrete frame Flugge solution does not allow for a pad-up region in the approach used. Hence, the pad-up was smeared into the skin using the ratio of pad-up volume to skin volume. Also, in the Flugge solution, the stringers are not discretely modeled but are smeared into the skin using

the ratio of stringer volume to skin volume. and in addition, a stringer correction is used to provide an effective resistance to bending in the axial direction. Note that for the discrete Flugge solution, only general recommendations are provided in the original Flugge paper (1952) to determine the effective skin width to calculate this axial bending stiffness correction. Separate FEM analyses were conducted (Kulak & Sklyut, n.d.) to fit this bending stiffness correction to a FEM model of a similar size aircraft and used for the results in Figure 51.

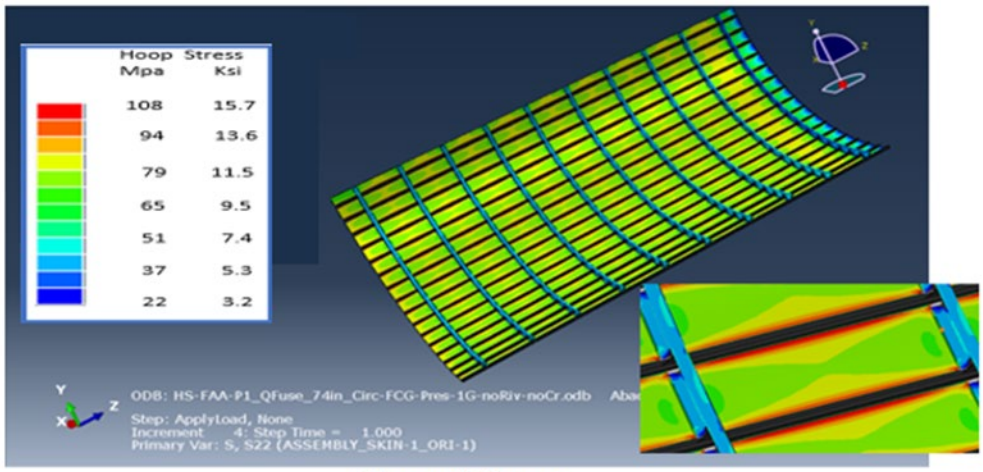

Hoop Stress

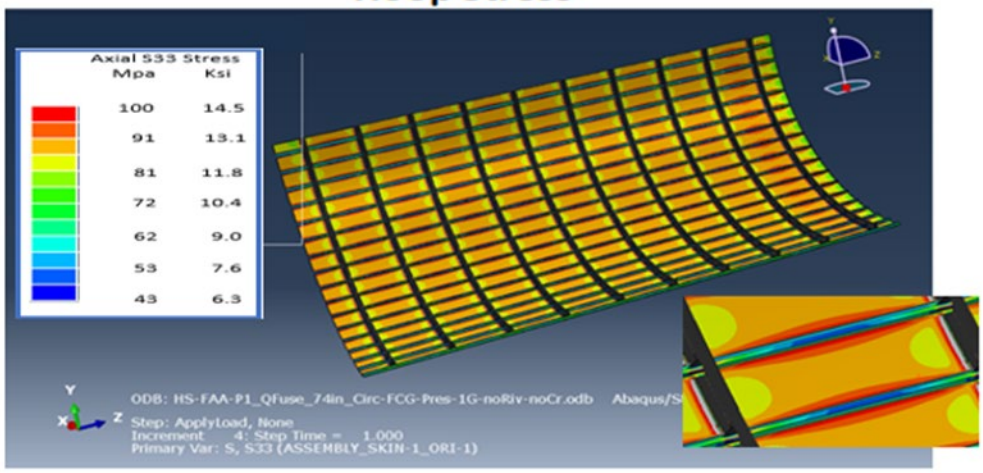

Axial Stress

Figure 52. Qsymm1 axial and hoop stress results for 1G + 9.9 psi (0.068 MPa)

Axial and hoop stress and strain results for the 1.04G + 9.9 psi (0.068 MPa) pressure condition for both the inside and outside skin surface are shown in Figure 53 and Figure 54. The 1.04G + 9.9 psi (0.068 MPa) loading condition was used as the “equivalent constant amplitude load” for the “as designed” FASTER Panel 1 testing for circumferential crack growth. This condition was determined by matching the K-control spectrum crack growth results on M(T) specimens to

constant amplitude crack growth in K-Control M(T) results (described in Section 5). Axial and hoop stresses and strains are shown in Figure 53 and Figure 54 for both the inside and outside skin surface for a circumferential path across stringers at the mid-bay location and for a longitudinal path across frames at the mid-bay location.

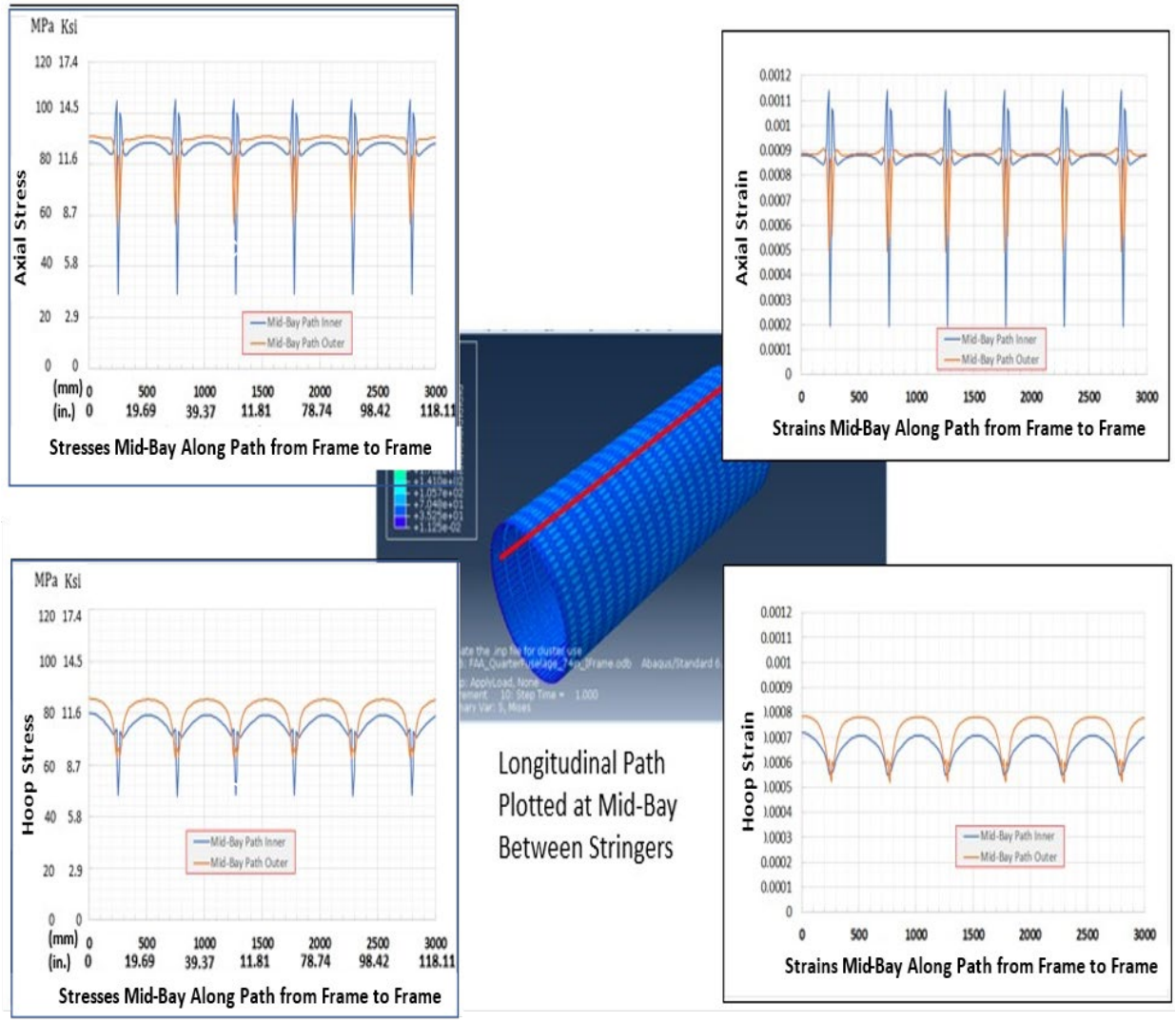

Figure 53. Qsymm1 axial and hoop stresses for 1.04G + pressure along a longitudinal path

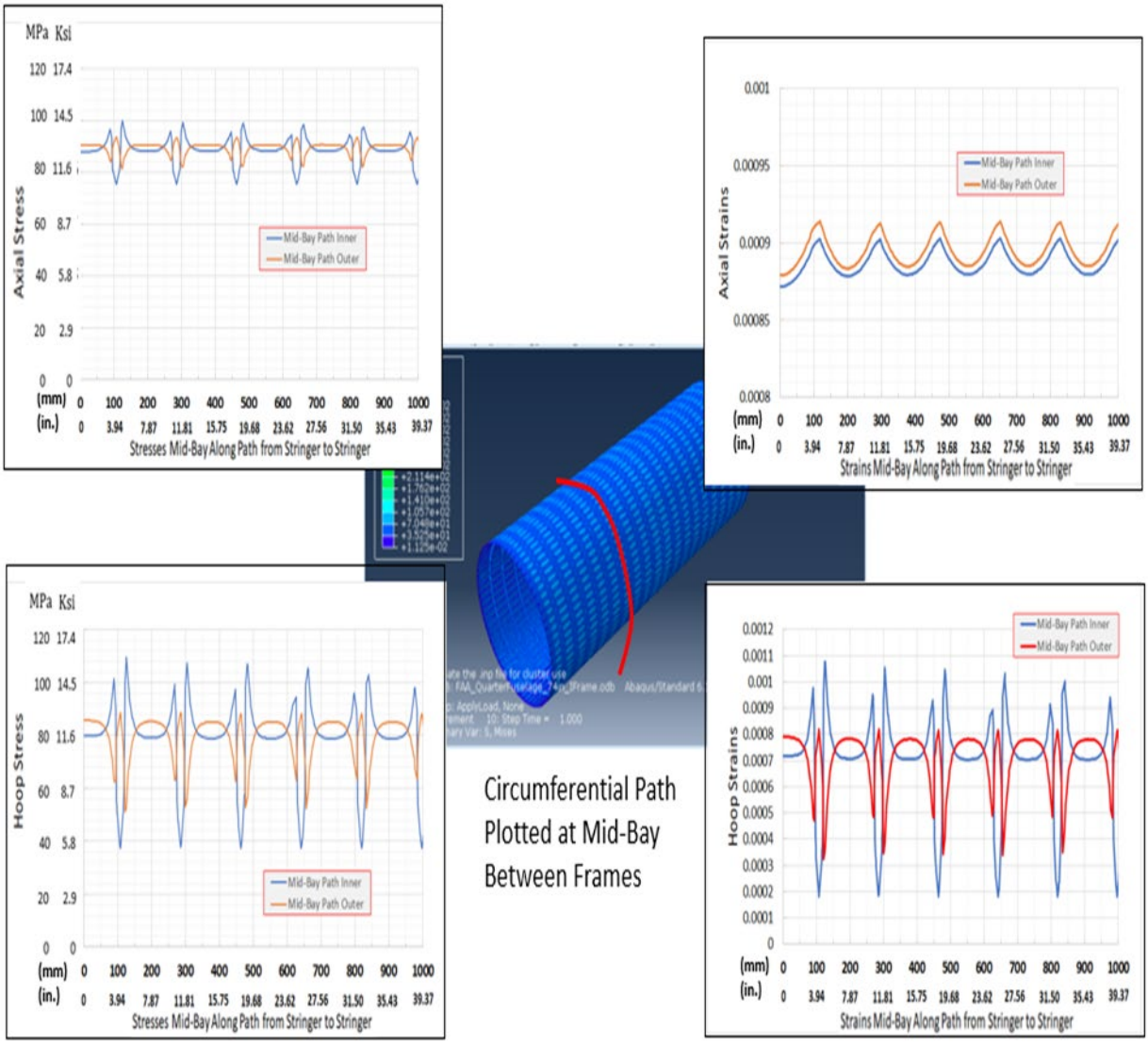

Figure 54. Qsymm1 axial and hoop stresses for 1.04G + 9.9 psi along a circumferential path

4.4 Qsymm1 circumferential stress intensity factors for as-designed Panel 1

The crack scenarios in the FASTER full-scale Panel 1 test (2524-T3) focus on repeat inspection intervals (circumferential and longitudinal) which were determined to be the critical sizing criterion for the as-designed crown Panel 1 at location STA 38. The stringer was assumed broken at the mid-bay skin to stringer fastener for the circumferential crack repeat inspection scenario, and a skin crack was grown from under the broken stringer in both directions symmetrically in the circumferential direction. For this program, the repeat inspection interval was defined to be the life of this skin crack from an inspectable size of 1.0 in. (25.4 mm) half-crack length to the full two bay crack when the skin crack reaches the adjacent stringers. For the circumferential

crack repeat inspection, a goal of two C-Check intervals, or 4 years, was chosen for the EMST panels, assuming a usage of 4 flights per day. This amounts to about 6,000 flights (rounded) and, considering a safety factor of two, a final goal of 12,000 flights was set for the repeat inspection. Thus, a total target life of 12,0000 flights was used to set the skin working stress target for sizing Panel 1 for the circumferential crack repeat inspection goal. The working stress target at 1.04G + 9.9 psi (0.068 MPa) of 13 ksi (89.6 MPa) equivalent constant amplitude axial skin stress was determined using K-control testing, as described in Section 5.

The ABAQUS Qsymm1 model was used to generate the total SIFs, Ktotal(a), for the circumferential cracks of various crack half-lengths, a. For the circumferential crack Qsymm1 FE model, non-linear rivets the load/displacement values in Table 2 were estimated and include hole elongation and bearing yielding. These were used in the crack bay for the frame and stringer connections to the skin. Surface-to-surface contact constraints were used in the crack bays to prevent penetration of the skin by the stringers and frames, as shown in Figure 55.

Table 2. Fastener nonlinear load displacement for NAS1097KE5 rivet (5/32 in. [3.97 mm] diameter, 100 degrees countersunk, 7050-T73) and NAS1097KE6 rivet

Non-linear load displacement relationship for rivets								
3/16 7050 rivet					**5/32 7050 rivet**			
F(N)	F(kips)	delta(in)	delta(mm)		F(N)	F(kips)	delta(in)	delta(mm)
0	0	0	0		0	0.00	0	0
3247	0.73	0.0029	0. 07366		2499	0.56	0.0020	0.0518
4804	1.08	0.0102	0.25908		3697	0.83	0.0072	0.1823
5560	1.25	0.0286	0.72644		4279	0.96	0.0201	0.5111
5560	1.25	0.06	1.524		4279	0.96	0.0422	1.0723

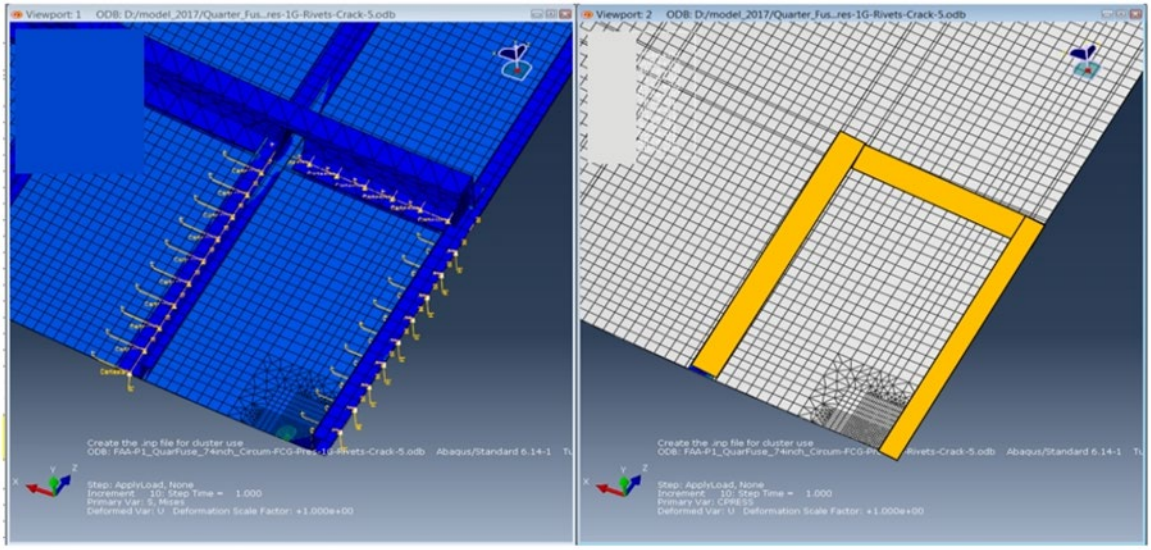

a) fasteners around double symmetry line crack b) contact surfaces around double symmetry line crack

Figure 55. Definition of rivet locations and contact surfaces for the ABAQUS Panel 1 circumferential crack growth in the skin with a broken stringer

The circumferential crack was modeled to act along the axial symmetry plane at the cylinder end. Plots of Qsymm1 results for a large circumferential crack in Figure 56 show the stresses and deformations as the crack approaches the adjacent stringers.

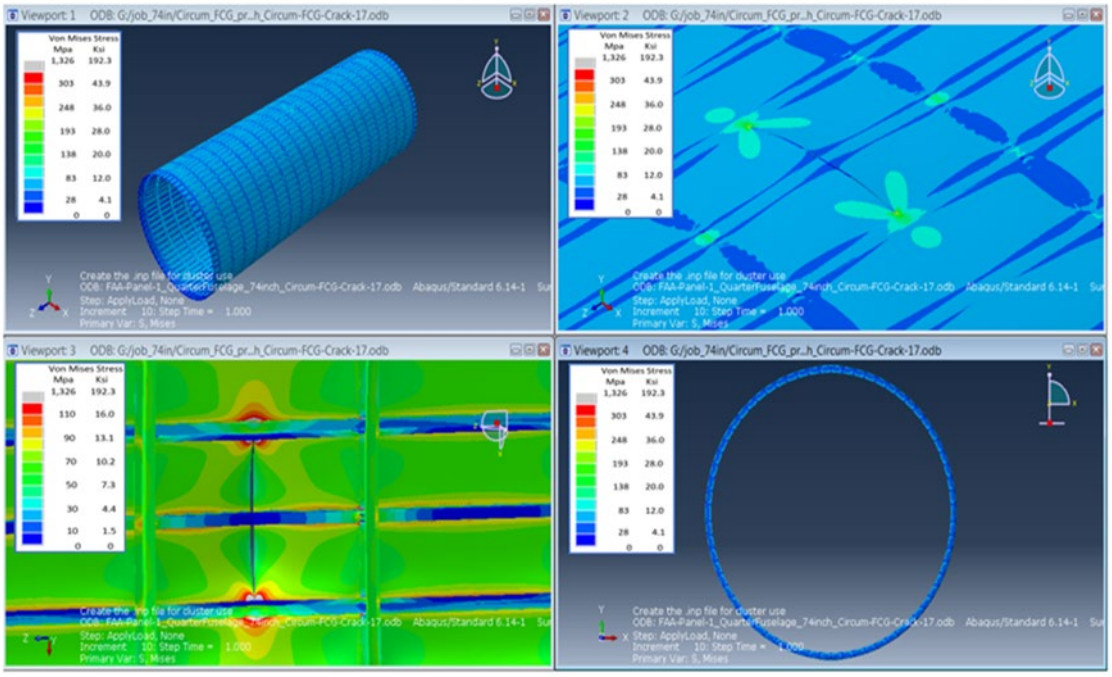

Figure 56. Qsymm1 results for circumferential crack growth with a broken stringer

The quarter symmetry Qsymm1 model is loaded by applying the 9.9 psi (0.068 MPa) pressure internally. Qsymm1 is also loaded at the cylinder end away from the symmetry plane by the axial load intensity from pressure plus the effective axial load intensity due to bending at the STA 38 crown location. As previously described in Section 1, simplifying assumptions were made regarding the relationship between the axial stresses due to bending in the fuselage and the effective axial loads in Panel 1. To simplify this axial loading due to bending, it was assumed the axial load intensity was constant along the Panel 1 leading and trailing edges. Also, it was assumed this axial load intensity did not vary between Panel 1 leading and trailing edges. The Panel 1 geometric mid-point axial load intensity solution from the simplified fuselage bending model (mid-panel at top of crown) was used as the representative axial load intensity for bending for Panel 1. This axial load intensity was applied as a constant load at the trailing edge of the Qsymm1 FE model with symmetry condition applied at the leading edge. This definition of axial load due to bending when applied to the Qsymm1 and the Panel 1 FE models results in the same stress distribution in all interior bays and is similar to the axial component of pressure. Thus, the axial loads due to pressure and those due to bending can be superimposed.

SIFs for a circumferential crack are shown in Figure 57 for the as-designed Panel 1 geometry at 9.9 psi (0.068 MPa) pressure, resulting in a Flugge characteristic skin stress of 5.576 ksi (38.4 MPa) plus the 1G bending skin stress of 7.130 ksi (49.16 MPa).

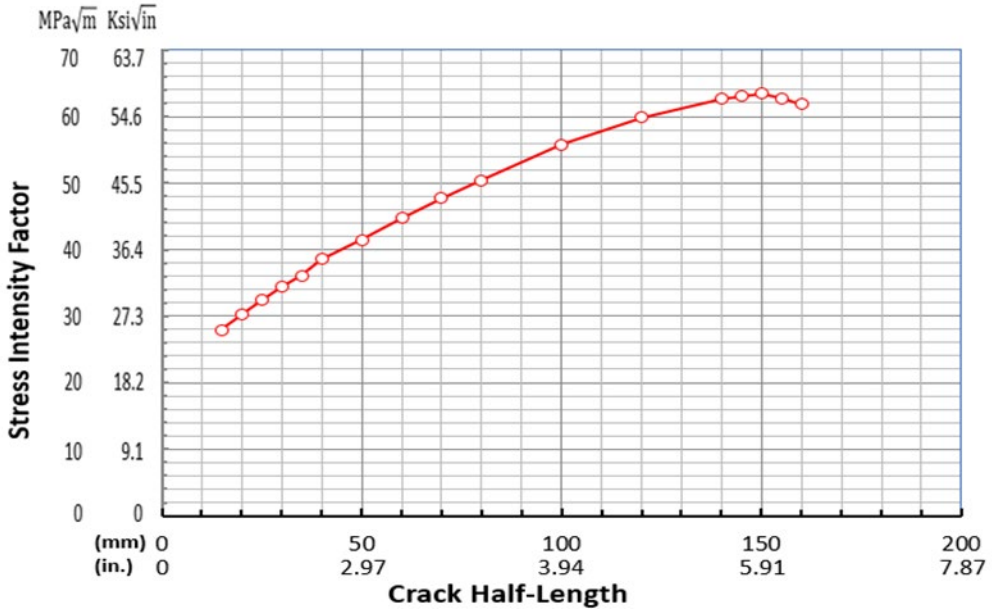

Figure 57. SIFs, Ktotal, for Qsymm1 in the circumferential skin crack under a broken stringer

Results for pressure only, 1G bending only, and combined pressure + 1G bending are plotted in Figure 58. The crack solution for 9.9 psi pressure + 1G compares well with a superimposed solution of pressure and 1G bending run verifying that superposition was applicable in the circumferential direction, since bulging is small. This shows that superposition of axial loads due to bending, the axial component, and pressure is possible for circumferential cracks.

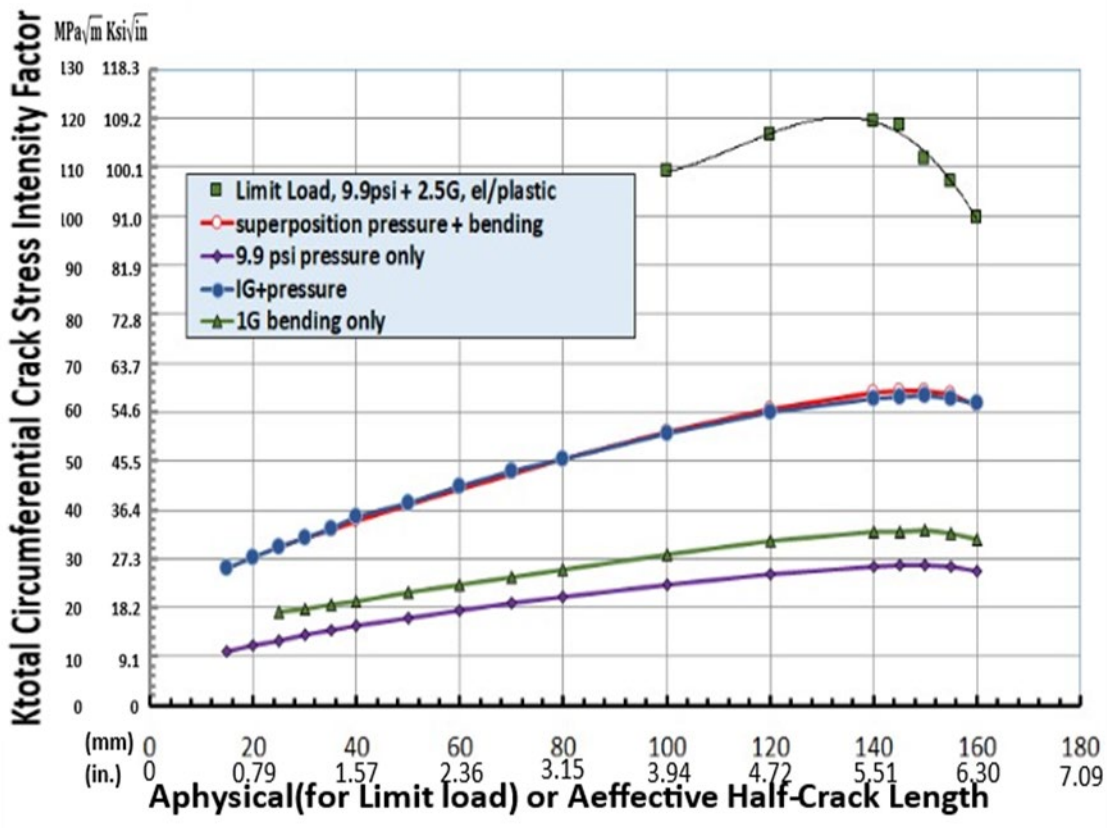

Figure 58. SIFs for a circumferential crack under a broken stringer

Finally, the results for a Qsymm1 analysis for the as-designed, 0.055 in. (1.4 mm) pocketed skin Panel 1 geometry for the limit load condition of 2.5G (resulting in 17.825 ksi [122.9 MPa] skin axial stress component from bending stress) plus the axial component of 9.9 psi (0.068 MPa) differential pressure (resulting in 5.576 ksi [38.4 MPa] stress) were shown in Figure 58 (total average skin axial stress = 23.401 ksi).

The material properties in Figure 59 were used for this non-linear rivet, elastic/plastic skin/stringer/frame solution. Since the plastic zone influences the crack compliance, the interpretation of the crack lengths in Figure 58 is “Aeffective” for the elastic FE solutions and “Aphysical” for the elastic/plastic FE solution at 2.5G + 9.9 psi (0.068 MPa). The crack tip stress intensities at 2.5G + 9.9 psi (0.068 MPa) pressure in Figure 59 were well below the Aeffective 2524-T3 L-T R-curve toughness value shown in Figure 60 (Wang, 2016; Bucci, Warren, &

Starke, 2000). The crack tip stress intensities were still expected to be below the R-Curve had it been measured as an Aphysical R-Curve. The primary objective of this non-linear plasticity analysis at limit load was to demonstrate a low level of permanent deformation at limit load such that the FASTER Panel 1 crack could be repaired for the next phase of testing.

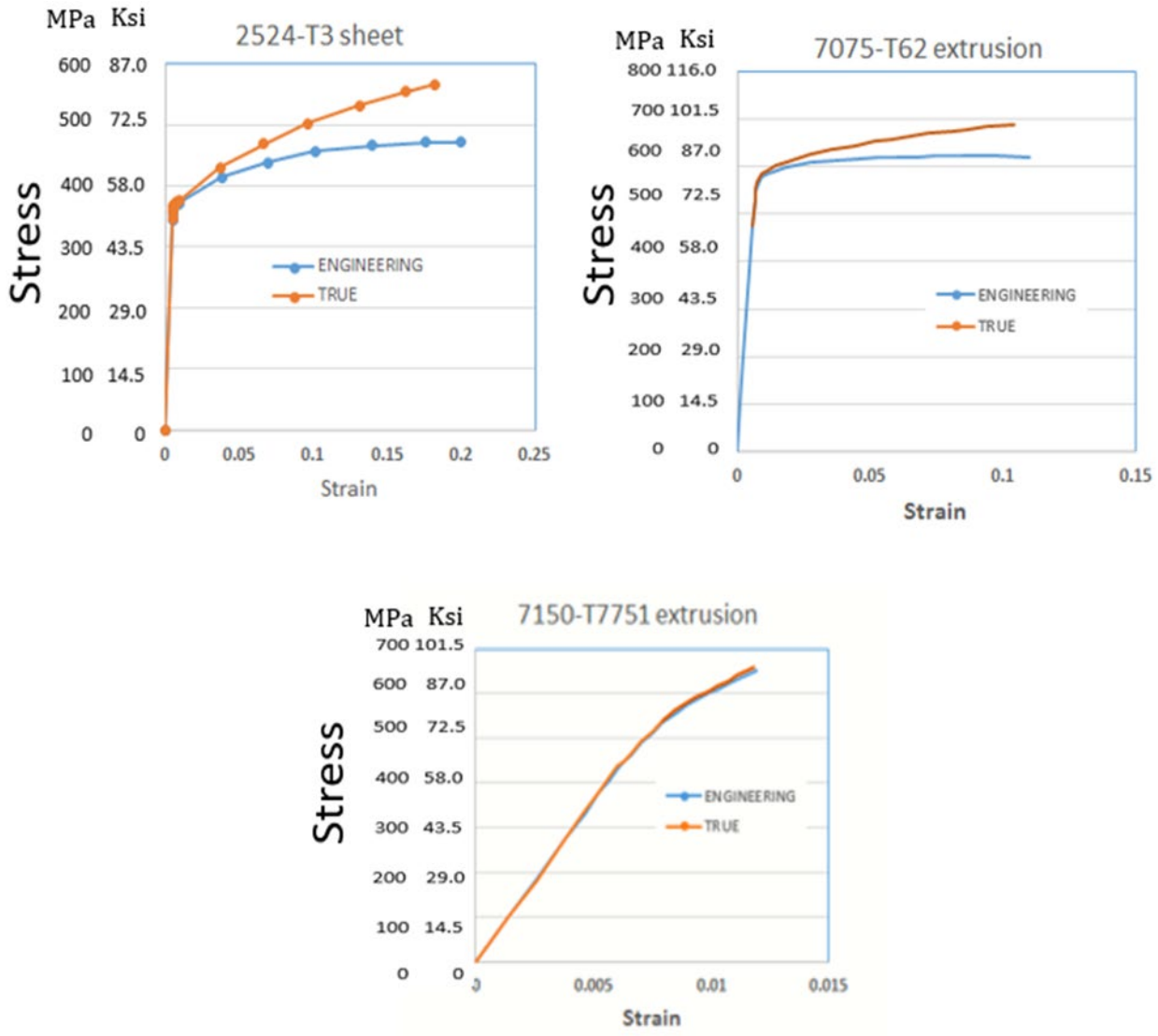

Figure 59. SIFs for a circumferential crack under a broken stringer

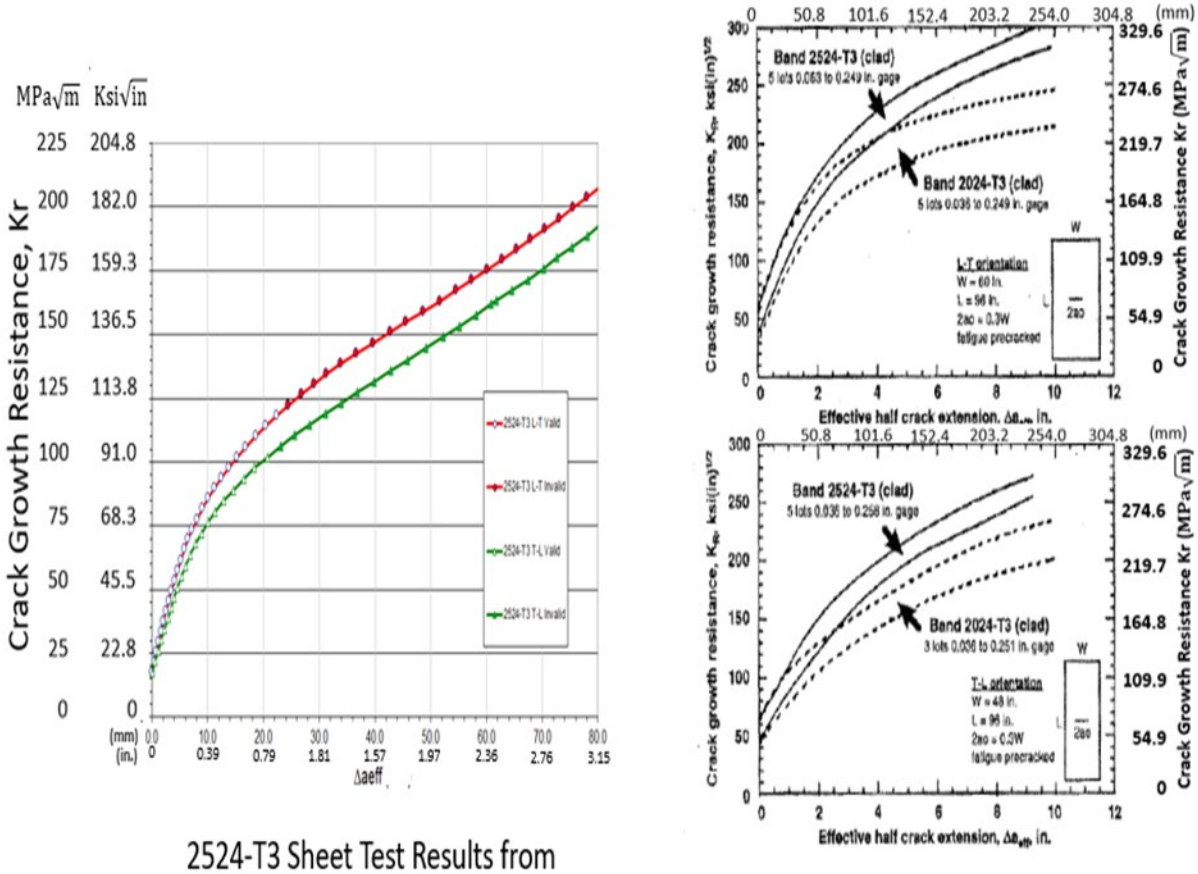

Ref. R.J. Bucci(former Alcoa), C.J Warren(former Alcoa), E.J Starke., "Need for New Materials in Aging Aircraft Structures", Journal of Aircraft, Volume 37, Number 1, Jan-Feb 2000.

Figure 60. Measured R-curves from 2524-T3 sheet used in Panel 1 and published data from wider 2524-T3 test panels

4.5 Qsymm1 longitudinal stress intensity factors for the as-designed Panel 1 (0.055 in. (1.4 mm) skin in pockets)

For the longitudinal crack repeat inspection scenario, the frame was assumed broken at the mid-bay skin-to-frame fastener, and a longitudinal skin crack was grown in the skin from under the broken frame fastener in both axial directions symmetrically. The repeat inspection interval in this program was defined as the life of this skin crack from a starting inspectable size of 1.0 in. (25.4 mm) half-crack length crack to the critical crack size. In this case, since a design goal was specified to carry a full two-bay crack at limit load, the life was defined when the crack reaches the adjacent frames. The repeat inspection goal was chosen to be 6,000 flights with a safety factor of 2.0. Thus, a total target life of 12,000 flights was used to set the working stress target for sizing Panel 1 for this longitudinal repeat inspection goal. A Flugge characteristic skin hoop

stress target of 10.35 ksi (71.4 MPa) at 9.9 psi (0.068 MPa) pressure was used based on previous studies (Kulak, n.d.). No axial stress from equivalent bending was used to be conservative.

For a frame broken at a fastener, the highest loaded rivets are the first adjacent intact rivets. To obtain a more rigorous stress intensity solution the rivets in the stringers and frames in the bay surrounding the cracks were included in the FE model. These rivets were modeled as non-linear springs with the load displacement relationship previously described in Table 1. Contact conditions were used between the stringer and frame attach flanges and skin in the local bay surrounding the crack to prevent penetration of the skin by the stringers and frames.

Stress plots of a Qsymm1 analysis for a half crack length of 5.9 in. (150mm) with a broken frame are shown in Figure 61. To obtain a better estimate of the SIF using the J integral approach, a finer in-plane mesh at the crack tip in the skin was subsequently used to develop the final as-built Panel 1 SIFs after a mesh convergence study in early 2020 (see Section 6). Unfortunately, at the start of the program, only one element was used through-the-skin thickness of the Qsymm 1 FE model of the as-designed Panel 1 geometry shown in Figure 61. The total SIFs, Ktotal, from the elastic, large displacement Qsymm1 FEM analysis for 9.9 psi (0.068 MPa) pressure load are plotted in Figure 62. The J integral values from the sheet mid-plane was used. The total SIF, Ktotal, was obtained by using equation $K = \sqrt{EJ}$ for the plain stress condition, where E is the skin elastic modulus and J is the J-integral.

Subsequent to the discussion above, the updated Qsymm1 model representing the as-built Panel 1 geometry included several changes, which had increasing and decreasing effects on Ktotal. These included the increased as-built pocket thickness in Panel 1; improved modeling conditions for axial load arms and skin hoop edge load arms based on experimental measurements; and an increased mesh density through the skin thickness. This will be discussed in detail in Section 6.

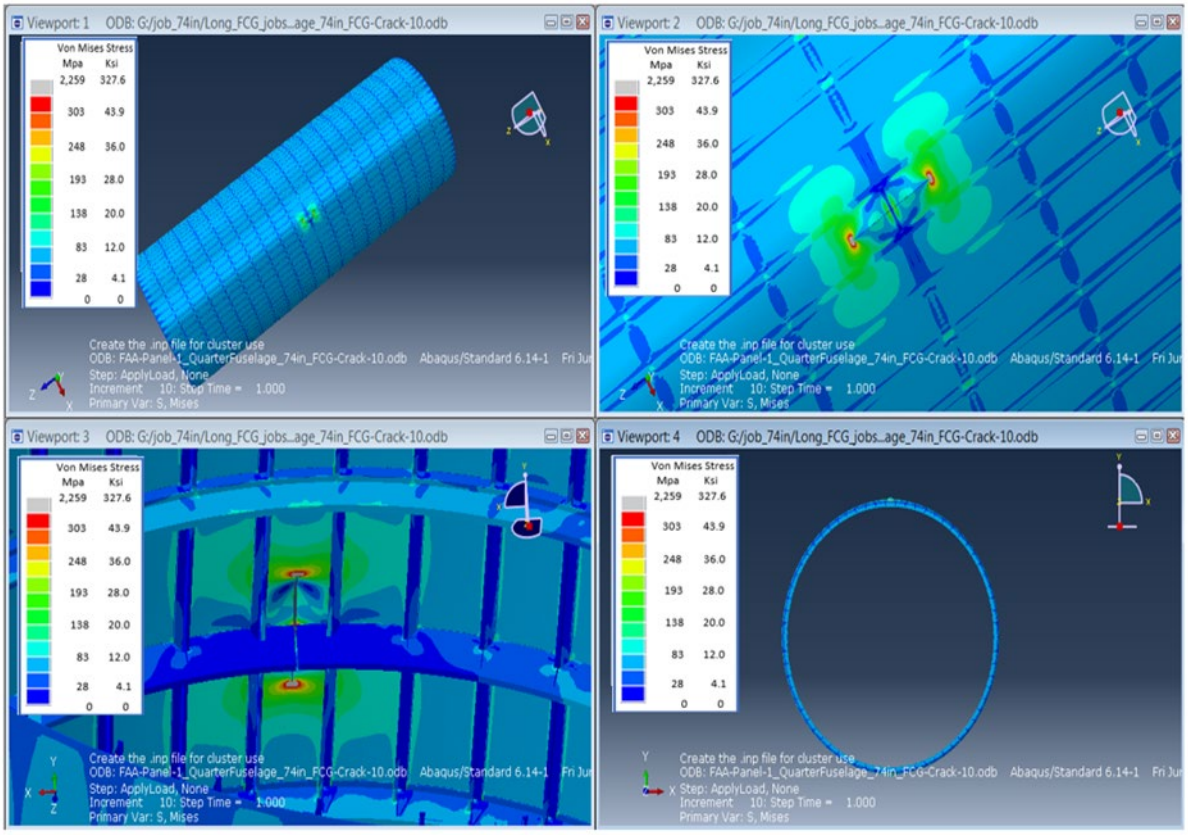

Figure 61. Results for the quarter symmetry model for 150mm (5.9 in.) half-crack length in the longitudinal direction with a broken frame

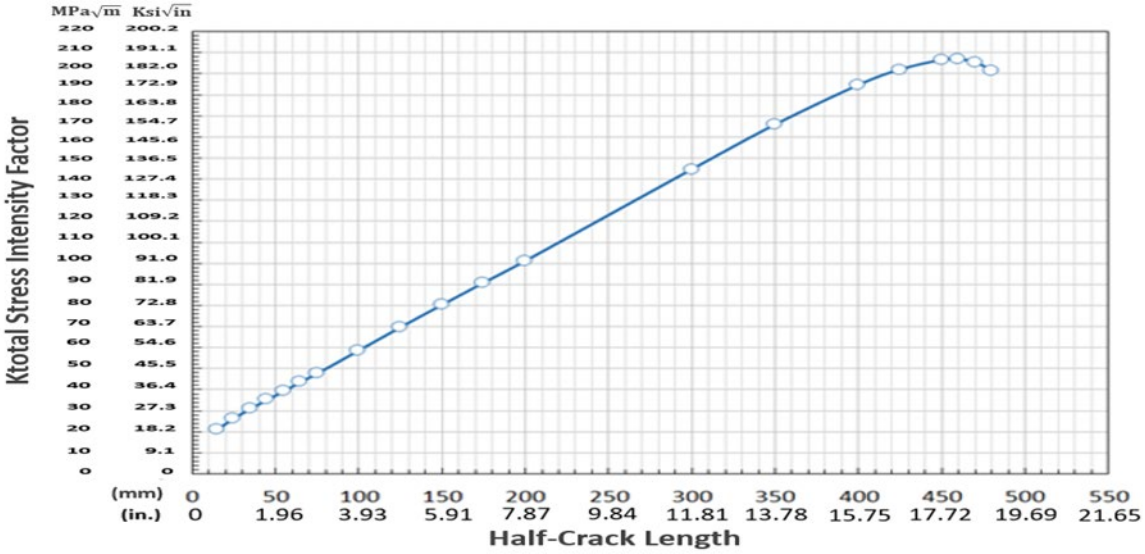

Figure 62. Longitudinal crack SIFs, Ktotal, for Qsymm1 representing the as-designed panel 1 geometry at 9.9 psi pressure

4.6 Qsymm1 elastic-plastic two-bay longitudinal crack stress intensity factors

A key design goal used in the fuselage trade study is the longitudinal two-bay crack scenario. In this scenario, the crack is two frame bays long with a central broken frame. Panel 1 was designed such that the critical crack size (the crack size when the panel fails at limit loads) extends to the adjacent intact frames, resulting in a total crack length of at least 40 in. (1.02 m).

To predict the SIFs for this two-bay longitudinal crack scenario an elastic/plastic FEM analysis was conducted using Qsymm1 (see Figure 59 for elastic plastic material properties). For the two-bay crack goal the limit load was defined to be 1.15 x 9.9 psi pressure (a total of 11.4 psi (0.0786 MPa)). The Flugge characteristic skin hoop stress for an undamaged Panel 1 at limit load is about 11.9 ksi (82.1 MPa). The half-crack Aphysical-based total SIF, Ktotal-Aphysical results for the elastic/plastic Qsymm1 analysis (with one element representing the skin thickness) were errantly run at 11.4 psi (0.079 MPa) pressure. Results are compared with the elastic Aeffective SIFs at 9.9 psi (0.068 MPa) in Figure 63. For small plastic zones, the effective crack length, Aeffective, is approximately equal to the physical crack length plus half of the plastic zone size in front of the crack. This relation may not be applicable for the large plastic zones in the residual stress analysis where the SIFs exceed 200 ksi*sqrt-in. (219.7 MPa*sqrt-m) and the zone is influenced by the intact adjacent frames or stringers.

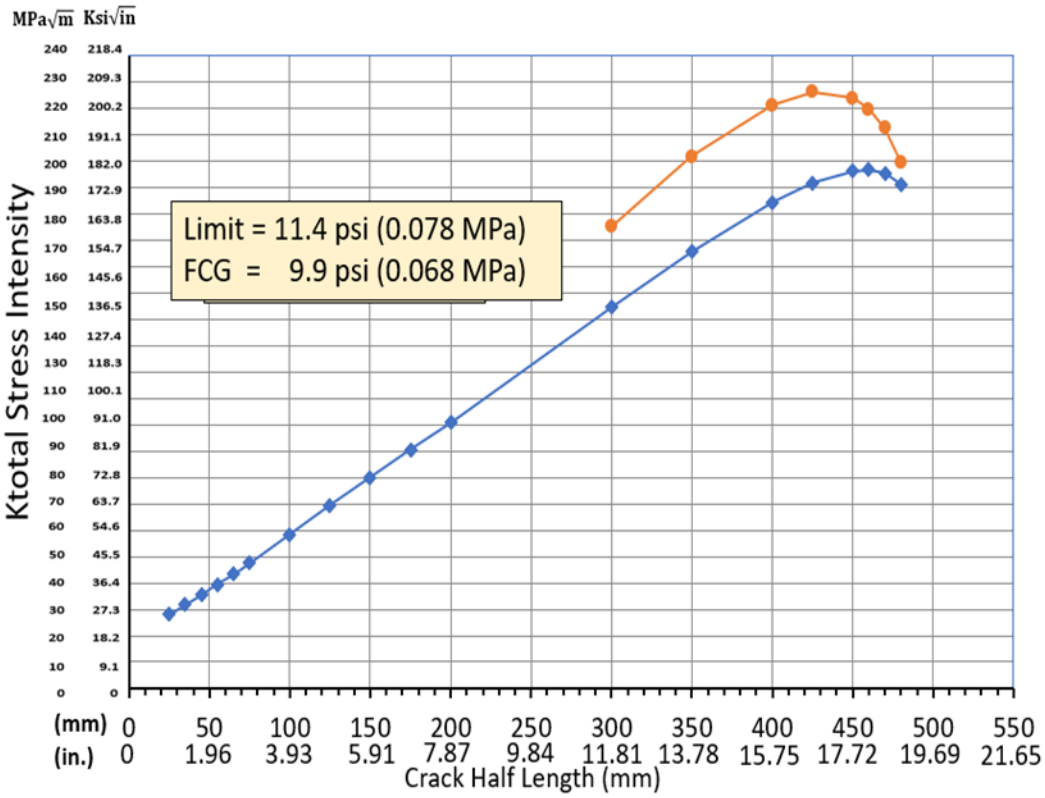

Figure 63. Longitudinal SIFs at limit load (11.4 psi pressure)

Conditions difficult to interpret arise with a plasticity analysis. For the crack approaching the intact adjacent frame, the Aphysical crack size is in front of the frame, while the Aeffective crack size could be beyond the frame because of the extensive plasticity zone. Also, the elastic solutions in Figure 63 are questionable for use in crack growth predictions without accounting for the plastic zone beyond about 50 ksi*sqrt-in. (54.9 MPa*sqrt-m), at which point the plastic zone is greater than 10% of the Aeffective crack size.

5 The use of K-control testing of M(T) specimens as a surrogate circumferential fatigue crack growth test for the full-scale Panel 1

For the circumferential crack repeat inspection scenario, the stringer is assumed broken at the mid-bay skin/stringer fastener, and a skin crack is growing from the fastener under the stringer in both directions symmetrically in the circumferential direction. For this program, the repeat inspection interval was defined to be the life of this skin crack from a starting inspectable size of 1.0 in. (25.4 mm) half-crack length crack to the critical crack size. In Panel 1 the skin critical

crack size in the circumferential direction was a two bay crack. The repeat inspection goal was chosen to be 6,000 flights with a safety factor of 2.0. For a typical FASTER frame test frequency of 0.05 Hz per pressure cycle, the testing time and resources for cycle-by-cycle spectrum testing of the circumferential crack growth using the adjusted Mini-TWIST spectrum would be excessive considering the number of panels to be tested, crack scenarios per panel, and the time frame of this multi-EMST panel testing program. In addition to scope and timing limitations, the program deemed it could be beneficial to the aerospace design community to investigate simplified test approaches that provide a reasonable representation of full-scale fuselage circumferential crack spectrum testing. An approach which is equally applicable to spectrum or constant amplitude loading would facilitate more representative structural trade studies early in design cycle efforts for new aircraft.

Early in this test program, a decision was made for the circumferential crack to be grown under an equivalent constant amplitude axial load which provides an equivalent crack growth life to spectrum loading for the defined repeat inspection goal using M(T) specimens. This equivalent constant amplitude load was determined by K-control testing as 13 ksi (89.6 MPa) at R = 0.05 for the as-designed 0.055in. (1.4 mm) skin pocket Panel 1 (see Section 2.2.5).

In Mosinyi, et al. (2007) FCG analysis was conducted for a series of loaded holes with diametrically equal cracks using both spectrum loading as well as constant amplitude loading to determine the equivalent constant amplitude loads for the fuselage panel. The challenge using M(T) specimens is that without K-control, the SIFs in the M(T) specimen are not the same as for the fuselage skin crack with a broken stringer or frame (or intact stringer or frame). Beta, β, for an M(T) specimen is defined as K/ (σ*sqrt [π*a]) where σ is the applied stress. As shown in Figure 64 the beta, β, solution for the standard M(T) center crack starts out lower than the ”as designed” circumferential fuselage crack with the broken stringer and increases as the crack grows while the fuselage skin mid plane circumferential crack beta with a broken stringer starts out higher than the M(T) specimen and decreases with crack length. Figure 64 shows the stress intensity from Qsymm1 Panel 1 fuselage model normalized by σ*sqrt [pi*a] where σ is the Flugge calculated characteristic circumferential skin stress. Thus, the life from M(T) testing will not reflect the circumferential life expected in the fuselage. Also, it is recognized that for spectrum loading, both the SIFs and the stress intensity gradients influence the plastic zones at the crack tips, crack retardation, and the crack growth life. Hence, the K-control approach was used in this program to keep the SIFs and gradients the same for the K-control M(T) specimen as the skin mid-plane in Panel 1 to provide a more representative life result even though the through thickness SIF in Panel 1 from the broken stringer may differ compared to the M(T) (no bending).

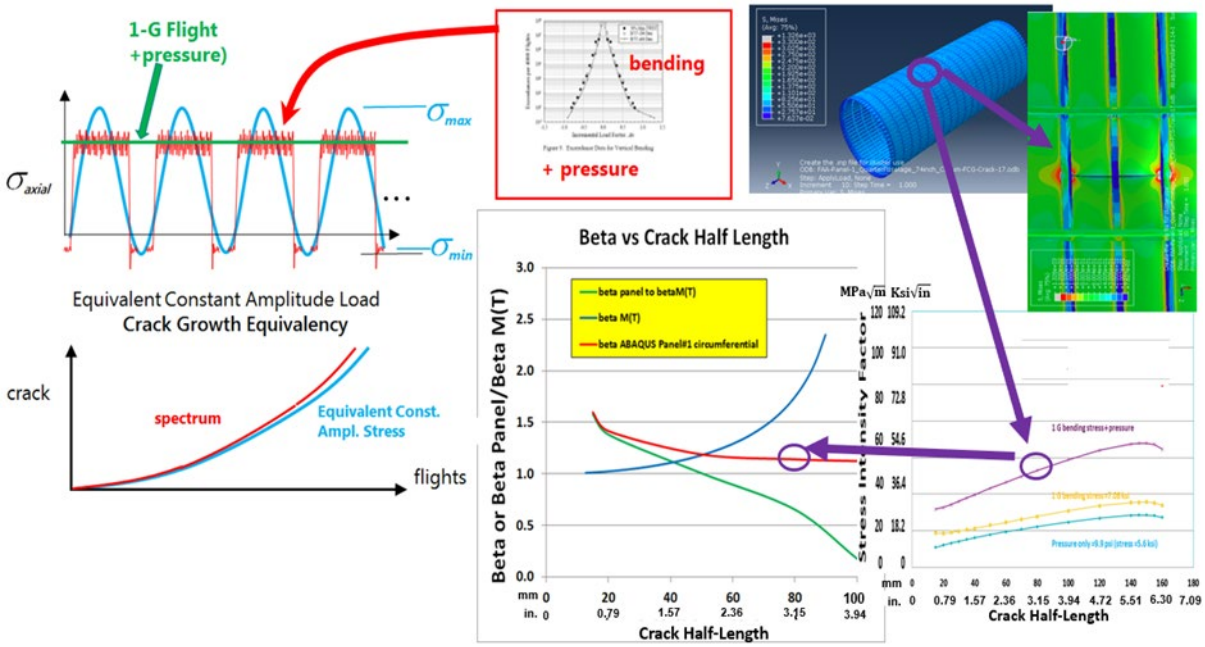

Figure 64. M(T) specimen testing to determine the equivalent constant amplitude axial load for circumferential crack growth

In the constant amplitude K-control approach used in this program, the M(T) specimen crack growth is driven by MTS software using an input Table defining the maximum SIF, K_{max}, versus crack half length. This Table was populated using Qsymm1 FE results shown in Figure 64 for the circumferential skin crack for various crack sizes under the broken stringer. Note that the K_{max} at the skin mid-plane was used in this study. It is recognized that the use of the mid-plane SIF does not account for skin bending effects from the broken stiffening element. When the skin crack is small a slower crack growth is expected from the resulting curved skin crack front compared to M(T) K-control testing using the SIF from the skin mid plane. K-Control corrections to account for this difference in bending SIF gradient through the thickness between the M(T) and Panel 1 skin was beyond the scope of the current program.

The objective is to apply the same SIFs versus crack length to the M(T) specimen as Panel 1. The use of Ktotal or K1 with or without plastic zone corrections will be discussed later. The K-control approach is used with the M(T) specimen and can be used for constant amplitude or spectrum loading. In principle, the K-control approach can potentially be used with any flat panel test (crack from open hole, edge crack, etc.) if the SIFs versus compliance relation for the specimen is provided to the K-control software.

5.1 Relation between K-control table and Qsymm1 undamaged fuselage skin stress for a given bending and pressure condition

The goal of this section is to clarify the relationship between the K-control Table and the undamaged Qsymm1 FE model fuselage axial skin stress for any combination of equivalent axial bending load intensity plus axial/hoop load intensities from pressure. Since Panel 1 loads have been determined by matching Panel 1 SIF solutions to Qsymm1 FE SIF solutions, this discussion applies to both the Panel 1 and Qsymm1 FE results. Recall that Panel 1 represents the conditions at the top of the fuselage at STA 38. The length of the curved front edge of Panel 1 is about 76.5 in. (1.94 m) along the arc, which means the corners extend +/- 28 degrees along the fuselage circumference from the top of the fuselage. Therefore, these Panel 1 corners are about 8.7 in. (221 mm) closer to the bending axis of the fuselage compared to the top of the crown. Thus, for a bending load there is approximately a 12 % lower bending stress at the corners of Panel 1 compared to the center point of Panel 1 because of the curved geometry. To simplify this comparative study, the axial load intensity at the top of the fuselage at STA 38 was used along the front and rear edges of Qsymm 1 and Panel 1. For Panel 1 and Qsymm1, a constant axial loading intensity ($pressure \times \frac{radius}{2}$) due to pressure was also applied on the Qsymm1 FE cylinder model end opposite to the axial symmetry plane. Due to skin pillowing in Panel 1 and Qsymm1 from the pressure load, there was a circumferential and longitudinal variation in skin stress within a bay, but the stresses bay-to-bay were identical in Qsymm1 away from the ends of the FE model and for the inside bays in Panel 1 under these loading conditions. The same axial loading as Qsymm1 would apply for Panel 1 if not for the doubler package used to apply the heavy loads and for the radial links in the FASTER fixture.

For Panel 1, the skin axial load distribution along the curved edges is found iteratively to match the stresses and SIFs for the same size circumferential cracks in Qsymm1. In the hoop direction, pressure was applied to the Qsymm1 model, and the symmetry BCs on the hoop edges produced the ($pressure \times radius$) hoop load intensity from pressure at STA 38. As with the axial loads, because of the doubler package, the hoop loading for Panel 1 (frame and skin load distribution along the hoop edges) are found iteratively to match the stresses and SIFs for longitudinal cracks in Qsymm1 for all crack cases.

To clarify the axial loading approach for Qsymm1, the cylindrical FE fuselage shell model does not have closed ends, and the axial load loads were applied manually at the cylinder end far away from the circumferential crack plane. The skin and stringer load intensities predicted by the Flugge smeared stiffness solution were applied to the 3D Qsymm1 FE model. Since the Flugge

load intensities are calculated using equilibrium, any differences between the 2D Flugge load solution and the 3D FEM model redistributed rapidly away from the loading edges.

The K-control software used for this test program uses an input K-control Table representing a piecewise linear fitting of the SIF K (Ktotal or K1, to be discussed later) as a function of the crack half-length for a given fuselage bending and pressure scenario. The MTS software at Arconic and the FAA Technical Center utilized a K-control software package developed by Donald (Donald, 1990). The software was implemented and validated for the modified mini-TWIST spectrum by Brazill (Brazill, 2016). Since the crack size in the M(T) specimen is determined through compliance, the software adjusts the M(T) load for the next cycle so the K solution for the M(T) matches that in the K-control Table linearly interpolated for that crack size. In this case the software solves for the M(T) applied stress, σ,MT, using Equation 1 below.

$$\beta, MT * \sigma, MT * \sqrt{\pi * a} = Ktable\ Interpolated\ Value\ for\ crack\ half\ length, a \quad 1$$

Stresses in each bay of the Qsymm1 cylinder FE model are the same and reflect the pillowing nature of the stresses inside the bay. Because the FE analysis is elastic and due to the symmetry of pressure and axial loading, if any FE axial and hoop stress is known for a given loading at the same or separate locations in a bay, then the rest of the axial and hoop stresses in the bay are uniquely defined. We have shown in the discussion about the results in Figure 10 that the Flugge stresses fall on the FE solution circumferential and longitudinal crack paths at about 25% of the distance from the broken stiffening element (see Figure 65 and Figure 66). Thus, we conveniently use the single Flugge stress to define a single solution from the Qsymm1 or Panel 1 FE models. This single FE solution for far field stresses produces a unique SIF versus crack length for the broken stiffening element condition. Thus, the Flugge stresses are used to uniquely define the vector of SIF versus crack length solutions from the Qsymm1 or Panel 1 FE model used to generate the K-control Table.

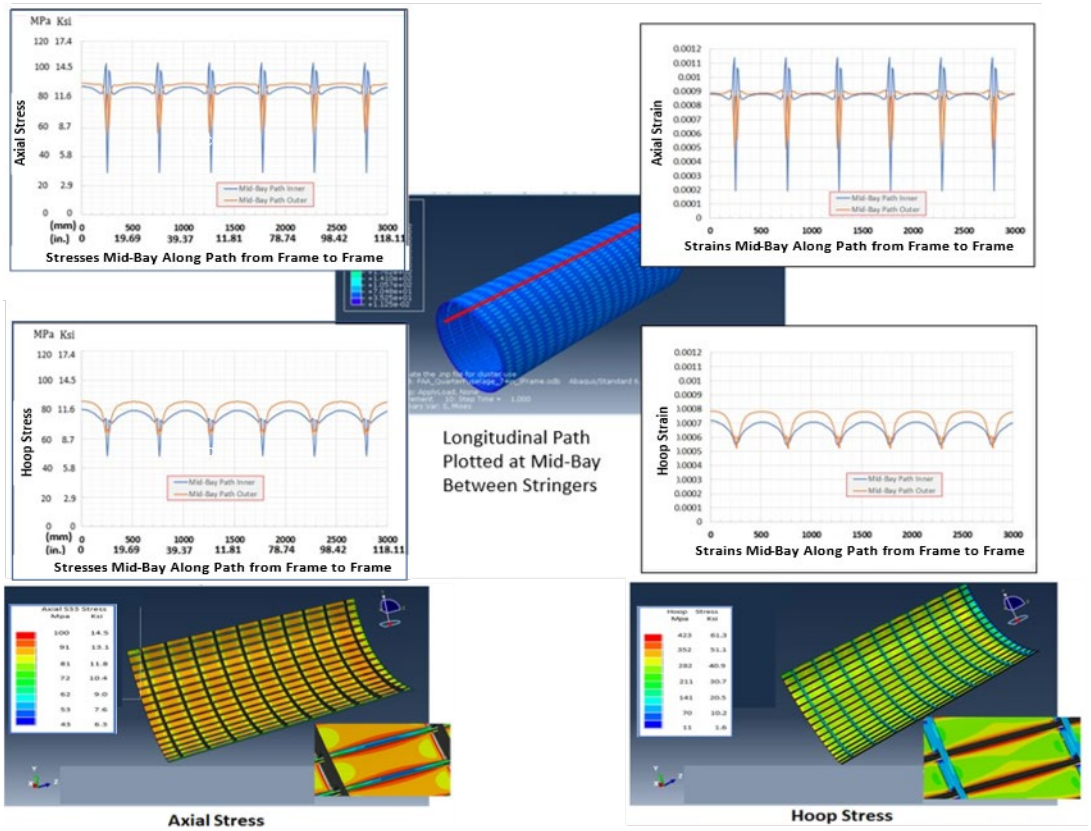

Figure 65. Qsymm1 results for 1.04G + 9.9 psi pressure

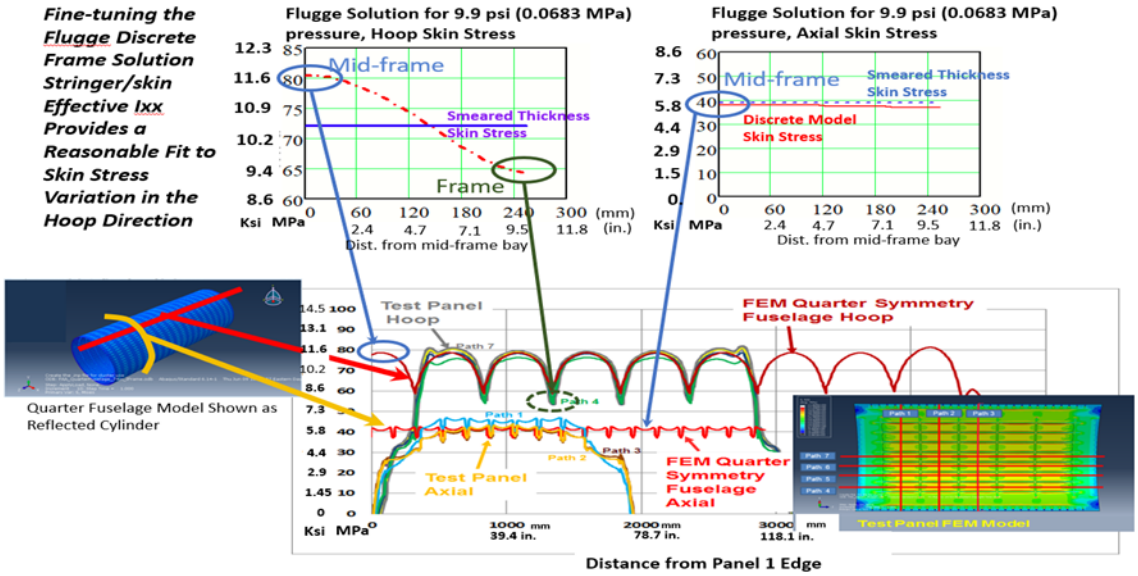

Figure 66. Use of the Flugge smeared stiffness skin stress for the K-control characteristic stress

5.2 Description of K-control spectrum used in this program

In the report by Steadman (2007), a spectrum was developed using flight recorded data from various commercial aircraft, including single-aisle aircraft. For the single-aisle aircraft, it was observed that the shape of the mini-TWIST exceedance data matched the flight recorded exceedance data reasonably well when the mini-TWIST acceleration factors were reduced by 50%, as shown in Figure 67. However, the 50% reduction factor was not conservative in the high exceedance regime (>100,000 per 4000 flights). The authors modified the number of cycles at mini-TWIST amplitude levels IX and X for all flight types, as shown in Figure 68, to make the modified mini-TWIST spectrum conservative relative to the flight measured data (Steadman, 2007; Mosinyi, Bakuckas, & Steadman, 2007). Both spectrums represent 4000 flights, but the original Mini-TWIST spectrum contained 58,422 flight cycles (plus 4000 landing loads were added for this study), while the new modified Mini-TWIST spectrum contains 91,496 cycles (plus 4000 landing loads added in this study).

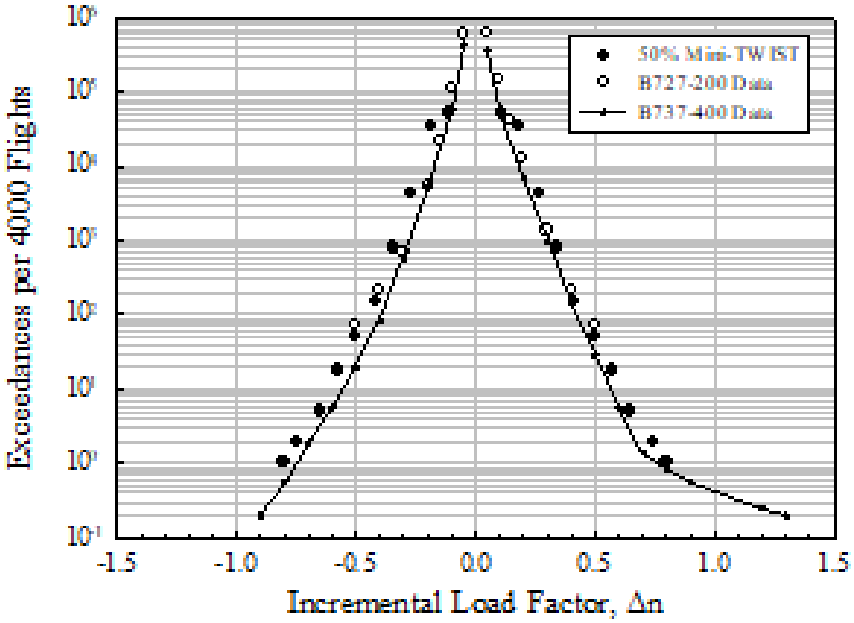

Figure 67. Comparison of the modified mini-TWIST Spectrum to B727 & B737 flight load data from Steadman

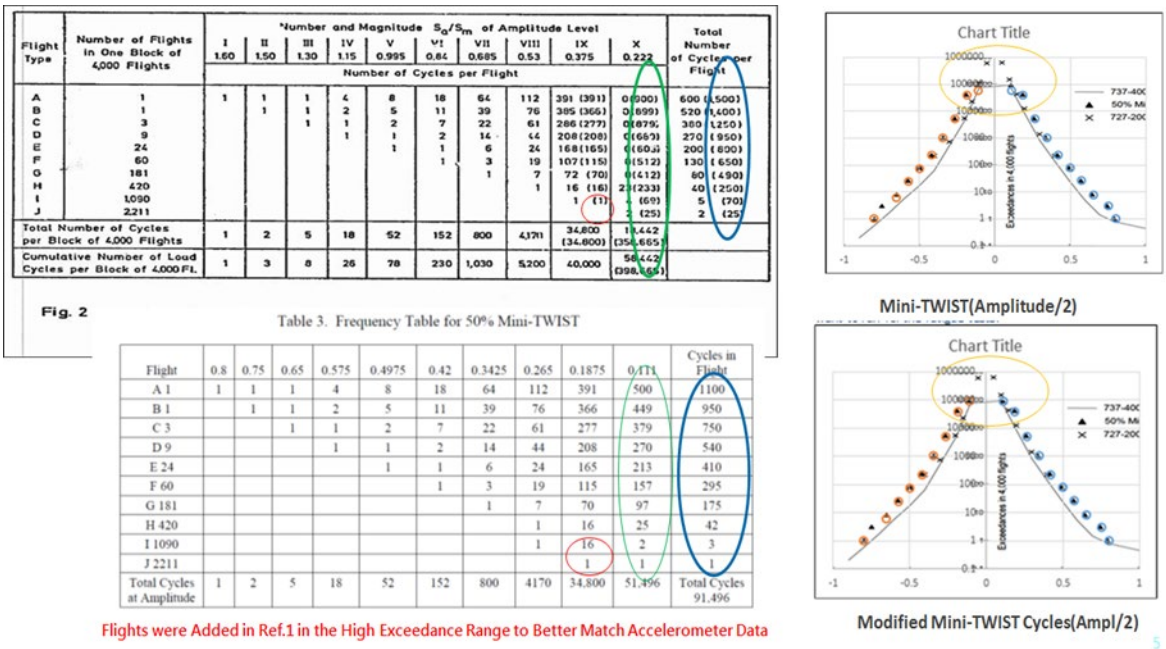

Figure 68. Comparison of modified mini-TWIST to mini-TWIST

Neither the original TWIST (deJonge & et al., 1973) or mini-TWIST (Lowak & et al., 1979) included landing loads, which make up the largest overall loading cycle per flight (the ground air ground cycle, GAG). The original mini-TWIST software was developed for wing bending excursions and was modified by Arconic to add a constant pressure component to the mean flight stress definition from which exceedance-based bending loads are added/subtracted, as well as to add a single landing load of equal magnitude between every flight in this modified mini-TWIST spectrum.

The key input and output parameters used in the Arconic software for the Panel 1 spectrum are shown in Figure 69 and are defined below. Note that *stress* refers to the Flugge characteristic stresses at the characteristic stress location.

- S_{1g} is the axial bending stress in the skin at 1G.
- S_{press} is the axial pressure skin stress.
- S_{mfs} is the mean flight stress in the skin, $Smfs = S_{1g} + S_{press}$.
- S_{max} is the skin maximum stress in the spectrum.
- α is the ratio of the landing stress to the 1G bending stress.

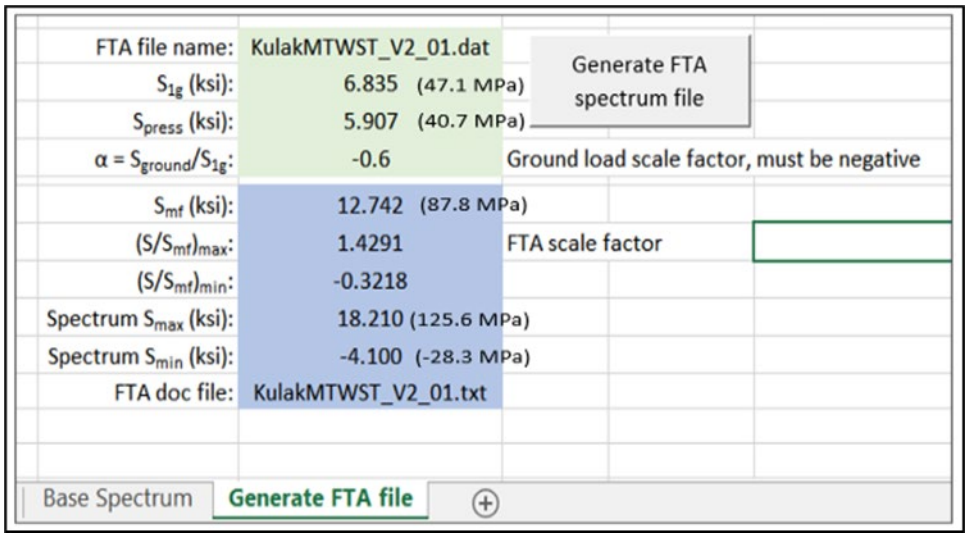

Figure 69. Modified mini-TWIST spectrum inputs and outputs for Panel 1

As discussed in Section 3.1, the spectrum was developed for the 78 in. radius using the Flugge smeared skin/stiffener/frame solution. This was the original radius chosen, and spectrum K-control testing was already underway before the decision was made to change the test panel radius to 74 in. (1.98 m) because the FASTER facility was already set-up and validated for this radius. The 1G + pressure flight stress levels between the 78 in. and 74 in. radius are within 5% of each other. Also, since the intention was that the same spectrum would be applied to all panels in an "apples-to-apples" testing approach, and considering that each OEM develops their own unique spectrum which could differ from the modified Mini-TWIST spectrum used herein, it was decided not to change the spectrum. The spectrum was generated for the as-designed Panel 1 with the skin pocket thickness of 0.055 in. and pad-up thickness of 0.063 in. The inputs from Table 3 for the 78 in. radius fuselage were used in the Arconic software (Brazill, 2016), as shown in Figure 69 to generate the spectrum for the Panel 1 K-control testing approach. The output is a spectrum stress endpoint-to-endpoint file.

A detailed description of the spectrum development is included in Appendix C.

Table 3. Bending and pressure stresses for a 74 in. (1.88 m) and 78 in. (1.98 m) radius fuselage

English Units								
	74” radius 9.9 psi pressure	**78” radius 9.9 psi pressure**	**74” radius, 1G+ 9.9 psi pressure**	**74” radius Stress Bending**	**78” radius. 1G+ 9.9 psi pressure**	**78” radius Stress Bending**	**74” radius, 2.5G +9.9 psi pressure**	**78” radius 2.5G +9.9 psi pressure**
No, press (lb/in)	733	772	733		772		733	722
Nx, press (lb/in)	366	386	366		386		366	386
Nx, bend (lb/in)	0	0	562		541		1,406	1,340
No/to (psi)	9927	10,463	9,927		10,463		9,927	10,463
Nx, press/ tx (psi)	4,613	4,861	4613		4,861		4,613	4,861
Nx, bend/ tx (psi)	0	0	7,082		6,817		17,708	16,877
skin hoop stress (psi)	10,350	10,991	10,866	536	11,426	435	11,687	12,197
skin axial stress (psi)	5,576	5,907	12,706	7,130	12,742	6,835	23,401	23,037
stringer stress (psi)	2,160	2,277	9,114	6,954	8,971	6,694	19,544	19,012
frame stress (psi)	8,511	8,971	6,693	-1,818	7,221	-1,750	3,956	4,595

SI Units								
	1.88 m" radius 9.9 psi pressure	**1.98 m radius 9.9 psi pressure**	**1.88 m" radius, 1G + 9.9 psi pressure**	**1.88m radius Stress Bending**	**1.98 m radius, 1G +9.9 psi pressure**	**1.98 m radius Stress Bending**	**1.88 m radius, 2.5G +9.9 psi pressure**	**1.98 m radius, 2.5G +9.9 psi pressure**
No, press (N/mm)	128	135	128		135		128	135
Nx, press (N/mm)	64	68	64		68		64	68
Nx, bend (N/mm)	0	0	98		95		246	235
No//to (MPa)	68	72	68		72		68	72
Nx, press/tx (MPa)	32	34	32		34		32	34
Nx, bend/tx(MPA)	0	0	49		47		122	116
skin hoop stress (MPa)	71	76	75	3.7	79	3.0	81	84
Skin axial stress (MPa)	38	41	88	49	88	47	161	159
stringer stress (MPa)	15	16	63	48	62	46	135	131
frame stress (MPa)	59	62	46	-13	50	-12	27	32

5.3 K-control constant amplitude test for the circumferential crack

The K-control software used in this testing program for constant amplitude and spectrum loading was developed by Donald (1990) and implemented for the modified mini-TWIST spectrum testing at the Arconic Technical Center by Brazill (2016). As previously discussed, the K-control method was used to determine an equivalent constant amplitude stress, $\sigma_{equiv,C.A}$, which produces the same life as the K-control spectrum crack growth test. The constant amplitude K-control Table was populated using the SIF solution from the Qsymm1 FE model, where Kmax was Ktotal and Kmin is determined by the R-Ratio (0.05 used in Panel 1 and M(T) testing). The Flugge characteristic stress associated with the K-control test (both spectrum Mfs and equivalent constant amplitude stress) is the characteristic stress in the undamaged stress Qsymm1 model which generates the skin mid-surface SIFs, for the repeat inspection damage scenario. An idealized view of the M(T) execution flow in the constant amplitude K-control test is illustrated in Figure 70 and is described by the following steps:

6. The physical crack length is measured using the compliance method as described in ASTM E647 Appendix A5 for an M(T) coupon (ASTM & s.l., 2015).
7. The SIF, K_{max}, at the measured crack half-length is interpolated from the input K-control Table populated by results from the Qsymm1 FE model.
8. The M(T) applied maximum stress, σmax , is determined by the FTA software system (Donald, 1990) controlling the MTS testing frame using the M(T) specimen geometry and the target K_{max}. The minimum stress, σmin, is determined by the R-ratio input (0.05 used here).

The cycle then repeats for the next crack length.

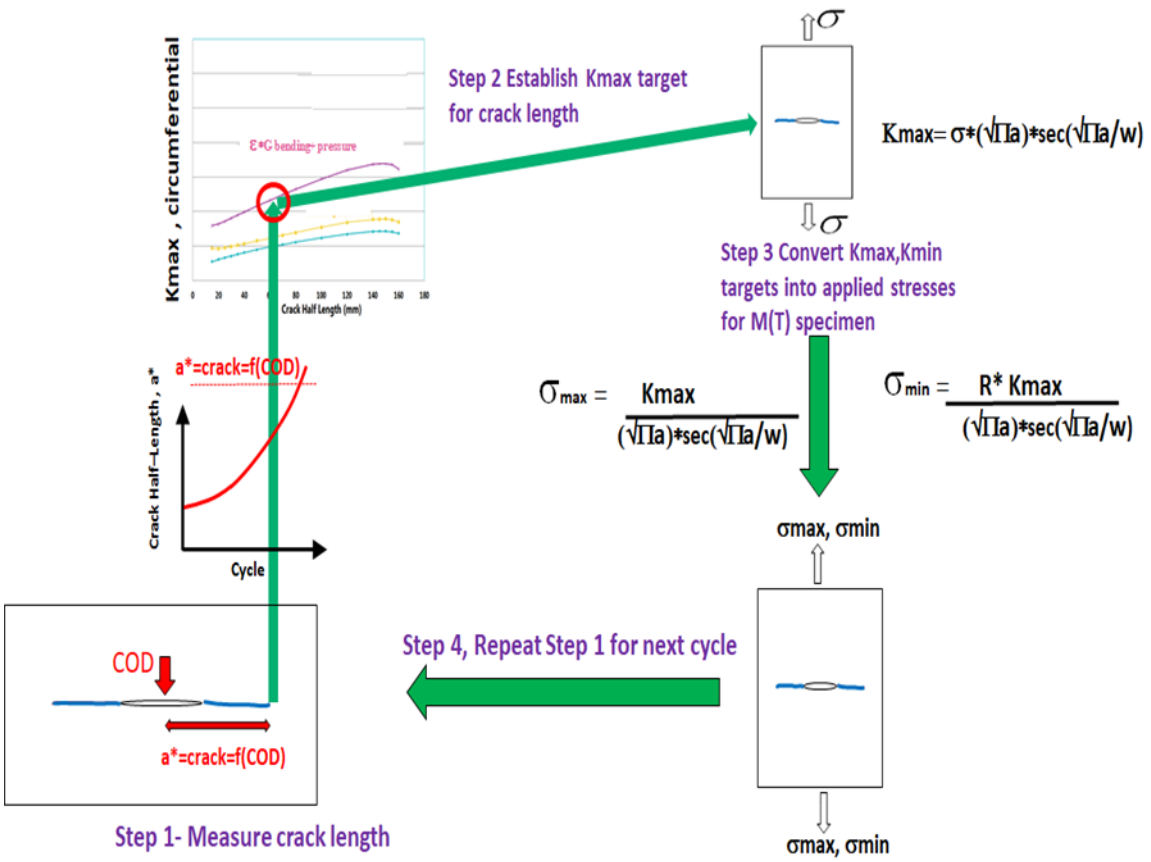

Figure 70. Idealized K-control approach for constant amplitude loading

A trial-and-error method is used to determine the constant amplitude equivalent characteristic stress, $\sigma_{equiv,C.A}$, where the constant amplitude K-control specimen life is equal to the spectrum K-control life. In this constant amplitude approach the pressure contribution to the fuselage skin stress was held constant at 9.9 psi (0.068 MPa) while the bending component was iteratively changed such that the total bending stress was σ_{1G} + scalefac x $\sigma_{1G,bending}$ where $\sigma_{1G,bending}$ is the equivalent axial skin stress due to bending at 1G, and scalefac represents the factoring (plus or minus) of this 1G bending skin stress used during constant amplitude K-control testing to equate the constant amplitude life with the spectrum life. At the converged solution, the equivalent constant amplitude skin stress, $\sigma_{equiv,C.A}$, is defined as:

$$\sigma_{equiv,C.A.} = \sigma_{press} + \sigma_{1.0G,bending} + scalefac \times \sigma_{1.0G,bending} \quad (2)$$

Rewriting Equation 2 to substitute the mean flight stress, σ_{mfs}, defined in this program as the skin stress at pressure + 1G ($i.e.\ \ \sigma_{Mfs} = \sigma_{press} + \ \sigma_{1.0G,bending}$):

$$\sigma_{equiv,C.A.} = \sigma_{mfs} + scalefac \times \sigma_{1G,bending} \quad 3$$

Solving for scalefac:

$$scalefac = (\sigma_{equiv,C.A.} - \sigma mfs)/\sigma_{1G,bending} \quad 4$$

The stress term, σ in Equations 2-4 represents the characteristic smeared Flugge axial skin stress at the Flugge characteristic location which defines the undamaged Qsymm1 FE analysis stress field in a given bay. Under elastic conditions, the term *scalefac* is just an elastic scaling factor. Therefore, the equivalent SIF, $K_{max,equiv}$, at $\sigma_{equiv,C.A}$ as a function of crack size, a, can be developed by superposition using *scalefac*, as defined in Equation 5 below.

$$K_{max,equiv,C.A.}(a) = K_{mfs}(a) + scalefac * [K_{@1Gbend}(a)] \quad 5$$

$$K_{min,equiv,C.A.}(a) = R * K_{max,equiv,C.A.}(a) \quad 6$$

where $K_{min,equiv,\,C.A.}(a)$ is determined by the R-Ratio of 0.05 used in this program and the term $K_{@1Gbend}(a)$ is the stress intensity from the equivalent axial skin load due to bending at 1G for crack size, a.

5.4 K-control spectrum test for the circumferential crack

The K-control software used in this testing program for constant amplitude and spectrum loading was developed by Donald (1990). The Arconic software (Brazill, 2016) as shown in Figure 69 generates the Flugge characteristic stress endpoints for the Panel 1 spectrum K-control testing. Before using the spectrum K-control approach, the spectrum characteristic stress, σ_i, at each endpoint, i, used for the circumferential crack growth is first normalized, $\sigma_{normalized,i}$, at each end point by the mean flight stress as shown for the first 500 endpoints (Figure 71). The mean flight stress, σ_{mfs}, for this program was defined as the skin axial pressure stress plus the skin 1G bending stress at the Flugge characteristic stress location previously defined.

$$\sigma_{normalized,i} = \frac{\sigma_i}{\sigma_{mfs}} \quad (7)$$

During the normalization process, the key parameter Fsf is calculated as the maximum normalized stress in the spectrum and stored for use in calculating the applied K-control M(T) stresses. For K-control testing, the K-control Table is populated with elastic Qsymm 1 SIFs generated for various crack sizes loaded to the spectrum maximum stress of 1.8*G plus pressure. This maximum axial stress at 1.8G plus pressure is exceeded about 1 time per 4,000 flights in the spectrum defined Figure 67. The term Fsf is defined for the modified mini-TWIST as:

$$Fsf = \frac{\sigma_{maxspectrum}}{\sigma_{mfs}} = \frac{\sigma_{mfs}}{\sigma_{pressure+1.8G}} \quad (8)$$

where Fsf was calculated using σ_{mfs} and $\sigma_{pressure+1.8G}$ values in Figure 69 as 1.4291.

A simple hypothetic example (see Figure 71) was constructed to illustrate the differences between the spectrum K-control and spectrum no K-control cases. Assume the observer does not know whether the adjusted min-TWIST spectrum loaded M(T) test was conducted with or without K-control. Also, it is assumed the crack growth test resulted in a parabolic crack half-length versus cycle endpoint test result, as shown in the lower plot in Figure 71. The K-control solution adjusts the spectrum endpoint loading on the M(T) specimen to effectively apply the as-built Panel 1 SIF, Ktotal, versus crack length solution to the specimen. The no K-control specimen can be thought of as applying the same modified mini-TWIST spectrum endpoint stresses to the M(T) using a K-control Table which is populated using the natural M(T) Kmax solution. The applied M(T) stresses and the M(T) SIFs, Ktotal, are compared to spectrum end points for the K-control and no K-control cases in the upper plot in Figure 71 for the first 500 cycles. As shown, the stress intensity histories are completely different for K-control versus no K-control for the same crack length versus spectrum cycle behavior. Thus, it can be concluded that the same materials tested in K-control versus no K-control would exhibit different crack growth lives.

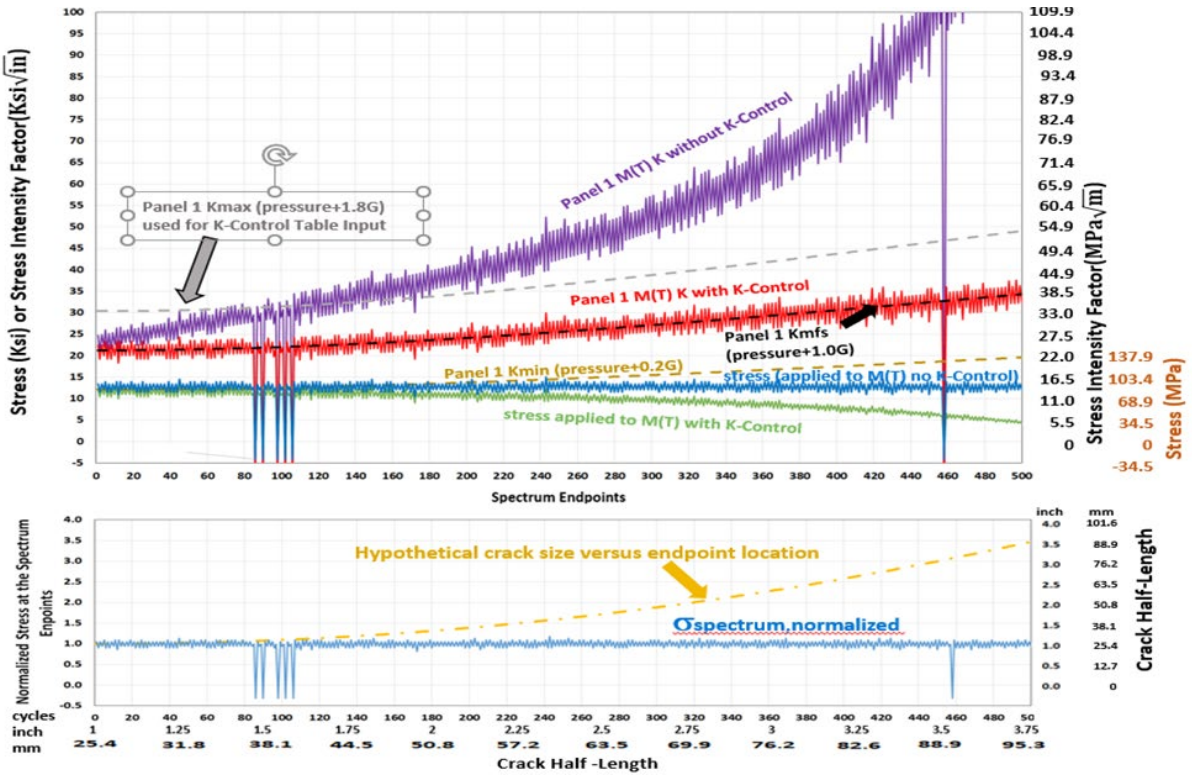

Figure 71. Inputs and results from a simplified hypothetic spectrum K-control example

The key assumption in the spectrum K-control methodology is that the SIF, K, is proportional to the applied loads at a given crack half-length, a*, which occurs at spectrum endpoint, i*. The SIF at crack half-length a* is calculated in Qsymm1 by inserting the crack, a*, into the stress field from the undamaged Qsymm1 FEM model. These stresses in the undamaged, elastic Qsymm 1 are nearly proportional to the loading for circumferential cracks. In cases of nonlinearity in the cracked Qsymm1 model, such as crack bulging for longitudinal cracks, this proportionality between the stress intensity and loading is not as linear. In this case, a set of solutions between the landing load and the 1.8G plus pressure load should be developed for a set of K-control tables from which the current K-control value is interpolated. As shown in Figure 58, for circumferential cracks, the assumption of the SIF, K, proportionality is a reasonable assumption, where elastic large displacement FE analyses results shows non-linear effects such as crack bulging and fastener non-linear load deformation are small.

An intuitive approach for this circumferential crack is used to derive the relationship between the SIFs developed at 1.8G plus pressure in the K-control Table and the stresses in the adjusted mini-TWIST spectrum. As previously mentioned, the SIF at crack half-length a* is calculated in Qsymm1 by inserting the crack into the undamaged stress field from the non-cracked Qsymm1 FEM model. These stresses in the undamaged Qsymm 1 are proportional to the loading when there are no significant sources of non-linearity, such as bulging and large-scale plasticity during

the circumferential crack growth phase. Therefore, doubling the uncracked Qsymm1 stresses will double the SIF, K, solution for any crack size, a*, when there are no significant sources of non-linearity, like crack bulging. In terms of spectrum cycle endpoints, doubling the non-cracked Qsymm1 stresses will double the SIF, K, solution at spectrum endpoint, i*, where the crack is a*. Stresses in the spectrum refer to the non-cracked Qsymm1 Flugge characteristic stresses (and location). This proportionality between the stress intensity and the undamaged Qsymm1 stress field results in the following relation:

$$\frac{K_{i*}}{K_{mfs,i*}} = \frac{\sigma_{c,i*}}{\sigma_{c,mfs,i*}} \qquad 9$$

where

- K_{i*} is the SIF for the current endpoint stress at the crack size, a*, which is measured at endpoint, i*.
- $K_{mfs,\,i*}$ is the SIF evaluated at the mean flight stress for the current crack size, a*, which exists at endpoint i*.
- $\sigma_{c,i*}$ is the total axial spectrum stress at endpoint, i*, representing the Flugge characteristic stress and location in the undamaged fuselage Qsymm1 FE model.
- σ_{mfs} is the mean flight stress (1G plus pressure stress) at the same Flugge characteristic stress location in the undamaged fuselage Qsymm1 FE model.

Recall that one pair of sigaxial, sighoop stresses at the characteristic Flugge location can describe the pillowing stress field in a bay in the elastic Qsymm1 FE analysis and is applicable to fracture mechanic calculations if there are no significant sources of non-linearities like bulging.

Using the proportionality between the undamaged fuselage skin spectrum stresses and SIFs exhibited in Equation 9, the following expression is written for the spectrum factor Fsf, which is a constant used in the K=Control algorithm:

$$Fsf = \frac{\sigma_{c,pressure+1.8G}}{\sigma_{c,mfs}} = \frac{K_{pressure+1.8G,i*}}{K_{mfs,i*}} \qquad 10$$

Where $\sigma_{c,pressure+1.8G}$ and $\sigma_{c,mfs}$ are the Flugge axial characteristic total axial stresses at pressure plus 1.8G bending and the Flugge characteristic total axial stress at the mean flight stress, Mfs. Solving for the stress intensity at the mean flight stress, $K_{mfs,i*}$:

$$K_{mfs,i*} = \frac{K_{pressure+1.8G,i*}}{Fsf} \qquad 11$$

To solve for the bending component of these SIFs we start with the definition of the mean flight stress below:

$$K_{mfs,i*} = K_{pressure+1.8G,i*} - K_{0.8G,i*} \quad 12$$

Substituting Equation 12 into Equation 11:

$$K_{0.8G,i*} = K_{pressure+1.8G,i*} - \frac{K_{pressure+1.8G,i*}}{Fsf} = K_{pressure+1.8G,i*} \times (1 - \frac{1}{Fsf}) \quad 13$$

Scaling equation 13 to the SIF at 1G:

$$K_{1G,i*} = K_{pressure+1.8G,i*} * [\frac{(Fsf-1)}{0.8*Fsf}] \quad 14$$

The mini-TWIST overall minimum SIF (1.0G-0.8G = 0.2G) at a given endpoint, i* (this minimum does not include the added landing loads), is calculated as the stress intensity at the mean flight stress, $K_{mfs,i*}$ (Equation 12), minus the bending stress intensity at 0.8G, $K_{0.8G,i*}$ (Equation 13) and is written as:

$$K_{mfs-0.8G,i*} = K_{pressure+1.8G,i*} \times \left[\frac{(2-Fsf)}{Fsf}\right] = K_{pressure+0.2G,i*} \quad 15$$

The SIF results $K_{pressure+1.8G,i}$, $K_{mfs,i}$, and $K_{pressure+0.2G,i}$ from the FE analysis for the as-designed 0.055 in. (1.4 mm) skin pocket thickness Panel 1 are plotted as the dashed curves in Figure 71 for the hypothetical crack growth analysis. Recall that the K at pressure + 1.8 G, $K_{pressure+1.8G,i*}$, is entered into the K-control Table using the FE model for various crack lengths, a*.

With K-control, the stress applied to the M(T) specimen at endpoint, i*, is the normalized characteristic endpoint stress at i*, $\sigma_{cn,i*}$, times the characteristic mean flight stress, $\sigma_{c,mfs}$, as defined in equation 16 below.

$$\sigma_{cn,i*} = \frac{\sigma_{c,i*}}{\sigma_{c,mfs}} \quad so \quad \sigma_{c,i*} = \sigma_{cn,i*} \times \sigma_{c,mfs} \quad 16$$

Using the proportionality approach, the stress intensity at the current endpoint cycle i* for crack half-length a* can be expressed in terms of the normalized stress at endpoint i*, $\sigma_{cn,i*}$ or the actual spectrum stress at endpoint i*, $\sigma_{c,i*}$ as:

$$\frac{K_{i*}}{K_{mfs,i*}} = \frac{(\sigma_{cn,i*} \times \sigma_{c,mfs})}{\sigma_{c,mfs}} = \sigma_{cn,i*} = \frac{\sigma_{c,i*}}{\sigma_{c,mfs}} \quad 17$$

Substituting Equation 11 (stress intensity at the mean flight stress) into Equation 17 and solving for the applied stress intensity, K_{i*}, yields:

$$K_{i*} = \frac{\sigma_{c,i*}}{\sigma_{c,mfs}} \times \frac{K_{1.8G+press,i*}}{Fsf} \quad 18$$

or, in terms of the normalized spectrum loading:

$$K_{i*} = \sigma_{cn,i*} \times \frac{K_{1.8G+press,i*}}{Fsf} \quad 19$$

The stress applied to the M(T) is determined using the standard M(T) solution for crack half length, a^*, at endpoint, i*:

$$\sigma_{K-Control,i*} = \frac{K_{a*}}{(beta,MT(a*)\times\sqrt{\pi\times a*})} \quad 20$$

where beta,MT(a^*) is the beta correction term for the M(T) specimen at crack size, a^*.

Using Equation 19, the applied stress, $\sigma_{K\text{-control},i*}$, for crack half length, a^*, at endpoint, i*, may be rewritten as:

$$\sigma_{K-Control,i*} = \frac{\sigma_{cn,i*}\times(K_{1.8G+press,i*}/Fsf)}{(beta,MT(a*)\times\sqrt{\pi*a})} \quad 21$$

Without K-control, the SIF, K_{MT} for the 7.874 in. (200 mm) M(T) specimen used in this program is calculated using the standard M(T) solution for the SIF (K_{MT}) at crack length, a_{i*}.

$$K_{MT} = beta,MT(a*) \times \sigma_{ci*} \times \sqrt{\pi * a*} = beta,MT(a*) \times \left(\sigma_{cn,i*} \times \sigma_{mfs}\right) \times \sqrt{\pi * a*} \quad 22$$

The no K-control stress intensities versus cycle endpoint are shown in Figure 71 (top figure, purple plot). These no K-control stress intensity endpoint values are significantly different from the stress intensity versus cycle endpoint for the example case with K-control (Figure 71, top figure, red plot). The same spectrum stresses were used (Figure 71, bottom figure, light blue plot, which is the same as the top figure, light blue plot) for the "no spectrum K-control" case. In this case, the mean SIF as well as the range (K_{max} - K_{min}) in stress intensity increases (Figure 71, top figure, purple plot), especially as the cracks approach the free edge of the MT specimen. Note, for spectrum K-control, both the applied stress and spectrum stress range (σ_{max} - σ_{min}) in this example (top figure, green plot in Figure 71) decreases with crack size to apply the stress intensity values in the K-control Table to the M(T) specimen. Thus, the crack life of the no spectrum K-control test is expected to be significantly different from life of the spectrum K-control Test.

The process flow for the spectrum K-control within the FTS software is shown in Figure 72 for this example case. For this example, we examine end points 64 and 65 shown in the upper right corner of Figure 72. As discussed, for spectrum testing, the K-control Table is populated using the Qsymm1 FE analysis SIFs, Kmax or K1max, versus crack length for the skin crack growing circumferentially from under a broken stringer for the maximum spectrum loading condition of

1.8G + pressure loading condition at the crown panel STA 38 location. The K Control Table is normalized by the width of the actual M(T) specimen.

In step 1, the physical crack length, a*, is measured using the compliance method as described in ASTM (2015).

In step 2, the SIF, $K_{1.8G+press,i*}$, for the measured crack half-length, a*, is interpolated from the input K-control table of SIFs versus crack lengths obtained from the Qsymm1 or Panel 1 FE models loaded at 1.8G + pressure. In this K-control approach, the M(T) specimen crack and crack gradient is the same as the crack size and crack gradient in Qsymm1 or Panel 1. Therefore, the same SIF is applied to the M(T) specimen as in the FEM analysis for the same crack size avoiding crack size and gradient issues. Since the M(T) specimen results are limited by the plastic zone interaction with the specimen edge in the 7.87 in. wide M(T) specimen, the crack results were only applicable to about 6.0 in. total crack length. Longer applicable crack results can be obtained using wider M(T) specimens.

In step 3, the FTA software system extracts the normalized characteristic spectrum stress $\sigma_{cn,i*}$ at endpoint, i*, and $\sigma_{cn,i*+1}$ at endpoint,i*+1 from the normalized stress endpoint file (for example, these values are 0.90 in step 64 and 1.10 in step 65; see Figure 72). It was shown that stress intensity targets for these two loading steps for the K-control M(T) test can be calculated using Equation 19, previously defined:

$$K_{i*} = \sigma_{cn,i*} \times \frac{K_{1.8G+press,i*}}{Fsf}$$

$$K_{i+1} = \sigma_{cn,i+1} \times \left(\frac{K_{1.8G+press,i+1*}}{Fsf}\right) \qquad 23$$

In step 4, these end point spectrum SIFs are converted into target stresses given the M(T) specimen with current crack-half length, a*. This process is repeated at for the next set of cycle endpoints i+2, i+3 and so on, until the end of the test.

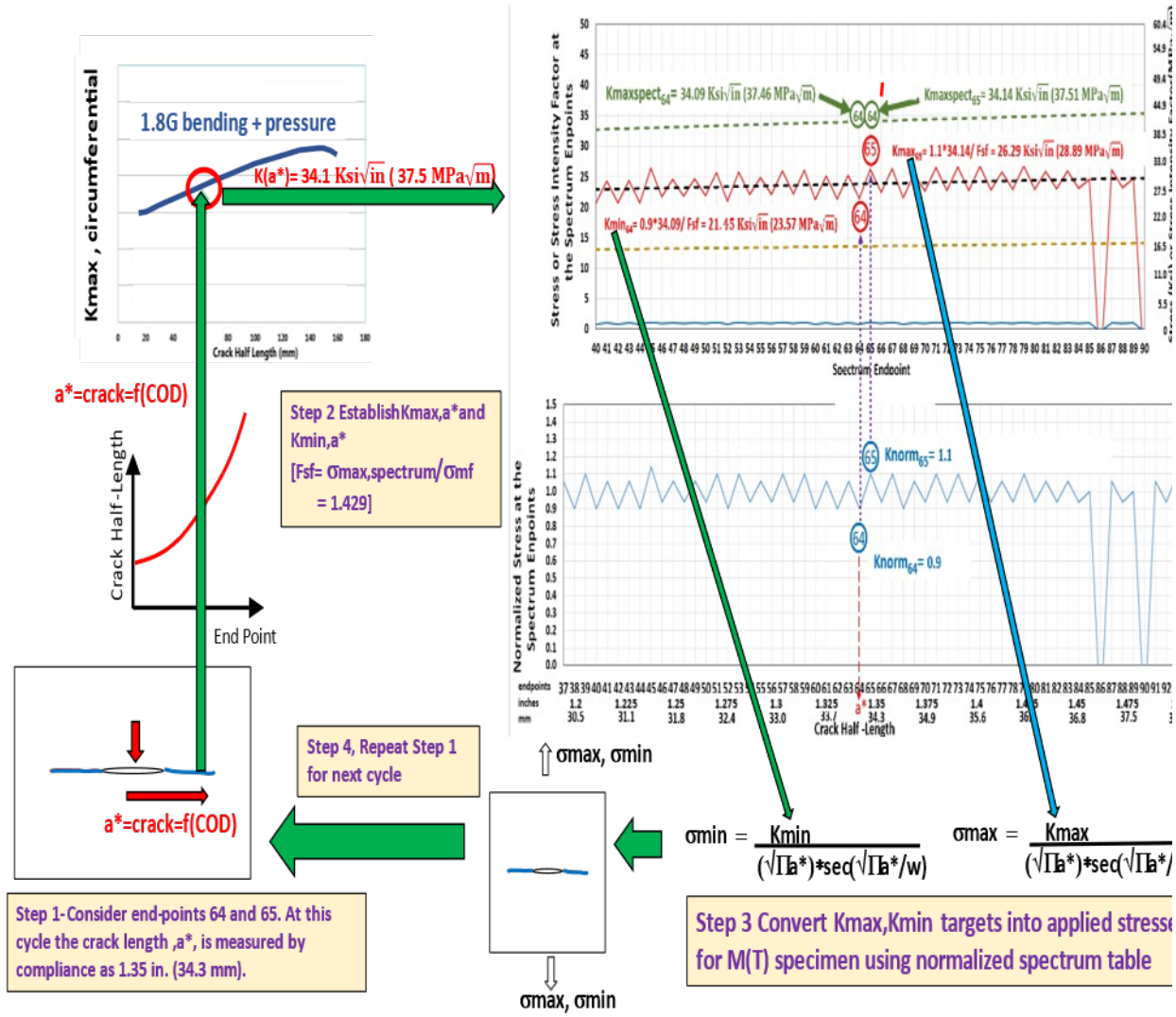

Figure 72. K-control approach for spectrum loading

With this K-control approach, the Kmax and Kmin versus circumferential crack length in the fuselage (from the Qsymm1 FE analysis) is the same as the Kmax and Kmin in the M(T) specimen for every spectrum end point for the same crack length. Since the Panel 1 SIFs were matched to the Qsymm1 SIFs, the M(T) results for spectrum loading are expected to match the spectrum crack growth results of Panel 1 if test load frequencies are kept the same in the FASTER test panel as in K-control test. Other effects in the circumferential direction, such as bulging, curvature effects on crack growth, skin bending due to the bending moment from the broken stringer, and roll forming residual stresses through the skin thickness were considered beyond the scope of this program.

5.5 Testing to determine the equivalent constant amplitude circumferential stress

The objective of the K-control test program was to determine the equivalent constant amplitude load which matches the spectrum life. As described in Section 2.2.4, the R-Ratio for the circumferential crack growth in the FASTER Panel was limited to R=0.05. Thus, the effective constant amplitude stress had to also be defined in terms of R=0.05. However, the spectrum K-control testing included a compression landing load at the end of every flight in the adjusted mini-TWIST spectrum. The specimen used for crack growth testing is shown in Figure 73.

The test setup used by Arconic is shown in Figure 74. The Arconic grips are barrel type bolt-actuated reverse wedge grips from MTS (circa 1974). Although the barrel grips are massive, which restricts the upper test frequency, they prevent backlash when going into compression. Because these specimens are thin and long, a buckling guide was attached to the testing machine uprights to prevent the specimen from moving out of plane. The specimen free length is 17.5 in. (444.5 mm), and the buckling guide used was 9.8 in. long (248.9 mm).

Even with this setup, two bolt-on buckling guides were used to prevent buckling of the remaining free length of the specimen. In this case, the compressive load for the 0.089 in. (2.26 mm) thick 2524-T3 M(T) specimens was still limited to -4.1 ksi (-28.3 MPa), which amounts to 60% of the 1G load bending load. The FAA Technical Center also ran replicate tests under the same spectrum without the compressive landing load to quantify the effect of landing loads on the spectrum FCG life. The K-control test specimens used the full thickness double clad as-received 0.089 in. (2.26 mm) 2524-T3 skin to allow for a higher compressive landing load during spectrum testing. However, the K-control Table represented SIF solution for the as-designed Panel 1 with the 0.055 in. (1.4 mm) pocketed skin construction. It was recognized that the crack growth in the machined 2524-T3 skin will differ from the as-received 0.089 in. (2.26 mm) double side clad material but will be consistent with the crack growth testing used to characterize 2524-T3, which was also done on the before full thickness and double side clad material.

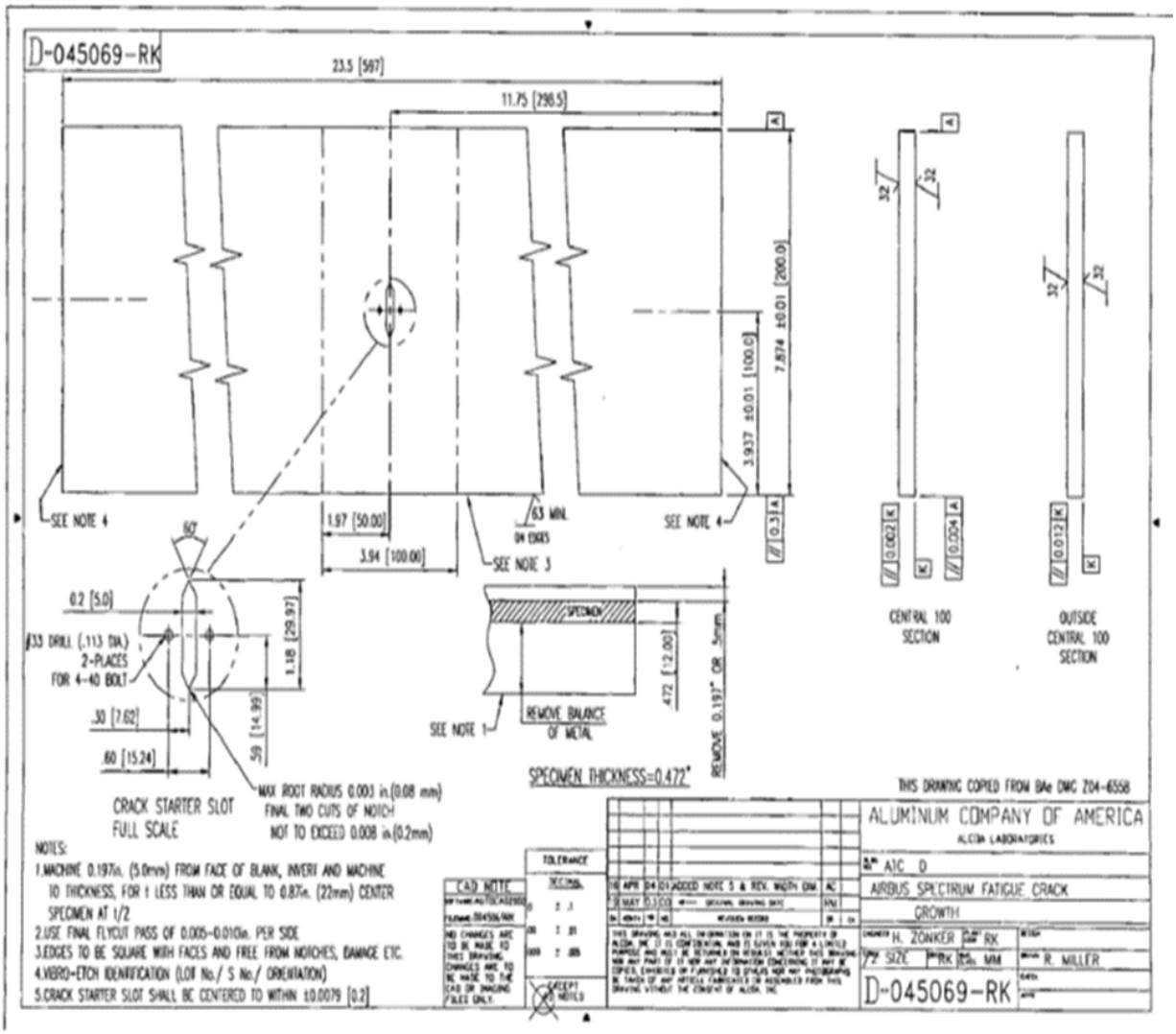

Figure 73. M(T) FCG specimen used in K-control testing program

Constant amplitude K-control M(T) testing was conducted to determine the equivalent Flugge characteristic stress that produces the same life as the spectrum-loaded K-control M(T) test. The K-control test results were for the as-designed Panel 1 with the skin pocket thickness of 0.055 in. (1.4 mm). The spectrum K-control Table represented the total SIF, Ktotal, for a circumferential skin crack growing from under a stringer broken midway between frames at the Panel 1 STA 38 crown location at the skin stress for pressure + 1.8G stress.

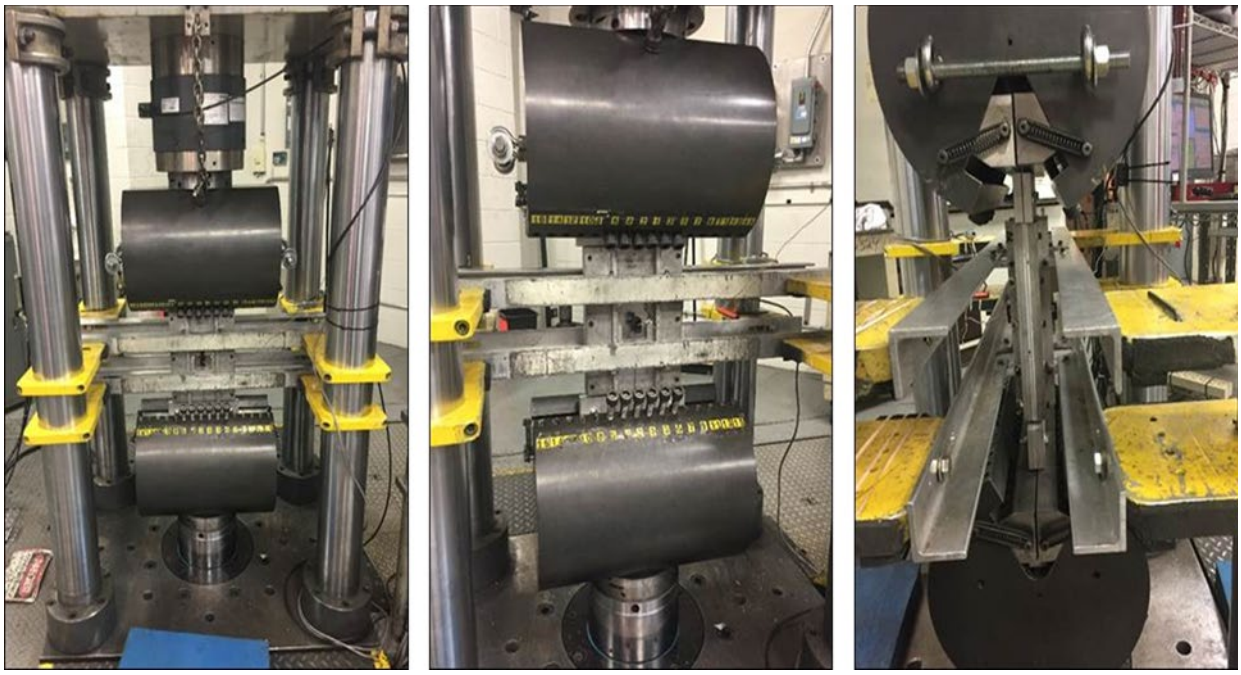

Figure 74. Arconic M(T) crack growth test setup developed to prevent buckling due to spectrum landing loads

First, two spectrum tests were conducted using spectrum K-control. Circumferential crack K-control M(T) specimens were tested using the modified mini-TWIST spectrum described in Appendix C representing a single aisle aircraft. Then, constant amplitude K-control tests were conducted iterating on the equivalent Flugge characteristic stress until a match of FCG life was found between the spectrum and constant amplitude K-control tests. M(T) specimens were also run without K-control to document the impact on crack growth life of using K-control. Spectrum K-control results at a mean flight stress, Mfs, of 1G + 9.9 psi (0.068 MPa) pressure load equal to 12.7 ksi are compared in Figure 75 with no K-control spectrum tests at the same 12.7 ksi (87.6 MPa) Mfs. For the no K-control test, the natural SIF in the 7.874 in. (200 mm) wide M(T) specimen determines the crack growth. Also plotted in Figure 75 are results for constant amplitude K-control tests versus conventional no K-control M(T) specimens at various characteristic stresses.

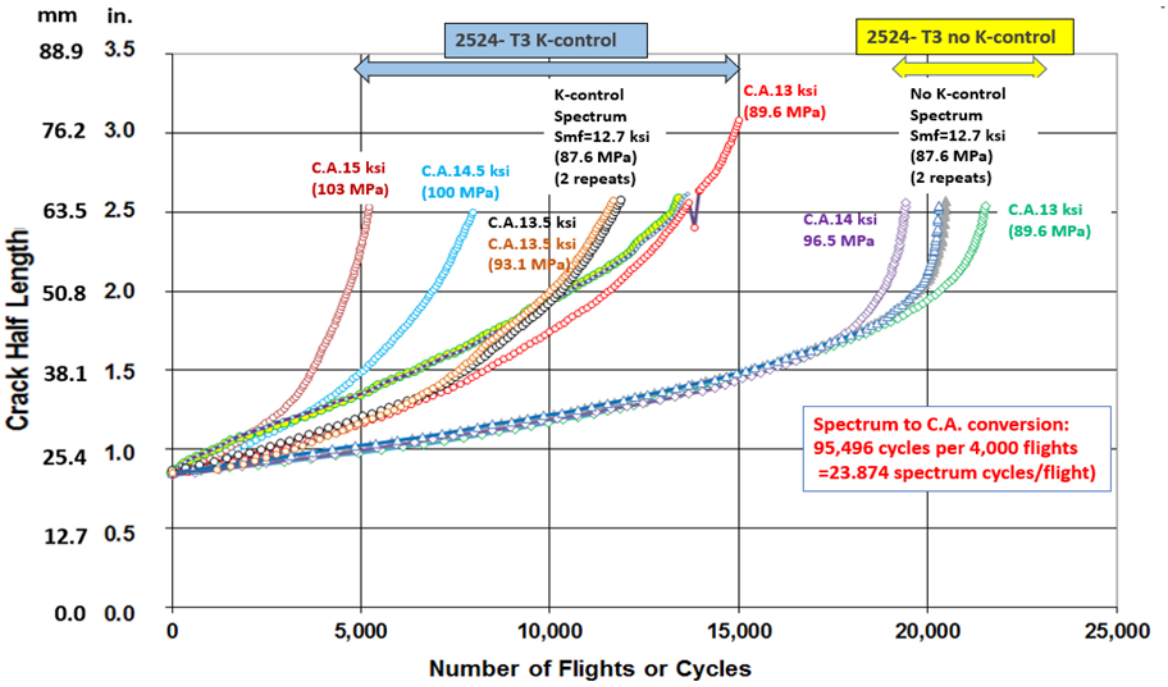

Figure 75. Constant amplitude and spectrum test results with and without K-control

The following observations were made:

- The life of the no K-control M(T) spectrum tests to 2.5 in. (63.5 mm) for the 7.874 in. (200.7 mm) wide M(T) specimen (20,300 flights) is much longer than the K-control spectrum life of 13,600 flights. Thus, using the M(T) with no K-control was not conservative for life prediction for this case.
- The shape of the crack versus life curve for the spectrum K-control test is not the same as the constant amplitude K-control test life curve.
- The spectrum results are repeatable for both K-control and no K-control spectrum tests.
- At the equivalent constant amplitude stress of 13 ksi (89.63 MPa) and R=0.05, the constant amplitude K-control life matched the life of the spectrum K-control tested at a 12.7 ksi (87.6 MPa) mean flight stress at a crack length of 2.5 in. (63.5 mm).
- For the same 2.5 in. (63.5 mm)crack size the equivalent constant amplitude stress for no K-control was 13.5 ksi (93.1 MPa) at R=0.05. Although a test was not conducted due to test setup limitation, it was expected that K-control constant amplitude tests at R = -0.5 representing constant amplitude ground-to-air loading would produce a maximum working stress for the repeat inspection interval lower than the 13.0 ksi spectrum Mfs that meets the repeat inspection goal at R = 0.5. See Section 2.2.5 for more details.

- The 7.874 in. (200 mm) wide specimen (Figure 75) provides valid data to about 3.0 in. (76.2 mm) half-crack length.
    - It appears that a wider specimen would have resulted in a longer life and slightly higher equivalent constant amplitude stress. To avoid extrapolation the K-control spectrum results at 12.7 ksi of 12,000 flights at 2.5 inches was considered a conservative goal for equivalent constant amplitude fitting.
- The equivalent (characteristic) stress applied to the M(T) specimen during K-control testing represents the axial skin stress due to pressure differential and the effective axial skin stress due to fuselage bending.
    - Since the axial stress due to pressure differential is constant, the axial bending stress in units of gravity acceleration, G, were varied in the constant amplitude K-control tests. An equivalent constant amplitude stress of 13 ksi resulted in a value of scalefac (recall $\sigma_{equivalent} = \sigma_{mfs} + scalefac * \Delta\sigma_{1Gbending}$ from Equation 3) of 0.04. Thus, the equivalent constant amplitude stress can be rewritten as $\sigma_{pressure} + 1.04 * \Delta\sigma_{1Gbending}$.
- An additional three repeat tests were conducted at the FAA Technical Center at the equivalent K-control constant amplitude stress of 13.0 ksi. These exhibited good agreement with the K-control spectrum, as shown in Figure 76.

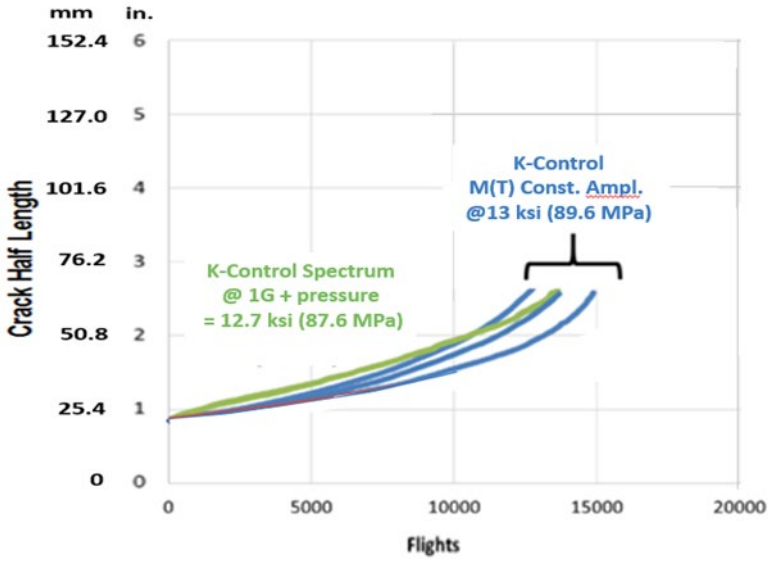

Figure 76. Additional results of Ktotal-control testing for modified mini-TWIST spectrum

5.6 Comparison of K-control tests with the FASTER Panel 1 test

This section examines the sensitivity of the K-control results to FE model mesh density, use of K1 versus Ktotal, and the effect of the plastic zone at the crack tip. These studies were done in an attempt to explain the longer as-built, as-FASTER-tested Panel 1 life compared to K-control test life. This study was done before it was realized that the as-built Panel 1 skin pocket was thicker than the as-designed Panel 1, resulting in the as-built SIFs to be lower. A new FE model was developed for the as-built Panel 1 which used the as-designed, as tested Panel 1 load but also included several modifications needed due to the load imbalance (described in Section 6.3). Based on this new FE model, the skin thickness increase alone would not account for the 13% estimated reduction in SIFs needed for the constant amplitude M(T) K-control testing program in order to match the Panel 1 circumferential crack growth. Therefore, the results of this study were useful to understand the sensitivities of the K-control approach.

The FASTER Panel 1 circumferential crack growth test was conducted at 1.04G + 9.9 psi (0.068 MPa), which resulted in an equivalent constant amplitude axial stress of 13 ksi (89.6 MPa) and R=0.05. The results are shown in Figure 77. The crack life counting for all K-control testing started at a crack half-length of 0.85 in. (21.6 mm). The K-control constant amplitude circumferential lives did not agree with the FASTER Panel 1 life. Ktotal was used for K-control and was calculated using the Qsymm1 FE model for the as-designed Panel 1 with the 0.055 in. (1.4 mm) pocketed skin. The longer life of the FASTER Panel 1 compared to the 13 ksi (89.6 MPa) K-control test indicates an estimated 13% stress intensity reduction is needed for the K-control Table SIFs, Ktotal, generated using the one skin element through the skin thickness Qsymm1 model in 2016. During the FASTER Panel 1 test, it was not known that Panel 1 was built to thicker skin pockets of 0.059 in. (1.5 mm). Potential explanations were explored, as described below.

The first area reviewed was the impact of skin mesh density through-the-thickness. It was questioned how much the representation of the as-designed Panel 1 skin thickness by one ABAQUS C3D20, 20-node solid element in the Qsymm1 model to develop SIFs used for the K-control testing may affected the SIF solution. The results for the as-designed, 0.055 in. (1.4 mm) skin pocket thickness, two skin elements through-the-thickness Panel 1 FE model are listed in Table 4. These results indicated an average 4.4% decrease in the K-control Table SIFs within the 0.8-1.6 in. (20-40 mm) crack range.

Another avenue explored was the issue whether Ktotal or K1 is more appropriate for the K-control Table. First, the crack was modeled on the front axial symmetry plane of the Qsymm1 cylinder which restricted the SIF to be K1 only. The circumferential crack in Panel 1 was placed

in an off-center bay and K2, and K3 components of Ktotal were expected. Also, the loading was not balanced since the as designed geometry loads were used with the as built geometry. These Panel 1 K2 and K3 components contributed to the Ktotal in Panel 1.

Table 4. As-designed Panel 1 FE model results — one C3D20 element versus two elements

crack length (in.)	**Ktotal-control table (2016) 1 elem. 0.055 in. skin@1.04G +9.9 psi Ksi*sqrt-in**	**Ktotal-control table (2018) 2 elem. 0.055 in. skin@1.04G +9.9 psi Ksi*sqrt-in**	**%diff Ktotal, 1 elem. vs 2 elem skin model**
0.79	28..1	26.6	-5.4%
0.98	30.2	28.9.	-4.3%
1.18	32.1	31.0	-3.4%
1.38	34.0	32.9	-3.2%
1.57	36.5	34.4	-5.8%
1.97	39.1	38.0	-2.8%
2.36	42.2	41.0	-2.8%
2.76	45.0	43.9	-2.4%
3.15	47.7	46.3	-2.9
crack length (mm)	**Ktotal-control table (2016) 1 elem. 0.055 in. skin@1.04G +9.9 psi MPa*sqrt-in**	**Ktotal-control table (2018) 2 elem. 0.055 in. skin@1.04G +9.9 psi MPa*sqrt-in**	**%diff Ktotal 1 elem. vs 2 elem skin model**
20	30.9	29.2	-5.4%
25	33.2	31.8	-4.3%
30	35.3	34.1	-3.4%
35	37.4	36.2	-3.2%
40	40.1	37.8	-5.8%
50	43.0	41.8	-2.8%
60	46.4	45.1	-2.8%
70	49.4	48.2	-2.4%
80	52.4	50.9	-2.9%

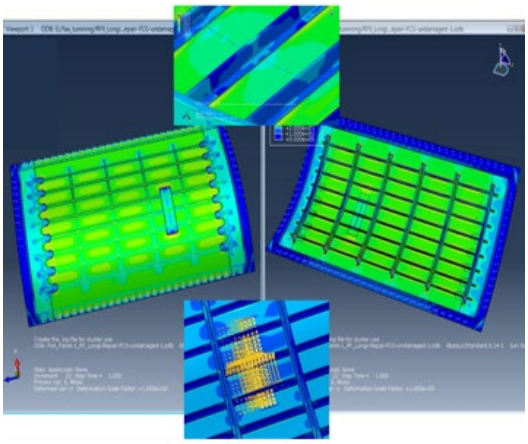

Results from a two-element skin thickness Panel 1 FE model used to calculate K1, K2, K3 components from the J integral are listed in Table 5. Since the MT specimen only exhibits Mode 1 crack growth it is driven by K1. Therefore, the use of the FE model K1 for K-control testing was evaluated. Results in Table 5 show the use of K1 rather than Ktotal would have represented another 2.0%-3% reduction in the stress intensity from the original one-element Qsymm1 results used in the K-control testing. The total reduction from the original Qsymm1 model SIF results

used in the K-control table using two elements through the skin thickness and the use of K1 now averaged about 6.4% lower in the 0.8-1.6 in. (20-40 mm) crack range. This was still not enough to account for the longer FASTER tested Panel 1 test life in Figure 77.

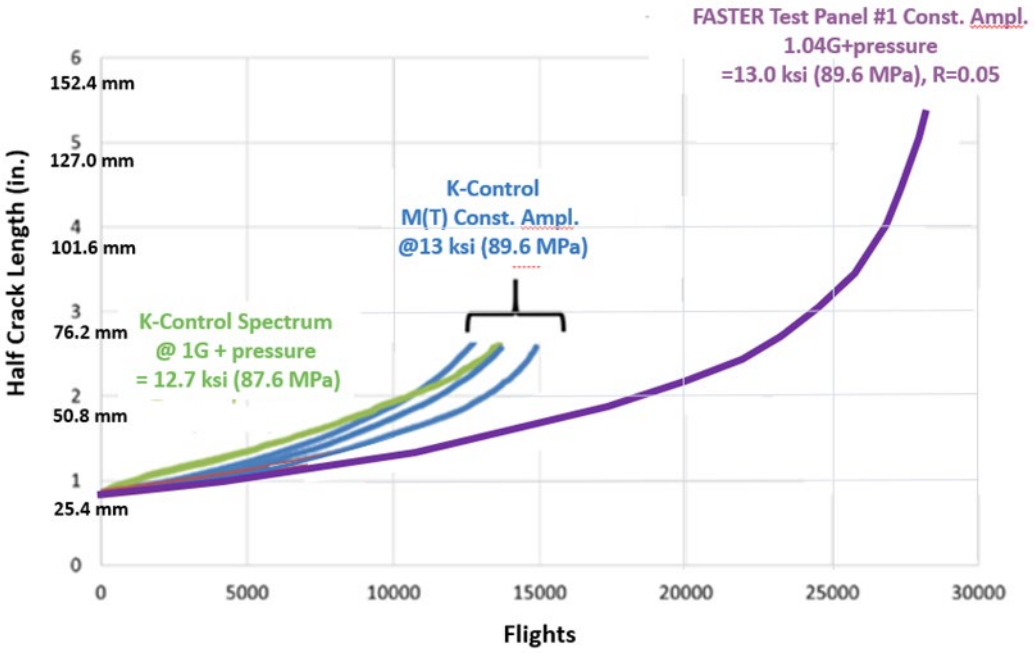

Figure 77. Results of the FASTER test Panel 1 versus the original K-control M(T) testing

A final hypothesis considered the differences in the compliance measurement for the crack length in the K-control test versus the interpretation of the crack used in the elastic, as-designed Panel 1 FE model. The physical crack half-length, Aphysical, was measured during the K-control test. However, the K-control Table represented Ktotal for an effective crack half length, Aeffective, since the Qsymm1 FE crack analysis was elastic. Thus, to be consistent, the K-control Table should have been generated by an elastic plastic FE analysis, thereby representing Aphysical crack sizes instead of Aeffective crack sizes. Therefore, a correction to the K-control Table was needed for the plastic zone sizes, which were large enough to differentiate Aphysical from Aeffective. A simple correction approach for the current elastic analysis-based K-control Table using the Irwin plastic zone prediction was used to estimate the impact (Figure 78).

Table 5. Comparison of panel 1 FE model Ktotal with K1

Crack length (in.)	**Ktotal-control table (2016) 1 elem. 0.055 in. skin@1.04G +9.9 psi Ksi*sqrt-in**	**Ktotal-control table (2018) 2 elem. 0.055 in. skin@1.04G +9.9 psi Ksi*sqrt-in**	**%diff Ktotal, 1 elem. vs 2 elem skin model**	**K1 (2018) 2 elem.0.055 in, skin @1.04G +9.9ps Ksi* Sqrt-in.**	**% difference Ktotal, 0.055 in, 2 elem vs K1, 0.055 in. 2 elem @1.04G +9.9psi**
0.79	28..1	26.6	-5.4%	26.2	1.3%
0.98	30.2	28.9.	-4.3%	28.3	2.1%
1.18	32.1	31.0	-3.4%	30.3	2.2%
1.38	34.0	32.9	-3.2%	32.2	2.1%
1.57	36.5	34.4	-5.8%	33.6	2.4%
1.97	39.1	38.0	-2.8%	36.9	2.9%
2.36	42.2	41.0	-2.8%	39.7	3.2%
2.76	45.0	43.9	-2.4%	42.3	3.6%
3.15	47.7	46.3	-2.9%	44.4	4.1%
Rack length (mm)	**Ktotal-control table (2016) 1 elem. 0.055 in. skin@1.04G +9.9 psi MPa*sqrt-in**	**Ktotal-control table (2018) 2 elem. 0.055 in. skin@1.04G +9.9 psi MPa*sqrt-in**	**%diff Ktotal, 1 elem. Vs 2 elem skin model**	**K1 (2018) 2 elem. 0.055 in, skin@1.04G +9.9 psi MPa*sqrt-in**	**% difference Ktotal, 0.055 in. 2 elem vs. K1, 0.055 in, 2 elem @1.046 +9.9 psi**
20	30.9	29.2	-5.4%	28.8	1.3%
25	33.2	31.8	-4.3%	31.1	2.1%
30	35.3	34.1	-3.4%	33.3	2.2%
35	37.4	36.2	-3.2%	35.4	2.1%
40	40.1	37.8	-5.8%	36.9	2.4%
50	43.0	41.8	-2.8%	40.5	2.9%
60	46.4	45.1	-2.8%	43.6	3.2%
70	49.4	48.2	-2.4%	46.5	3.6%
80	52.4	50.9	-2.9%	48.8	4.1%

The Aphysical crack half-length is measured by unloading compliance in the M(T) specimen and is related to the Aeffective crack length as defined below:

$$Aeff, M(T) = Aphy, M(T)° + \Delta a, pl.zone, M(T) \quad 24$$

Where Aeff,M(T) is effective total crack half-length in the M(T) specimen, Aphy,M(T) is the Aphysical crack half-length compliance measurement in the M(T) specimen, and Δa,pl.zone, M(T) is the effective increase in crack size due to the plastic zone.

The K-control Table was populated using an elastic Qsymm1 FEM model; therefore, the crack lengths are considered Aeffective, as defined in Equation 25.

$$Aeff, Qsymm1 = Aphy, Qsymm1° + \Delta a, pl.zone, Qsymm1° \quad 25$$

Where Aeff,Qsymm1 is effective crack half-length from the Qsymm1 analysis, and Aphy,Qsymm1 is the physical crack size in Qsymm1. The effective crack size was modeled in the elastic Qsymm1 FE model and Δa,pl.zone, Qsymm1 is the apparent increase in crack size due to the plastic zone.

In the K-control approach, the SIF, K_{Qsymm1}, in the Qsymm1 FE model of Panel 1 is set to equal the SIF, $K_{M(T)}$, in the M(T) specimen. The plastic zone is related directly to the stress intensity K in the valid M(T) test region (before yielding reaches near the free edge of the M(T) specimen). Therefore, Qsymm1 and the K-control M(T) should have the same plastic zone sizes (same plastic zone size at the same SIF), the same physical crack sizes, and the same effective crack sizes as defined by Equations 26, 27, and 28.

$$\Delta a, pl.zone, Qsymm1 = \Delta a, pl.zone, M(T) \quad 26$$

$$Aphy, Qsymm1 = Aphy, M(T) \quad 27$$

$$Aeff, Qsymm1 = AeffM(T) \quad 28$$

The relationship between the M(T) crack measured, Aphy,M(T), and the Qsymm 1 elastic FE Model K-control Crack Aeff,M(T) for Panel 1 is shown in Figure 78. The MTS software measures the Aphy,M(T) crack length using the unloading compliance. Therefore, the Aeffective Panel 1 K-control Table (red curve in Figure 78) was converted to an Aphysical K-control Table (dark blue dashed curve in Figure 78). For the small-scale plastic zone, the plastic zone correction size was estimated using Equation 29. *Rpl* is the radius of plastic zone, pl.

$$rpl = \frac{1}{2} * \frac{1}{\pi} * \left({}^{K1}/_{\sigma ys}\right)^2$$

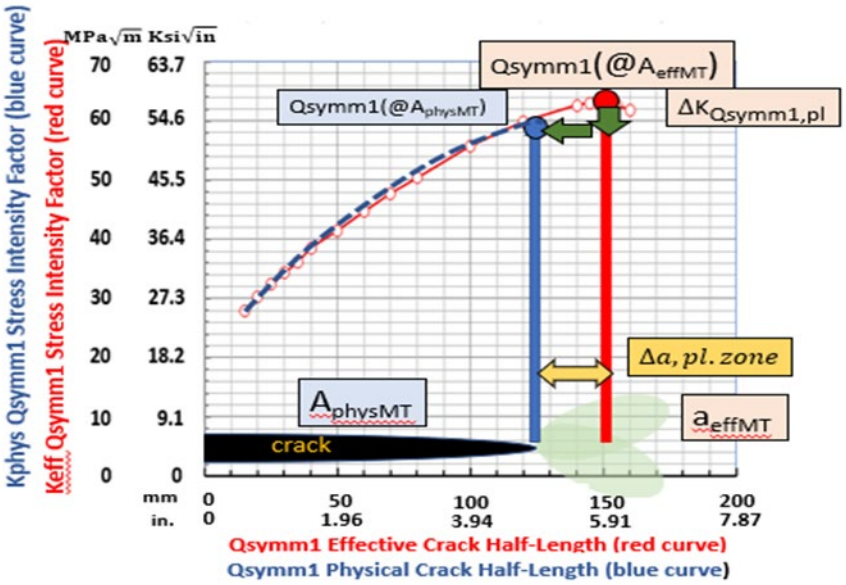

Figure 78. Corrections to convert the Aeffective crack K-control table to an Aphysical K-control table

The SIFs in the K-control Table, K,Qsymm1 (Aeff), were corrected at each effective crack half-length by multiplying the current K-control Table values based on Panel 1 (Aeff) by the ratio of the SIF for Aphysical divided by the SIF at the effective crack size, Aeff, for Qsymm1, as defined in Equation 29. Note, the mode 1, K1 SIF was used for the plastic zone size correction in Table 6.

$$K1correction = \frac{\beta,Qsymm1@(Aeff-ry@Aeff)\sqrt{\pi(Aeff-ry@Aeff)}}{\beta,Qsymm1(@Aeff)\sqrt{\pi(Aeff)}} \quad 29$$

where β,Qsymml1@(Aeff-ry@Aeff) and β,Qsymm1(Aeff) are the beta factors for the M(T) specimen evaluated at the crack size in the parenthesis. The plasticity correction results in approximately an additional 2% decrease over the Panel 1 K1 only results in the stress intensities in the crack ranges from 0.8-1.6 in. (20-40 mm), as shown in Table 6.

Additional K-control tests were conducted by manually reducing the K-Control Table by about 13% in the crack ranges from 0.8-1.6 in. (20-40 mm) from the original the Ktotal-Control Table, as shown in Figure 79. The results shown show a good match to the as-built FASTER Panel 1 life. Thus, the SIFs used for these K-control tests (final two columns in Table 6) results should be in the ballpark for those in the as-built Panel 1 SIFs in the FASTER test.

Table 6. Comparison of original K-control (2016) to K1-Control (2020) with skin mesh refinement and use of K1 with plastic zone correction

Crack length (in.)	**Ktotal-control table (2016) 1 elem. 0.055 in. skin@1.04 G +9.9 psi Ksi*sqrt-in**	**Ktotal-(2018) 2 elem. 0.055 in. skin@1.04 G +9.9 psi Ksi*sqrt-in**	**%diff Ktotal, 1 elem. vs 2 elem skin model**	**K1 (2018) 2 elem.0.055 in, skin @1.04G +9.9ps Ksi* Sqrt-in.**	**% difference Ktotal, 0.055 in, 2 elem vs K1, 0.055 in. 2 elem @1.04G +9.9psi**	**K1 control table, 0.55 in. skin (2018) with K1 and plastic zone correction, 1.045G +9.9psi, Ksi* sqrt-in.**	**% difference K1 vs K1m plast**	**%difference Ktotal-control, 1el(2016) vs K1-Control, 2 elem +plast**	**Final K-control table at 1.3 ksi matching Panel 1 Ksi* sqrt-in.**	**% difference final K-control at 1.3 ksi vs Ktotal-control, 1 el (2016), Ktotal**
0.79	28..1	26.6	-5.4%	26.2	1.3%	25.7	1.9%	8.4%	24.4	13.2%
0.98	30.2	28.9.	-4.3%	28.3	2.1%	27.8	1.8%	7.9%	26.4	12.6%
1.18	32.1	31.0	-3.4%	30.3	2.2%	29.9	1.3%	6.9%	28.3	11.7%
1.38	34.0	32.9	-3.2%	32.2	2.1%	31.4	2.5%	7.6%	29.8	12.3%
1.57	36.5	34.4	-5.8%	33.6	2.4%	32.9	1.9%	9.8%	31.3	14.4%
1.97	39.1	38.0	-2.8%	36.9	2.9%	35.8	2.9%	8.3%	34.0	13.0%
2.36	42.2	41.0	-2.8%	39.7	3.2%	38.2	3.8%	9.6%	36.3	14.0%
2.76	45.0	43.9	-2.4%	42.3	3.6%	39.7	6.1%	11.7%	37.9	15.9%
3.15	47.7	46.3	-2.9	44.4	4.1&	40.1	9.6%	15.8%	38.5	19.4%

Crack length (mm)	Ktotal-control table (2016) 1 elem. 0.055 in. skin@1.04G +9.9 psi MPa*sqrt-in	Ktotal-control table (2018) 2 elem. 0.055 in. skin@1.04G +9.9 psi MPa*sqrt-in	%diff Ktotal, 1 elem. Vs 2 elem skin model	K1 (2018) 2 elem. 0.055 in, skin@1.04G +9.9 psi MPa*sqrt-in	% difference Ktotal, 0.055 in. 2 elem vs. K1, 0.055 in, 2 elem @1.046 +9.9 psi	K1-control table, 0.565 in. skin (2018) with K1 and plastic zone correction, 1.04G+9.9psi MPa*sqrt-m	%difference K1 vs K1, plast	%difference Ktotal-control, 1el(2016) vs K1-Control, 2 elem +Plast	Final K-control table at 1.3 ksi matching Panel 1 MPa* sqrt-m	% difference final K-control at 1.3 ksi vs Ktotal-control, 1 el (2016), Ktotal
20	30.9	29.2	-5.4%	28.8	1.3%	28.3	1.9%	8.4%	26.8	13.2%
25	33.2	31.8	-4.3%	31.1	2.1%	30.5	1.8%	7.9%	29.0	12.6%
30	35.3	34.1	-3.4%	33.3	2.2%	32.9	1.3%	6.9%	31.1	11.7%
35	37.4	36.2	-3.2%	35.4	2.1%	34.5	2.5%	7.6%	32.7	12.3%
40	40.1	37.8	-5.8%	36.9	2.4%	36.2	1.9%	9.8%	34.3	14.4%
50	43.0	41.8	-2.8%	40.5	2.9%	39.4	2.9%	8.3%	37.4	13.0%
60	46.4	45.1	-2.8%	43.6	3.2%	41.9	3.8%	9.6%	39.9	14.0%
70	49.4	48.2	-2.4%	46.5	3.6%	43.7	6.1%	11.7%	41.6	15.9%
80	52.4	50.9	-2.9%	48.8	4.1%	44.1	9.6%	15.8%	42.3	19.4%

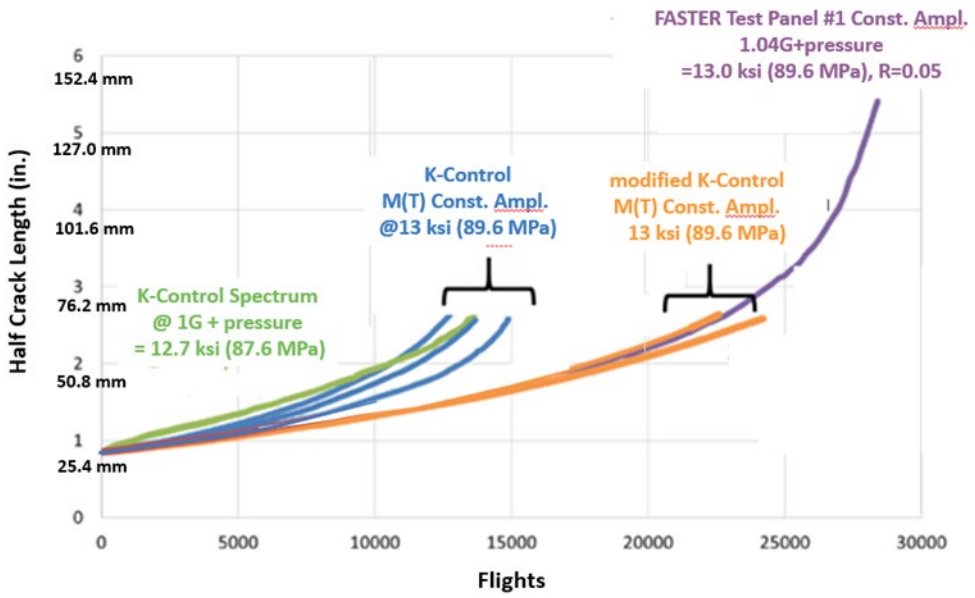

Figure 79 .Results of FASTER test Panel 1 compared with modified K1-control M(T) testing with plasticity correction

Now that the K-control SIFs that provide a good fit to the FASTER Panel 1 life (see Figure 79) have been established (last two columns in Table 6), these SIFs can be compared to the final as-built, FASTER-tested Panel 1 SIF solutions. It turns out that the as-built Panel 1 FE model with all corrections to be described below exhibited Ktotal SIF solutions surprisingly similar to the as-designed Panel 1 Ktotal SIFs, with the more refined two-element FE model listed in column 3 of Table 6 (Ktotal 2018, 2 element, 0.055 in. skin @1.04G +9.9 psi). Therefore, by analogy, the K1 SIFs and K1 with plastic zone correction SIFs for the as-built Panel 1 are expected to be similar to the respective K1 SIFs for the as-designed Panel 1 (columns 5 and 7 of Table 6).

As mentioned above, the as-built Panel 1 FE model with all corrections exhibited Ktotal SIF solutions surprisingly similar to the as-designed Panel 1 Ktotal SIFs when the more refined two-element FE model was used. Measurements of strain at various points on the as-built FASTER Panel 1 and the as-built Panel 2 displacements at the load arms indicated that adjustments were needed to the as-built Panel 1 FE model (discussed in detail in Section 6).

Adjustments included the increased pocket skin thickness in the as-built Panel 1; changes in axial load arm and skin edge BCs to resolve the measured load point displacement and measured panel strains; and the use of increased mesh density through the skin thickness (see impact of mesh density described in Section 6.4). The as-built Panel 1 SIFs were calculated using eight elements througthe skin thickness based on the results of the mesh convergence study (see Section 6.4). The net effect of these adjustments resulted in the as-built Panel 1 Ktotal SIFs with eight

elements through the thickness (yellow triangles) to be less than 1% lower than the as-designed Panel 1 Ktotal solution with two elements (solid red circle). Therefore, if the circumferential crack Ktotal SIFs of the as-designed and as-built Panel 1 are similar, then it would be expected that likewise, the K1 SIFs and the K1 with plastic zone correction SIFs for the as-designed and as-built Panel 1 would also be similar to the results in columns 5 and 7 of Table 6. In this case, the estimated SIFs for the as-built Panel 1 (estimated using column 7 of Table 6) are still about 4-5% too high to match the FASTER crack growth results from Panel 1. Some of this difference may be attributed to variability in crack growth due to crack surface morphology which has been observed on previous tests. Fracture surfaces exhibiting a slant morphology grew faster than V-shaped fracture surfaces, which could account for some or all of this 4-5% difference. The fracture surfaces of the FASTER-tested Panel 1 will have to be compared with the K-control test surfaces to see if there are differences. Another possibility leading to a 4% reduction of SIFs in column 7 of Table 6 is to account for a curved crack front in the Panel 1 skin due to bending loads from the broken stringer. In this case, the use of the skin mid-plane SIF solution for the M(T) K-control test which does not have any skin bending would be too high to represent the crack growth in Panel 1. A Panel 1 skin SIF solution below the mid-plane may be a better choice. Additional tests are being considered to develop a better understanding of the differences in Panel 1 circumferential crack growth test results versus K-control testing.

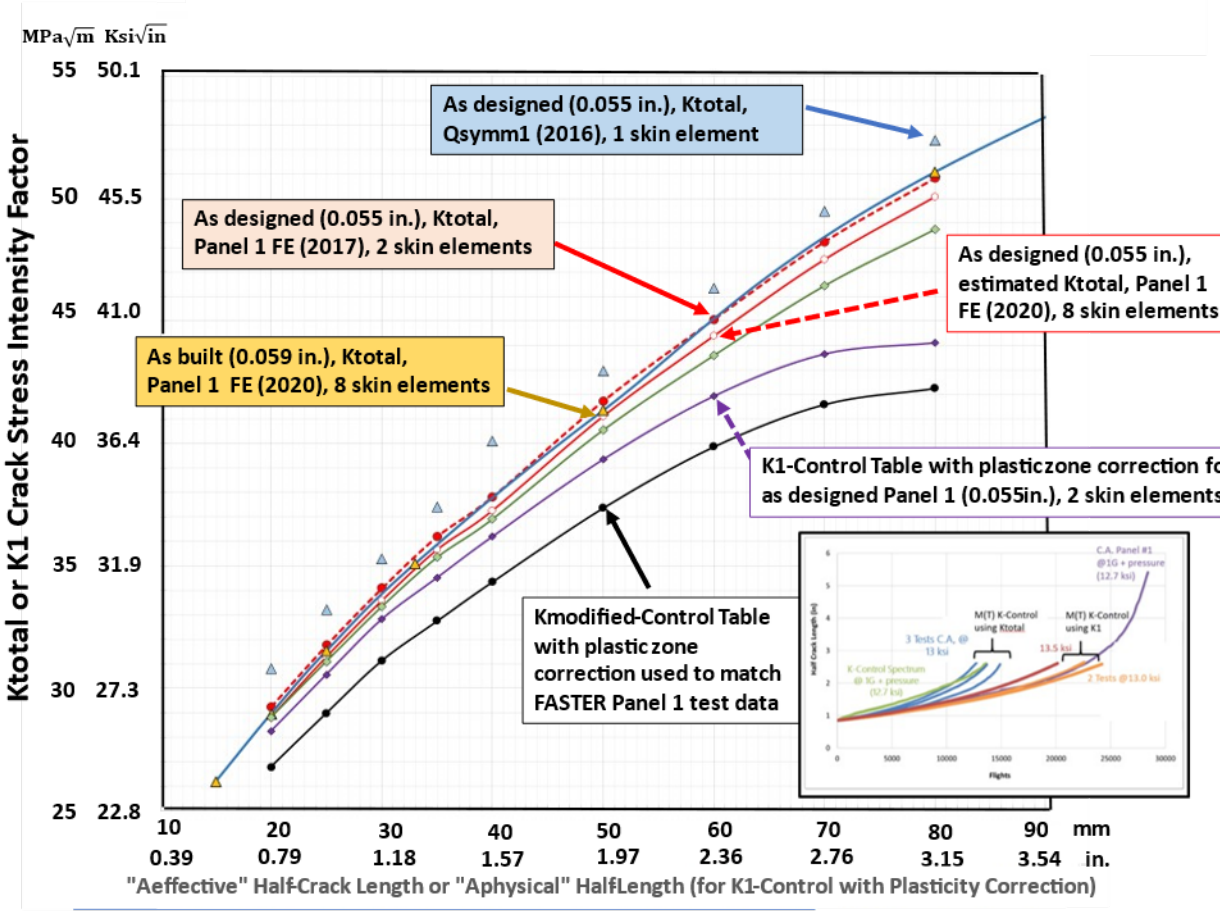

Figure 80. As-built Panel 1 stress intensity solutions vs. new as-designed Panel 1 solution for axial load arm displacement = -1.0 mm and radial link displacement = 0.0 mm

5.7 Final comments on circumferential crack growth spectrum testing approach

The following comments are to clarify the role of spectrum in this FASTER Panel testing program for the circumferential crack growth testing phase. Recall that one of the primary objectives was to compare the behavior of new metallic materials solutions and advanced design concepts for the single-aisle aircraft. To compare “apples to apples,” it is important to test the panel under spectrum conditions for crack growth in the circumferential direction. Defining the different flight load types in a fleet of aircraft needed to construct a representative spectrum is within the domain of the aircraft manufactures and is beyond the scope of this program.

The goal of this program was to test a reasonably representative spectrum in magnitude and exceedance profile, as well as to test all panels in an “apples-to-apples” manner. However, in practicality, the program discovered that it was not possible to build thin-skinned EMST panels to the same thicknesses, and by keeping loads constant, the variations in stress and SIFs would

lead to large variations in life. For this reason, the testing plan for Panels 2 and beyond was modified to follow another approach for the “apples-to-apples” comparison. It was decided that the best approach was to adjust loads on each panel to keep the SIF solutions versus crack size the same for all panels. Since the stringer-to-skin and frame-to-skin AS/Bt ratios are now different between Panel 1, Panel 2, and Panel 3, adjusting for loading based on cross-sectional area changes would not result in the same SIF solutions between panels. Also, because the doubler reinforced load introduction areas of Panels 1-3 were kept the same, the impact of the panel reinforced doubler edge stiffness relative to the panel interior stiffness for a constant area correction would have to be accounted for in the loading. Finally, since repeat inspection was the primary panel sizing criterion, it was determined that it would be easier to draw conclusions regarding panel performance by keeping the SIF the same for Panels 2 and 3.

One approach to utilize the Panel 1-3 data is to use the FASTER panel test results in conjunction with supplemental testing to first validate that K-control testing reproduces the FASTER panel crack growth results. Then, spectrum K-control testing can be used to establish skin working stress targets for the circumferential repeat inspections for all ESMT Panel concepts at several locations in the crown. The same goes for the longitudinal inspections. A new sizing study could then be conducted to compare the performance of the various EMST panel configurations.

6 Finite element modeling of Panel 1

6.1 Original 2016-2017 as-designed Panel 1 FE modeling

This section describes the FE modeling work used to generate the loads for the as-designed, 0.055 in. (1.4mm) skin pocket thickness Panel 1. These loads were unknowingly used to test the as-built, 0.059 in. skin pocket Panel 1, because the as-built skin pocket thickness discrepancy was not detected until after the crack growth testing was completed. The as-designed Panel 1 loads were generated by matching the as-designed Panel 1 FE model stress intensity solutions with the as-designed Qsymm1 FE model. At that time, both the Qsymm1 and as-designed Panel 1 FE models used one C3D20, 20 node solid element through-the-skin thickness. A refined in-plane mesh was used at the crack tip. There are several aspects of the Panel 1 load introduction and the FASTER attachment/loading setup that required a different FE modeling approach in the as-designed Panel 1 compared to the Qsymm1 FE model where cylindrical symmetry BCs were used with pressure and axial loads. Also, recall the discussion in Section 5 where it was discovered that the modeling the circumferential crack on the Qsymm1 FE model symmetry plane resulted in a pure K1 opening mode, which did not reflect the off-center bay positioning of the circumferential crack in Panel 1 resulting in small K1, K2, and small K3 (from bulging) SIFs.

This section details the as-designed Panel 1 FE modelling work in the 2016-2017 timeframe. Most of the results in this section are for the one-element through-the-skin thickness FE model, except where noted. Recall that after testing Panel 1, it was discovered that the Panel 1 skin was built to an increased thickness of +0.004 in. (0.102 mm) in the chem-milled pockets, and the SIFs were recalculated in 2020 for the 0.059 in. (1.5 mm) thick skin pocket as-built Panel 1. Measurements of strain in Panel 1 and LVDT panel displacements at the load arms in Panel 2 indicated that small adjustments were needed to the original 2016-2017 modeling BCs for the new as-built Panel 1 FE modeling. These adjustments to the original Panel 1 FE model included the increased as-built pocket thickness in Panel 1 and included boundary condition adjustments to better model axial bending moments introduced when the as designed FASTER Panel 1 loads were applied to the as built Panel 1. Also, a boundary condition at the skin edge used to stabilize the solution which was to be removed in the final solution step was discovered and the small error in results was corrected (to be discussed later). Finally, a meshing approach was developed, which allowed a significant increase in mesh density through the skin thickness with a relatively small increase in computational resources. The combined effects of these adjustments (with plus and minus effect on SIF's) resulted in the final 2020 as-built Panel 1 SIFs, which surprisingly compared well to the as-designed Panel 1 SIFs when two elements were used through the skin thickness (Figure 80).

The as-designed Panel 1 test article was shown in Figure 4. A full set of engineering drawings is included in Appendix A. The 2524-T3 skin radius was 74 in. (1879.6 mm). A pocketed skin construction was used as shown in Figure 5 with a skin thickness of 0.063 in. (1.6 mm) in the pad-up skin under the frames and stringers and a thickness of 0.055 in. (1.4 mm) in the pocketed regions. The two-piece 7075-T62 shear tie/frame design used for Panel 1 is shown Figure 47. The frame was extruded, stretch-formed, and quenched/tempered. The shear ties were hydroformed and quenched/tempered. There were six frames and eight stringers in the as-designed Panel 1 FE model. The frame spacing was 20 in. (508 mm) and the AS/BT ratio of frame area/effective skin area was 0.294. The 7150-T77511 stringer was shown in Figure 48. The stringer spacing is 7.0 in. (177.8 mm) and AS/BT ratio of the stringer area to skin effective area was 0.393. The rivets fastening the stringers/frames to the skin were NAS1097KE5 (0.156 in. (3.97 mm) diameter, 100 degrees countersunk, 7050-T73). An elastic modulus of 10.2 Msi (70.3 GPa) was used for the skin and 10.4 Msi (71.7 GPa) was used for the stringers and frame.

Panel 1 was loaded through the skin by actuators axially and in the hoop direction. The frames are also loaded in the hoop direction at each frame end by individual actuators. The test panel was loaded internally by pressure. There is only one source of constraint (acting as a safety feature) in the FASTER test panel. These are the radial links attached to each frame at both ends

(Figure 44) which restrain the panel from moving in the radial direction. To simplify the FE modeling, the radial links were assumed to be rigid (e.g., zero radial displacements were applied to the frames at the radial links attachment point). To represent the FASTER loading, the as-designed Panel 1 FE model actuator loads were applied tangent to the FE model skin edges and frame load points, and pressure was applied internally in the model. The Qsymm1 to Panel 1 approach shown in Figure 43 was used for the load development of the as-designed Panel 1 loads. If Panel 1 did not have the thick edge doublers package to distribute the large point loads from the actuators, the Panel 1 loads could be determined directly (as a FE substructure) from the Qsymm1 FE model results. To account for the edge doublers, an iteration approach was used for the Qsymm1 to Panel 1 loading development with the goal of achieving the same SIFs versus crack size as Qsymm1 while minimizing radial link reaction loads. Note that any imbalance in applied loads balanced by the radial link reactions.

As described above, the effect of the radial links should be small and localized when the Qsymm1 to Panel 1 approach is used (see Figure 43). However, for the FASTER Panel 1 circumferential crack growth test, the as-designed Panel 1 loads were applied to the as-built Panel 1 geometry. The effect of using this imbalanced load relative to the as-built Panel 1 geometry introduced a global bending moment from the axial loads (reacted by the radial links), which introduced vertical movement at the axial load actuators. For FE modeling, a constant radial displacement boundary displacement was applied at the axial actuator load arm to skin connection points to offset the effect of this unintended bending moment produced by the axial loads. The as-designed FASTER test Panel 1 model is shown in Figure 81. The length is 125 in. (3.175 m), and the width is 76.5 in. (1.94 m) measured as the arc length for the 74 in. (1.88m) radius. The test panel finite element model has 6 frames and 8 stringers and 35 chem-milled skin pockets.

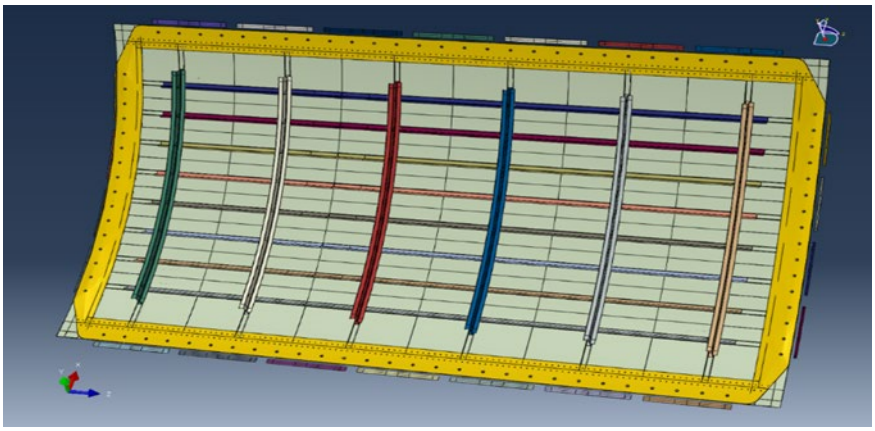

Figure 81. ABAQUS FEM model of Panel 1 (note that mesh is not shown)

Heavy skin doublers were used in the Panel 1 test article, as previously shown Figure 45 and in Figure 82 around the panel edges to apply the large point loads to the skin in both the axial and hoop directions. An iterative solution method was necessary to determine the test panel loads needed to reproduce the SIFs and stresses in the Qsymm1 model. The FASTER system of load actuators was described in Section 3. For hoop loading, there are seven actuators on each side, and each actuator has four load arms which distribute the actuator load equally. In total, there are 28 loads along both the top and bottom hoop edges for a total of 56 hoop loading points on the skin, as indicated by the edge holes shown in Figure 81. The spacing between each hoop direction loading arm hole is about 4 in. (101.6 mm). When the panel is pressurized, the panel hoop loading actuator arms do not restrict the panel from moving freely in the radial (U1) direction in a cylindrical coordinate system where U1 = radial direction, U2 = circumferential direction, and U3 is axial in the cylindrical length direction.

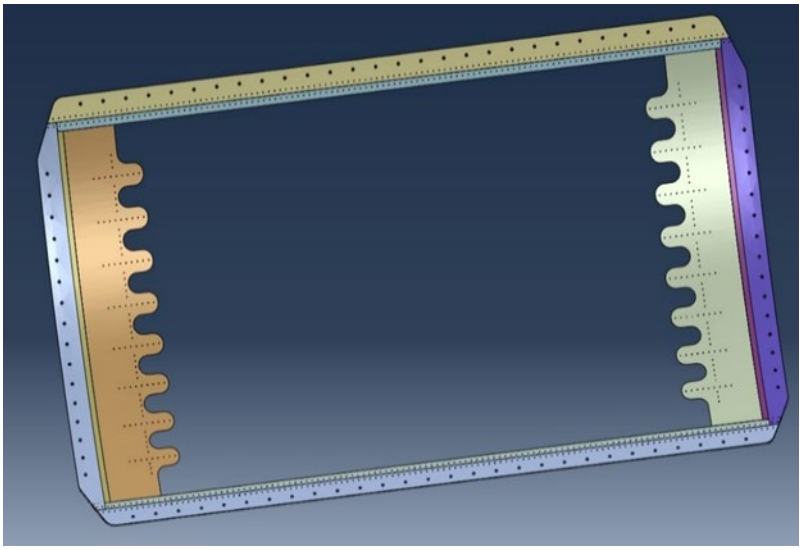

Figure 82. Edge doublers used in Panel 1 FE model

An iterative approach was used to determine the axial, hoop, and frame actuator loads applied (each actuator can be loaded independently) to the as-designed Panel 1 FE model to reproduce the stresses and SIFs in the Qsymm1 quarter symmetry model. In the first step, cylindrical symmetry edge displacement BCs were enforced in the as-designed Panel 1 FE model along the two hoop edges at each actuator load arm attachment point to the skin (Figure 83). Also, a cylindrical symmetry condition was applied at the frame actuator to frame load points (Figure 83). The radial link constraints were not included in this first iteration step. The axial strains from the Qsymm1 model were used to apply a trial displacement to the undamaged Panel 1 FE model at the connection points between the axial load arms and the skin. Pressure was applied internally. The reaction loads from FE analysis in step 1 were used as loads for step 2.

In step 2, the actuator arm reaction loads from step 1 were converted to actuator loads by summing the reactions for the four arms for each of the eight axial actuators (four per edge) and spreading that load equally to each load arm. The same is done for the 14 hoop actuators along the edges of the panels. The frame is loaded by one actuator arm, and frame loads are set equal to the frame reaction loads from step 1. The only displacement constraints were the radial links.

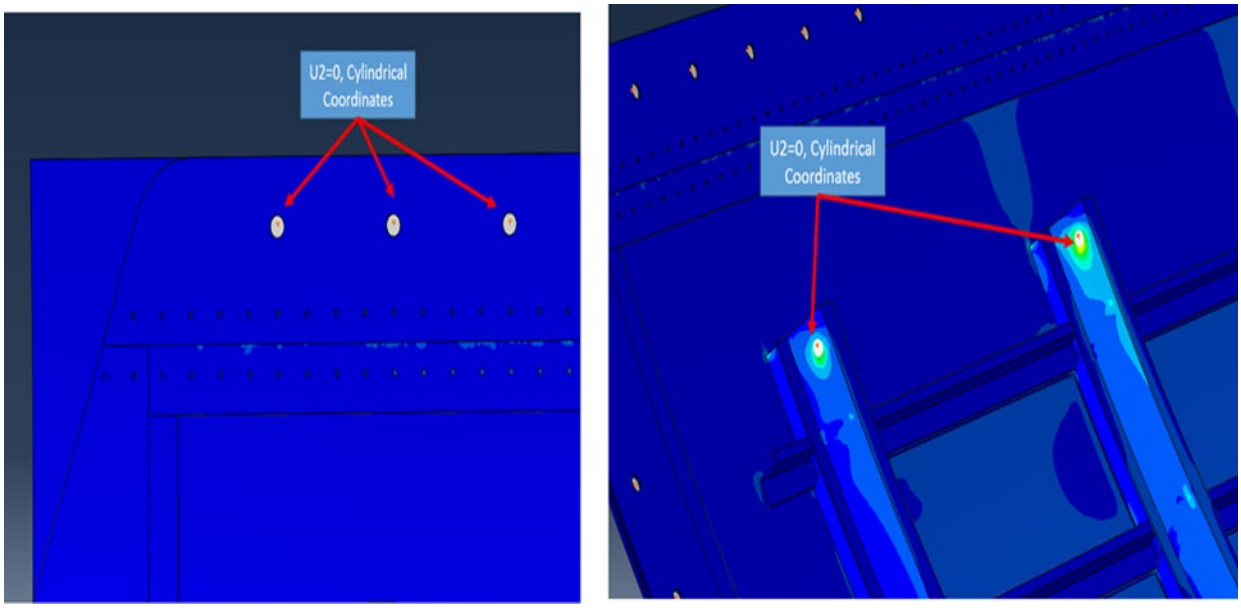

Figure 83. Cylindrical symmetry conditions applied at actuator load points

Next actuator loads are iteratively adjusted and applied to the as-designed Panel 1 FE model until the SIFs are the same as in the QSymm1 model. These load locations are the same as described in step 2. As in step 2 the radial link boundary condition is applied as a zero-radial displacement at the frame attachment. The radial link only permits a load to be developed in the radial direction.

It was discovered after the as built FASTER Panel 1 testing that the skin at the Panel 1 hoop edge actuator load points in the FE model was unintentionally constrained in steps 3+ to a zero radial displacement, as idealized in Figure 84. Note that the forces shown in Figure 84 are the applied forces from step 1. This radial constraint at the skin edge created a small radial reaction at the hoop edge of Panel 1 (Figure 84). This step 3+ solution approach was conducted in two steps because the FASTER fixture is designed to rely on load equilibrium to improve NLGEOM convergence. The intention was to establish equilibrium in the first step and then to remove this skin constraint in the second solution step and reestablish equilibrium, but unfortunately the displacement was unintentionally not removed in this solution step. This error in SIF was a few percent but corrected in the 2020 as-built Panel 1 FE model for the 0.059 in. pocketed skins. The steps were iterated upon until a good match was made to the Qsymm1 cylindrical model.

Another small difference between the Panel 1 FE model and the Qsymm1 FE model was the inclusion of the elastomeric seal used to contain the pressure. The effective pressurized area of skin inside of the rubber seal begins approximately 4 in. away from the skin panel edge, as shown in Figure 84 and Figure 85. To simulate this test condition, pressure loads are applied to the skin area inside the seal in the Panel 1 FE model. This small deviation from a true pressurized stiffened panel is also accounted for by the iterative approach. Results in the bay region where the cracks are grown in Panel 1 are shown in Figure 86 to Figure 88.

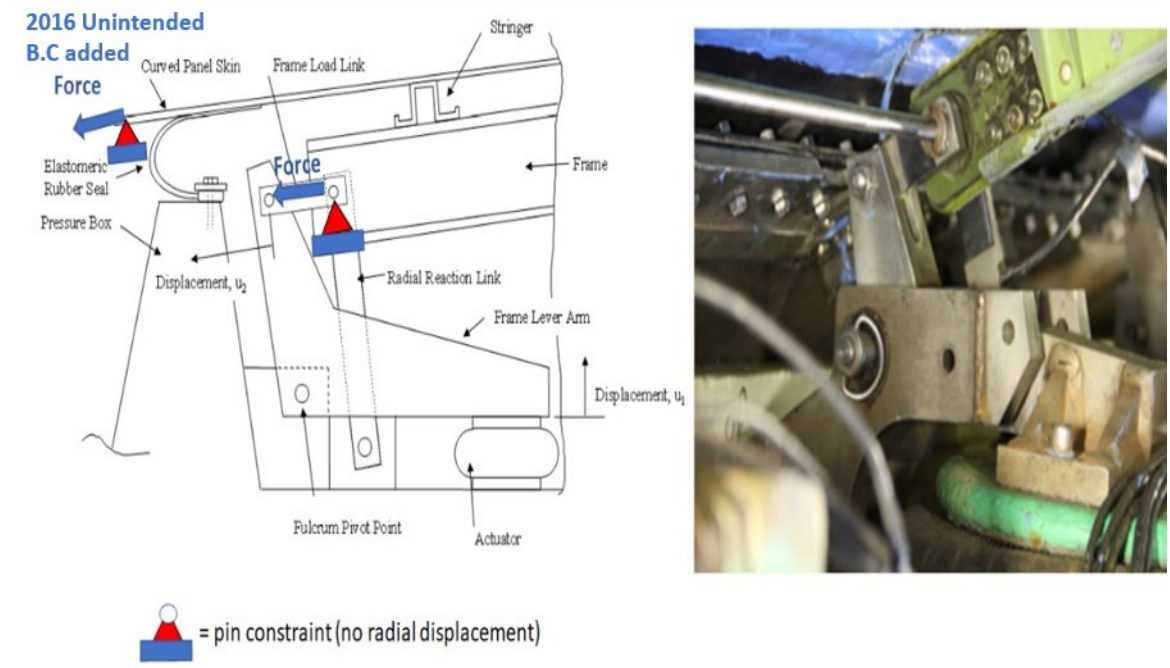

Figure 84. Detail of a radial link in the FASTER fixture

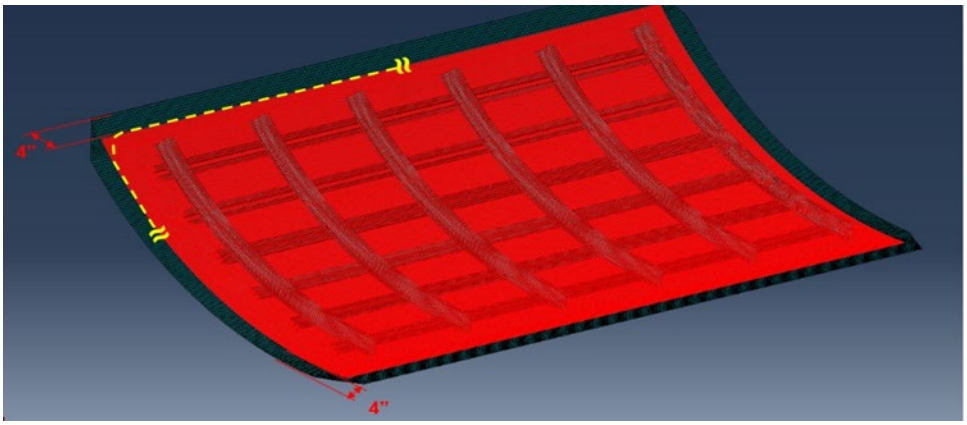

Figure 85. Panel 1 FE model showing the elastomeric seal (dark blue edge)

In general, a good fit to the Qsymm1 SIF solution was obtained for the crack sizes especially at the smaller crack sizes most of the life of the panel occurred.

The undamaged, as-designed Panel 1 FE results at 9.9 psi (0.068 MPa) pressure showed good agreement when compared with the Qsymm1 FE results, as shown in Figure 86. Similar results for the 1G plus 9.9 psi (0.068 MPa) condition were also in good agreement with the Qsymm1 results in the bays region where the cracks are grown in Panel 1 (Figure 87 and Figure 88). It was determined through Panel 1 FE analysis that no adjustments to the actuator loading during FASTER Panel 1 testing were necessary to match the SIFs in the Qsymm1 FE model for similar circumferential crack or longitudinal crack scenarios.

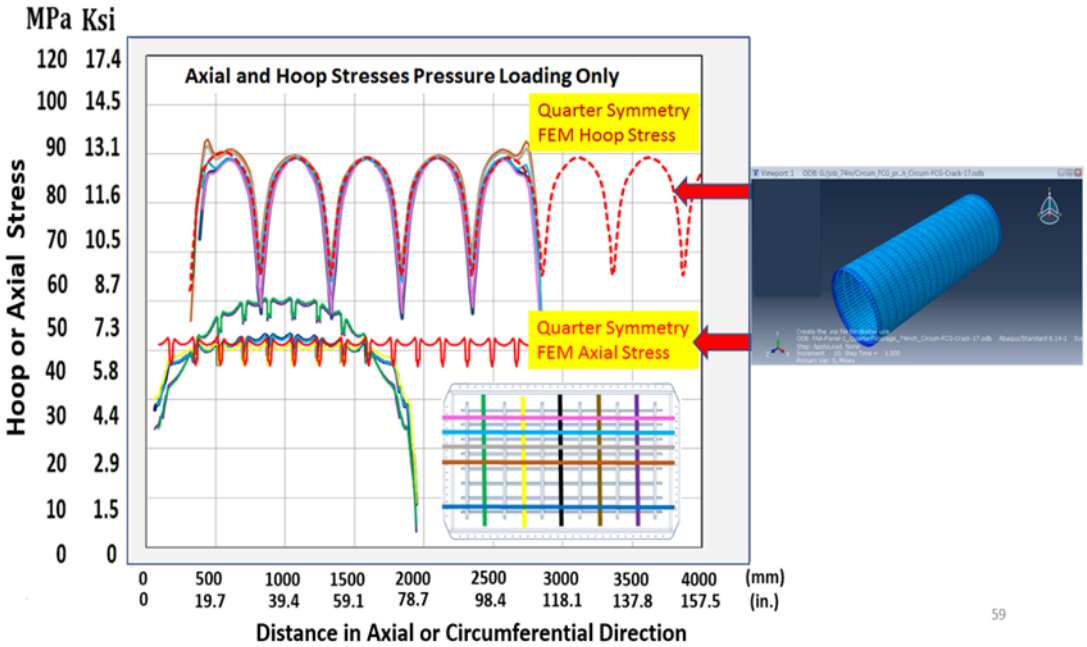

Figure 86. Comparison of Panel 1 FEM stresses to Qsymm1 at 9.9 psi pressure

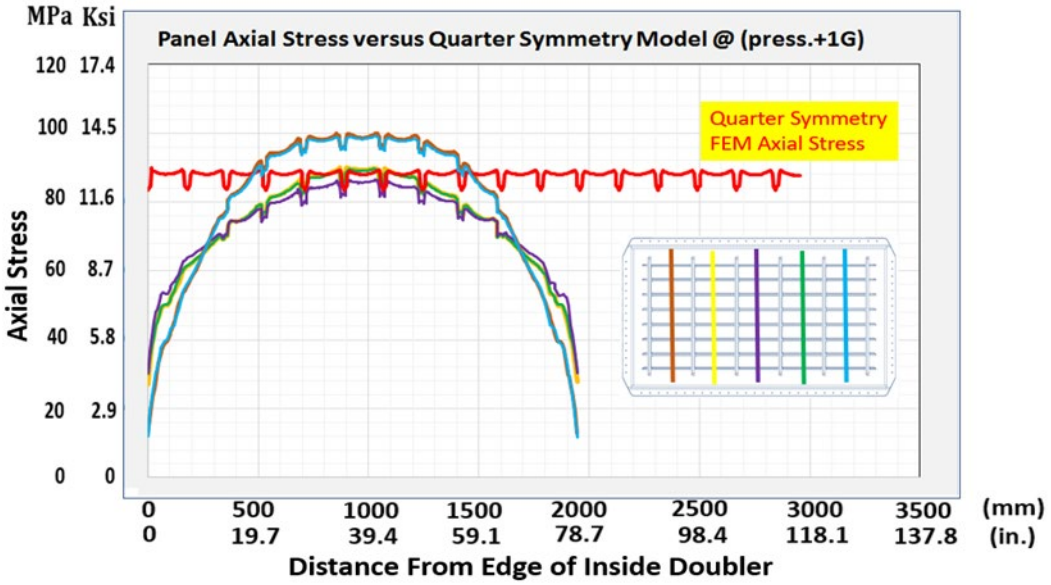

Figure 87. Panel 1 axial stress comparison with Qsymm1 model at 9.9 psi+1G

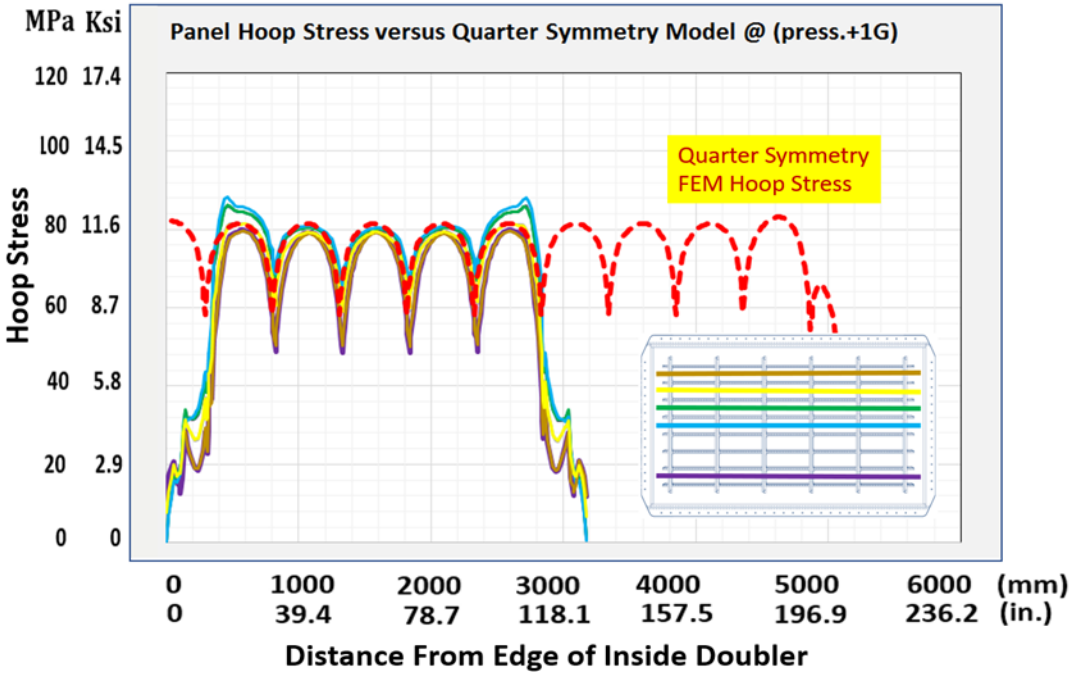

Figure 88. Panel 1 hoop stress comparison with Qsymm1 model at 9.9 psi+1G

6.2 Panel 1 loads

Loads developed for the as-designed Panel 1 are shown in Figure 89 for 2.5G bending only and in Figure 90 for 9.9 psi (0.068 MPa) pressure only. As shown in Figure 91, there is very little impact of bulging for cracks in the circumferential direction, even when the ABAQUS FE

NLGOEM corrections for large displacements were used, so the pressure and 2.5G results can be scaled and superimposed to generate solutions for various pressure and bending scenarios in this direction.

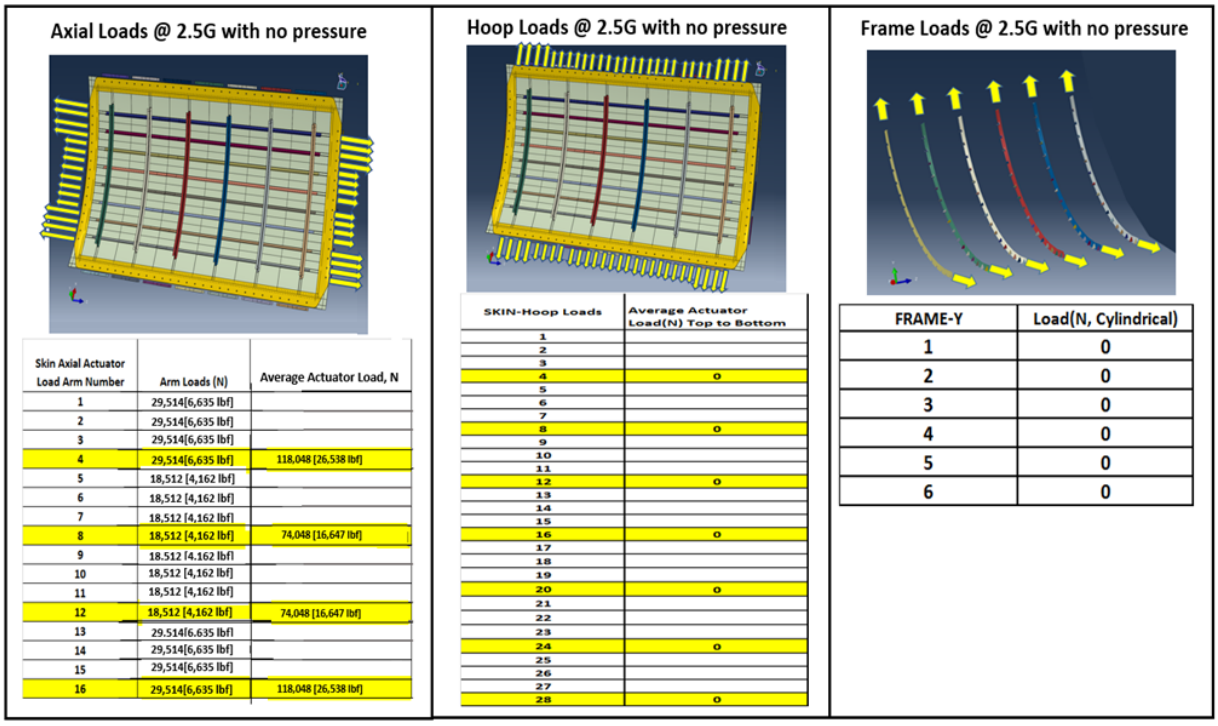

Skin Axial Actuator Load Arm Number	Arm Loads (N)	Average Actuator Load, N
1	29,514[6,635 lbf]	
2	29,514[6,635 lbf]	
3	29,514[6,635 lbf]	
4	29,514[6,635 lbf]	118,048 [26,538 lbf]
5	18,512 [4,162 lbf]	
6	18,512 [4,162 lbf]	
7	18,512 [4,162 lbf]	
8	18,512 [4,162 lbf]	74,048 [16,647 lbf]
9	18.512 [4.162 lbf]	
10	18,512 [4,162 lbf]	
11	18,512 [4,162 lbf]	
12	18,512 [4,162 lbf]	74,048 [16,647 lbf]
13	29.514[6.635 lbf]	
14	29,514[6,635 lbf]	
15	29,514[6,635 lbf]	
16	29,514[6,635 lbf]	118,048 [26,538 lbf]

SKIN-Hoop Loads	Average Actuator Load(N) Top to Bottom
1	
2	
3	
4	0
5	
6	
7	
8	0
9	
10	
11	
12	0
13	
14	
15	
16	0
17	
18	
19	
20	0
21	
22	
23	
24	0
25	
26	
27	
28	0

FRAME-Y	Load(N, Cylindrical)
1	0
2	0
3	0
4	0
5	0
6	0

Figure 89. Panel 1 actuator loads for 2.5G bending with no pressure

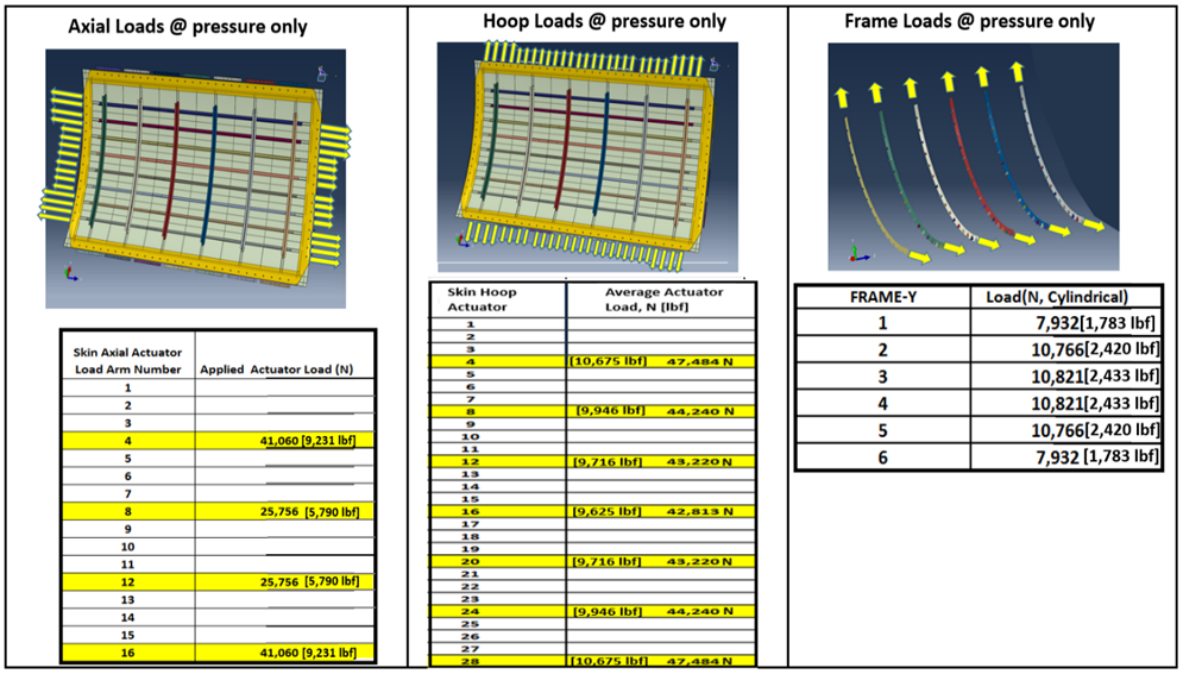

Skin Axial Actuator Load Arm Number	Applied Actuator Load (N)
1	
2	
3	
4	41,060 [9,231 lbf]
5	
6	
7	
8	25,756 [5,790 lbf]
9	
10	
11	
12	25,756 [5,790 lbf]
13	
14	
15	
16	41,060 [9,231 lbf]

Skin Hoop Actuator	Average Actuator Load, N [lbf]
1	
2	
3	
4	[10,675 lbf] 47,484 N
5	
6	
7	
8	[9,946 lbf] 44,240 N
9	
10	
11	
12	[9,716 lbf] 43,220 N
13	
14	
15	
16	[9,625 lbf] 42,813 N
17	
18	
19	
20	[9,716 lbf] 43,220 N
21	
22	
23	
24	[9,946 lbf] 44,240 N
25	
26	
27	
28	[10,675 lbf] 47,484 N

FRAME-Y	Load(N, Cylindrical)
1	7,932[1,783 lbf]
2	10,766[2,420 lbf]
3	10,821[2,433 lbf]
4	10,821[2,433 lbf]
5	10,766[2,420 lbf]
6	7,932 [1,783 lbf]

Figure 90. Panel 1 actuator loads for 9.9 psi pressure only

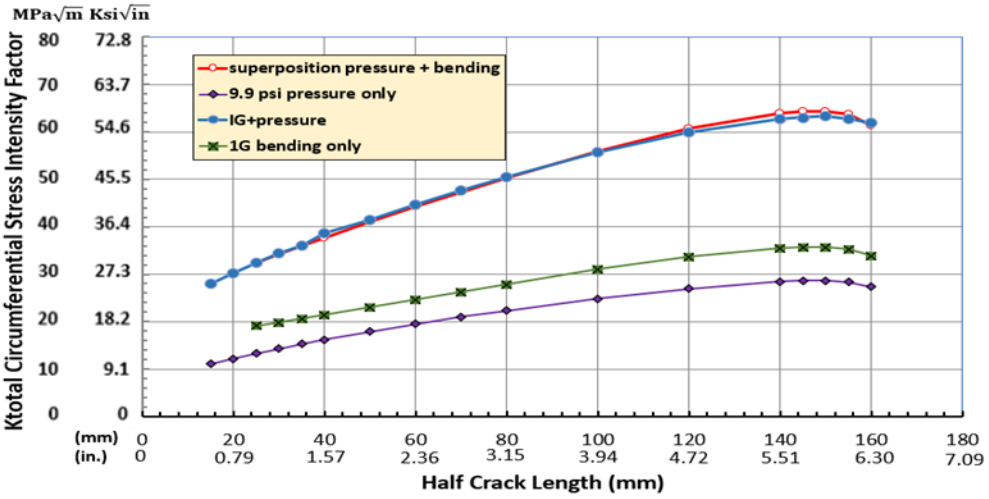

Figure 91. Comparison of superposition of SIFs using Qsymm1 results versus Qsymm1

6.3 Adjustments for FASTER axial arm loads developed for the as-built Panel 1

The FASTER load frame applies discrete actuator loads along the axial edge, hoop edges, and frame ends. The radial links restrict Panel 1 radial movement at the frame ends (see Figure 44).

In the Panel 1 FE model, the hoop and axial actuator loader arms were assumed to only apply load tangent to the skin or frames. When the same geometry is used for both the Qsymm1 and Panel 1 FE models, the axial actuator arm loads are balanced not only for the front axial edge to rear axial edge, but also are balanced about the global XX axis through the centroid of the Panel 1 cross-section (see Figure 92) to prevent a bending moment. This was the case for the as-designed 0.055 in. skin pocket thickness design. However, when the as-designed Panel 1 loads were applied to the as-built 0.059 in. skin pocket Panel 1 FE model with the different cross-section, a bending moment was generated about the global XX axis shown in Figure 92.

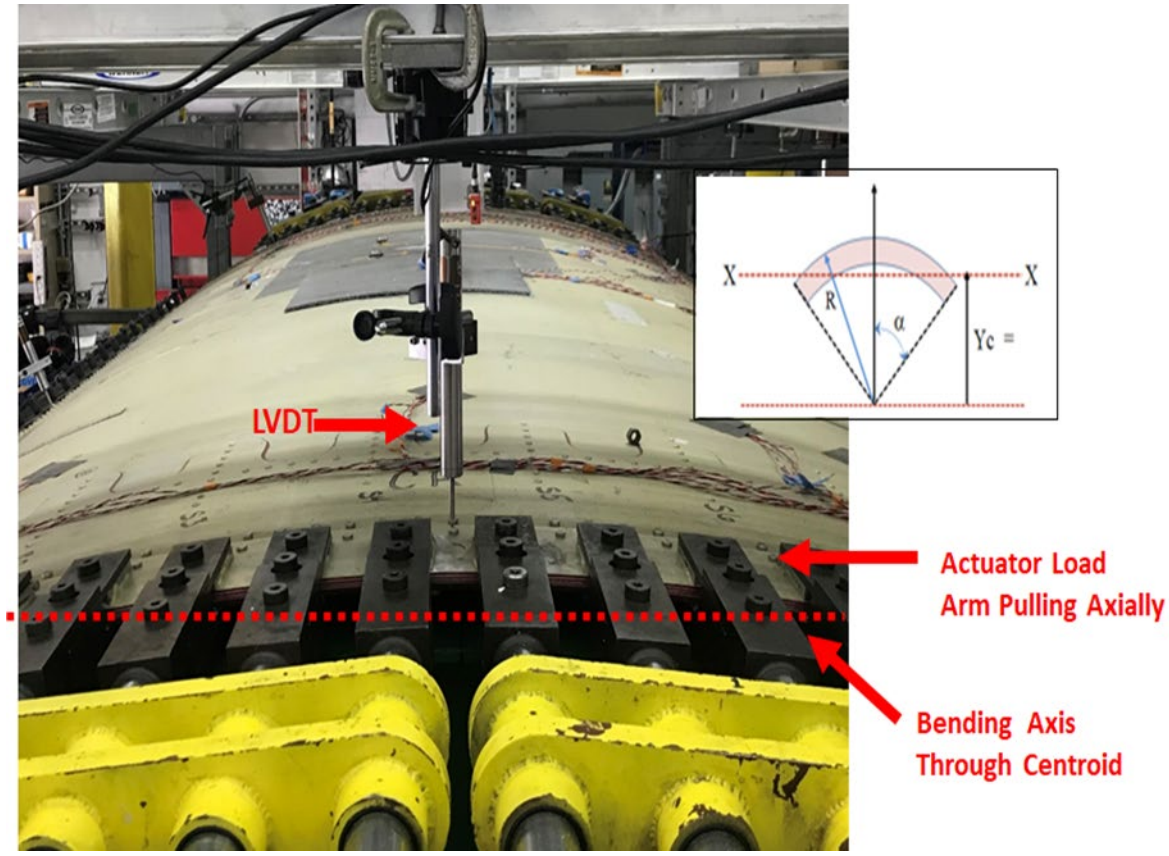

Figure 92. Panel 1 showing axial load arms, the centroid of the cross-section, and LVDT

Strain gage readings of test Panel 1 and Panel 2 and LVDT measurements of Panel 2 confirmed this effect. To account for this effect for the as-built Panel 1 FE model, various FE analyses were conducted by adjusting the radial movement at the axial load arms and radial link displacements as shown in Figure 93 and Figure 94 to match strain gage data. A radial movement of -0.039 in. (-1.0 mm) at the axial edge load arms was applied as a boundary condition while the radial link boundary condition was kept equal to 0.0 in. at the frame attachment point in the solution providing the best fit to the strain gage results. Note, the -0.039 in. (-1.0 mm) movement in the

Panel 1 FE coordinate system is a +0.039 in. (+1.0 mm) outward radial movement of Panel 1 in the FASTER Panel 1 test coordinate system.

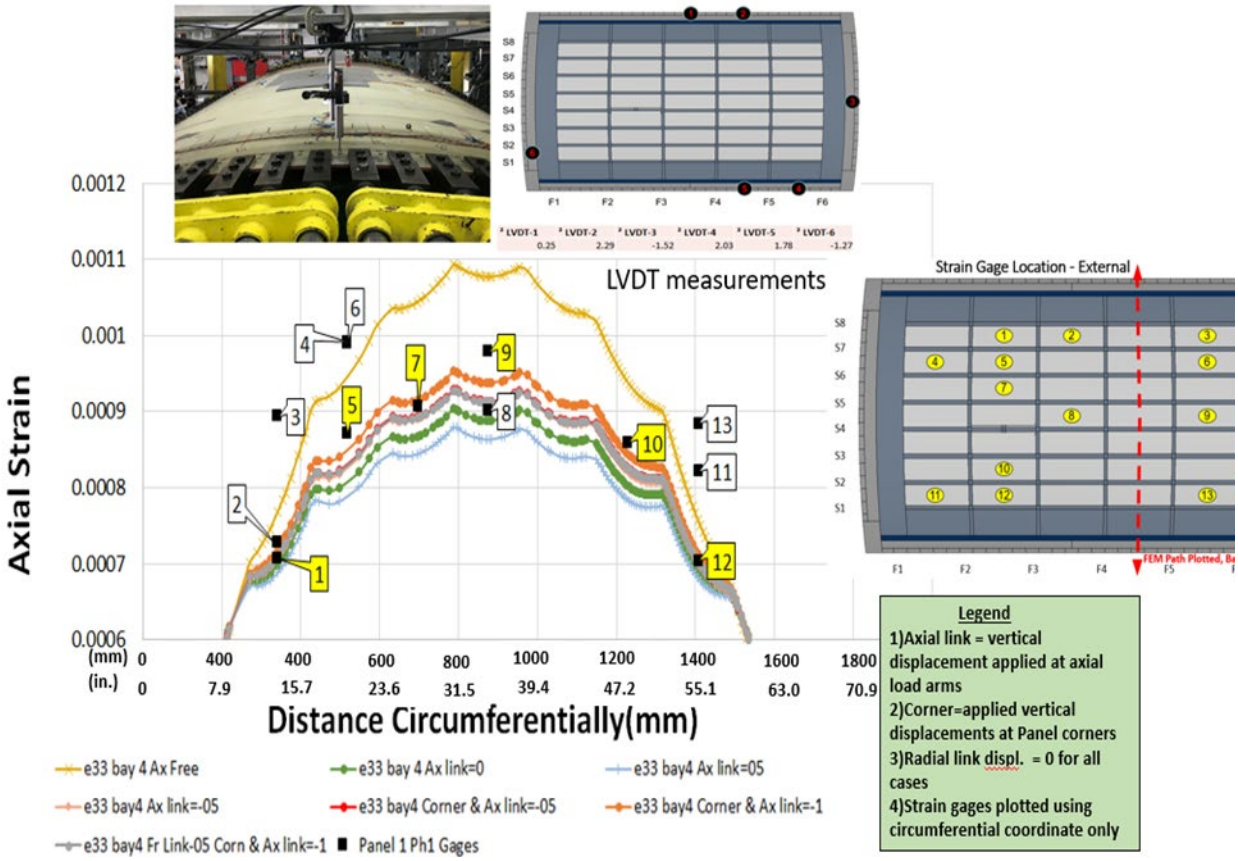

Figure 93. Comparison of axial strain gage measurements with Panel 1 FE analyses assuming various displacement BCs at axial loader arms

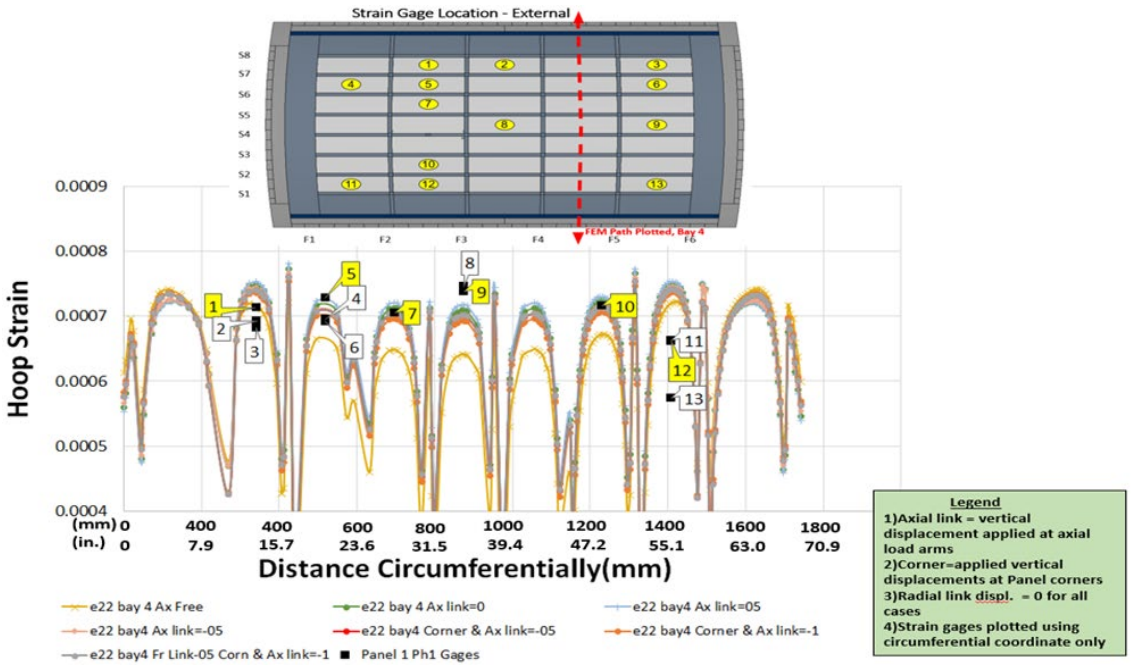

Figure 94. Comparison of hoop strain gage measurements with Panel 1 FE analyses for various displacement BCs at axial loader arms

These as-built Panel 1 stress intensity solutions were used to re-evaluate the as-built Panel 1 crack growth results. Also, these new stress intensity solutions and boundary conditions were used to generate loads for Panel 2 and Panel 3 to insure the same ("apples-to-apples") SIFs were used for Panel 2 as Panel 1. The impact of axial arm movement increased the circumferential crack SIFs for the as-built Panel 1 for all crack sizes, while the increased thickness in the as-built Panel 1 lowered the circumferential crack SIFs for all crack sizes. The net effect for the final SIFs for Panel 1 when including the effect of the mesh refinement to eight elements through-the-skin thickness (discussed in the next section) and removing the unintentional radial constraint at hoop edge of Panel 1 resulted in the SIFs for the as-built Panel 1 (yellow triangles in Figure 95) to be closer than expected to the original 2016 as-designed Panel 1 solution using two skin elements (red circles in Figure 95).

It should be noted, however, that a more appropriate comparison would be for an as-designed Panel 1 with eight-element discretization through the skin model like that used in the new as-built Panel 1 FE analysis. The as-designed model was not rebuilt, but SIFs were estimated for eight elements through the skin thickness (red open circles in Figure 95). This estimate was based on results from mesh study described in Section 6.4. As shown in Figure 95b, the as-built Panel 1 Ktotal solution is about 3-6% lower than the Qsymm1 result with one element for the skin thickness used for K-control testing and the as-built Panel 1 K1 solution. The K1 results for the two-element as-designed Panel 1 indicate that with the plasticity correction, the SIFs would

still be about 4% higher on the estimated SIFs required to match the FASTER tested Panel 1 circumferential crack results shown in Figure 77. As discussed in the previous section, the use of the mid-plane for the Panel 1 SIFs may not reflect the stringer bending effect on the distribution of the SIF through the Panel 1 skin thickness and subsequent crack growth. Additionally, the morphology of the crack surface may not be the same in the K-control tests.

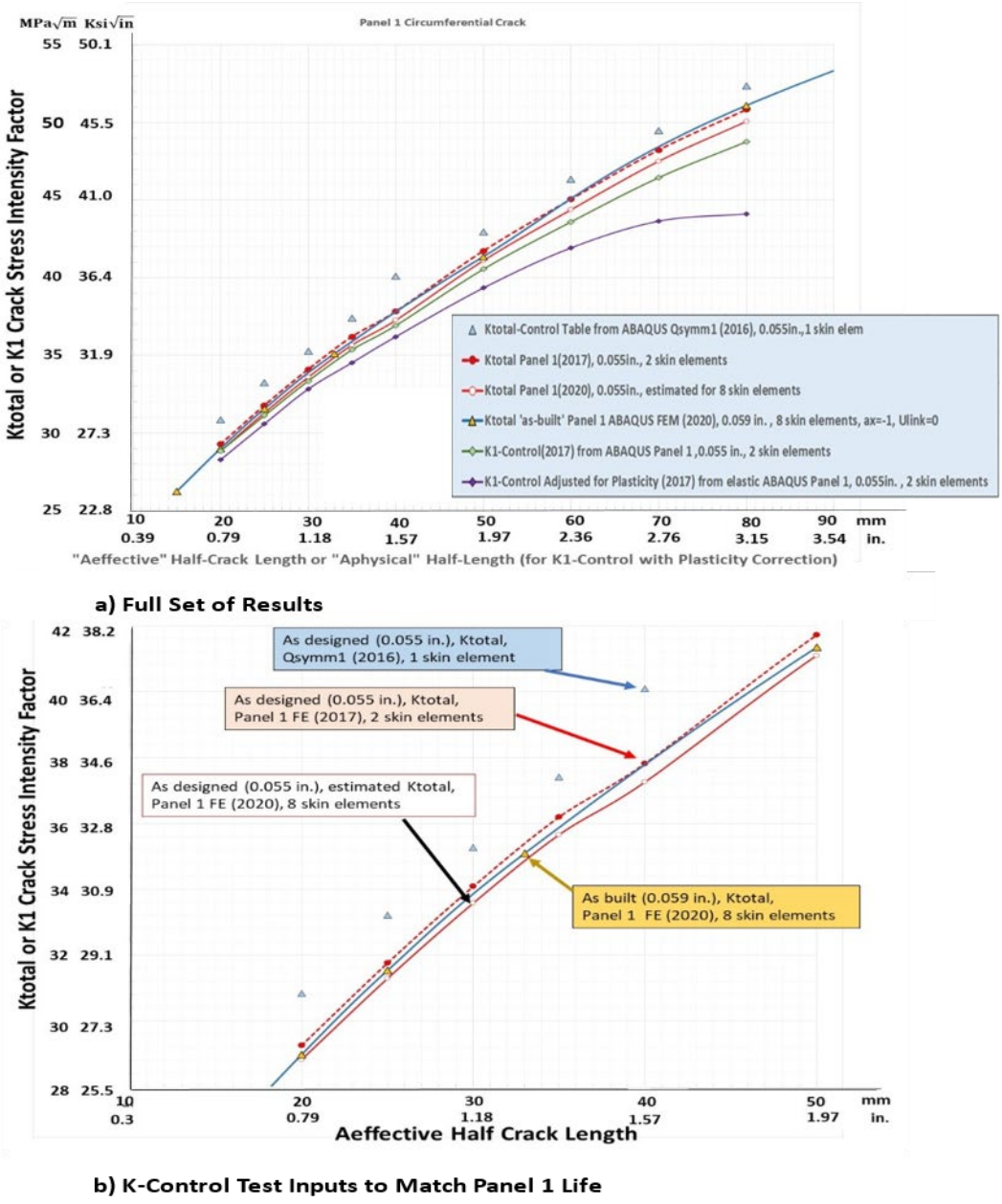

Figure 95. Results showing final as-built Panel 1 SIFs to be similar to the two-skin element as-designed Panel 1 SIFs

6.4 Effect of skin thickness discretization on Panel 1 solutions

The first as-designed Qsymm 1 and as-designed Panel 1 FE models were developed in 2016 using one ABAQUS C3D20 solid element through-the thickness to minimize solution time and cost due to the large displacement correction for crack bulging effects and the iterative approach needed to solve for Panel 1 SIFs. The as-designed Panel 1 FE model was refined to two elements through-the-thickness when follow-up K-control testing required the extraction of K1, K2, K3 SIFs. For a one-element skin, the Panel 1 FE model solid element mid-side nodes are on the skin mid-plane. A two-skin element Panel 1 FE model is not only more flexible, but the skin mid-plane is at the interface between elements. These effects reduced the one-element solution SIFs by about 3-6% (see Table 4 in the relevant crack size range).

In 2018, more detailed analyses were undertaken to study the effect of skin mesh through-the-thickness discretization on the SIFs. It was hypothesized that convergence of the SIFs at the mid-plane was influenced by the discretization and by whether an even or odd numbers of elements was used through the skin thickness. For an even number of elements, there are more nodes on the mid-plane for SIF extraction. Also, the extraction of stresses and strains using the element shape functions at the element surface nodes versus the element middle results in differences in the calculation of the J integral.

Two meshing strategies were studied (Figure 96) using a simplified Qsymm1 model (no rivets or contact elements were used to reduce solution time) for the as-built Panel 1 skin thickness of 0.059 in. (1.5mm) in the pockets and a 1.38 in. (35 mm) half- crack loaded at 1.04G + 9.9 psi (0.068 MPa). The first goal was to compare the results of a transition mesh (with many elements through-the-skin thickness near the crack tip transitioning to a smaller number of elements through-the-skin thickness away from the crack tip) to a mesh where the number of elements through-the-skin thickness is the same everywhere in the bay. The second goal was to study the impact of the number of elements through-the-skin thickness on the SIF. In all cases, the in-plane dimensions of the elements were the same between transition and non-transition meshes.

First, the results for the Ktotal SIF determined by averaging all layers was compared to the K solution at the mid-plane for the as-designed Qsymm1 (with rivets and contact element) model. Results are shown in Figure 97. The transition mesh result (orange curves) for two elements was similar to the two-element mesh over full-bay, as-designed Panel 1 analysis conducted in 2016 (green diamond) while substantially reducing the solution times by about a factor of eight for the four-element through-the-thickness case.

The through thickness averaging involved averaging stress intensity results for all element planes through the thickness of the skin (skin surface results were excluded). This average stress converged with the mid-plane only SIF when 6-8 elements were used through-the-thickness. For this example, there is little, if any, skin membrane stretching. Therefore, the bending effect on the stress intensities above the mid-plane average out the stress intensities below the mid-plane in this averaging method, effectively smoothing the oscillations seen in the mid-plane stress intensity. However, in cases where there is a complex loading this thickness averaging may result in differences with the mid-plane results. The oscillations in the mid-plane SIF solutions, Ktotal, are thought to be a shape function stress/strain extraction difference between the mid-element (for odd number of elements) and element surface nodes (for even number of elements).

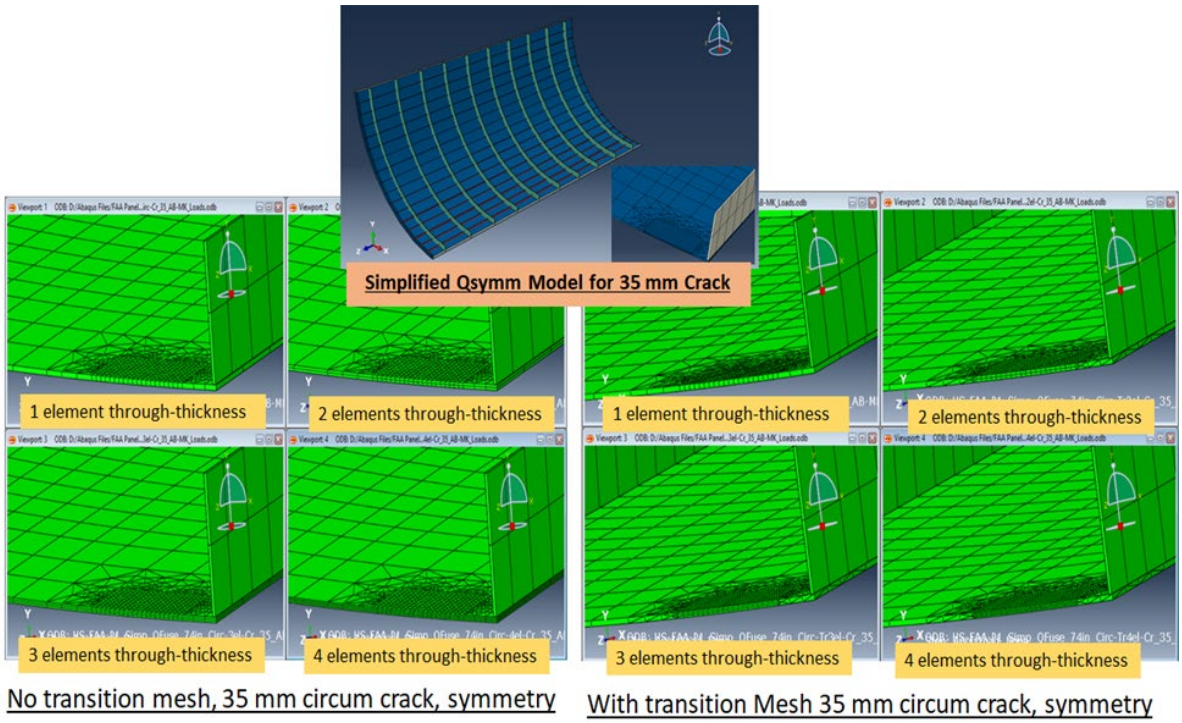

Figure 96. Meshes used to study skin through-the-thickness mesh discretization

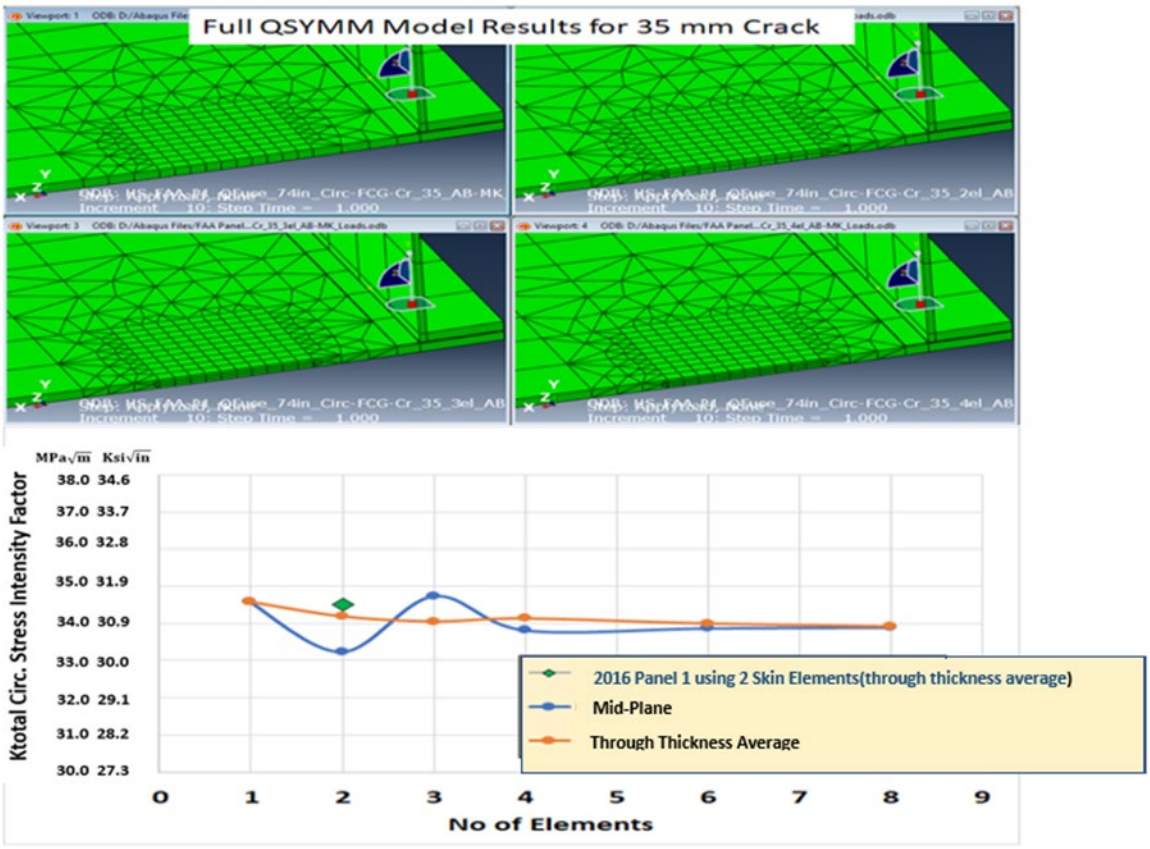

Figure 97. Full Qsymm1 FE model Ktotal versus number of skin elements through-the-thickness for a 35 mm crack half-length

A larger study was done to compare the transition mesh results to the non-transitional mesh for the simplified Qsymm1 FE model with no rivets and stringer/frame to skin contacts. The impact of the element in-plane size is shown in Figure 98 for a 1.97 in. (50 mm) crack in the as-built Panel 1 FE model for transitional element meshes of two and eight elements through-the thickness. The results show that a 0.079 in. (2 mm) in-plane element size provides nearly the same results as a 0.039 in. (1 mm) element size when eight elements are used through the thickness. For the as-built Panel 1, the final analyses for the SIF solutions were developed from the mid-plane using the transitional mesh with eight elements through the skin thickness.

The results for the two mesh types (transitional mesh from many layers to fewer layers versus the same number of elements through-the-thickness in the entire bay) shown in Figure 99 compare well to each other and demonstrate that the oscillation effect for an even and odd number of elements is not related to the transition mesh.

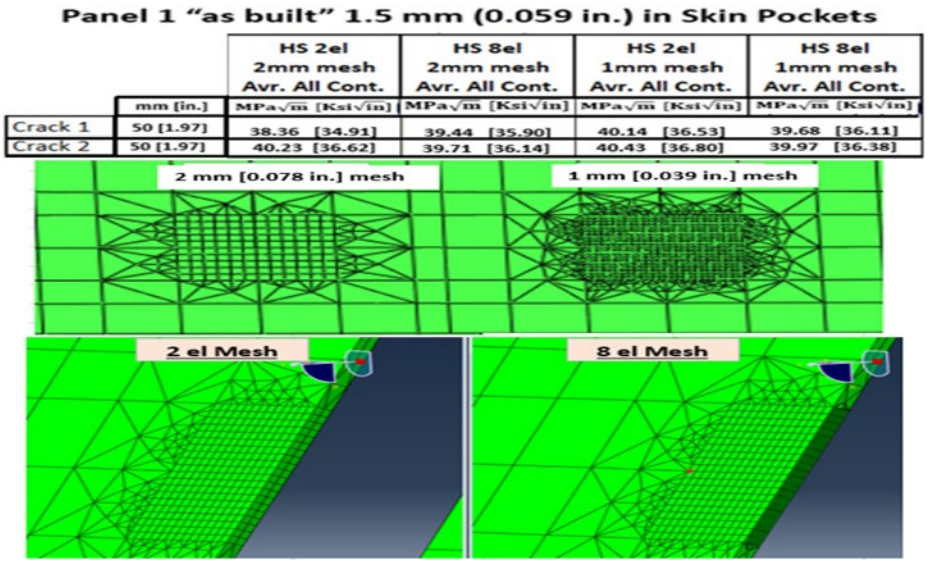

Figure 98. Panel 1 results for 1.0 and 2.0 mm in-plane mesh size for two- and eight-element meshes through-the-thickness of the skin

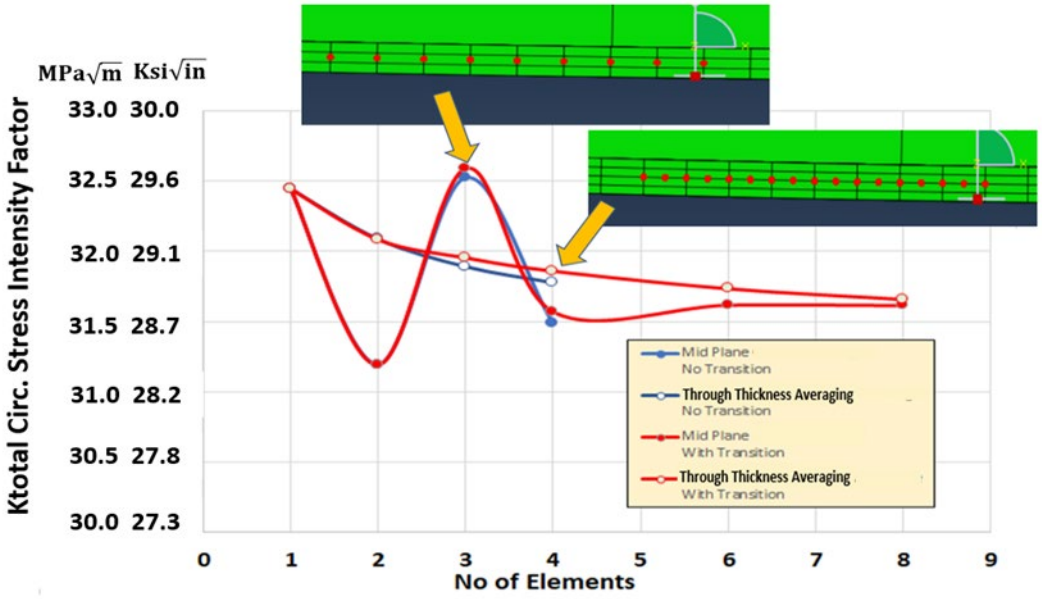

Figure 99. Stress intensity Ktotal versus number of skin elements through-thickness

6.5 Panel 1 circumferential crack growth modeling

The circumferential crack in Panel 1 was grown from a skin crack centered in a fastener hole under a broken stringer at the mid-bay location. For the circumferential repeat inspection scenario, the central stringer S4 was severed mid-bay between frames F2 and F3, as shown in Figure 100. The mid-bay fastener was removed, and a starter notch was cut into the skin, as

shown in Figure 101. The crack was then grown to the adjacent stringers loaded by the equivalent constant amplitude loading, which produces the same life as the spectrum loading in the spectrum K-control test. This was determined to be an equivalent constant amplitude axial stress (Flugge characteristic stress) of 13.0 ksi evaluated at 1.04G + 9.9 psi pressure, as described in Section 5. Actuator loads are shown in Figure 100.

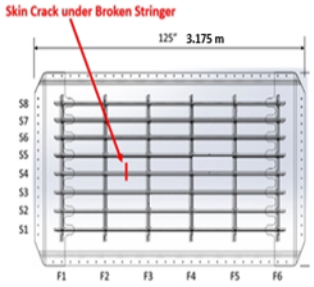

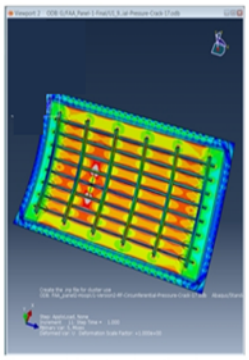

FEM Model Showing 2-Bay Crack

Axial Loads @ pressure + 1.04G Bend.

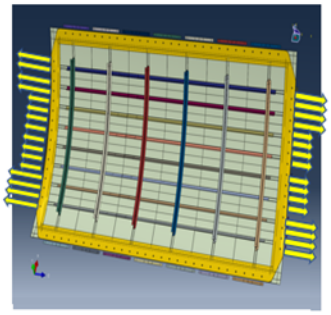

Skin Axial Actuator Load Arm Number	Arm Loads (N)	Average Actuator Load, N
1	22,544[5,068 lbf]	
2	22,544[5,068 lbf]	
3	22,544[5,068 lbf]	
4	22,544[5,068 lbf]	90,168 [20,271 lbf]
5	14,140 [3,179 lbf]	
6	14,140 [3,179 lbf]	
7	14,140 [3,179 lbf]	
8	14,140 [3,179 lbf]	90,168 [20,271 lbf]
9	14.140 [3.179 lbf]	
10	14,140 [3,179 lbf]	
11	14,140 [3,179 lbf]	
12	14,140 [3,179 lbf]	90,168 [20,271 lbf]
13	22.544[5.068 lbf]	
14	22,544[5,068 lbf]	
15	22,544[5,068 lbf]	
16	22,544[5,068 lbf]	90,168 [20,271 lbf]

Hoop Loads @ pressure + 1.04G Bend.

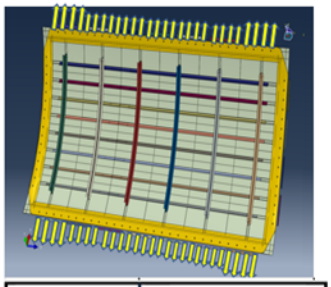

Skin Hoop Actuator	Average Actuator Load, N [lbf]
1	
2	
3	
4	[10,675 lbf] 47,484 N
5	
6	
7	
8	[9,946 lbf] 44,240 N
9	
10	
11	
12	[9,716 lbf] 43,220 N
13	
14	
15	
16	[9,625 lbf] 42,813 N
17	
18	
19	
20	[9,716 lbf] 43,220 N
21	
22	
23	
24	[9,946 lbf] 44,240 N
25	
26	
27	
28	[10,675 lbf] 47,484 N

Frame Loads @ pressure +1.04 G Bend

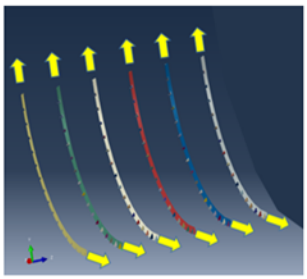

FRAME-Y	Load(N, Cylindrical)
1	7,932 [1,783 lbf]
2	10,766[2,420 lbf]
3	10,821[2,433 lbf]
4	10,821[2,433 lbf]
5	10,766[2,420 lbf]
6	7,932 [1,783 lbf]

Figure 100. Panel 1 actuator loads for 1.04G bending with pressure

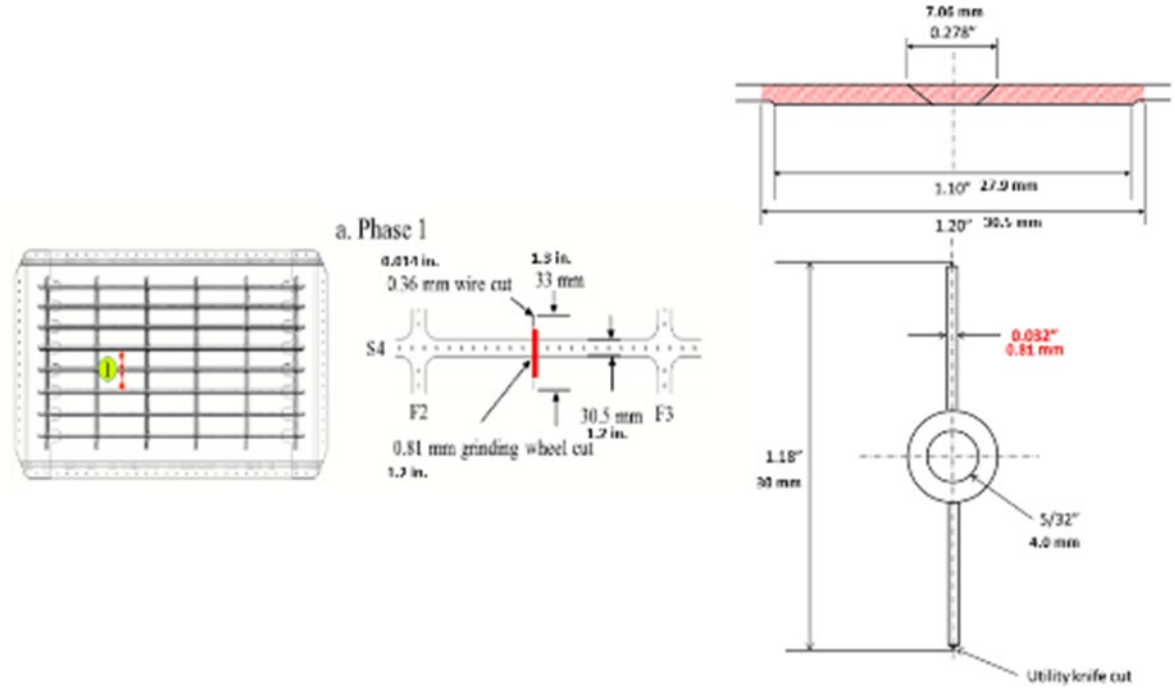

Figure 101. Starting notch for a circumferential crack at the mid-bay stringer to skin fastener

This section summarizes the various circumferential SIFs, K, developed from 2016 to 2020 for the test Panel 1. The modeling approaches and BCs have changed over the years, as previously discussed. Results are identified by year, number of skin elements through-the-thickness, and boundary condition type where possible. Stress intensity solutions for Panel 1 are compared in Figure 102. The actuator loads are the same for all results in Figure 102, but geometry and BCs changed. The following comments apply:

- The top curve (light blue triangles) represents the one skin element Qsymm1 results, which were used for the as-designed Panel 1 Ktotal-Control Table at the equivalent constant amplitude circumferential stress of 13 ksi (at 1.04G + 9.9 psi (0.068 MPa) pressure).
- By comparing the as-designed Ktotal-Control plot (light blue triangle) from the Qsymm1 one skin element through-the-thickness model to the Ktotal solution for the as-designed two skin element FASTER Panel 1 FE model with 0.055 in. (1.4mm) skin pocket thickness at 1.04G + 9.9 psi (0.068 MPa) pressure (red filled circle), it is shown that the latter FEM model reduced the one element Ktotal solution by an average of about 3.6% in the relevant crack range.
- The two element Panel 1 FE model K1 SIF solution (green diamond) for the as-designed Panel 1 with 0.055 in. (1.4 mm) skin pocket thickness at 1.04G + 9.9 psi (0.068 MPa)

pressure shows a reduction of about 2.7% compared to the Ktotal SIF solution for the same two element Panel 1 FE model (see Table 6) .

- The Panel 1 FE model K1 solution with the plastic zone correction based on converting the K-control Table into an Aphysical-based K-control Table are plotted as purple diamonds. This model representing the as-designed Panel 1 with 0.055 in. (1.4mm) skin pocket thickness at 1.04G + 9.9 psi (0.068 MPa) pressure shows a reduction of about 3% compared to the K1 solution without plastic zone corrections. Note that for this plot, the x-axis crack half-length is interpreted as Aphysical in Figure 102.
- The final as-built 0.059 in. skin pocket thickness Panel 1 FE model Ktotal SIF solution (yellow triangle) with adjusted axial loader arm BCs and eight elements through-the-thickness is similar to the as-designed 0.055 in. (1.4 mm) skin thickness two-element Panel 1 FE model Ktotal solution (red circle plot). A more appropriate comparison would be to an eight-element as-designed Panel 1 stress intensity solution. This was estimated as the white filled circle plot in Figure 102 based on results from the mesh study described in Section 6.4. The eight-element as-built Ktotal solution is shown to be between the two-element and the estimated eight-element as-designed Panel 1 Ktotal solution in Figure 1b.

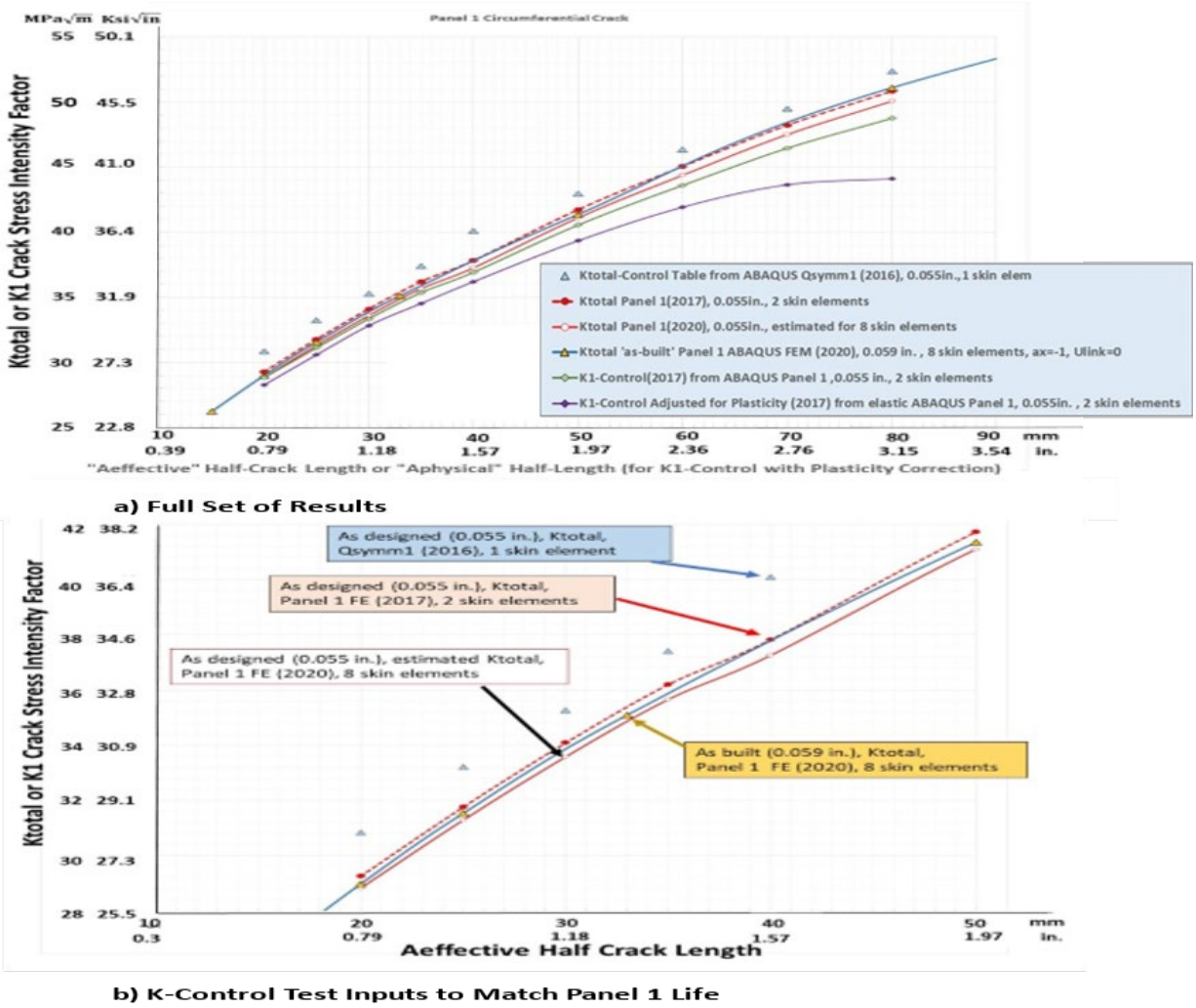

Figure 102. Circumferential crack Panel 1 final Ktotal solution compared to various solutions from 2016

6.6 Panel 1 circumferential two-bay crack at limit load

The circumferential crack was evaluated for the as-designed 0.055 in. skin thickness Panel 1 for a two-bay skin crack with a central broken stringer at limit load. For this study, limit load was defined as 9.9 psi (0.068 MPa) pressure + 2.5 G bending load. The elastic/plastic material properties used in the analysis are shown in Figure 103. The actuator loads used to load the ABAQUS test panel model are shown in Figure 104. A two-bay crack analysis was conducted for a conservative load condition of 3.4 G bending + 9.9 psi (0.068 MPa) pressure (Figure 105) to ensure yielding in the stringers and skin was not excessive, leaving Panel 1 unrepairable. The as-designed Panel 1 SIFs, Ktotal, at limit load (2.5G + 9.9 psi) are compared in Figure 106 to the results at 1G and the results at 9.9 psi (0.068 MPa) pressure. These results are for the as-designed Panel 1 geometry with one C3D20 element representing the skin thickness.

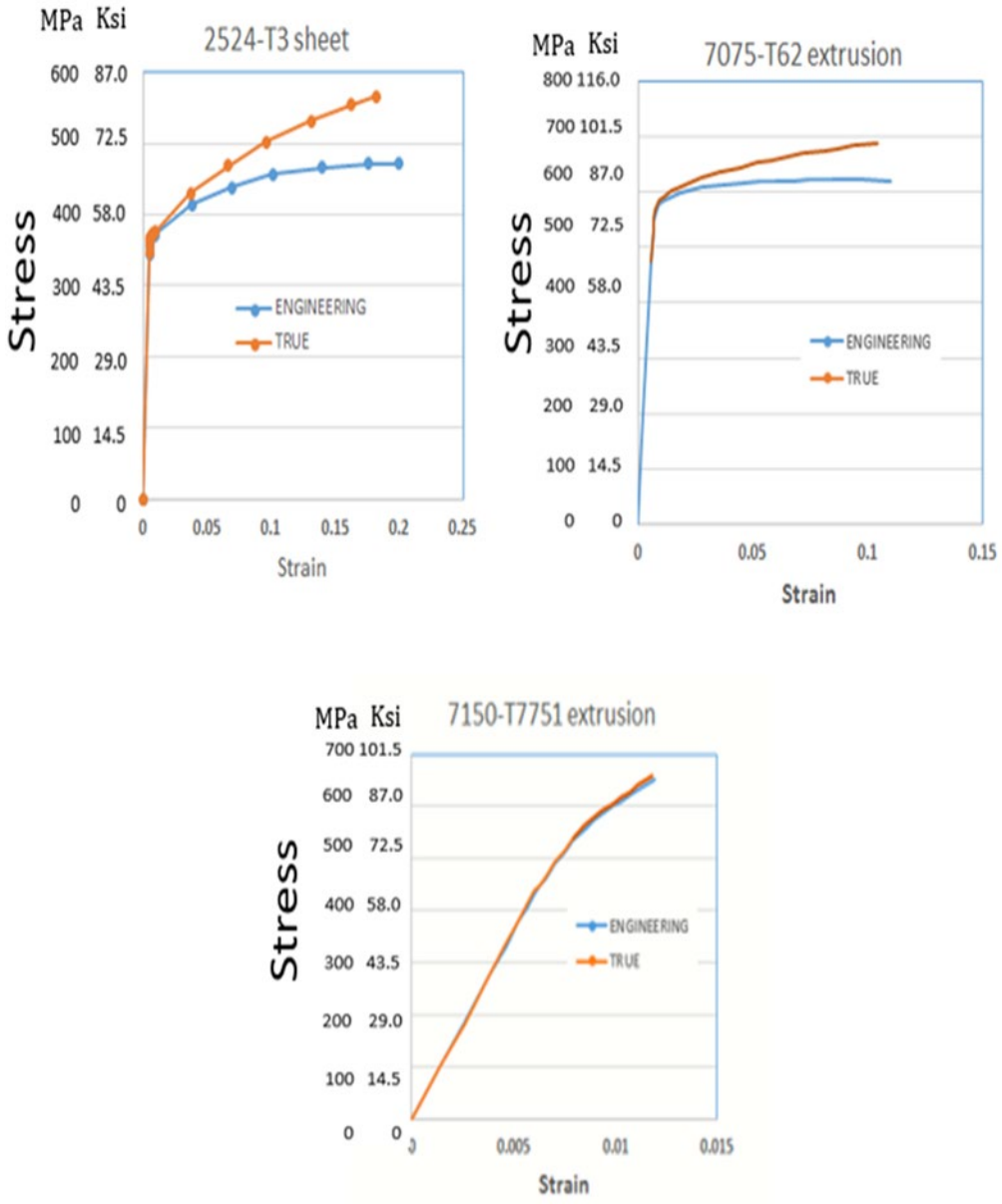

Figure 103. Elastic/plastic property inputs for 2524-T3 sheet, 7075-T62 formed sheet, and 7150-T7751 extrusion stringer

The interpretation of the crack length for the limit load in Figure 106 is Aphysical crack length and is Aeffective for the elastic analyses at the 1G and the 9.9 psi loading condition.

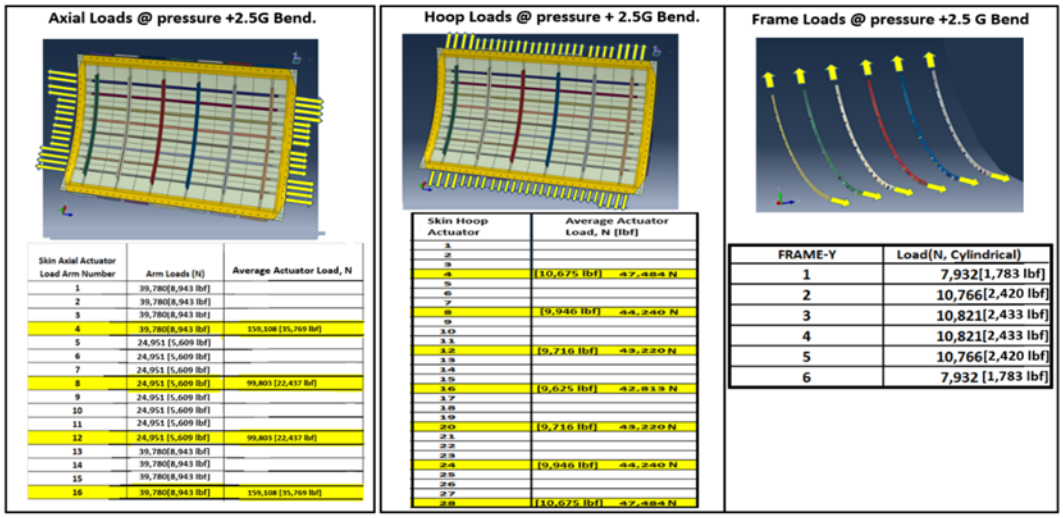

Skin Axial Actuator Load Arm Number	Arm Loads (N)	Average Actuator Load, N
1	39,780[8,943 lbf]	
2	39,780[8,943 lbf]	
3	39,780[8,943 lbf]	
4	39,780[8,943 lbf]	159,108 [35,769 lbf]
5	24,951 [5,609 lbf]	
6	24,951 [5,609 lbf]	
7	24,951 [5,609 lbf]	
8	24,951 [5,609 lbf]	99,803 [22,437 lbf]
9	24,951 [5,609 lbf]	
10	24,951 [5,609 lbf]	
11	24,951 [5,609 lbf]	
12	24,951 [5,609 lbf]	99,803 [22,437 lbf]
13	39,780[8,943 lbf]	
14	39,780[8,943 lbf]	
15	39,780[8,943 lbf]	
16	39,780[8,943 lbf]	159,108 [35,769 lbf]

Skin Hoop Actuator	Average Actuator Load, N [lbf]
1	
2	
3	
4	[10,675 lbf] 47,484 N
5	
6	
7	
8	[9,946 lbf] 44,240 N
9	
10	
11	
12	[9,716 lbf] 43,220 N
13	
14	
15	
16	[9,625 lbf] 42,813 N
17	
18	
19	
20	[9,716 lbf] 43,220 N
21	
22	
23	
24	[9,946 lbf] 44,240 N
25	
26	
27	
28	[10,675 lbf] 47,484 N

FRAME-Y	Load(N, Cylindrical)
1	7,932[1,783 lbf]
2	10,766[2,420 lbf]
3	10,821[2,433 lbf]
4	10,821[2,433 lbf]
5	10,766[2,420 lbf]
6	7,932 [1,783 lbf]

Figure 104. Actuator loads for the circumferential crack at limit load (2.5G + 9.9 psi)

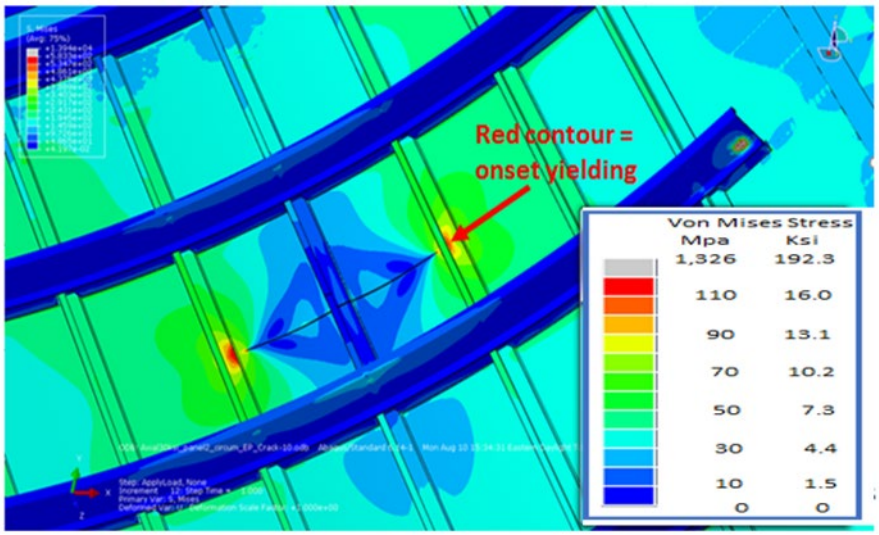

Figure 105. Panel 1 skin and stringer yield areas at 3.4G + 9.9 psi

The circumferential two-bay crack (Figure 107) was evaluated for the as-designed Panel 1 for a two-bay skin crack with a central broken stringer. Note that an Aeffective crack R-curve is shown for the 2524-T3 skin in Figure 107. An Aphysical-based crack length R-curve may be more appropriate for prediction of skin failure at the high stress intensity values where large plastic zones occur. Since the Aeffective SIFs are well below the Aeffective R-Curve, it was felt that an additional analysis using an estimated Aphysical R-Curve for skin failure was not necessary. The conclusion was that Panel 1 will not fail and should be repairable after the limit load test.

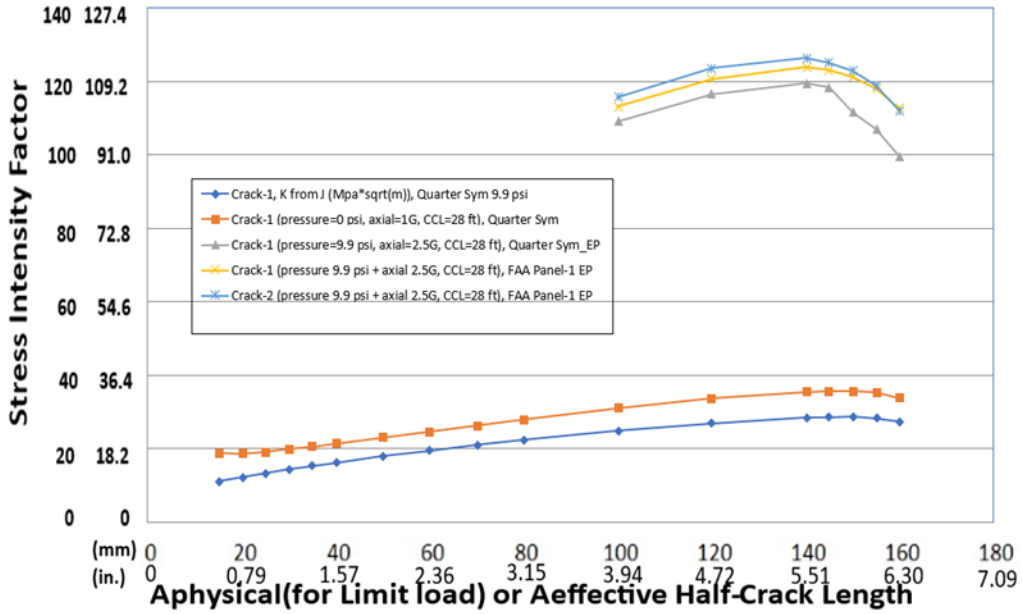

Figure 106. Ktotal at limit load compared to 1G + 9.9 psi load

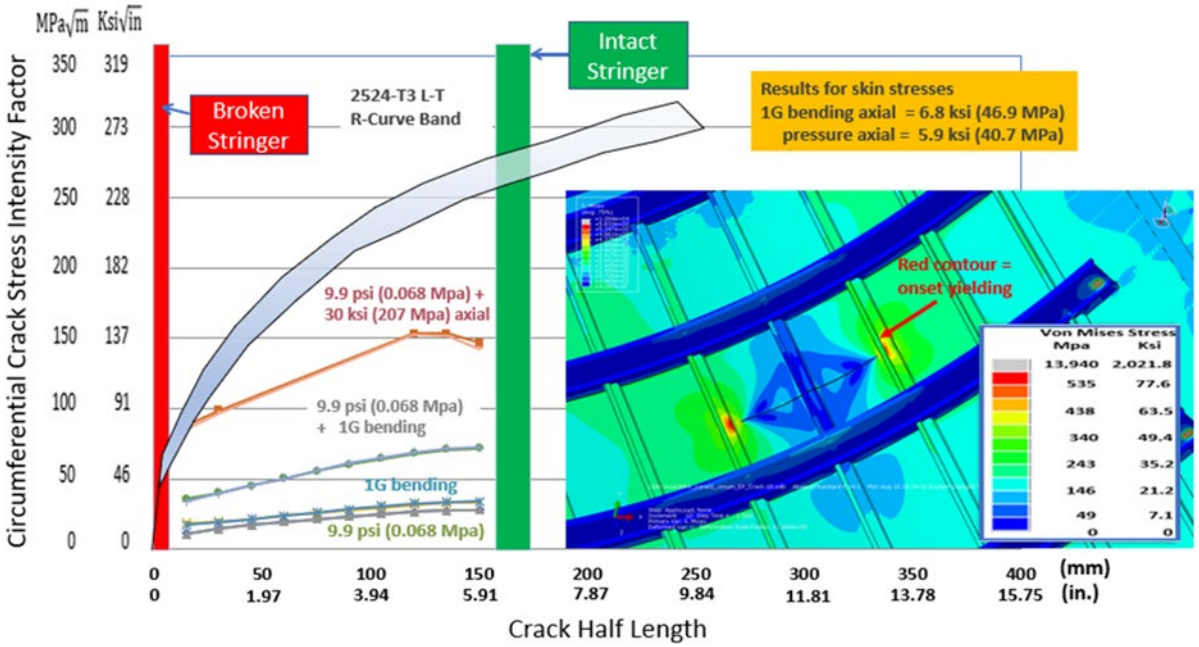

Figure 107. Panel 1 results at 3.4G + 9.9 psi (0.068 MPa) pressure

6.7 Panel 1 stresses at 9.9 psi pressure load after repair

After the circumferential crack growth testing of Panel 1 the circumferential crack was repaired (Figure 108). A skin patch was used to repair the skin crack, and an extrusion splice doubler was used to repair the stringer. To support the engineering design of the repair, an analysis was

conducted on a preliminary proposed repair (Figure 109) for the as-designed Panel 1, 0.055 in. (1.4 mm) skin. A skin patch thickness of 0.063 in. (1.6 mm) was used. The size of the skin patch is 6 in. (152.4 mm) in the longitudinal direction and 21 in. (533.4 mm) in the circumferential direction. A 10 in. (254 mm) section of the original 7150 extrusion stringer was used to repair the broken stringer.

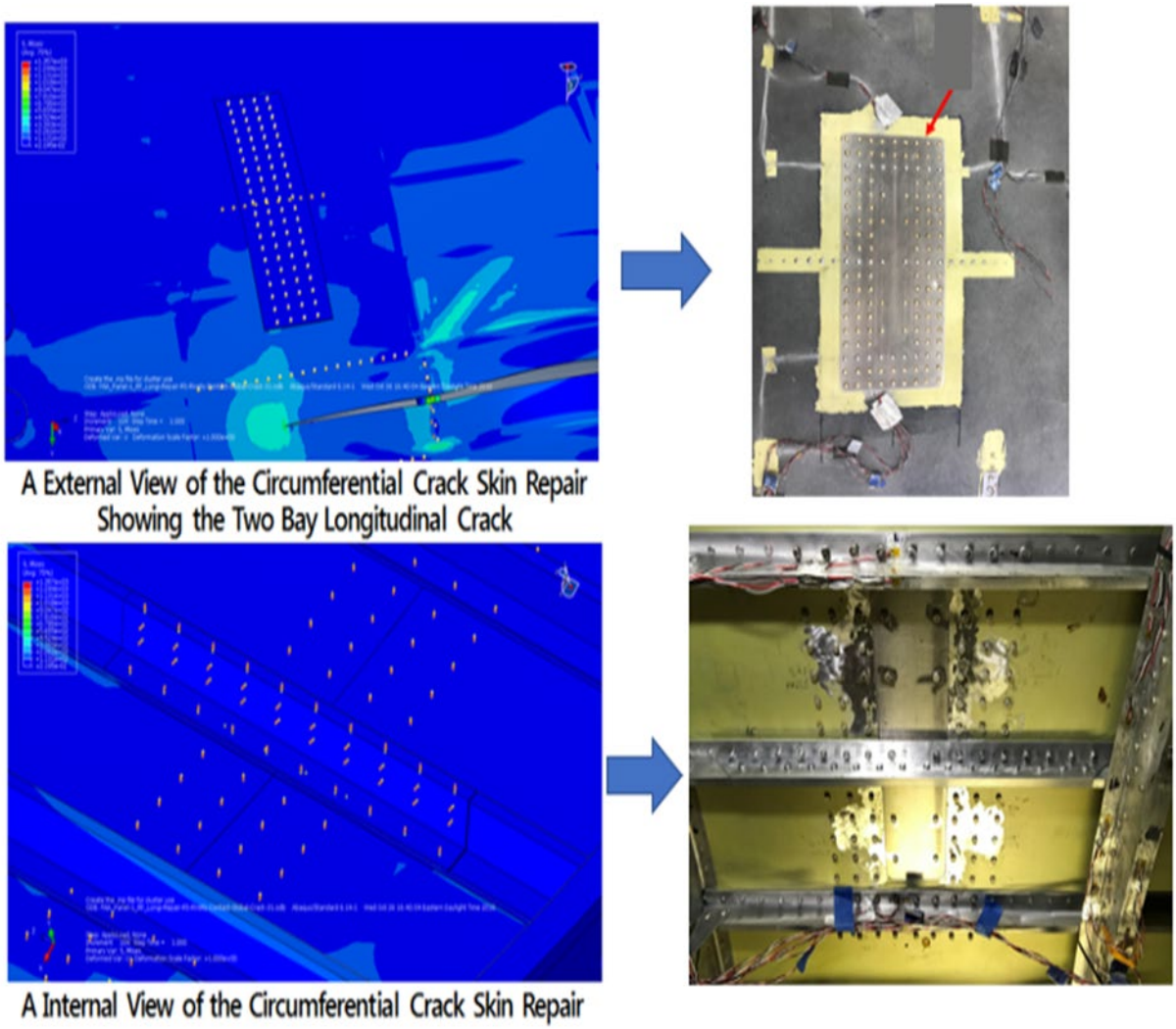

Figure 108. ABAQUS Panel 1 model and repair detail of the circumferential crack

The axial and circumferential skin stresses in the as-designed, repaired Panel 1 are compared to the as-designed, 0.055in. (1.4 mm) skin Qsymm1 model in Figure 110. These results show that there is a local stress disturbance in the repair area and in the first bay surrounding the repaired crack. However, stresses in bay 4, where the longitudinal crack growth and residual strength tests will be conducted, were virtually unchanged. This supports the placement of the longitudinal crack in Panel 1 for the next step of testing without the need to adjust the Panel 1 longitudinal crack loads.

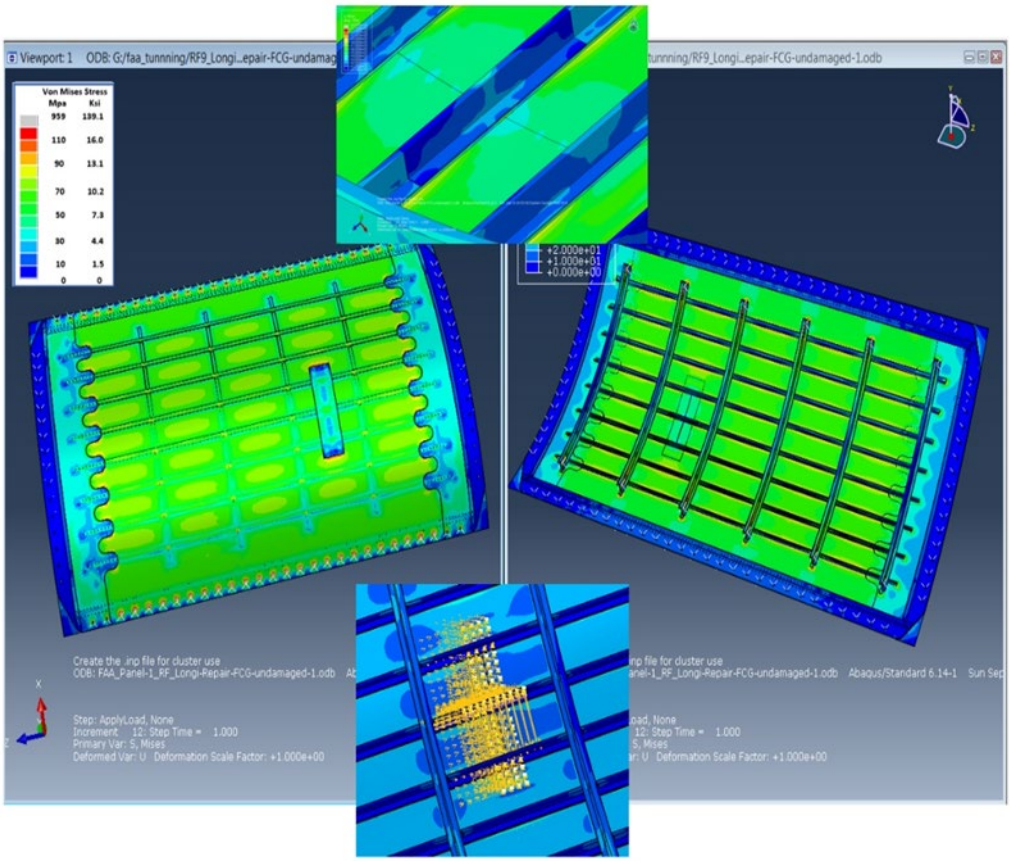

Figure 109. Panel 1 FE model after repair of Panel 1 (0.055 in. (1.4 mm) skin)

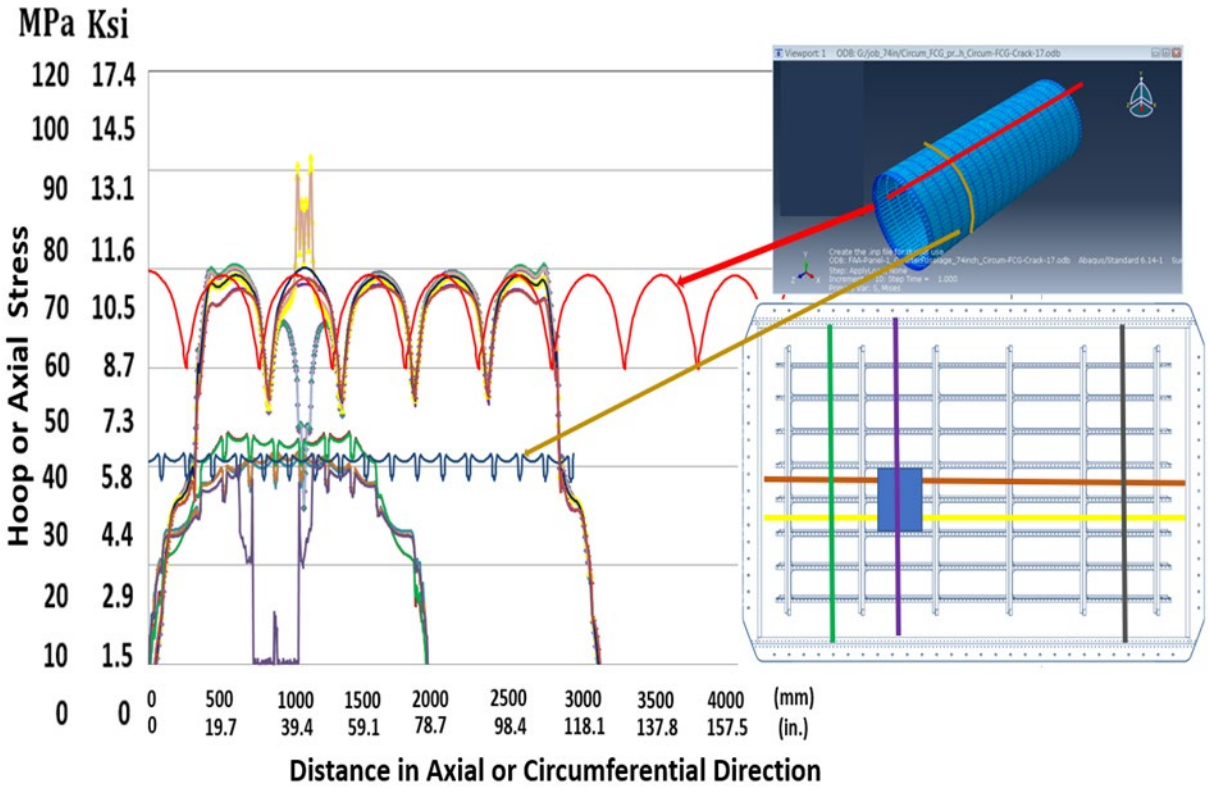

Figure 110. Skin stresses with repair of circumferential crack and broken stringer

6.8 Panel 1 crack #2 — testing of crack turning scenario

The crack scenario for Phase 2 is shown in Figure 111. This longitudinal crack #2 was added to the original test plan to develop crack turning data for the evaluation of crack turning predictive approaches. The starting crack was located mid-bay between frame F4 and F5. A crack 5.5 in. (139.7 mm) long and 0.032 in. (0.81 mm) wide was cut along the chem-milled pocket edge along the stringer at the location shown in Figure 112.

The panel was pre-cracked at 70% pressure loading (Figure 113) from an initial total crack length of 5.5 in. (139.7 mm) to a final size of 6.0 in. (152.4 mm). For purposes of post-test evaluation, the growth from 5.5 in. (139.7 mm) to 6.0 in. in total length was considered non-steady state crack growth, and life counting started when the crack reached 6.0 in. total length (152.4 mm). Panel 1 was loaded (see Figure 114) by constant amplitude pressure at an R-ratio of 0.05.

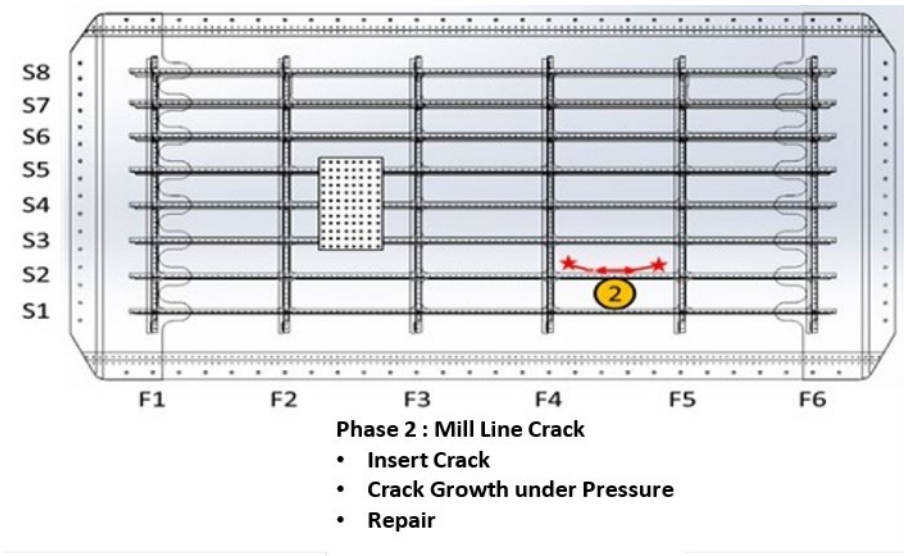

Figure 111. Panel 1 longitudinal crack turning scenario

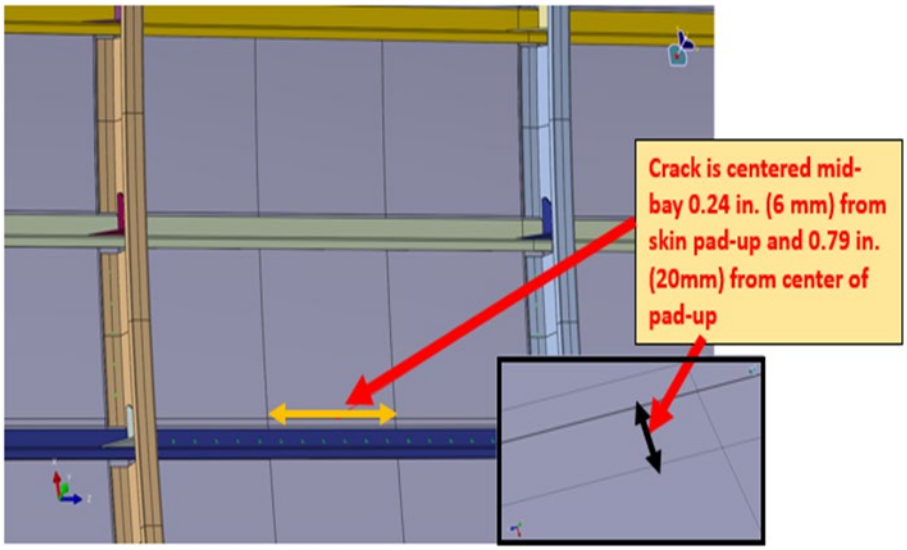

Figure 112. Location of longitudinal crack #2

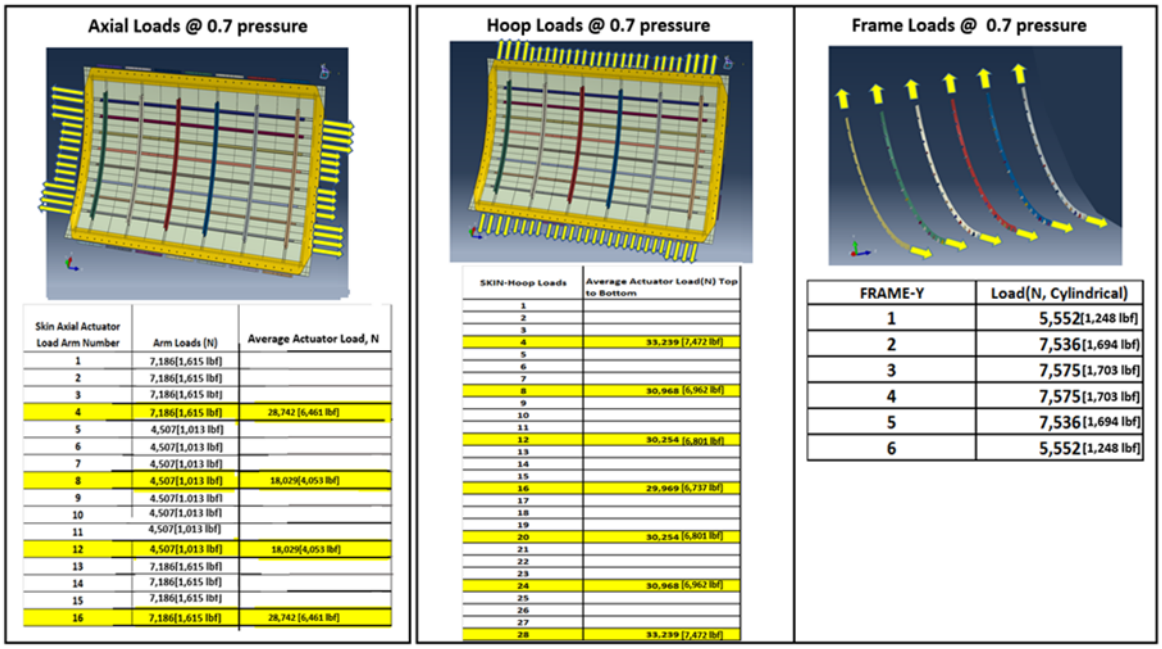

Skin Axial Actuator Load Arm Number	Arm Loads (N)	Average Actuator Load, N
1	7,186[1,615 lbf]	
2	7,186[1,615 lbf]	
3	7,186[1,615 lbf]	
4	7,186[1,615 lbf]	28,742 [6,461 lbf]
5	4,507[1,013 lbf]	
6	4,507[1,013 lbf]	
7	4,507[1,013 lbf]	
8	4,507[1,013 lbf]	18,029[4,053 lbf]
9	4,507[1,013 lbf]	
10	4,507[1,013 lbf]	
11	4,507[1,013 lbf]	
12	4,507[1,013 lbf]	18,029[4,053 lbf]
13	7,186[1,615 lbf]	
14	7,186[1,615 lbf]	
15	7,186[1,615 lbf]	
16	7,186[1,615 lbf]	28,742 [6,461 lbf]

SKIN-Hoop Loads	Average Actuator Load(N) Top to Bottom
1	
2	
3	
4	33,239 [7,472 lbf]
5	
6	
7	
8	30,968 [6,962 lbf]
9	
10	
11	
12	30,254 [6,801 lbf]
13	
14	
15	
16	29,969 [6,737 lbf]
17	
18	
19	
20	30,254 [6,801 lbf]
21	
22	
23	
24	30,968 [6,962 lbf]
25	
26	
27	
28	33,239 [7,472 lbf]

FRAME-Y	Load(N, Cylindrical)
1	5,552[1,248 lbf]
2	7,536[1,694 lbf]
3	7,575[1,703 lbf]
4	7,575[1,703 lbf]
5	7,536[1,694 lbf]
6	5,552[1,248 lbf]

Figure 113. Pre-cracking loads for longitudinal crack #2 turning scenario at 70% pressure

This pressure load was synchronized with the panel axial constant amplitude load applied to simulate the axial component of pressure. The pressure and the axial component of pressure loads were applied in a sinusoidal manner to a maximum pressure of 9.9 psi (0.068 MPa) with a frequency of 0.033 HZ (1 cycle per 30 seconds).

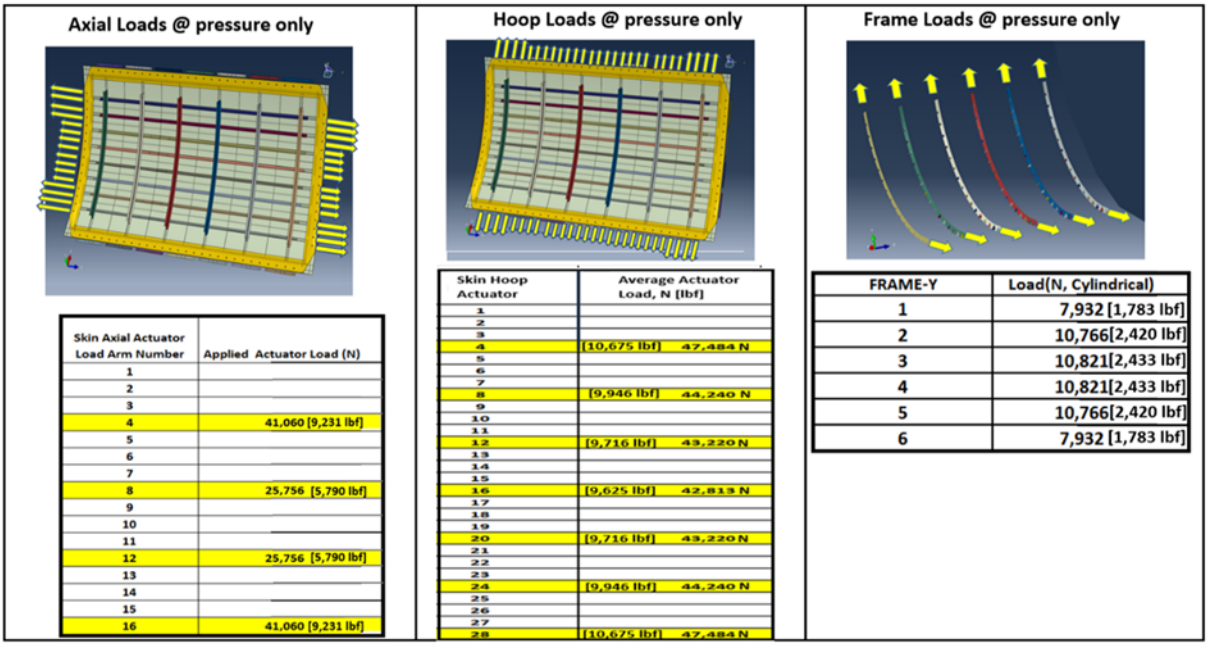

Skin Axial Actuator Load Arm Number	Applied Actuator Load (N)
1	
2	
3	
4	41,060 [9,231 lbf]
5	
6	
7	
8	25,756 [5,790 lbf]
9	
10	
11	
12	25,756 [5,790 lbf]
13	
14	
15	
16	41,060 [9,231 lbf]

Skin Hoop Actuator	Average Actuator Load, N [lbf]
1	
2	
3	
4	[10,675 lbf] 47,484 N
5	
6	
7	
8	[9,946 lbf] 44,240 N
9	
10	
11	
12	[9,716 lbf] 43,220 N
13	
14	
15	
16	[9,625 lbf] 42,813 N
17	
18	
19	
20	[9,716 lbf] 43,220 N
21	
22	
23	
24	[9,946 lbf] 44,240 N
25	
26	
27	
28	[10,675 lbf] 47,484 N

FRAME-Y	Load(N, Cylindrical)
1	7,932 [1,783 lbf]
2	10,766[2,420 lbf]
3	10,821[2,433 lbf]
4	10,821[2,433 lbf]
5	10,766[2,420 lbf]
6	7,932 [1,783 lbf]

Figure 114. Loads for Panel 1 longitudinal crack #2 and crack #3 at 9.9 psi (0.068 MPa)

Before Panel 1 modeling, an FE study was conducted to verify the ABAQUS FE modeling approach to determine the crack turning T-stresses. The study involved a bi-axially loaded square plate for various levels of bi- axiality, as shown in Figure 115. Results shown in Figure 116 agree with results in the literature (Sutradhar & Paulino, 2004).

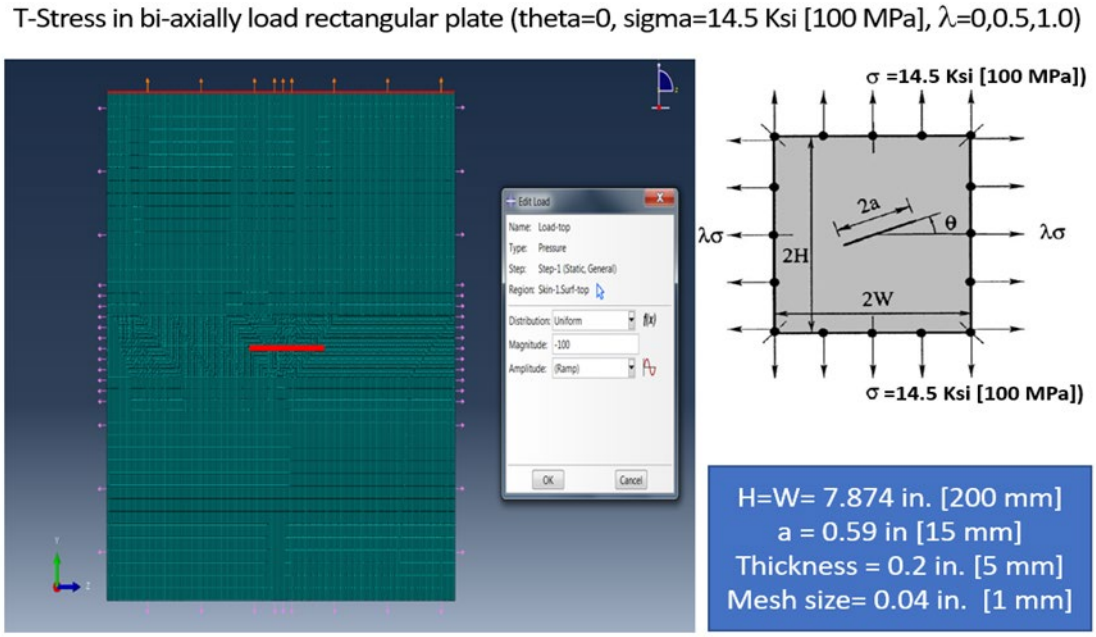

Figure 115. ABAQUS FEM model for T-stresses in a bi-axially loaded plate

An FE analysis was conducted for a one-bay crack turning scenario in Panel 1 starting at mid-bay and growing along the stringer pad-up (referred as mill line crack) for various crack sizes. A stress plot for a 12.0 in. (304.8 mm) crack is shown in Figure 117. The ABAQUS FE model is shown for a 6.0 in. crack (152.4 mm) along with the local sub-structure crack model in Figure 118 and Figure 119. The model represented the as-designed, 0.055 in. (1.4 mm) pocketed skin with two elements representing the skin thickness. The objective of this analysis was to determine the K1 and K2 SIFs and the crack turning T-stress at 6.0 in. (152.4 mm) where pre-cracking ended and crack growth life counting began. Stress contour plots for various sized cracks are shown in Figure 120, Figure 121, and Figure 122. The direction of crack turning for a positive ABAQUS K2 stress intensity was interpreted by observing the node movement behind the crack tips in Figure 123, where both crack tips show the tendency to turn upward towards the mid-bay. Mode 1 (K1) stress intensity solutions are compared with Mode 2 (K2) SIFs in Figure 124 for a 9.9 psi (0.068 MPa) pressure load.

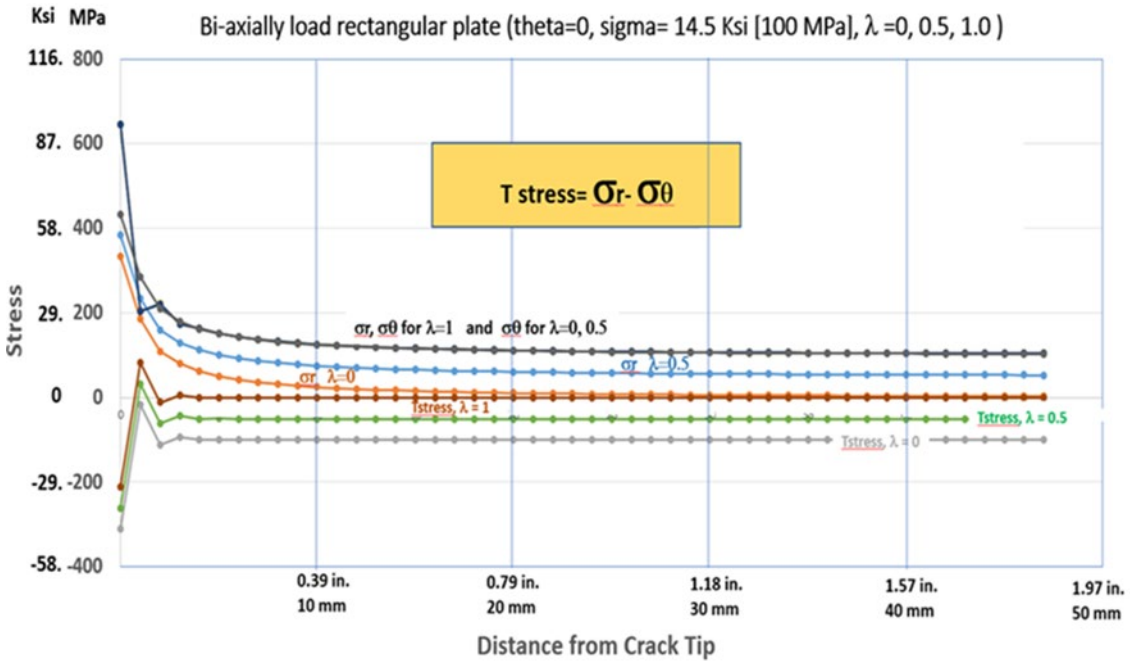

Figure 116. FEM results for T-Stress in bi-axially loaded plate

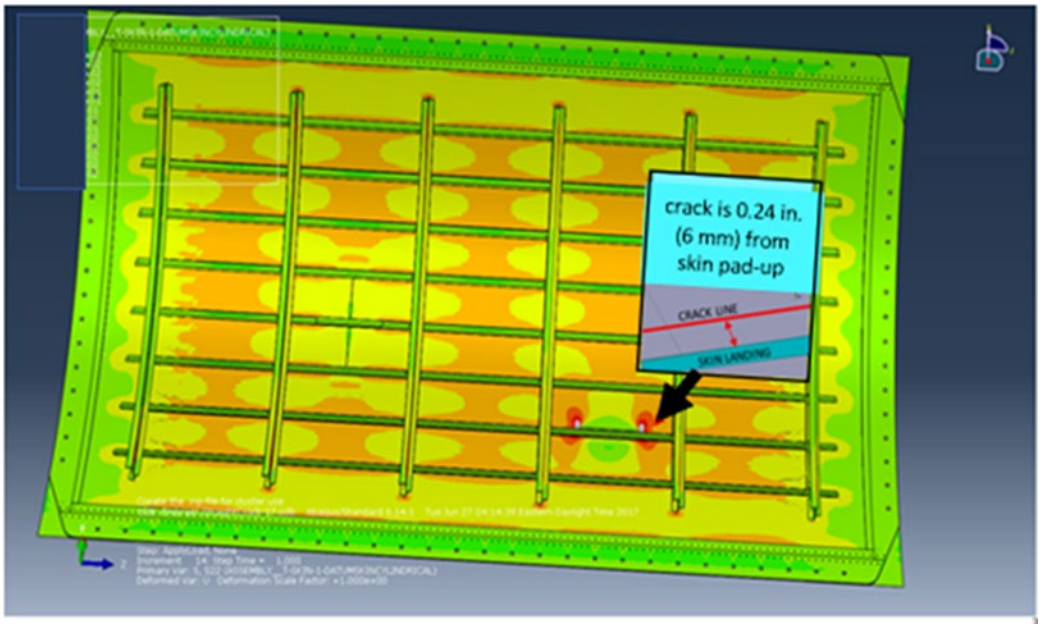

Figure 117. As-designed Panel 1 crack turning FE model for a 12.0in. (305 mm) starting crack total length

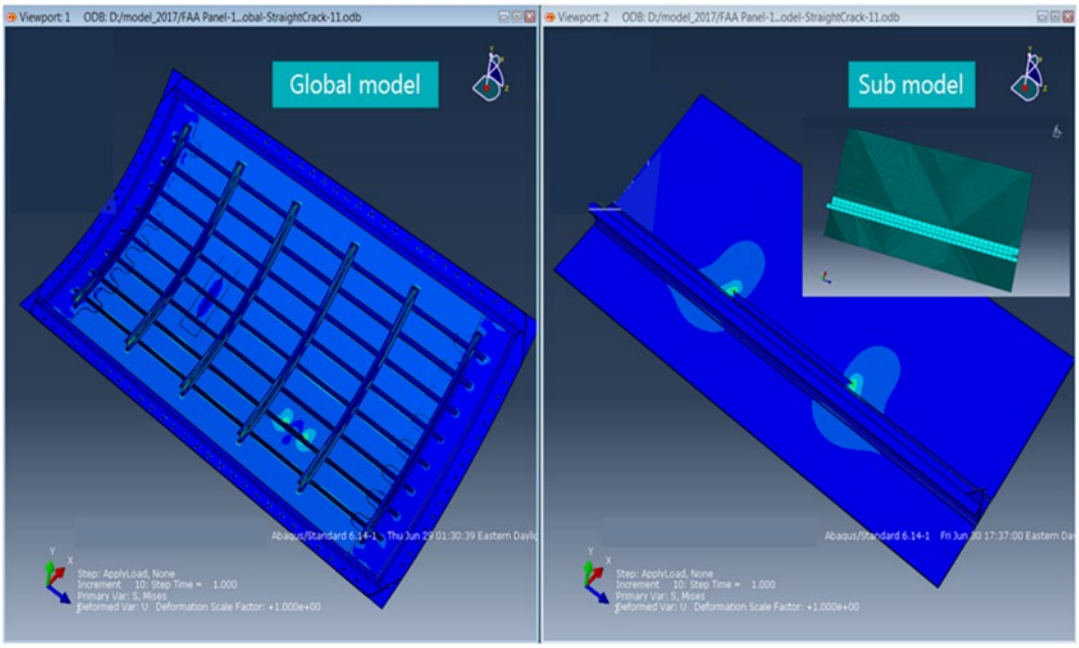

Figure 118. Sub-structure model used for the as-designed Panel 1 cack turning analysis

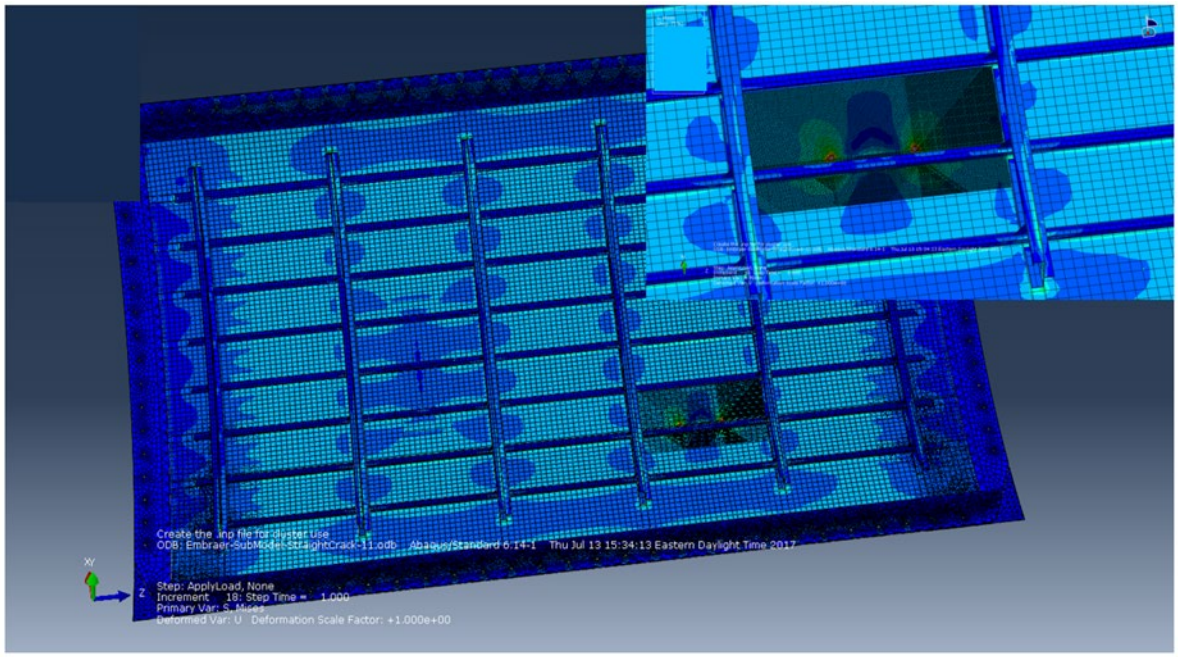
Figure 119. FE model of the as-designed Panel 1 showing the sub-structure detail

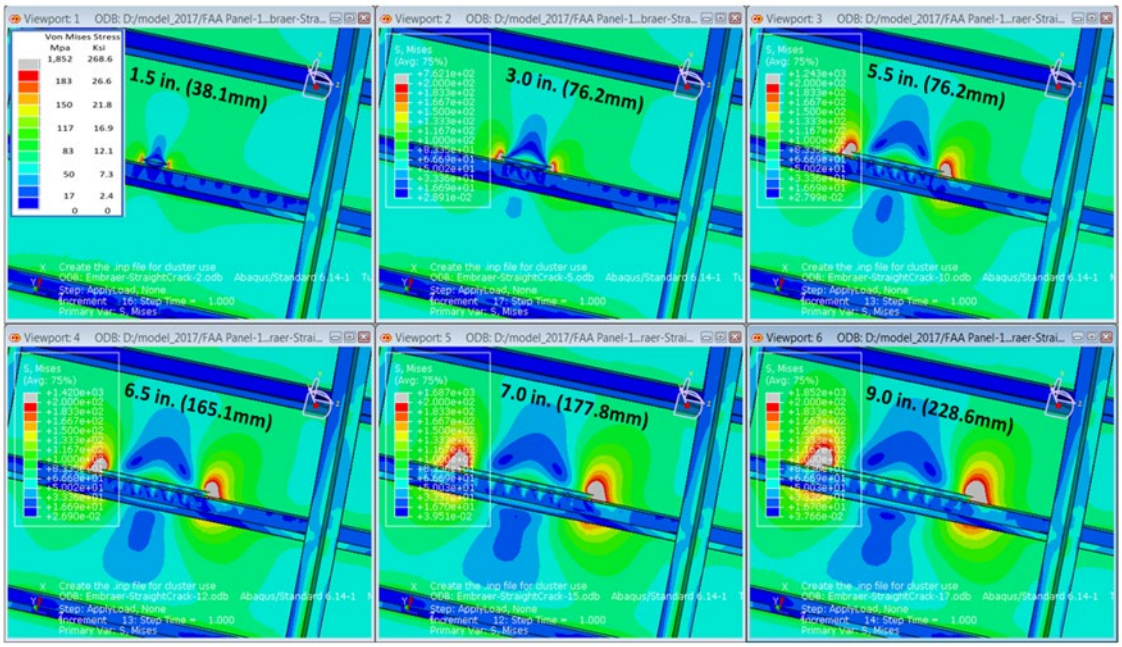

Figure 120. FEM Von Mises stress contour plots for various crack lengths along the stringer (internal view)

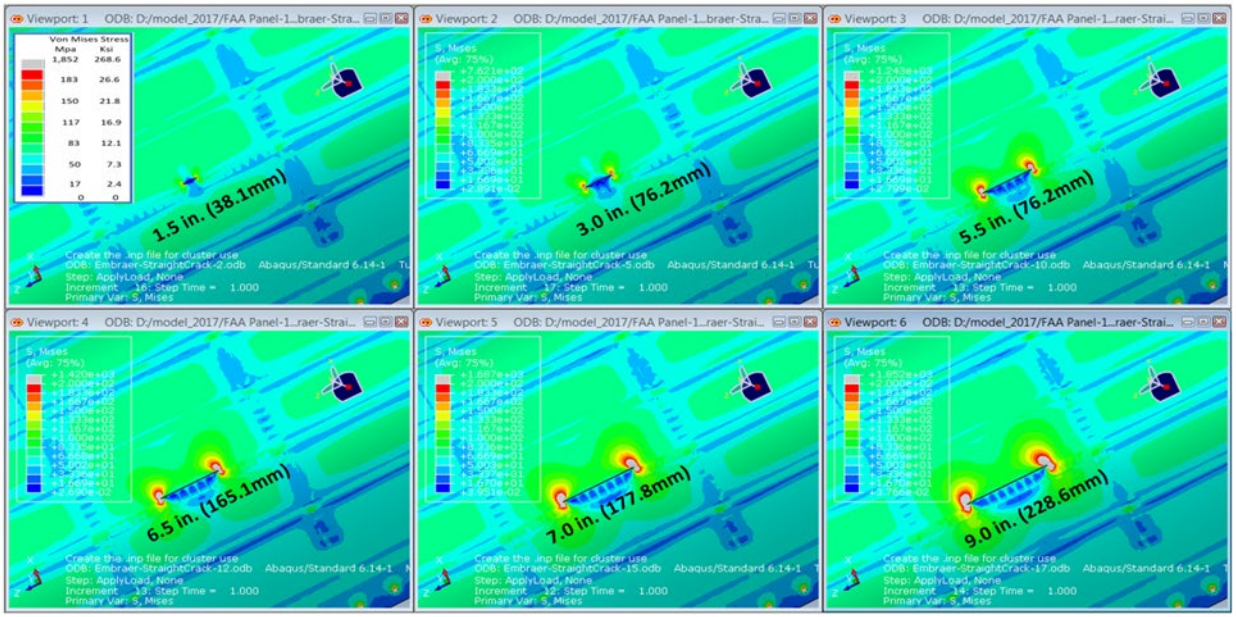

Figure 121. FEM Von Mises stress contours for various crack lengths along the stringer (external view)

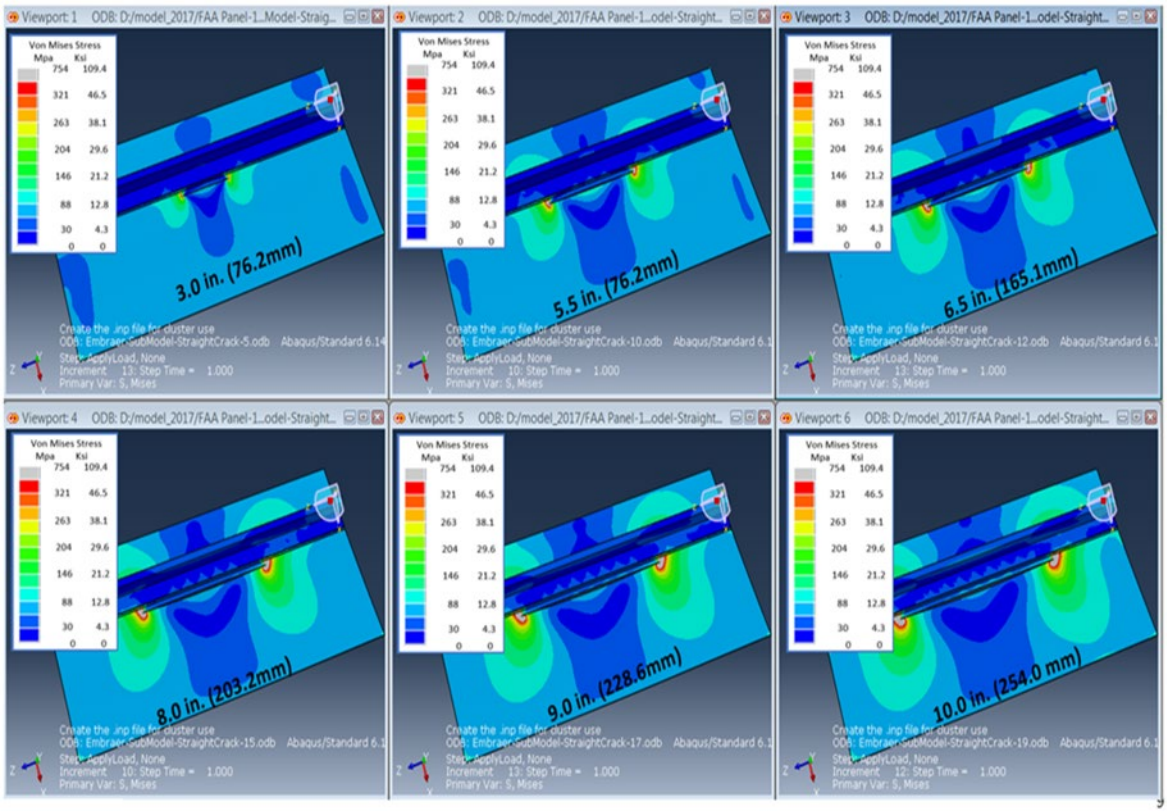

Figure 122. As-designed Panel 1 sub-model Von Mises stresses for various crack lengths along the stringer

The T-stress was calculated for the 6.0-inch crack (152mm) by subtracting the hoop stresses (S22) from the axial stresses (S33). The resulting T-stress on the crack plane in front of the crack is shown to be negative (Figure 125) for pressure only and slightly positive for the load case of pressure plus 1G bending. It was decided to test Panel 1 with pressure only because the mode 1 (K1) SIFs are larger in hoop loading only, even though the starting T-stress was slightly negative.

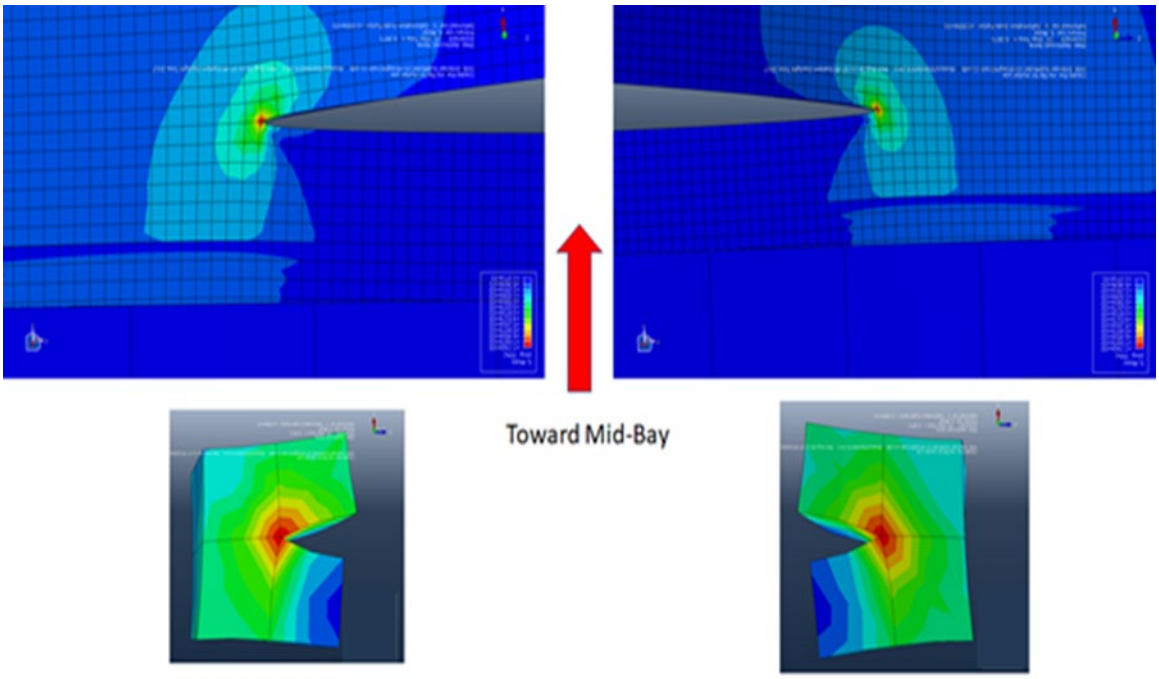

Figure 123. Direction of crack turning for positive K2 in ABAQUS model

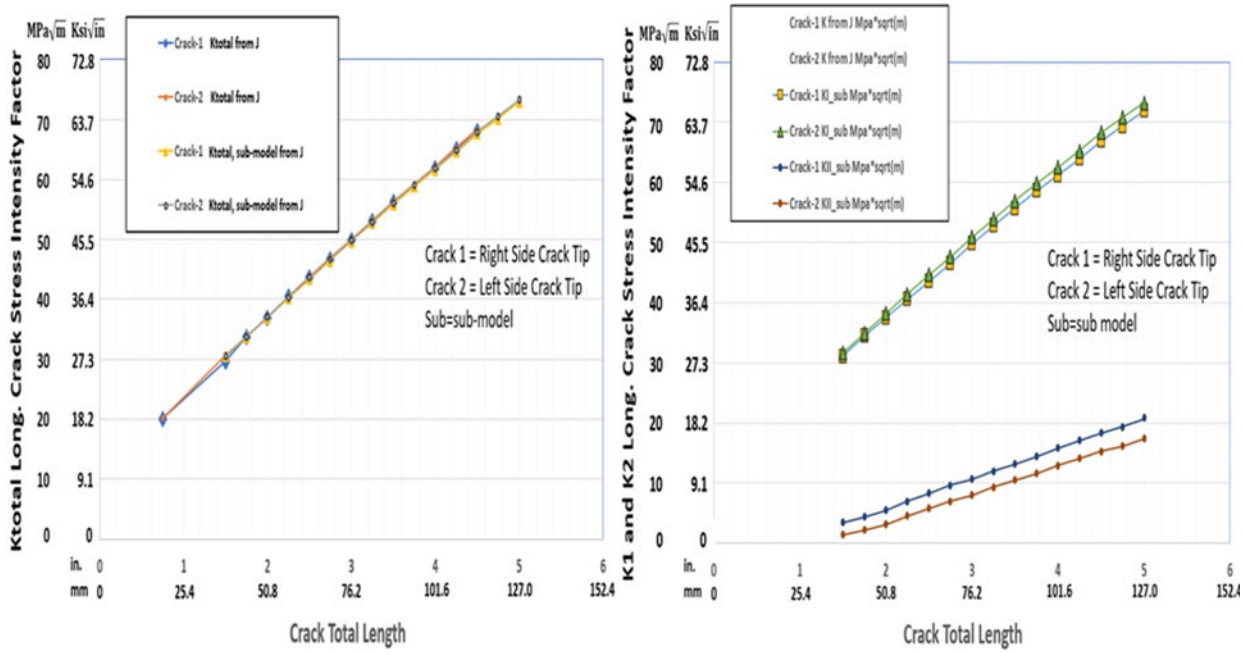

Figure 124. Results for K1 and K2 for various crack lengths along the stringer mill line

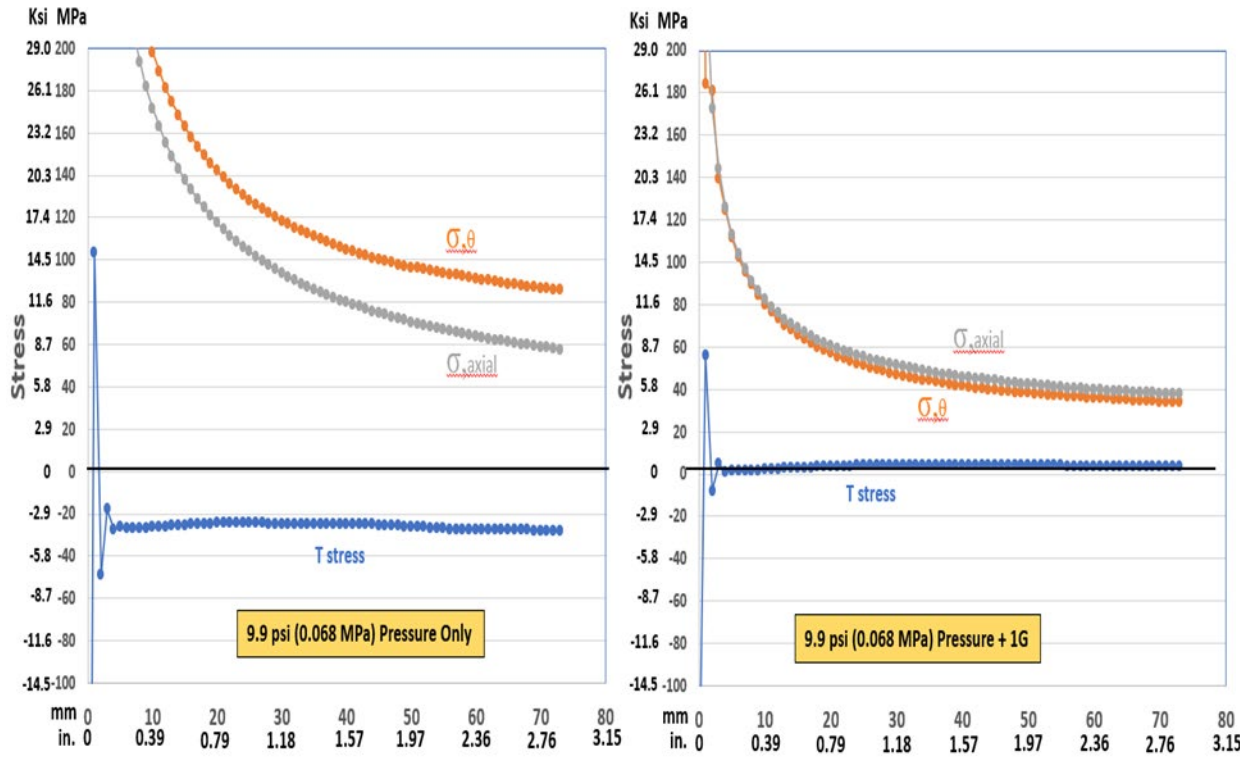

Figure 125. Calculation of T-stress for a 6.0-inch total crack length

6.8.1 Prediction of crack growth life and trajectory

The crack growth life and trajectory for the as-designed, 0.055 in. (1.4 mm) skin thickness Panel 1 for 9.9 psi (0.068 MPa) pressure only) was estimated as follows:

1. The 6.0 in. (152.4 mm) crack tips are located at -3.0 in. (76.2 mm) and +3.0 in. (-76.2 mm) in a local crack coordinate system located along the stringer with the (0,0) location at the crack center which is located mid-bay.

2. The crack tips on the right and left sides are assumed to be a reflection about the crack centerline for this simplified analysis and were assumed to exhibit the same growth rate. Thus, only the crack trajectory on the right crack side of Figure 119 is predicted.

3. For the first calculation the K1, K2 SIFs and T stress for the straight crack with tip at +3.0 in. (76.2 mm) are used to calculate the crack angle for the principal stress direction. This principal stress direction angle was calculated with and without T-stress, and the larger of the two angles was used to be conservative. The SIF K1 for a crack oriented in the principal stress direction was then calculated.

- The crack growth rate at this stress intensity, K1, was obtained using the da/dn versus delta-K curve for the 2524-T3 skin material in the L-T direction (assuming there is no appreciable theta variation in da/dn, which may not always be the case).
- For a piecewise solution, it was assumed that the crack grows at a constant growth rate and at a constant angle for the next 0.394 in. (10mm).
- It is recognized that the smaller this incremental length (0.394 in. (10mm) is, the more refined the calculation will be.
- The number of cycles to traverse this 0.394 in. (10mm) segment length is estimated as 0.394 in. (10mm) divided by the crack growth rate da/dn at the K1 obtained at the beginning of the increment.

4. For the second calculation, K1, K2, and T stress are calculated using a FE model with the updated crack, which includes the 6.0 in. (152.4 mm) initial straight length crack plus a 0.394 in. (10mm) crack extension at the previous increment angle on each side of the crack (see Figure 126).
    - Using the K1, K2, and T-stress from this FE solution, the new principal stress direction is calculated as well as the incremental crack turning angle.
    - Keep in mind that the previous total crack angle defines the reference direction for the incremental angle change at the current FE model crack tip. Therefore, the crack angle calculated is an increment to the previous crack turning angle.
    - The incremental turning angle is calculated with and without the T-stress, and the maximum angle of the two is used.
    - The K1 for the updated crack angle is used to establish the crack growth rate.
    - It is assumed that the crack grows at a constant growth rate and at a constant angle for the next 0.039 in. (10mm) distance.
    - The number of cycles to traverse this second 0.039 in. (10mm) segment is estimated as 10 mm (0.39 in.)/dadN.
    - These steps are repeated until the crack turning is completed.

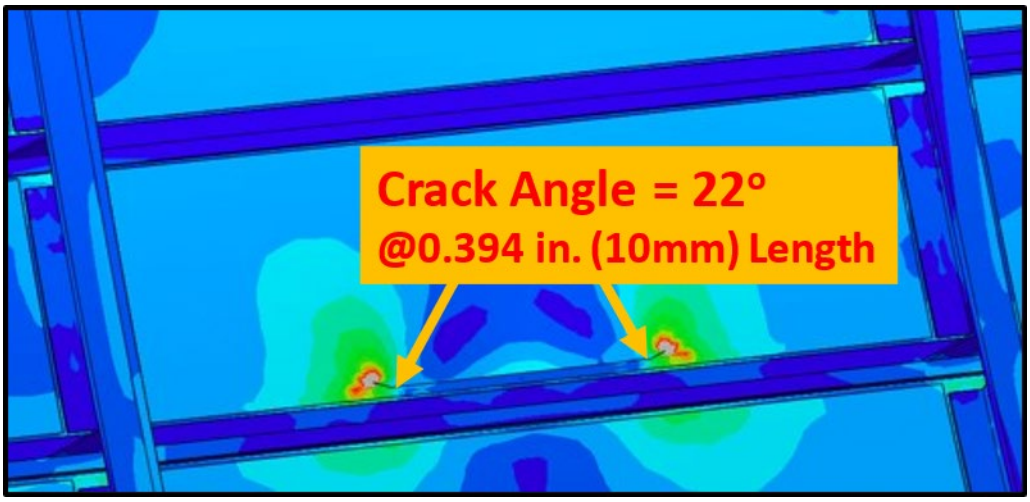

Figure 126. ABAQUS FE model after the first crack turning segment

The calculations for the as-designed, 0.055 in. (1.4 mm) are described next. For the 6.0 in. (152 mm), the starting crack right (+3.0 in. (76.2 mm)) crack tip SIF, K1 was 45 ksi*sqrt-in. (49.4 MPa*sqrt-m) for pressure loading only, and K2 was -9.1 ksi*sqrt-in. (-10.0 MPa*sqrt-m), and the Tstress was -27 ksi (186 MPa). Using the T stress (with the principal stress direction evaluated 0.05 in.(1.27mm) from the crack tip), the principal crack direction was 12°. When the T stress was not included, the angle was 22° (Figure 126 and Figure 127). The larger of the two angles 22° was used for the first step of crack growth prediction.

In this first step, a virtual 10 mm (0.39 in.) crack (Figure 126 and Figure 127) was grown from the tips of the 6.0 in. (152 mm) total length crack at a direction angle of 22º. To determine the growth rate along the 10 mm length (0.39 in.) at 22º , the stress intensity, K1, for the crack oriented at 22º was calculated as 47 ksi*sqrt-in. (51 MPa*sqrt-m), and K2 was zero, as expected, since this was the calculated principal stress direction in step 1. At 51 MPa*sqrt-m (47 ksi*sqrt-in) and a R-ratio of 0.05, the crack would be growing about 0.012 mm (0.0047 in.) per cycle (see Figure 128). It was assumed that the crack grew at this average rate for 10mm (0.39 in.) of growth at 22º for about 909 cycles.

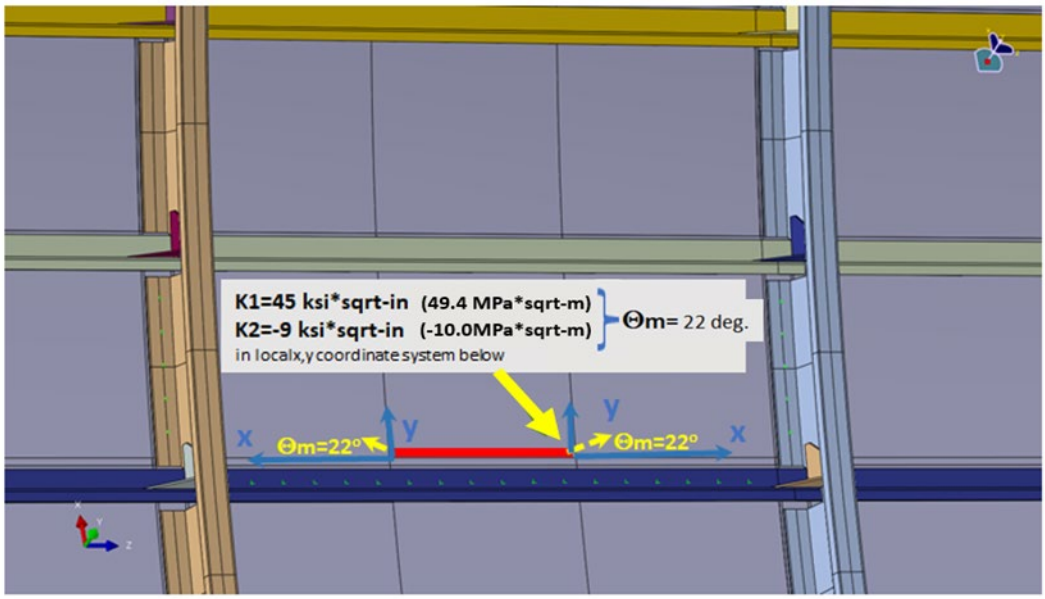

Figure 127. At 6 in. total length, the crack is assumed to grow at 22° for 10 mm

At the end of this first 10 mm of crack growth, K1, K2, and T stress were calculated (see crack tip in Figure 126 and Figure 129) at the FE model crack tip in the coordinate system oriented at 22°, and these were used to calculate the next turning angle increment. The results of K1=56.9 ksi*sqrt-in. (62.5 MPa*sqrt-m), K2 =-1.3 ksi*sqrt-in. (1.4 MPa*sqrt-m) and Tstress= -3.6 ksi (24.8 MPa) were used to calculate the next crack turning angle increment as 2.6°. Again, the T-stress incremental turning angle was smaller, and the principal stress incremental turning angle of 2.6° was used as shown in Figure 130. The total crack angle was now 22° plus 2.6° or 24.6°. In this direction of 24.6,° the K1 was 56.4 ksi *sqrt-in. (62 MPa*sqrt-m) and K2 was zero. The estimated crack growth rate is 0.001 in./cycle (0.03 mm/cycle) for a life of 333 cycles in this increment.

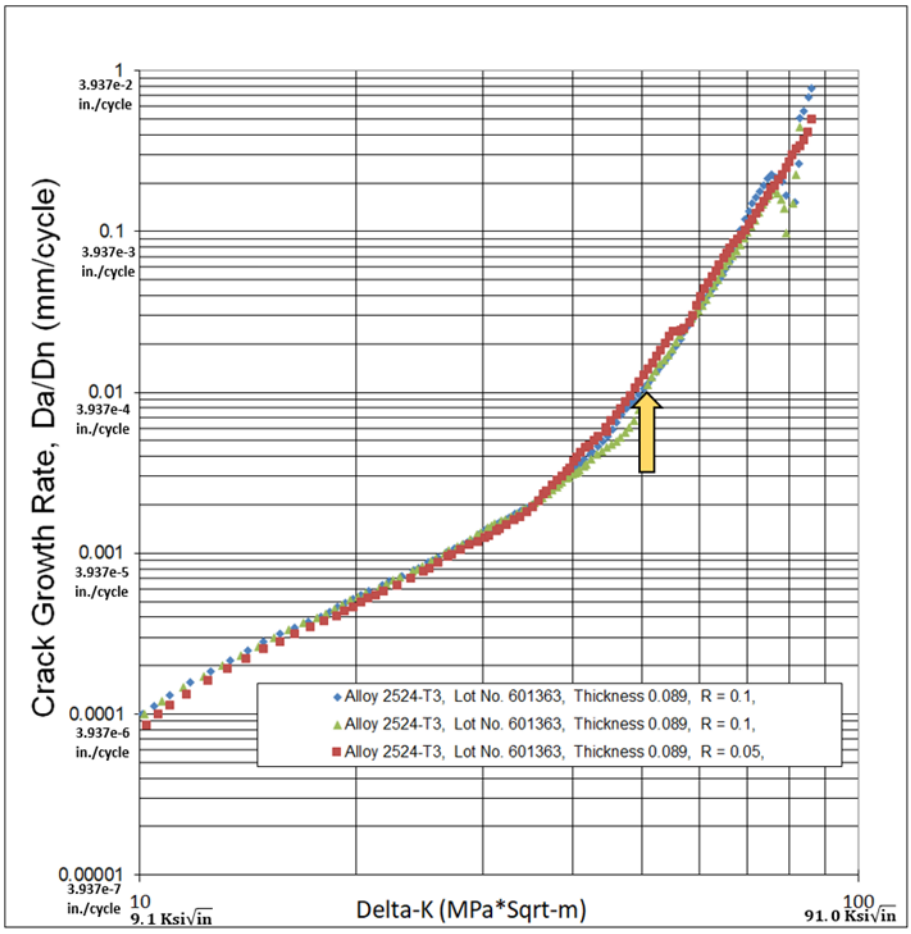

Figure 128. Crack growth rate, da/dN, for 2524-T3 in T-L direction

The results from a four-step estimate of crack life and trajectory analysis are detailed in Figure 131. The estimated life is the sum of the four segments is 1434 cycles (909, 333, 125, and 67 cycles).

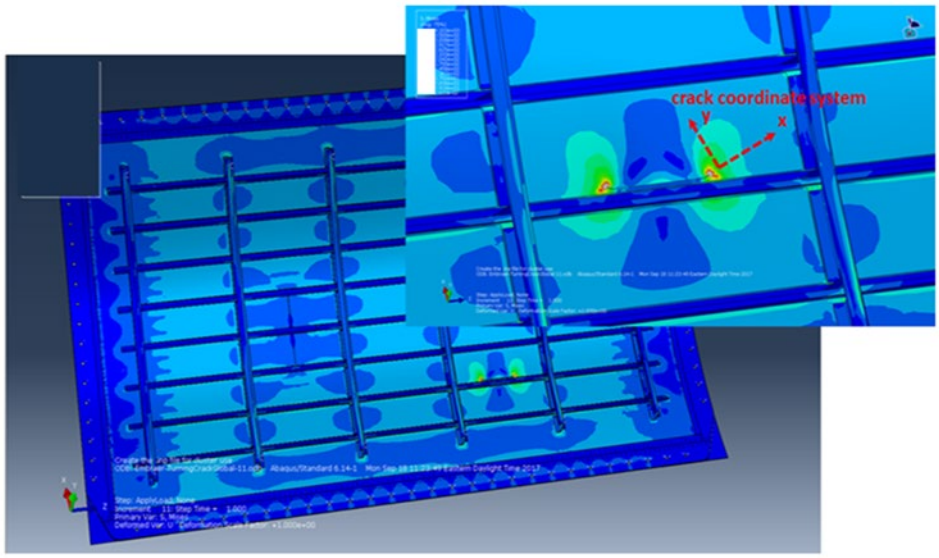

Figure 129. ABAQUS FE model coordinate system for K1, K2 calculations after the first crack turning segment

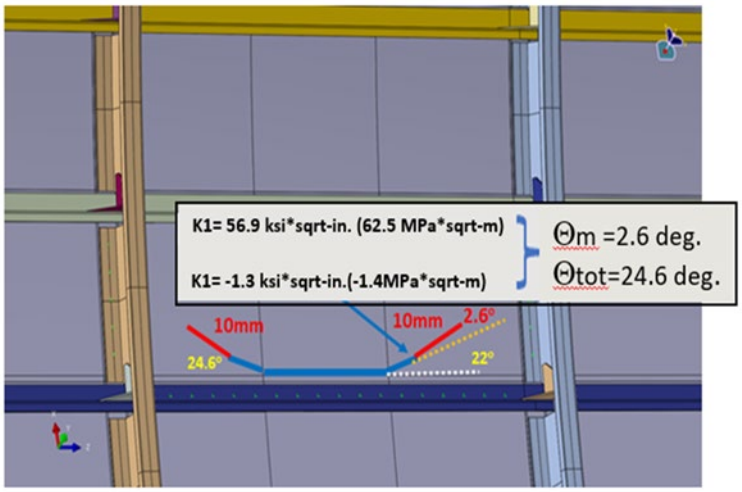

Figure 130. Calculated angle for second crack turning segment

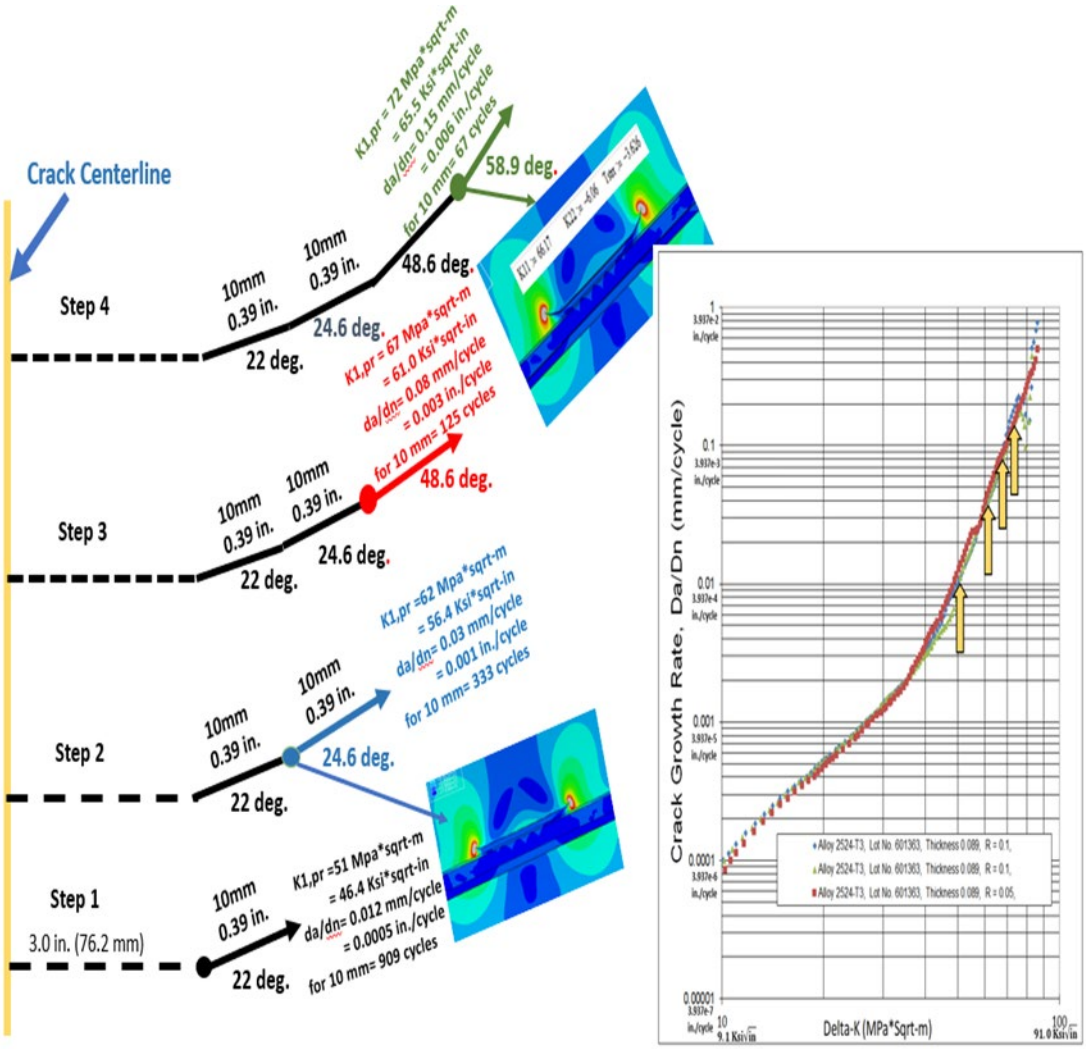

Figure 131. Summary of the four-step prediction of crack turning life

6.9 Analysis of phase 2, crack #2 repair

After the Panel 1, Phase 2 longitudinal one-bay crack turning test, the crack was repaired. A FEM analysis was conducted on a trial repair to determine if this repair in combination with the previous repair on the circumferential crack would affect the stresses in the Phase 3 longitudinal two-bay crack growth repeat inspection and residual strength scenarios (see Figure 132 and Figure 133). A skin patch of 0.063 in. was riveted using three rows of rivets to the skin in the stringer/frame bay where the “mill line” crack test was conducted. The skin patch extended to the adjacent bay below the Phase 2 crack and was fastened by three rows of fasteners (Figure 132). The skin patch ran over the stringer (stringer fasteners were removed and the patch re-fastened with the stringers). The FEM analysis for the as-designed Panel 1 was conducted before Panel 1 was tested. Note that during the FASTER testing, the Phase 1 circumferential and Phase 2

turning crack locations were mirror imaged in the test panel compared to the Panel 1 FE model as shown in Figure 132. The resulting axial stresses and hoop stresses for 9.9 psi pressure are plotted in Figure 133 and show that although the stresses in the patch repaired bays were altered by the repair, the stresses in the bays where the Phase 3 longitudinal crack will be conducted were not affected significantly.

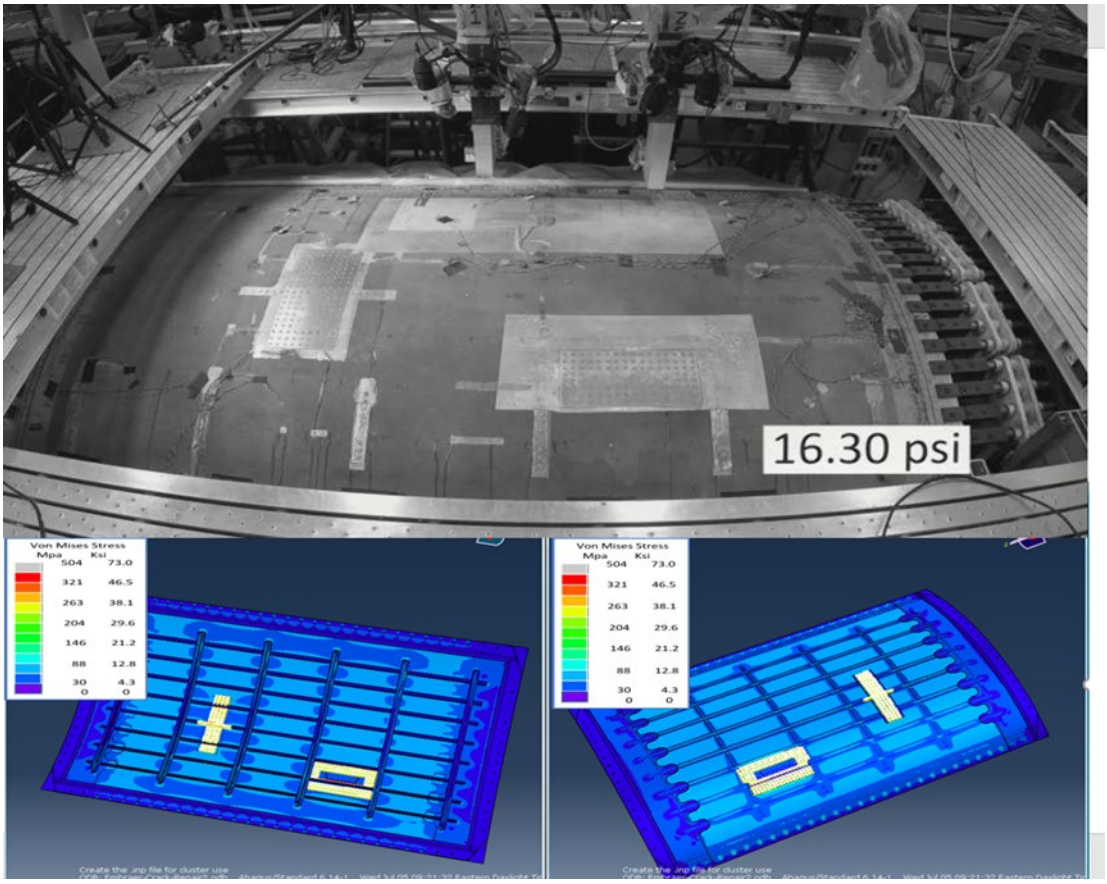

Figure 132. External view of Panel 1, Phase 2 crack repair and FEM model

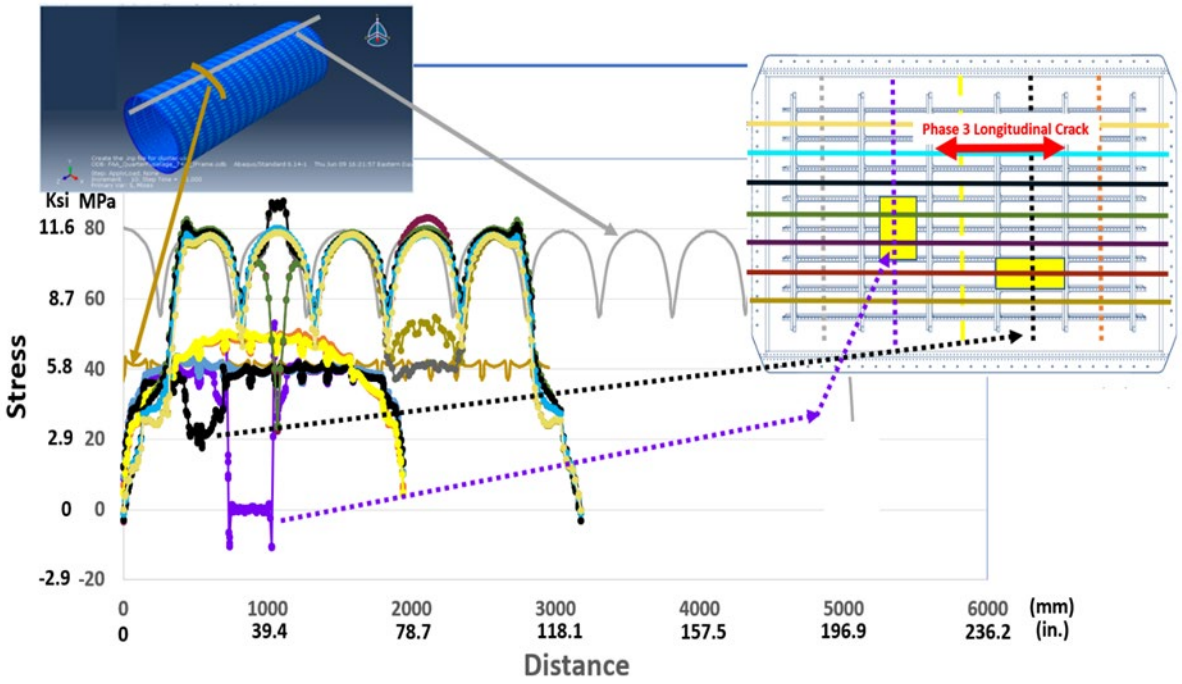

Figure 133. Axial and hoop stresses after repair of Phase 2 crack at 1G+9.9 psi

6.10 Panel-1 two-bay longitudinal fatigue crack growth modeling at 9.9 psi pressure

The as-designed, 0.055 in. (1.4 mm) Panel 1 longitudinal crack growth repeat inspection scenario was evaluated for a skin crack growing from the fastener under a broken central frame under cyclic pressure loading of 9.9 psi (0.068 MPa) (Figure 134). The central frame F4 was severed mid-bay between stringers S6 and S7. The crack was grown towards the adjacent frames, and then the panel was tested for residual strength. The goal for the repeat inspection interval was 6,000 flights with a safety factor of 2, or a total of 12,000 flights. For future aircraft, it was assumed the goal would be to achieve these inspections at a higher operating pressure of 9.9 psi (0.068 MPa) used in this test.

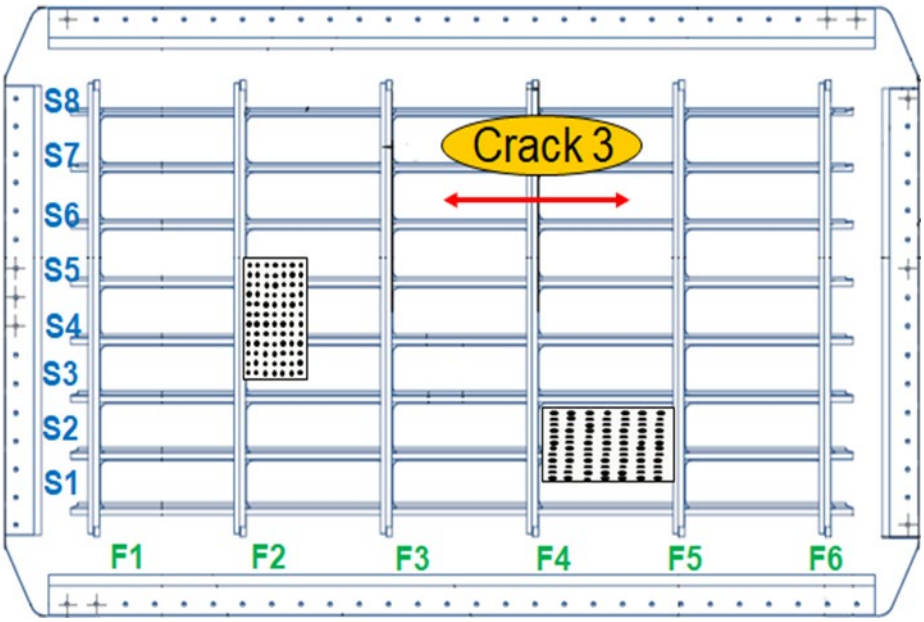

Figure 134. Location of the longitudinal two-bay crack

An ABAQUS FEM model was built for the as-designed, 0.055 in. (1.4 mm) skin thickness Panel 1 using two ABAQUS C3D20 element through-the-skin thickness. The repair patch for the Phase 2 crack was not included in this analysis, because the Phase 2 crack turning test was added to the testing program after this analysis was completed. Stress contour plots (Von Mises stress) are shown in Figure 135 for various size cracks.

The ABAQUS model in Figure 135 was subsequently modified to include the Phase 2, Crack 2 repair. The SIFs, Ktotal, results for the as-built, 0.059 in. Panel 1, Crack 3 longitudinal crack and the as-designed, 0.055 in. Panel 1, Crack 3 longitudinal cracks are compared in Figure 136 and Figure 137 for various FE models from 2016 to 2020. The test conditions are documented in these figures (see loads in Figure 114). As discussed previously, no actuator load adjustments were made during the FASTER Panel 1 crack growth testing or in the FE analysis for the various crack sizes.

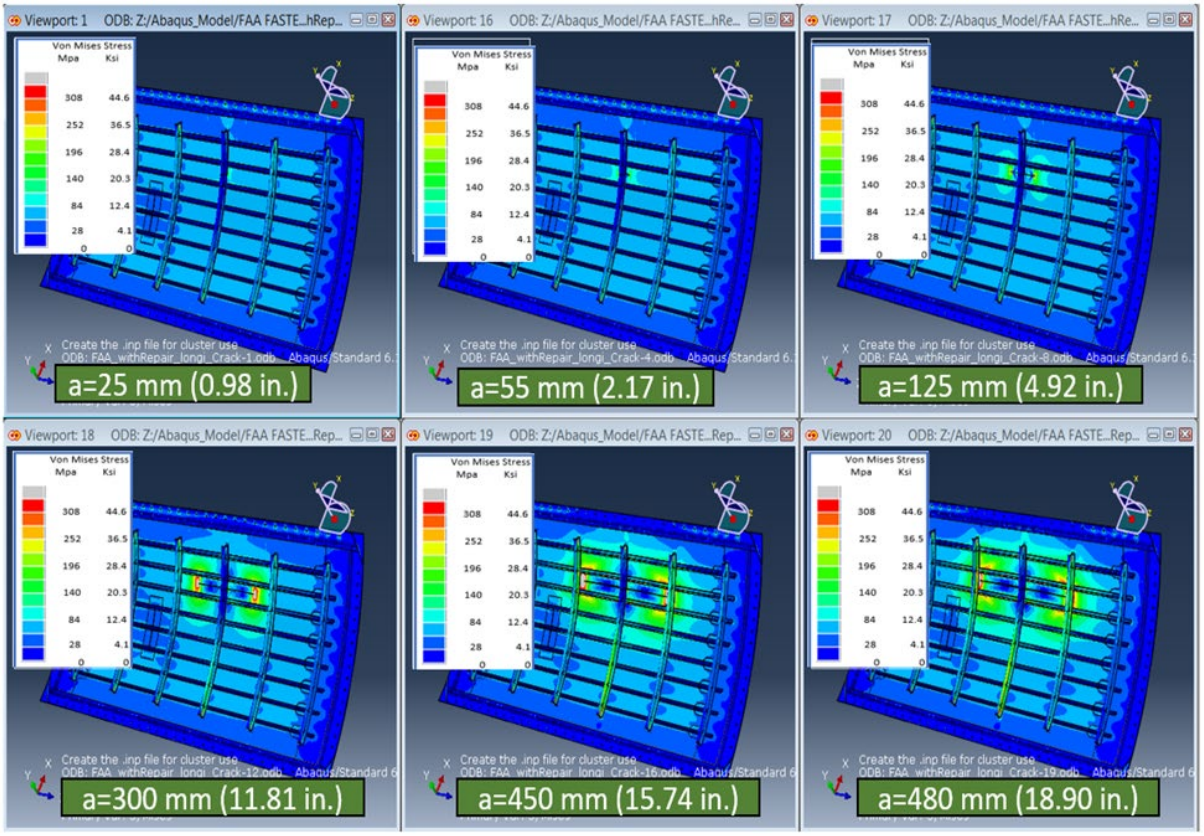

Figure 135. Von Mises stresses for various as-designed Panel 1, Phase 3 longitudinal cracks

The following comments are made regarding the results in Figure 136 and Figure 137:

- The one skin element, 0.055 in. (1.4 mm) pocket thickness Panel 1 (2016) FE results (red solid square) agree well with the one element, 0.055in. (1.4 mm) skin Qsymm1 FE model (grey solid square) for crack sizes up to 7.87 in. (200 mm). This demonstrates that the global to local approach used for Panel 1 loading worked well for crack sizes contributing to the majority of life.
- The two skin element, as-designed 0.055 in. skin thickness (1.4 mm) Panel 1 (blue solid triangle) model shows a reduction of 1.5% at a crack half-length of 1.0 in. (25mm) and a reduction of 6% at a crack half-length of 5.91 in. (150 mm) compared to the one skin element, 0.055 in. (1.4 mm) Panel 1 (red solid square) results.
- The eight-skin element, as-built 0.059 in. (1.5 mm) skin thickness Panel 1 results (yellow solid circle) show a small additional reduction of 1% at 5.91 in. (150 mm) crack lengths over the two-element as-designed, 0.055 in. (1.4 mm) Panel 1 (blue solid triangle) results. This as-built Panel 1 analysis (yellow solid circle) included the same boundary condition adjustments as the final as-designed Panel 1 circumferential crack analysis.

- The eight-element, as-built 0.059 in. (1.5 mm) skin thickness Panel 1 results for both crack tips (light green diamond and white circle) with the axial loader arm displacement of -0.039 in. (-1.0 mm) radially in the FE coordinate system shows a reduction of about 3% at 1.77 in. (45mm) and 6% at 3.94 in. (100 mm) crack length over the two-element as-designed, 0.055 in. (1.4 mm) Panel 1 solution (blue triangle).

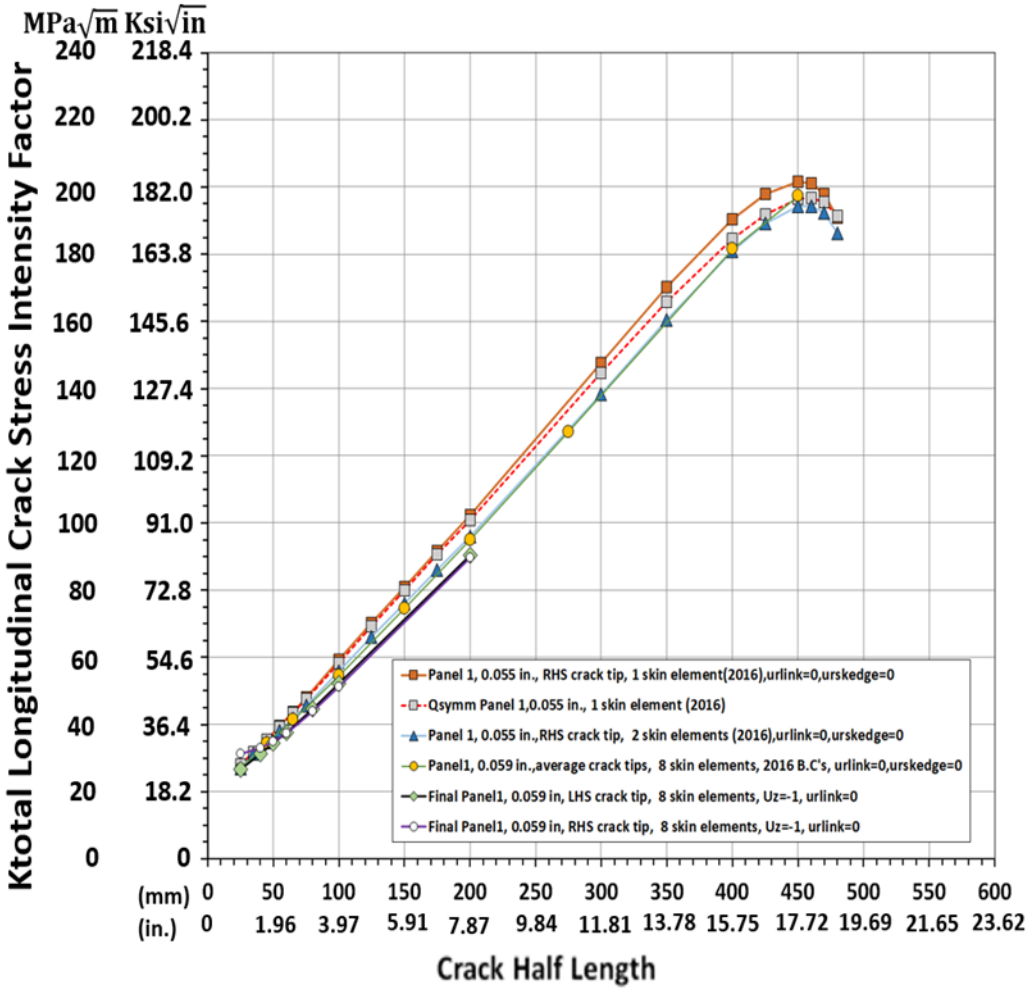

Figure 136. Comparison of the 2016 Panel 1 as-designed SIF solutions to the 2020 as-built longitudinal crack solutions

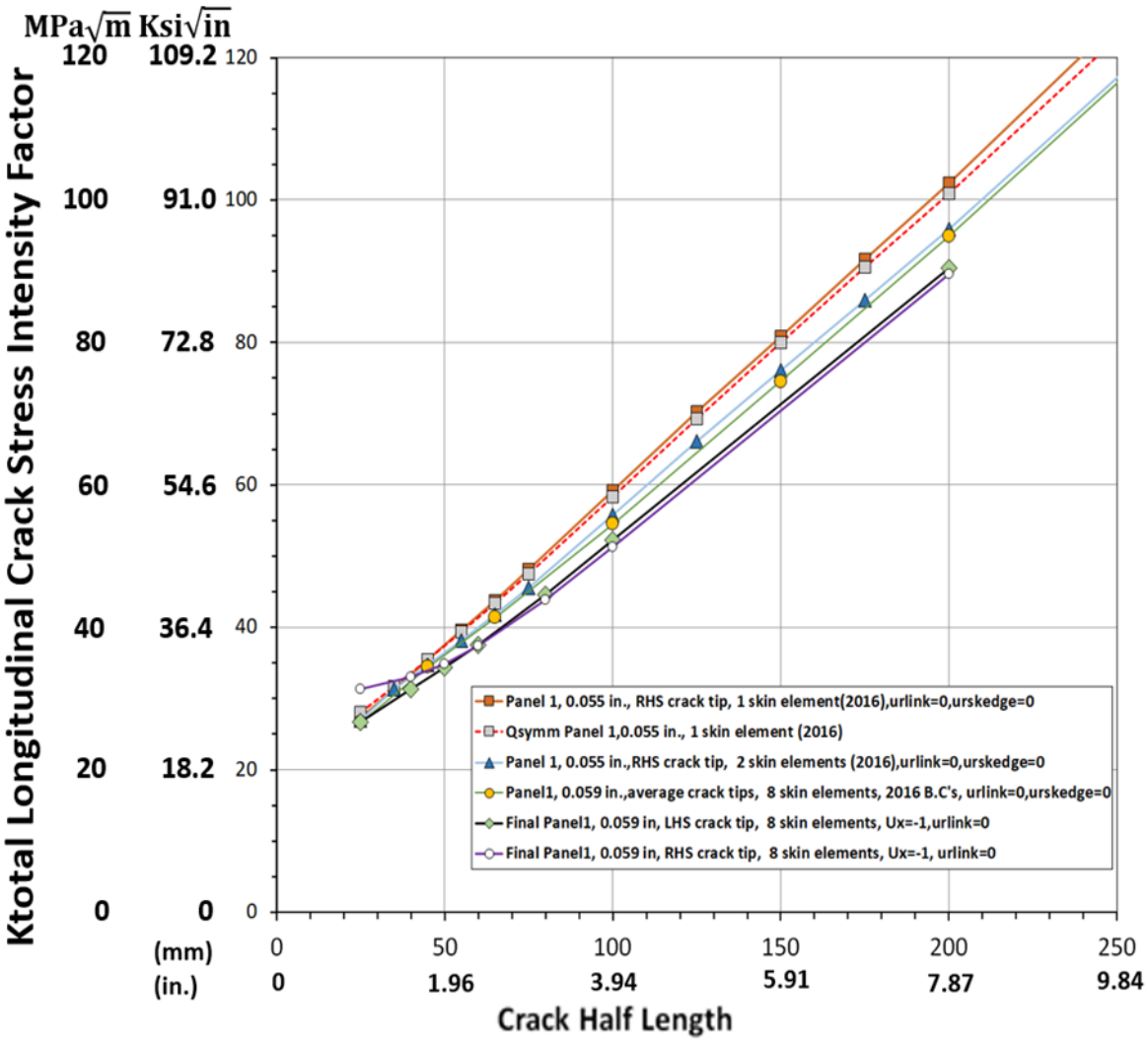

Figure 137. Detail of the 2016 Panel 1 as-designed stress intensity

- The eight-element as-built, 0.059 in. (1.5 mm) skin thickness Panel 1 results for both crack tips (light green diamond and white circle) with the axial loader arm displacement of -0.039 in. (-1 mm) in the FE coordinate system is considered the final solution for the as-built Panel 1.
    - Note that between 0.98 in. (25mm) and 1.97 in. (50 mm), there appears to be a local influence of the frame rotation. It was not determined how much of this is due to the non-symmetric location of the crack in the test Panel. That is, the broken frame distance (see Figure 134) to the panel hoop edge on the lower side is longer than to the upper hoop side; therefore, the panel flexibility against rotation and bending displacement in the frame direction is different on each side of the crack.

- This differential displacement/rotation of the frame in Panel 1 is shown in Figure 138. This effect is an artifact resulting from the non-symmetric crack placement in a finite width (frame direction) panel.
- In a full 360-degree fuselage, the frame flexibility on each side of a broken frame would be similar at the top crown location (when the broken frame is far from the pressure bulkheads and other major geometry disruptions).
- During the testing of Panel 1, considerable crack binding was experienced for the smaller crack lengths, which may partially be related to this differential displacement/rotation.

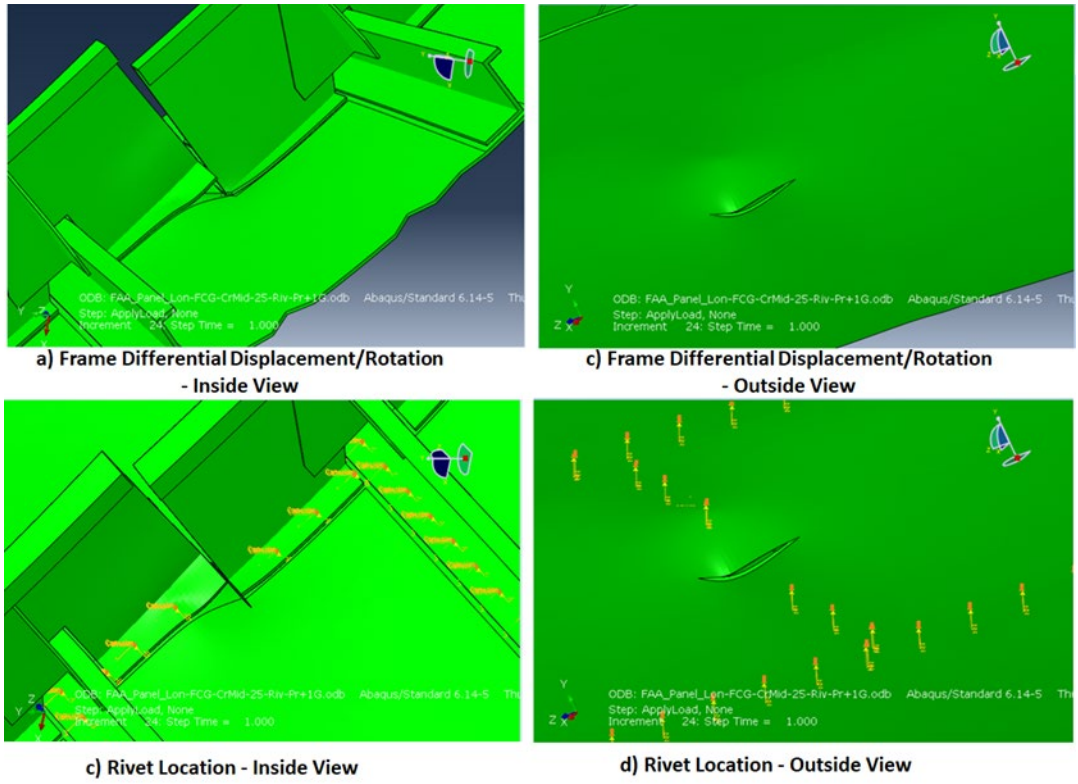

Figure 138. Frame differential displacement and rotation due to non-symmetric Panel 1 longitudinal crack placement

6.11 Longitudinal two-bay crack residual strength

The longitudinal crack residual strength goal was defined in this program to be a two-bay skin crack with a central broken frame loaded at 1.15 x pressure loads. The SIFs, Ktotal, at this limit load condition for the as-designed, 0.055 in. (1.4 mm) pocket skin Panel 1 show good agreement with the 0.055 in. (1.4 mm) pocket skin Qsymm1 FE model in Figure 139. Actuator loads for 9.9

psi (0.068 MPa) previously shown in Figure 113 were scaled by a factor of 1.15 for the limit loads. See Figure 103 for properties used in ABAQUS FE model. The elastic/plastic analysis SIFs are plotted as Aphysical. The elastic analysis SIFs are plotted as Aeffective. The Panel 1 longitudinal crack was grown to about 8 in. half crack length. For crack growth to this size, the two-bay crack, the SIFs at 1.15 x pressure shown in Figure 139 were below the crack resistance R-Curve for 2524-T3, so Panel 1 was not expected to fast fracture during the pressure driven longitudinal crack growth portion of the FASTER Panel 1 test.

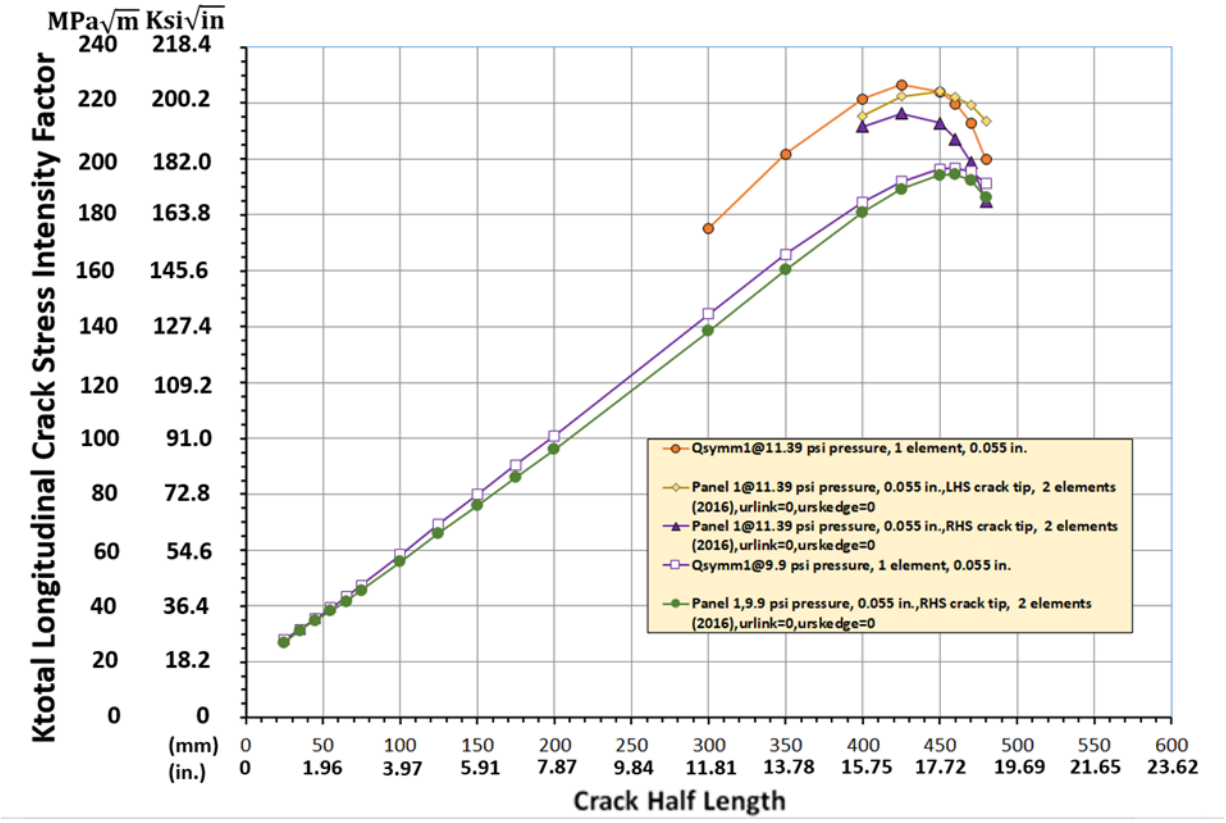

Figure 139. Comparison of as-designed, 0.055 in. skin thickness Panel 1 Ktotal for the longitudinal two-bay crack at 1.15 x pressure limit load with results at 9.9 psi

Results of the elastic plastic analysis at 1.15 x pressure load are replotted in Figure 140. This analysis did not include rivet failure, shear tie failure, and frame failure. A separate analysis was conducted for the full two-bay crack and will be discussed later. Note that an Aphysical R-Curve was not available for use with the elastic/plastic ABAQUS FE analysis results . The Aphysical R-Curve in Figure 140 was estimated by a FE analysis of the 43 in. (1.09 m) wide panel Aeffective based R-Curve shown in Figure 141 (Bucci, et al., 2000). The Aphysical R-Curve was estimated using the Aeffective COD and test load data for various points measured on the Aeffective R-Curve. Both elastic/plastic and elastic FE models were needed for each crack size converted to Aphysical. For a given Aeffective crack size, the Aphysical crack tip in the

elastic/plastic FE model was iteratively moved until the COD in the elastic/plastic FE analysis was the same as the COD in the elastic FE model with the Aeffective crack. Both FE models were loaded to the same experimental measured load for the given Aeffective crack size being converted. The resulting stress intensity of the Aphysical crack was extracted using the J-integral.

The approach in Figure 140 (see orange and yellow solutions at limit load) was used to establish whether the crack resistance R-Curve is greater than the SIFs at limit load for crack sizes up to 8 inches (203 mm) to cover the sizes in the FASTER tested Panel 1 longitudinal crack phase (beyond this the SIF is so high that few additional crack growth cycles are added). The interpretations of the graphs in Figure 140 were documented in Section 2.2.7. As mentioned in Section 2.2.7, FE analyses with rivet failure and frame/shear ties failure should be done for large cracks approaching the adjacent frames to determine the shape of the upper brown dashed line in Figure 140. Recall that the upper and lower brown dashed curves are only hypothetical in Figure 140. In the current program, only one detailed analysis was conducted and described below.

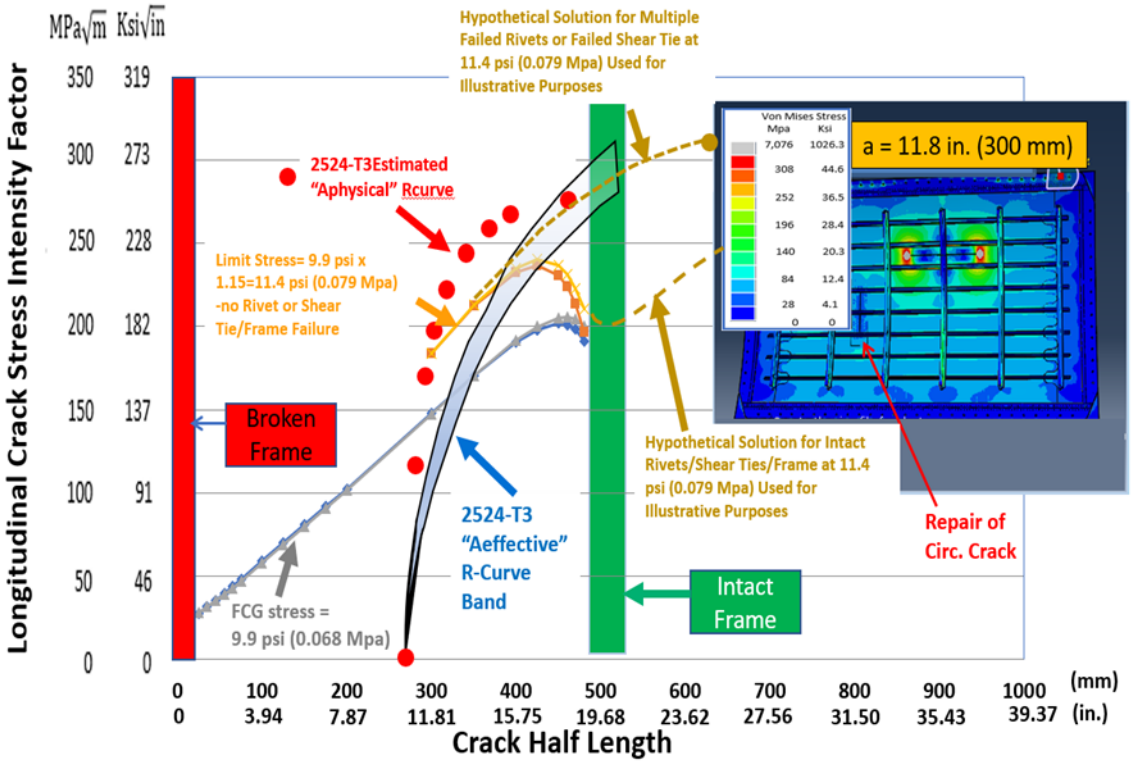

Figure 140. Analysis of Panel 1 longitudinal two-bay crack at limit pressure of 1.15 x pressure, or 11.385 psi (0.0785 MPa)

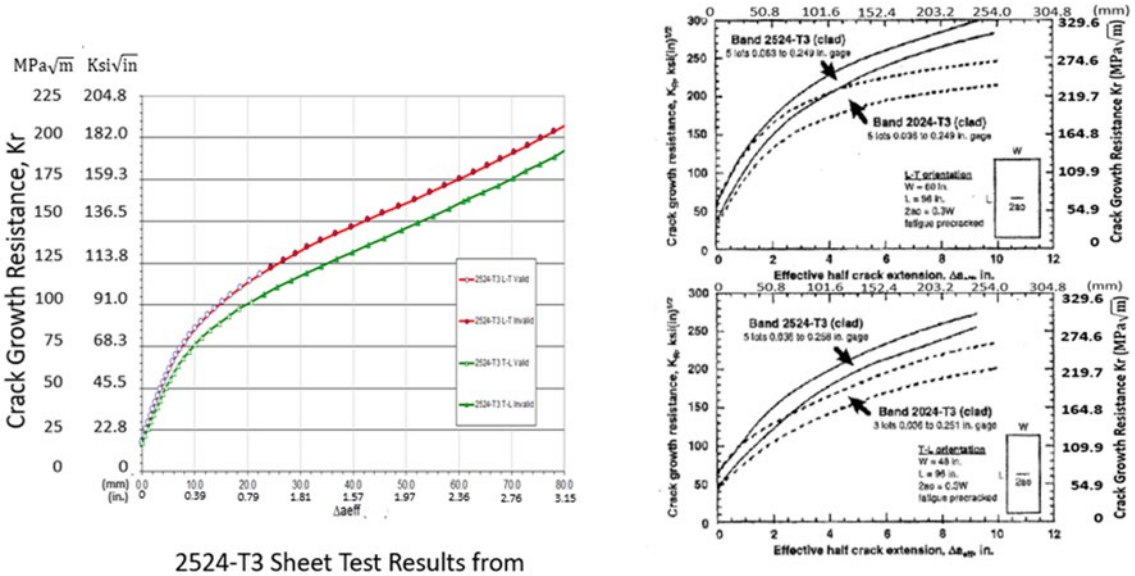

Figure 141. R-Curve for same lot 2524-T3 used in Panel 1 and wide panel data from Bucci, et al., used to estimate Aphysical based R-Curve

A detailed FE analysis was conducted to demonstrate one approach for estimating failure for the full Panel 1 longitudinal two-bay crack scenario. This involved modeling complex behavior in the panel, including:

- Elastic/plastic behavior of the skins, shear ties, and frames
- An effective non-linear rivet load displacement relationship that captures hole skin bearing yielding for a highly loaded rivet
- Capability in the FE model to capture rivet failure/unloading or frame/shear tie failure
- A four-bay crack analysis for the R-Curve failure approach as the crack stably extended into the bays beyond the adjacent frames

These predictions were still considered a rough estimate, because there were severe limitations to using the FE analysis approach with the R-Curve for this type of failure analysis. These limitations include:

- The extensive plasticity in the skin when the crack is approaching the frame indicated that while Aphysical was still in front of the frame, Aeffective could be beyond the frame, which makes it difficult to interpret results.

- It is difficult and time consuming in a FEM analysis to iteratively capture a) the slow stable tearing process and include b) the impact of the plasticity on the frame/skin/rivet interactions, as well as c) potential failures of rivets and shear ties/frames.

Perhaps a better approach to predict the residual strength is to use the crack tip opening angle (CTOA) approach proposed by Wells (1961) and discussed in Newman & James (2001). However, this was beyond the scope of the program.

An ABAQUS simulation was conducted for the as-designed 0.55in. (1.4 mm) pocketed skin Panel 1 with two C3D20 skin elements for the two-bay crack to estimate the loads needed to fail Panel 1. The elastic/plastic analysis model included non-linear fasteners and stringer, skin, and frame plasticity. As shown in Figure 142a, full two-bay crack extending from frame fastener to frame fastener would exhibit skin slow stabile tearing into the bays beyond the adjacent frames. A simplified piecewise approach was used to estimate the skin tearing, fastener non-linear load displacement, and fastener failure, and to check for shear ties/frame failure. Key elements of the incremental loading prediction approach are shown in Figure 143 and are described below.

- Detailed sub-models were used to generate the SIFs for cracks on both sides of the four-bay crack.
- Stringer-to-skin and frame-to-skin contact regions were defined to prevent penetration in key regions.
- Non-linear fastener load displacement data was used. When the fastener exceeds the last displacement entered in the fastener load displacement input Table (see Table 2), the fastener is unloaded, representing fastener failure. Also, since the crack plane extends through to the skin fastener in this FE model, this adjacent frame fastener is considered failed when the crack extends beyond this fastener into adjacent bays 3 and 4.
- Elastic plastic properties are used for the skin, stringers, and frame (see Figure 103).
- The shear tie and frame are modeled as a single detail to simplify the analysis, as shown in Figure 143. Failure of the shear tie/frame is assumed when the average strain in the attach leg reaches 2.5% between rivets based on prior data with “dog-bone” type skin/stiffener specimen testing with fastened holes (Mohaghegh, 1985). Another area of potential failure is the “mousehole” cutout corner regions that allow the stringers to pass through. However, the mesh was not fine enough at the shear tie “mousehole” cutouts to capture the stress concentrations, and engineering judgement was used to check for failure at this location.

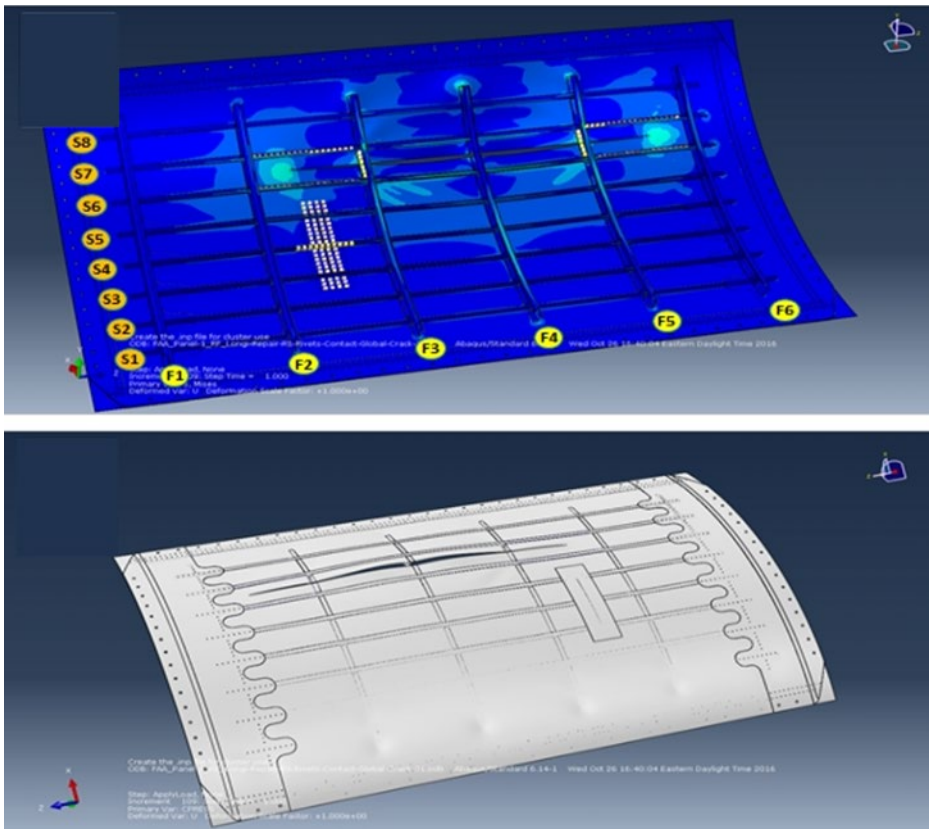

Figure 142. FE model (mesh not shown) of test Panel 1 showing a crack grown in the skin from the central broken frame

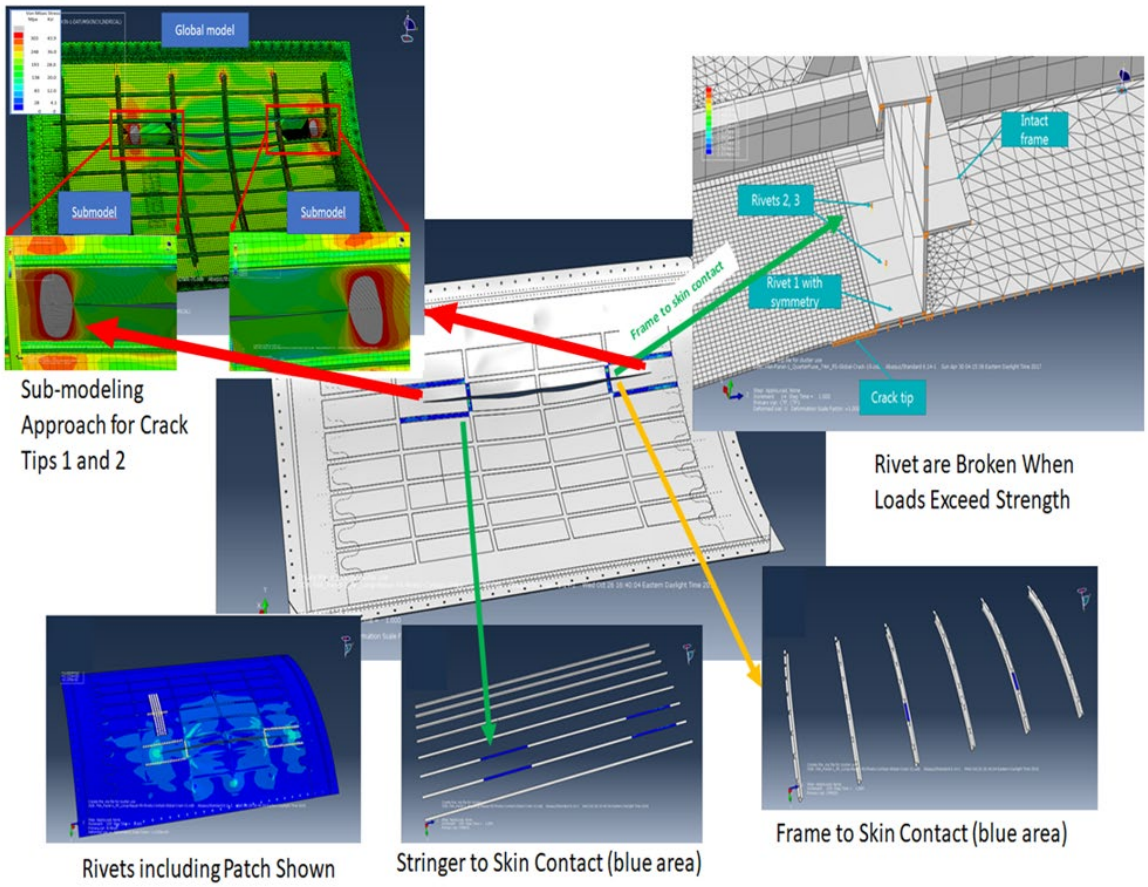

Figure 143. FEM approach for two-bay longitudinal crack elastic/plastic R-Curve analysis

The results of the iterative steps for the Panel 1 failure load analysis are shown in Figure 144. The goal was to provide a rough estimate of the pressure needed to fail the panel for a starting crack size of 19.68 in. (500 mm). To establish analysis Point 1 in Figure 144, an elastic/plastic analysis was conducted for the limit pressure of 9.9 × 1.15 psi, or 11.385 psi (0.0785 MPa) for the 19.68 in. (500 mm) starting size to establish the Ktotal for this condition. Using the Ktotal, the delta Aphysical skin tearing was determined from the Aphysical R-Curve. The crack was extended this amount and Ktotal recalculated. Point 1 was established as this new Ktotal.

The frame-to-skin rivet at the crack centerline (Rivet 1) was released before the loading, because the crack extension was beyond Rivet 1 at the end of this first step. Adjacent frame rivets 2 and 3 on each side of the center rivet in the crack path were checked for failure. Rivet 2 had reached a high load but had not reached the maximum displacement. Also, frame/shear tie and mousehole failure was checked and estimated to be intact. Point 2 was established by starting with the Point 1 four-bay crack and arbitrarily extending the crack 5.3 in. (135 mm) to a total half-length of 25 in. (635mm), and an elastic/plastic analysis was conducted at the same limit pressure of 1.15 × pressure, or 11.385 psi (0.0785 MPa), as Point 1 to determine the SIF, Ktotal, (with the center

rivet removed and the adjacent rivets not carrying any additional load at this point in accordance with the non-linear load displacement in Table 2). A Ktotal was calculated for this condition, and the results were plotted as Point 2 in Figure 144. The results were checked for rivet or frame failure.

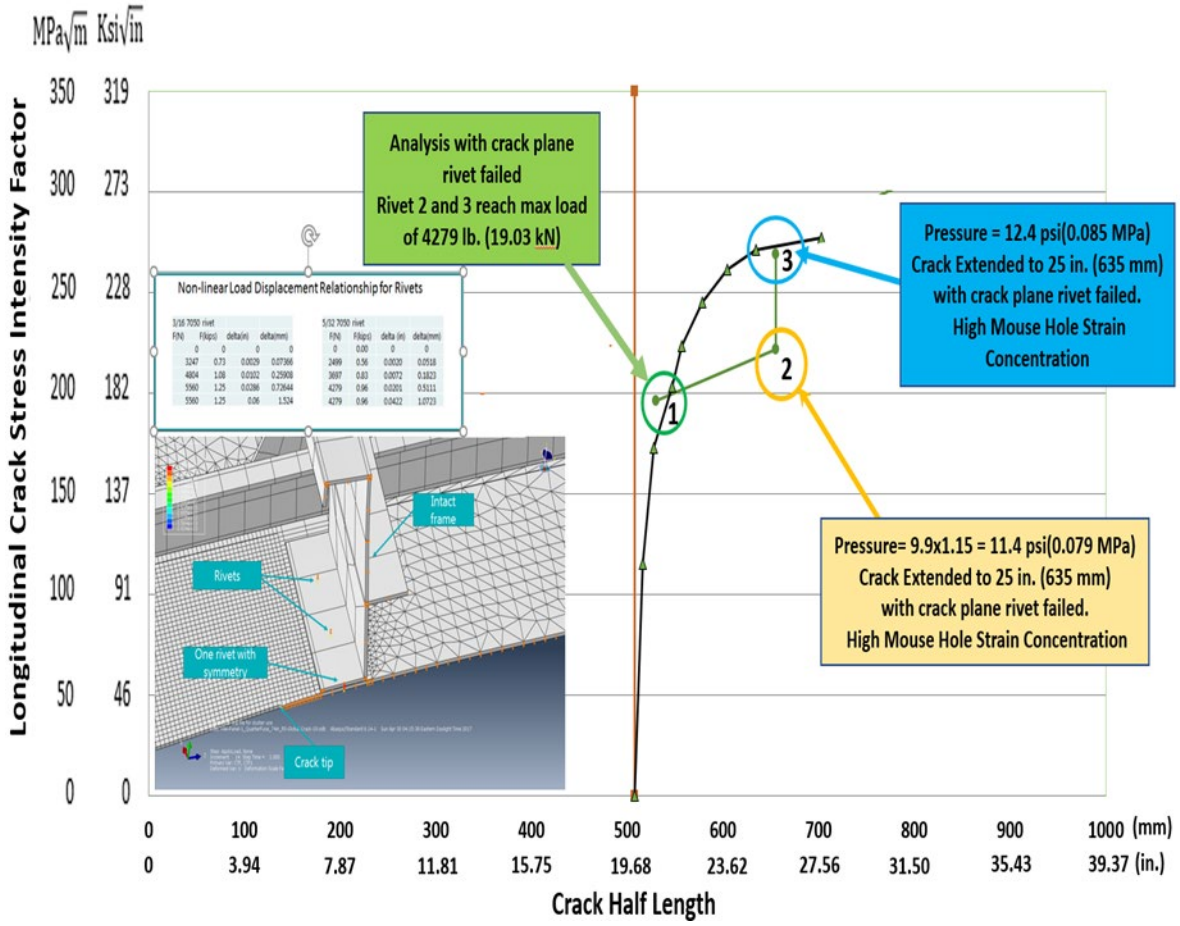

Figure 144. First three iteration steps in Panel 1 longitudinal two-bay crack analysis

A final analysis was done, starting with the crack size at Point 2 and increasing the pressure (keeping the current crack length) constant until the SIF, Ktotal, at this total crack extension of 5.3 in. (135 mm) was coincident with the estimated Aphysical R-Curve crack resistance at this same total crack extension of 5.3 in. (135 mm). This solution is shown as Point 3 in Figure 144. The pressure required to reach Point 3 was 12.4 psi (0.085 MPa). Note that at this point, the Ktotal was nearly equal to the peak crack resistance at Point 3 (R-Curve flattens). Therefore, no more iterations were undertaken. It was recognized that the smaller the extension of the crack, the more accurately the results would follow the Aphysical R- Curve. It was felt that the current ballpark prediction could be revisited after the Panel 1 test, if needed, to refine the analysis.

7 Repeat inspection and limit loads for Panel 2

This section discusses the impact of testing the as-built Panel 1 to limit loads developed for the as-designed Panel 1. This section also discusses the limit loads development for the as-built Panel 2. Panel 2 was built with a pocketed skin thickness of 0.05 in. (1.27mm) in the pocketed region compared to 0.059 in. (1.5 mm) in the skin pockets of the as-built Panel 1. The extrusions maintained their target thickness, and thus the Axx/Bts in Panel 2 were larger than the as-built Panel 1. The program team decided to test the circumferential and longitudinal cracks in Panel 2 and Panel 3 using loads that produced the same respective SIFs in the as-built Panel 1 (longitudinal and circumferential). Since Panel 2 crack growth loads were derived matching SIFs to the as-built Panel 1, the circumferential limit load cannot simply be established by multiplying the axial loads by a factor of 2.5. Circumferential limit load was established by locating Panel 2 in the fuselage crown based on a separate sizing study for each panel using the generic methods described in Section 2. The results of a study will be discussed for estimated circumferential repeat inspection working stress targets for Panel 2 comprised of a 2060-T8 Al-Li skin, 2055 Al-Li extruded stringers, and 2099 integral frames from extrusions.

This section provides detailed information used to scale the Panel 2, Phase 1 circumferential crack growth loads to obtain the limit loads for the locations in the crown for Panel 2 as determined by a separate sizing study using the methods described in Section 2. Estimated circumferential repeat inspection working stress targets for the 2060 skin materials were used. The limit load for Panel 3 was calculated in a similar manner, although the details are not included in this document.

As described in Section 2, the sizing study for Panel 2 materials and geometry includes the same design goals for static failure, buckling, inspections, etc. as Panel 1. Skin working stress targets for each design goal (such as the skin stress needed to meet an inspection goal for the defined Axx/Bt ratios) were estimated for the sizing study. The calculation of the ultimate and limit bending loads are summarized as follows:

1. The simplified fuselage bending model shown in Figure 11 determines the *axial bending moment* at limit load along the length of the fuselage using the maximum of the gust accelerations or the regulation specified maneuver acceleration for the type class of aircraft (2.5 G in this case; see Figure 11).
2. This maximum acceleration in step 1 (gust versus maneuver) was applied to the entire fuselage where MTOW load is multiplied by the maximum acceleration G factor at limit (normally a factor of 2.5). This acceleration-scaled MTOW load is distributed uniformly

along the fuselage length for simplicity. The calculation of the bending moment along the length of the airplane is statically determinate for the model in Figure 11 and does not change throughout the rest of the sizing study iteration loops as the panel geometries change along the circumference and length of the fuselage. Note, the weight of the fuselage structure is included in the MTOW.

3. The bending moment at ultimate is 1.5 times the maximum bending moment at limit. The bending moment at limit divided by 2.5 is the 1G bending moment.

4. The axial load intensities and stresses in the crown due to bending for 1G, limit, and ultimate were defined by the equations for a cylindrical cross-section beam, and these values change in the iterative looping process used in the sizing study. For instance, for the simplified approach in this study the 1G axial bending stress in the crown is equal to:

$$(LimitMoment(STAxx)/2.5G) \times radius(STAxx) \Big/ Ixx(STAxx) \quad (30)$$

where Ixx(STAxx) is the moment of inertia of the cross-section at location STAxx. Ixx(STAxx) depends on the all the inputs in the sizing methods that are used to ensure all design goals are met (materials, geometry, minimum gage, Axx/BT, etc.) as defined in Section 2.
The bending axial load intensities in the crown at 1G are defined using the beam equation for stress times the thickness:

$$(LimitMoment(STAxx)/2.5G) \times radius(STAxx) \times tavcr(STAxx) \Big/ Ixx(STAxx) \quad (31)$$

where tavcr(STAxx) is the average crown cross-section smeared thickness at STAxx.

5. By calculating axial stresses in the crown from the bending moment based on the cross-sectional moment of inertia (Figure 13), Ixx, at the various STA locations and adding the axial component of the pressure stress, the total axial stresses at 1G + pressure, limit + pressure, and ultimate + pressure can be determined.

6. For the hoop direction, skin stresses from the 9.9 psi (0.068 MPa) pressure load were used for the longitudinal crack growth in the crown. This was done in the sizing approach using the current iteration values of skin thickness, the input constant Axx/Bts, and the Flugge equations. Longitudinal cracks for Panel 1 were grown for 9.9 psi (0.068 MPa)

pressure-based hoop stresses, and only the axial load component of pressure was applied. The limit pressure was defined as 1.15 × 9.9 psi (0.068 MPa) or 11.4 psi (0.072 MPa).

A separate sizing study was done for the as-built Panel 1 geometry to establish the location in the crown where the panel would have been located to meet the repeat inspection goals given the pocketed skin thickness change from 0.055 in. (1.4mm) to 0.059 in. (1.5 mm) in the as-built geometry. This study was used to determine the new limit load for the circumferential crack for the as-built Panel 1. Recall that the thickness change was not discovered until after the Panel 1 test for the as-designed limit load. This new limit load for the as built Panel 1 would have provided a more rigorous test for the as-built Panel 1 compared to the limit load developed for the thinner as-designed Panel 1 for the FASTER test.

For the Panel 2 limit load, two separate sizing studies were conducted to determine a more realistic location in the crown for the as-built Panel 2. In the first, the same as-built Panel 1 skin axial working stress target of 12.1 ksi (83.4 MPa) at 1G plus 9.9 psi (0.068 MPa) pressure was used for Panel 2. Recall that the goal for the thinner skinned as-designed Panel 1 was an axial skin stress target of 13 ksi at 1.04G + pressure based on K-control testing which converts to 12.1 ksi (83.4 MPa) at 1.0G + pressure for the thicker skinned as built Panel 1. An additional sizing study was done for Panel 2 to develop limit loads assuming a hypothetical anticipated improvement in the skin axial working stress target for crack growth for the 2060-T8 skin.

It should be emphasized that no K-control testing was done to establish this new axial skin working stress target hypothesis for the 2060 skin material, since testing for a 2060-T8 working stress target for circumferential crack growth was beyond the scope of the program. Instead, an axial skin working stress target of 13.5 ksi (83.1 MPa) was estimated for Panel 2 at 1G + pressure given that 2060 exhibits improved growth characteristics in Da/Dn testing compared to 2524-T3. This second sizing study may be interpreted as finding the Panel 2 location in the crown, which takes advantage of a potential performance improvement for circumferential repeat inspections. To summarize this hypothetical limit load case for Panel 2, the FASTER crack growth testing for Panel 2 was conducted for a location in the crown where the SIFs based on FE analyses were the same as the SIFs for the as-built FASTER-tested Panel 1. The circumferential crack limit load for Panel 2 was calculated at the crown location, where the as-built Panel 2 exhibited an estimated 13.5 ksi (93.1 MPa) skin working target stresses for circumferential crack growth. If a higher working stress is established for Panel 2, this new limit load test could be used to establish critical crack sizes during circumferential crack growth and ensure the panel meets the design goal definitions of being able to carry a two-bay circumferential crack at the location in the crown where Panel 2 would be located for the higher estimated working stress for

circumferential crack growth. More details of crack growth and limit load testing are described below.

The decision to apply the same SIF to Panel 2 as the as-built is detailed as follows. Because the Panel 1 skin thickness difference was not known at the time of Panel 1 FASTER testing, the as-designed Panel 1 loads were used to test the thicker skin, as-built FASTER Panel 1. This thicker Panel 1 skin lowered the axial skin stress during the circumferential crack growth test at 1G + 9.9 psi pressure from 12.7 ksi (87.6 MPa) to about 12.1 ksi (83.4 MPa). The ideal "apples-to - apples" comparison would have been to test the same geometry Panel 1 and Panel 2 to the same loads, and thus to exhibit the same SIFs (apart from small modulus differences). Since this was not possible considering the pocketed skin differences in Panels 1 versus 2, various approaches were considered for Panel 2 testing. The first approach involved keeping the average cross-sectional stresses the same for Panel 2 as the as-tested Panel 1 and conducting post-test FEM and crack growth simulations to estimate the fine tune performance of Panel 2 relative to Panel 1. It was felt that this approach would add too much reliance on post-test fracture mechanics analysis for the interpretation of experimental test results for the differing AS/BT geometries. It was decided to test Panel 2 to loads that produced the same SIFs as the as-built, FASTER-tested Panel 1 and then use analysis in conjunction with supplemental testing of smaller specimens to compare performance of Panels 1 and 2 at the same location in the fuselage.

Before we discuss the Panel 2 loads, it is useful to review the effect of the as-designed versus as-built Panel 1 loading by examining the results of several separate sizing studies. For these studies, it is recognized that changes in skin thickness and/or changes to Axx/BT ratios result in changes in SIFs, which, in turn, could change the axial and hoop skin working target stresses necessary to meet a given inspection goal. However, it was beyond the scope of this study to determine the new working stress targets using K-control testing for the as built versus as designed Panel 1 geometry.

For these studies, it was assumed that axial skin working stress targets for the as-built Panel 1 were the same as those established for the as-designed Panel 1 using K-control testing (12.7 ksi [87.6 MPa] at 1G + pressure).

The results of sizing studies for Panel 1 are shown in Figure 145. The blue line represents the as-designed Panel 1 at the fuselage crown location STA 38 sized for an axial skin working stress target of 12.7 ksi (87.6 MPa) based on K-control testing. The purple line represents the as-built Panel 1, which was tested to the same load intensities as the as-designed Panel 1, since we were unaware at the time of testing of the skin pocket thickness difference. For the FASTER Panel 1 test load intensities used the Flugge characteristic skin stress in the thicker, as-built Panel 1 was

not 12.7 ksi (87.6 MPa), but was about 12.1 ksi (83.4 MPa). The bottom green circle shows the estimated location for the as-built Panel 1 based on a new sizing study to locate the thicker skinned as-built Panel 1, if the Panel 1 skin stress was kept at the12.7 ksi (83.4 MPa) axial skin working stress target at 1G plus pressure establish by independent specimens using K-control testing (see Section 5). The upper green circle represents the estimated limit load for this same Panel 1 study. This is the estimated limit load if the thicker skin as-built Panel 1 were to be placed in the crown of the same aircraft used for the as-designed Panel 1 study for the skin axial working stress target of 12.7 ksi (83.4 MPa). The FASTER as-built Panel 1 test (purple line in Figure 145) was actually loaded to an in-fuselage axial target of 1,766 lb/in. (309 N/mm) at the circumferential crack limit load. The limit loads for the thicker skin as-built Panel 1 sized to 12.7 (83.4 MPa) axial skin working stress target was determined to be 1,916 lb/in. (336 N/mm). Thus, the FASTER as-built Panel 1 was tested to about 92% of the estimated geometry-based limit load.

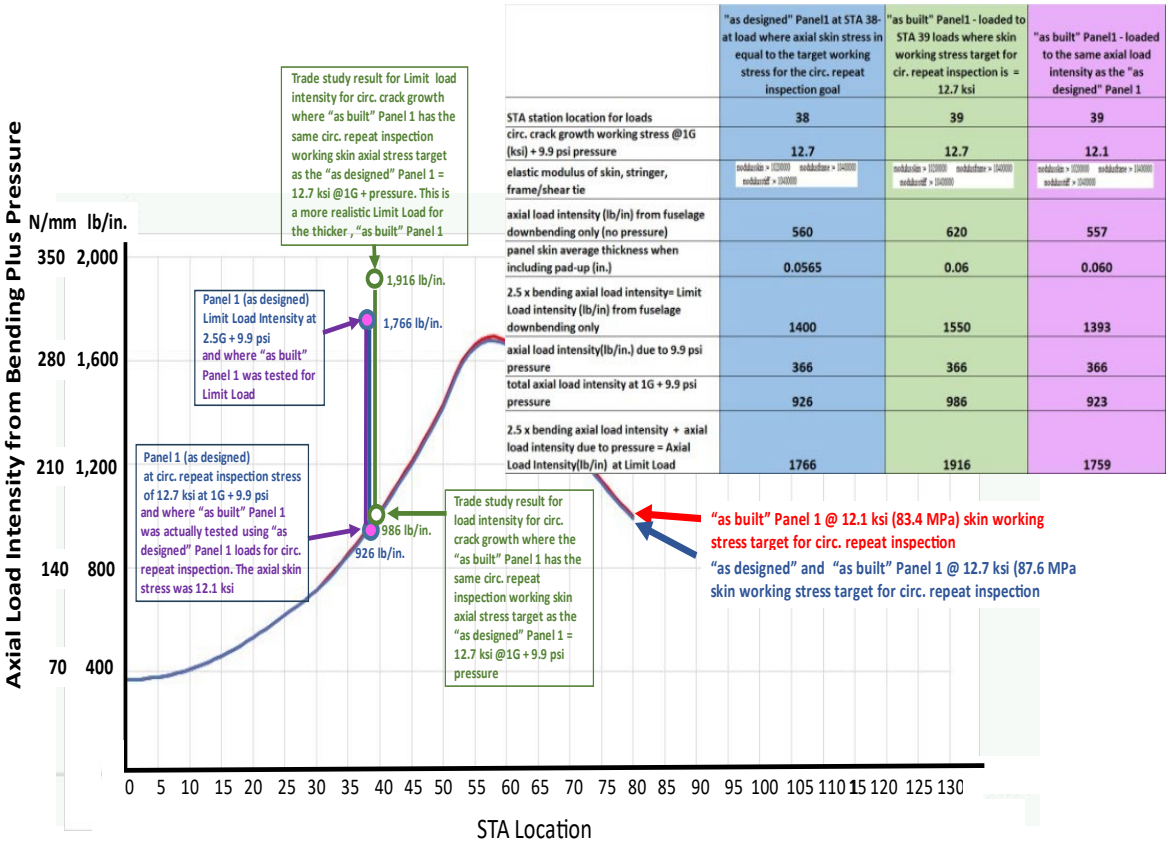

	"as designed" Panel1 at STA 38- at load where axial skin stress in equal to the target working stress for the circ. repeat inspection goal	"as built" Panel1 - loaded to STA 39 loads where skin working stress target for cir. repeat inspection is = 12.7 ksi	"as built" Panel1 - loaded to the same axial load intensity as the "as designed" Panel 1
STA station location for loads	38	39	39
circ. crack growth working stress @1G (ksi) + 9.9 psi pressure	12.7	12.7	12.1
elastic modulus of skin, stringer, frame/shear tie			
axial load intensity (lb/in) from fuselage downbending only (no pressure)	560	620	557
panel skin average thickness when including pad-up (in.)	0.0565	0.06	0.060
2.5 x bending axial load intensity= Limit Load intensity (lb/in) from fuselage downbending only	1400	1550	1393
axial load intensity(lb/in.) due to 9.9 psi pressure	366	366	366
total axial load intensity at 1G + 9.9 psi pressure	926	986	923
2.5 x bending axial load intensity + axial load intensity due to pressure = Axial Load Intensity(lb/in) at Limit Load	1766	1916	1759

Figure 145. Location in fuselage of as-designed Panel 1 versus as-built Panel 1

As mentioned above, the team decided that Panel 2 would be tested using loads designed to maintain the same SIFs versus crack length as the as-built, FASTER-tested Panel 1 (see Figure 146 for the circumferential crack growth FASTER loads). These loads for the as-built Panel 2

were determined by iteratively scaling the FASTER Panel 1 axial test loads and applying these to the as-built Panel 2 FE model until a good fit for the as-built, as-tested Panel 1 SIF solutions versus crack length was obtained. The hoop load intensity was kept the same during iterations, since the pressure was the same for every iteration.

For the Panel 2 FASTER longitudinal crack testing, the pressure applied to the Panel 2 FE model was scaled until a good fit to the Panel 1 longitudinal crack SIFs was obtained at 8.24 psi (0.0568 MPa). The longitudinal crack limit load was 1.15 times the operating differential pressure goal of 9.9 psi (0.068 MPa) (as opposed to the pressure of 8.24 psi used to match SIFs for longitudinal crack growth testing in Panel 1).

The total axial load intensity applied to Panel 2 at 1G plus pressure is comprised of the following elements:

- Axial loads representing fuselage bending-induced axial loads at the top center point of Panel 2 in the crown
- The axial component of the pressure loads
- The additional axial loads applied to the panel needed to stretch the heavy edge buildup doublers (acting as a frame around the edges of the skin)

To uncouple the Panel 2 added loads due to this edge doubler effect (see total loads in Figure 146) from the Panel 2 bending and pressure loads, a Qsymm2 analysis (quarter symmetry cylindrical FE model for the as-built Panel 2) was conducted at a crack length of 11.3 in. (287 mm) crack to match the stress intensity of the as-built Panel 1 FE model with the same 11.3 in.(287 mm) crack for the 1.04G + 9.9 psi (0.068 MPa) condition. Qsymm2 results for the total axial load intensity in Qsymm2 only contain bending and pressure components; there are no doublers in Qsymm2 for load introduction. For bending (as described in Section 2), a uniform axial load intensity is applied to the Qsymm2 cylinder, simulating the axial bending load intensity at the top midpoint crown location of Panel 2 (note that this Qsymm2 model is not simulating a cylinder in bending). These axial and hoop loads are intending to produce the same stresses in the hoop and axial directions in each interior bay Qsymm2. The axial component of the pressure load intensity per inch arc length is known from static equilibrium to be pressure × radius/2, or 9.9 psi x 74 in. x 0.5 = 366.3 lb/in. (64.1 N/mm).

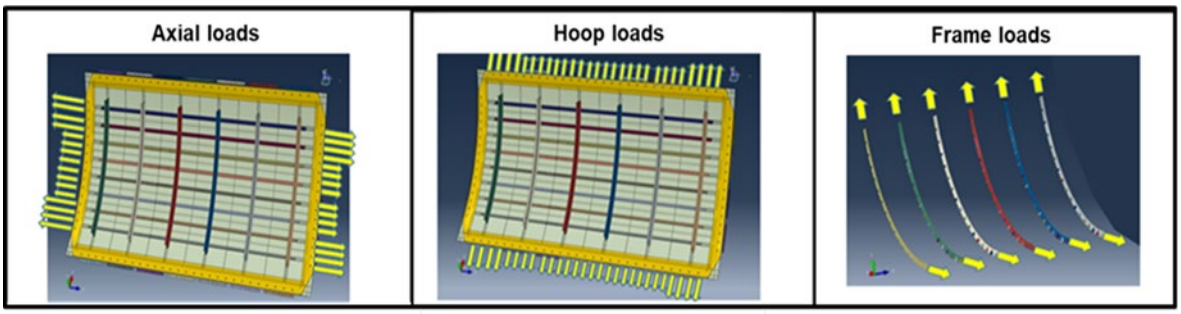

Skin Axial Actuator Load Arm Number	Applied Load (lbf)
1-4	17,738
5-8	11,126
9-12	11,126
13-16	17,738

Skin Hoop Actuator Load Arm Number	Applied Load (lbf)
1-4	10,458
5-8	9,729
9-12	9,500
13-16	9,408
17-20	9,500
21-24	9,729
25-28	10,458

Frame Number	Applied Load (lbf)
1	2,036
2	2,673
3	2,686
4	2,686
5	2,673
6	2,036

Figure 146. FASTER actuator loads for the Panel 2 Phase 1 fatigue test

Since the SIFs are equal between the as-built FE Qsymm2 model and the as-built Panel 2 FE model, the axial load intensities and hoop load intensity components due to bending and pressure are considered to be the same between Qsymm2 and the Panel 2 FE model. In other words, if there were no doubler buildup at the Panel 2 FE model edges and the appropriate BCs were used for the Panel 2 FE model to simulate the conditions in a circular fuselage, the load intensities at the Panel 2 edges would be the same as those in the Qsymm 2 FE model. The loads due to the doublers in the Panel 2 FE model can be determined by subtracting the load intensity due to the axial component of pressure and the axial load intensity due to bending from the total axial load intensity. Details of these calculations are described below.

a. The total axial load (including bending plus pressure) at 1.04G + 9.9 psi pressure was 98,074 lbs. (436.3 kN) for the 116.2 in. (2.95 m) arc length in the Qsymm2 FE model.
b. The total axial load intensity from Qsymm2 at 1.04G + pressure is the total axial load, 98,074 lb, divided by the Qsymm2 FE model circumferential edge length of 116.2 in. (2.95 m) which equals 98,074 lbs. (436.3 kN)/116.2 in. (2.95 m) = 843.3 lb/in. (147.7 N/mm).
c. The pressure axial load intensity from Qsymm2 (pressure × radius x 0.5) equals 366.3 lb/in. (64.2 N/mm).
d. The axial load intensity due to the uniform loads simulating bending load intensity at the top center of Panel 2 is the total load intensity at 1.04G + pressure from step b minus the

axial pressure component and was calculated as 843.3 lb/in. (147.7 N/mm) – 366.3 lb/in. (64.2 N/mm) = 477.0 lb/in. (83.5 N/mm) at 1.04G.

e. The axial bending load intensity at 1G can be calculated by dividing the result at 1.04G by a factor of 1.04 and is 477.0 lb/in./1.04 = 459.0 lb/in. (80.4 N/mm).
f. The as-tested location of Panel 2 (for equal stress intensity to the as tested Panel 1) is shown in Figure 147 (lower orange filled circle) to be near station 34 with a total axial stress intensity of 459.0 lb/in. (80.4 N/mm) from bending plus an axial stress intensity of 366 lb/in from pressure, which equals 825 lb/in. (144.5 N/mm) at 1G plus 9.9 psi (0.062 MPa) pressure.

In the sizing study described above, the as-built Panel 2 was sized to exhibit equal SIFs to the as-built Panel 1. In this study, the red filled circle in Figure 147 represents the case where the skin working stress was reduced to develop the same SIFs as the as-built Panel 1. The orange open circle in Figure 147 (847 lb/in. [148.3 N/mm]) shows a similar result for a solution where the skin circumferential crack growth target stress in the as-built Panel 2 was fixed to be 12.1 ksi (83.4 MPa) which was the actual Flugge characteristic skin stress applied to the thicker skin as built Panel 1 by the FASTER fixture. In this case, an “equal skin stress” criterion (Panel 2 to Panel 1) produced results similar to an equal SIF criterion.

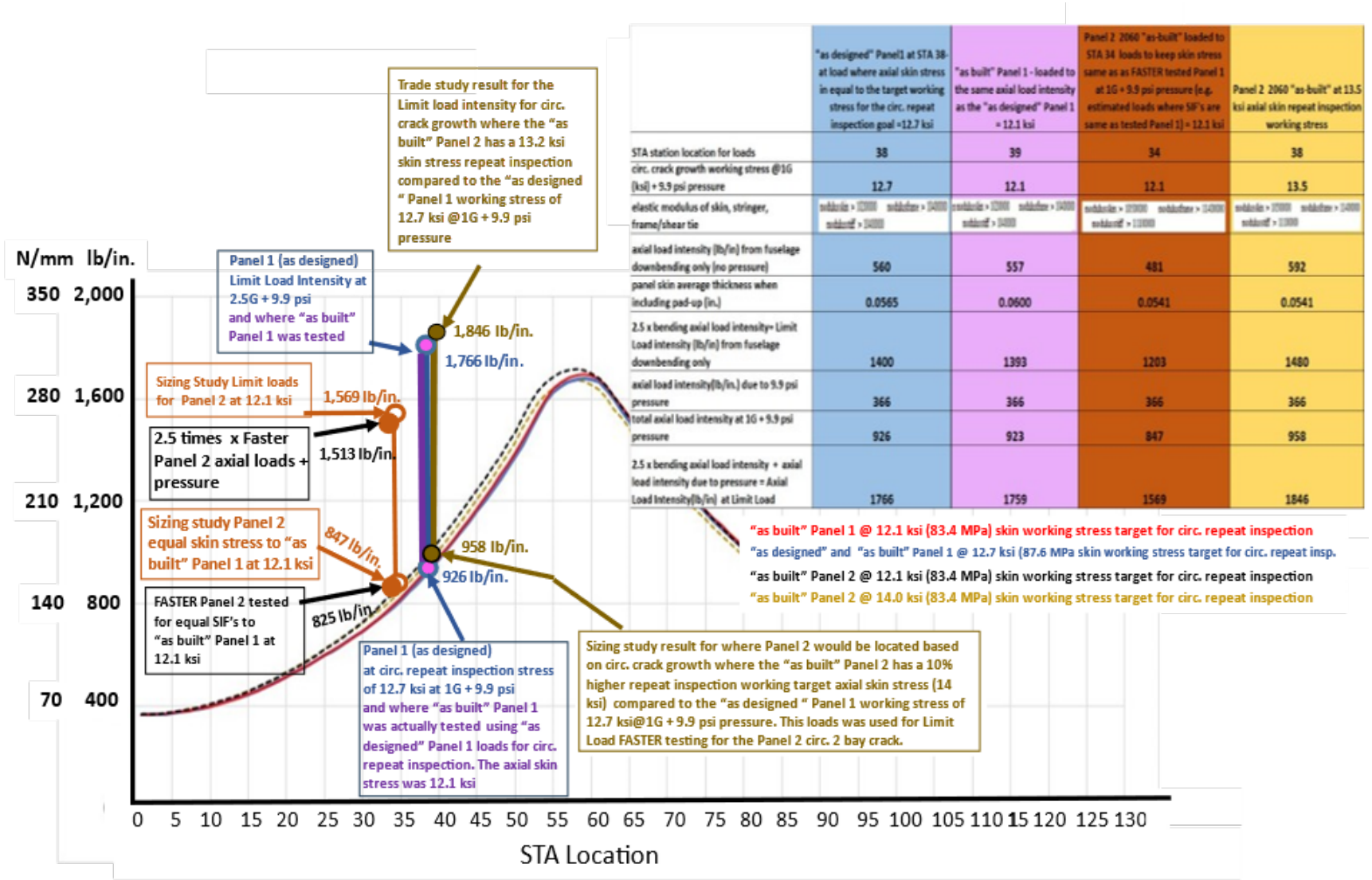

Figure 147. Location of Panel 2 for various sizing studies

A final sizing study was done to locate the as-built Panel 2 in the crown using a higher axial skin stress working target anticipating the 2060-based Panel 2 skin to perform better in FCG than 2524-T3. The bottom brown filled circle in Figure 147 represents the location of Panel 2 assuming a higher working stress target of 13.5 ksi (93.1MPa) for the circumferential crack repeat inspection. The top brown filled circle is total axial limit load intensity for this skin axial working stress target (2.5 times the 1G intensity plus the pressure load intensity). These results show the higher circumferential crack growth working target stress in the as built Panel 2 (0.05 in. [1.27 mm] in the pocketed region plus 0.063 in. [1.58 mm] in the pad-up region for an estimated average thickness of 0.54 in. [1.35 mm]). Note, that the pad-up regions add a smaller amount to the average 0.060 in. 1.52 mm) smeared thickness in Panel 1, because the 0.063 in. (1.58 mm) pad-up is only 0.004 in. (0.10 mm) above the 0.059 in. pocket thickness in the as-built Panel 1. This STA 38 location (brown filled circle) for the as-built Panel 2 in the crown may be interpreted as where the Panel 2 would be located to take advantage of a potential higher performance for circumferential repeat inspections. Note that the trade study load intensities do not include the extra loads needed to stretch the Panel 2 edge doublers; these extra loads were in Figure 146 because the Panel 2 FE model loads were iteratively determined to generate the same SIFs as Panel 1.

The following summarizes the Panel 2 FASTER loading conditions for the circumferential crack. For the final Panel 2 loading conditions for circumferential crack growth, Panel 2 was located where the SIFs are the same for the as-built and FASTER tested Panel 1 (bottom orange filled circle in Figure 147), while the limit load was calculated at the crown location where a hypothetical as-built Panel 2 with a 13.5 ksi (93.1 MPa) skin axial working stress target for circumferential crack growth would be located in the fuselage (top brown filled circle in Figure 147).

The actuator loads for the Panel 2 limit loads for the STA 38 location (using the 13.5 ksi (93.1 MPa) skin axial working stress target) which include doubler loads were calculated as follows:

1. The as built Panel 2 FE model axial load from bending at 1.04 G is the bending axial load intensity at 1.04 G (477 lbs./in. (83.5 N/mm)) times the panel circumferential direction edge length and was calculated (from Qsymm2 — see step d above) as 477 lb/in. (83.5 N/mm) x 116.24 in. (2.95 m is the Panel 2 FE axial edge length)) = 55,446 lb (246.6 kN).
2. The Panel 2 FE axial load from pressure is 366.3 lb/in (80.38 N/mm) x 116.24 in. (2.95 m) = 42,579 lb (189.4 kN).

3. The total axial load at 1.04G plus pressure in Qsymm2 is 55,446 lb (246.6 kN) from bending plus 42,579 lb (189.4 kN) from pressure, totaling 98,074 lbs. (436.3 kN).
4. The proportion of axial load due to bending to the total axial load in the Panel 2 FE is 55,446 lb (246.6 kN)/98,025 lbs. (436.3 kN) = 0.556.
5. Recall that the axial load from bending is intended to represent the load intensity at the top midpoint of Panel 2 (fuselage top). This axial load due to bending is applied as a constant load intensity to the front and rear edges of Qsymm2. Therefore, the axial load due to bending only (not including the doubler loads) is treated as a constant load intensity along the front and back edge of Qsymm2 FE model in the same manner as the axial component of pressure is added as a constant load intensity to the edges of Qsymm2.
    - Recall that the goal of the loading is to ensure the interior bays in Qsymm2 and Panel 2 have the same SIF solutions (by analogy the same far field stresses). Qsymm2 does not differentiate between a "unit" axial load from bending and a "unit" axial load from pressure since they are both constant load intensities along the Qsymm2 edge. In the same manner the distribution of a unit pressure induced load intensity or bending load unit load intensity is the same when applying loads to Panel 1 with the goal to obtain 1) the same average load intensity and 2) a uniform axial strain even though the doubler corners are very stiff (same strained shape as Qsymm1). The main difference is that an additional axial load intensity is required to account for the massive doubler frame to be stretched to the same shape as the Qsymm2 FE model.
    - Following the discussion above, this additional doubler load distribution is the same shape along the front and rear Panel 2 edge as the pressure or bending load intensity on these edges and is proportional to the total bending and pressure load intensities. This distribution of axial load intensity along the front or back panel edges is referred as the *unit edge doubler load distribution*.
    - The unit edge doubler load distribution needed to maintain the correct strained shape on Panel 1 or 2 resembles a parabolic shape load distribution with higher loads at the corners (stiffer region due to doubler layup) and lower at the middle of the Panel 1 or 2 edge.
    - The additional units of the *unit edge doubler distribution* axial loading needed to stretch the doubler frame of Panel 2 is proportional to the amount of axial

bending load intensity plus the axial pressure load intensity. The proportion of doubler contribution due to axial bending load at 1G + pressure (see Figure 146) was calculated previously in step 4 to be 0.566. The proportion of the axial load due to pressure is therefore 1- 0.566 = 0.434. These are important numbers used to calculate the loads to achieve limit load where the pressure component of load at the 1G + pressure solution is kept constant but the bending loads are multiplied by a factor 2.5.

6. Recalling that the FASTER actuator loads for the Panel 2 circumferential crack growth were developed for equal SIFs to the as-built Panel 1 circumferential crack. These loads include the extra doubler loads. The total axial load applied to Panel 2 in Figure 146 is 57,728 lbs. (256.8 kN), the bending component (including doublers) in the FASTER Panel 2 loads shown in Figure 146 is 0.566 x 57,728 lb = 32,674 lb (145.3 kN) at 1.04G. Scaling this bending component load to 1G equals 32,674 lb /1.04 =31,417 lbs. (139.7 kN). Thus, the 1G load can be scaled by a factor of 2.5 for the bending contribution.

7. The axial pressure component (including doublers) in the FASTER Panel 2 loads shown in Figure 146 is calculated as (1-0.566) x 57,728 lb = 25,054 lb (111.4 kN). This pressure load is the same whether evaluating loads at 1G bending, 1.04 G bending, or the limit condition of 2.5G bending. These components of axial and pressure 1G loads from the FE analysis of Panel 2 and used for FASTER testing of the circumferential crack in Panel 2 were used as described below to calculate the axial limit loads for Panel 2.

The results for a separate sizing study for the as built Panel 2 for an axial skin working stress target of 13.5 ksi (93.07 MPa) were shown for 1G plus 9.9 psi (0.062 MPa) pressure in Figure 147 (bottom brown filled circle). This solution was obtained by first scaling the FASTER-tested Panel 2 circumferential crack growth loads (Figure 146) at 1.04G (steps 6 and 7 above) to determine the loads at 1G + 9.9 psi (0.062 MPa) pressure loads at the STA 38 location. Then these 1G + pressure loads at STA 38 can be scaled to 2.5G + pressure at limit loads as follows:

- The load intensity representing bending at the top center of the crown for Panel 2 at 1G + 9.9 psi (0.062 MPa) for the 13.5 ksi (93.07 MPa) circumferential crack working target stress at this location STA is 592 lb/in (103.7 N/mm) at STA 38 (see Table at upper right of Figure 147).

- The Qsymm 2 FE model axial skin load intensity representing bending at the top center of the crown for Panel 2 at 1G + 9.9 psi (0.062 MPa) at STA 34 (the location where the

Panel 2 SIFs are equal to the FASTER tested Panel 1 SIFs) was equal to 459 lb/in (80.4 N/mm) (see step e above).

- The ratio of the 13.5 ksi skin axial load intensity due to bending to the Qsymm2 axial load intensity (STA 34 location) due to bending is 592 lb/in. (103.7 N/mm) divided by 459 lb/in (80.4 N/mm), or 1.291.
- The next step is to calculate the total axial loads (including bending loads, doubler loads, and pressure loads) for the Panel 2 1G plus pressure condition assuming the 13.5 ksi (93.1 MPa) axial skin working stress target location STA 38. Recall that the FASTER Panel 2 circumferential crack growth bending load at 1G from step 6 was 31,417 lb (139.7 kN) which includes the doubler loads. Scaling this by the ratio of bending load at STA38 divided by the bending load at STA 34 of 1.291 in step iii the STA 38 Panel 2 bending load plus doubler load is calculated as 31,417 lb (139.7 kN) × 1.291 =40,548 lbs. (180.4 kN). The pressure axial loads, including the axial doubler loads caused by pressure for the STA 34 FASTER Panel 2 crack growth test, were calculated in step 7 as 25,054 lb (111.4 kN). These pressure loads remain the same at STA 38 because the pressure × radius/2 load intensity remain constant at the fuselage STA location where the radius is constant. Therefore, the total axial 1G + pressure loads including doublers at the STA 40 location is 40,528 lbs. (180.4 kN) from bending + 25,054 lbs. from pressure (111.4 kN) = 65,582 lbs. (291.7 kN).
- The limit loads for the 13.5 ksi (93.1 MPa) axial skin working stress target at STA 38 is 2.5 x 1G bending loads + pressure loads = 40,548 lbs. (180.4 kN) x 2.5 + 25,054 lbs. (111.4 kN) = 126,424 lbs. (562.4 kN). These Panel 2 FASTER actuator loads for the circumferential crack limit load are shown in Figure 148.

For the Panel 2 longitudinal crack growth at STA 34 , the crack growth test was conducted using a pressure of 8.24 psi (0.057 MPa). This pressure was determined where the longitudinal crack SIFs from the as-built Panel 2 FE model were equal to the longitudinal crack SIFs for the as-built Panel 1 FE model (recall that only the axial load component from the pressure plus the extra doublers loads and the hoop loads due to pressure plus extra hoop doubler loads were used for the longitudinal crack growth scenario). For the Panel 2 longitudinal crack residual strength, the limit condition is defined as 1.15 x 9.9 psi pressure.

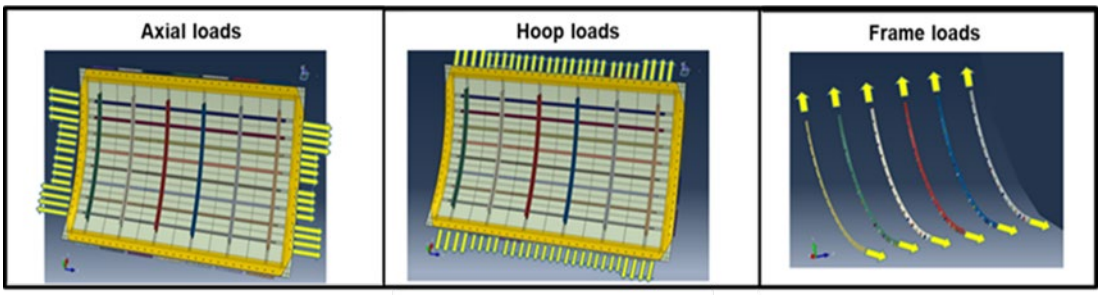

Skin Axial Actuator Load Arm Number	96% of target limit load (lbf)
1-4	37,019
5-8	23,220
9-12	23,220
13-16	37,019

Skin Hoop Actuator Load Arm Number	Applied Load (lbf)
1-4	10,458
5-8	9,729
9-12	9,500
13-16	9,408
17-20	9,500
21-24	9,729
25-28	10,458

Frame Number	Applied Load (lbf)
1	2,036
2	2,673
3	2,686
4	2,686
5	2,673
6	2,036

Figure 148. FASTER fixture actuator loads for Phase 1 limit load

8 Conclusions

A collaborative effort, initially with the FAA and Arconic and eventually including Embraer and NIAR, was established to design, build, and test full scale panels representing EMST to conduct research into areas of airframe safety and structural integrity that are of importance and mutual interest to the industry and the FAA. These technologies represent key improvements in materials, structural design, and manufacturing approaches.

This report describes the methodology used to locate and size test Panel 1 in a generic single-aisle fuselage that is applicable to Panels 2 and 3. The approach for this panel testing program was to conduct “apples-to-apples” fuselage panel testing under the same conditions at a key location in the crown of a generic, OEM-independent single-aisle commercial aircraft defined in this study. The generic aircraft defined for this study’s goals includes assumed simplified performance, life, and inspection goals. Also, simplified loading and design methodologies were used to meet static strength, buckling, fatigue, and damage tolerance goals.

Panel 1 (2524-T3 skin with 7150-T77511 stringers and 7075-T62 shear ties and frames) was sized, and the FASTER test fixture loading was developed for the Panel 1 location at STA 38, where damage tolerance was the key sizing criterion in both the longitudinal and circumferential direction. Phase 1 of Panel 1 included a test for circumferential crack growth from under a broken stringer at mid-bay. This crack was repaired and then tested. Panel 1 was tested for a mid-bay longitudinal crack growing along the pad-up mill line where crack turning was

expected. This crack was repaired, and then Panel 1 was tested for longitudinal crack growing from a broken frame/shear tie mid-bay. Finally, this crack was to be tested for residual strength.

The “apples-to-apples” testing was initially defined to test all panels to the same cross-sectional areas and to the same loads. However, it was found that Panel 1 was built to a skin pocket thickness of 0.059 in. (1.5 mm) instead of 0.055 in. (1.4 mm). In this case, because the panel skins were thin, even a small manufacturing tolerance of 0.005 in. (0.127 mm) resulted in a significant thickness difference in the chem-milled skin pockets in Panel 1 and 2. This pocket thickness change would have significantly changed the SIFs if the different skin pocket thicknesses in Panels 1, 2, and 3 were tested to the same loads. Thus, manufacturing differences in skin pocket thickness were accounted for by adjusting loads for each panel, and crack growth testing was conducted for Panels 1, 2, and 3 to the same SIFs versus crack size relationship based on FE analysis.

This report describes the sizing and load development of the as-designed Panel 1. A quarter symmetry (Qsymm1) FE model was used to develop target loads and target SIF solutions for Panel 1. A global fuselage model to local test Panel 1 FE analysis approach was used to determine the loading for the as-designed Panel 1 to achieve these target stress Qsymm1 intensity factors. The as-designed Panel 1 circumferential crack growth constant amplitude loading was developed using K-control M(T) testing by equating the spectrum K-control results to those of an equivalent constant amplitude K-control load.

The as-built Panel 1 skin pocket thickness difference was not discovered until after Panel 1 testing. Thus, the as-designed Panel 1 loads were used to test the as-built Panel 1. Subsequent analyses were conducted to understand the effect of this geometry difference. The loading imbalance presented some difficulties in modeling the as-built Panel 1. The set of as-designed Panel 1 loads introduced an extra bending moment because the balanced as-designed Panel 1 axial loads were no longer balanced about the new neutral axis of the cross-section of the as-built Panel 1. Adjustments to the as-built Panel 1 model BCs were made based on strain gage measurements of Panel 1 and LVDT measurements of Panel 2 during testing. A mesh convergence study was conducted. Final stress intensity solutions were provided for both the longitudinal and circumferential crack growth directions for the as-built Panel 1. These results will be used to interpret the results of the FASTER Panel 1 test results.

Finally, corrections for Panel 2 crack growth and limit loads were developed to account for the skin pocket difference in the as-built Panel 2 compared to the as-built Panel 1.

9 References

14 CFR § 25.571 Damage-tolerance and fatigue evaluation of structure. (2023, January 18). Retrieved from eCFR.gov: https://www.ecfr.gov/current/title-14/section-25.571

ASTM, & s.l. (2015). ASTM. *ASTM, E647*.

Astori, P., Hupperts, J., & van Tooren, M. (2003). *Loads development for two aircraft fuselages using FAR criteria and parametrised FE-models.* Delft Universtiy of Technology.

Bertoni, M., Fernandez, F., & Miyazaki, M. (2014). Fuselage technology demonstrator. Orlando: AeroMat. Retrieved June 16-19, 2014

Beumler, T. (2014). Development of thin-walled FML-structures. Orlando: AeroMat.

Brazill, R. L. (2016). Arconic software (internal). s.l. Retrieved from https://doi.org/10.1111/blar.12417

Bucci, R., Warren, C., & Starke, E. (2000). Need for new materials in aging aircraft structures. *Volume 37*. doi:10.2514/2.2571

Chaves, C. (2017). A review of aeronautical fatigue investigations in Brazil. *35th ICAF Conference.* Nagoya.

deJonge, J., & et al. (1973). *A standardized load sequence for flight simulation test on transport aircraft wing structures.* Netherlands: National Aerospace Laboratory (NLR). doi:NL TR 73019 U

Donald, K. (1990). Automated variable-amplitude fatigure crack growth technology. (A. International, Ed.) Kansas City, Missouri. Retrieved from https://doi.org/10.1520/STP25037S

Federal Avaiation Administration. (1993, February 10). *Policy Statement PS-ANM100-1993-00047.* Retrieved from Dynamic Regulatory System: https://drs.faa.gov/browse/excelExternalWindow/F031FE97DEB457BD86256C300072A592.0001

Federal Aviation Administration. (2011, January 13). *Advisory Circular 25.571-1D.* Retrieved from Damage Tolerance and Fatigue Evaluation of Structure: https://www.faa.gov/documentLibrary/media/Advisory_Circular/AC_25_571-1D_.pdf

Flugge, W. (1952). *Stress problems in pressurized cabins.* (NACA, Ed.) doi:s.l. NACA TN2612

Heinimann, M., & et al. (2007). Validations of advanced metallic hybrid concepts with improved damage tolerance capabilities for next generation lower wing and fuselage applications. *s.n.* Naple, Italy.

Hibbit, Karlson, & Sorenson. (2018). ABAQUS.

Kok, L., Poston, K., & Moore, G. (2011). Bombardier aerospace FSW demonstrator. *ICAF*, *26th.* Montreal.

Kulak. (2015). Flugge stringer/skin local bending stiffness factor.

Kulak, M. (2018). *Fuselage sizing module for Mathcad*(n.l.).

Kulak, M., Sklyut, H., s.l., & n.d. (n.d.). Private Arconic Correspondence.

Kulak, n.d., & s.l. (n.d.). Longitudinal crack growth working stress used in some trade studies. *Private Arconic documentation*.

Lowak, H., & et al. (1979). *MINITWIST - A shoratened version of TWIST.* Laboratorium fur Betriebstigkeit (LBF).

MMPDS. (2015). *Metallic Materials Properties Development and Standardization (MMPDS) Handbook.* Battelle Memorial Institute.

Mohaghegh, M. (1985). Tension Analysis of Stiffened Aircraft Structures. *AIAA-85-0795-CP*. Retrieved from https://doi.org/10.2514/6.1985-795

Mosinyi, B., Bakuckas, J., & Steadman, D. (2007). Destructive evalatuion and extended fatigue testing of retired transport aircraaft. *Extended Fatigue Testing, s.l.*, *4.* doi:DOT/FAA/AR-07/22,V4

Newman, J. C. (1992). Effects of constrain on crack growth under aiarcraft spectrum loading,NASA Technical Memorandum. *Aluminum-Lithium Alloys, Processing, Properties and Applications*. Elseview, s.l.

Newman, J. C., & James, M. (2001). A review of the CTOA/CTOD fracture criterion. *Engineering Fracture Mechanics*.

Prasad, E. N., Gokhale, A. A., & Wanhill, R. (2014). Aluminum-Lithium Alloys : Processing, Properties, and Applications. *Elsevier Science*.

PTC, s.l., & s.n. (2019). Mathcad. *15*.

Schmidt, H. (2005). Damage tolerance technology for current and future aircraft structure. *Proceedinds of 23rd ICAF Symposium.* Hamburg.

Silva, D., & al., e. (2017). Manufacturing of a fiber metal laminate lower wing cover demonstrator. *Proceedsing of AeroMat.* Charleston.

Steadman, D. (2007). *Destructive evaluation and extended fatigure testing of retired transsport aircraft.* Data Analysis Report, s.l., Data Analysis Report. doi:DOT/FAA/AR-07/22, V5

Stonaker, K., Bakuckas, W. I., & Freisthler, M. (2015). Materail characterization of aluminum lithium alloys used in aerospace applications. *Proceedings of the 28th ICAF Symposium*, *1.* Helsinki.

Sutradhar, A., & Paulino, G. (2004). *Symmetric Galerkin boundary element computation of T-stress.* Engineering Analysis with Boundary Elements.

Swift, T. (1974). The application of fracture mechanics in the development of the DC-10 fuselage. (s.l., Ed.) *Fracture MEchanics of Aircraft Structures*. doi:AGARD-AG-176,1974

Tian, Y., & Bakuckas, J. (2019). *Full-scale aircraft structural test evaluation and research (FASTER) fixture.* Capabilities Description and User Manual, s.l. doi:DOt/FAA/TC-TN19/6

Tian, Y., & et al. (2023). Test and analysis of fuselage structure to assess emerging metallic structures technologies. *31st ICAF Symposium.* Delft.

Tian, Y., Stanley, D., & Bakuckas, J. (2021). Assessment of emerging metallic structures technologies through test and analysis of fuselage structures: Panel 1. doi:DOT/FAA/TC-21/25

Wang, G. (2016). R-curve results for 2524-T5 sheet.

Wells, A. (1961). Unstable crack propagation in Metals: Cleavage and fast fracture. *Crack propagation symposium.*

A Panel 1 design drawings

Figures

Figure A-1. Panel 1 drawing #1 ..... A-2
Figure A-2. Panel 1 drawing #2 ..... A-3
Figure A-3.Panel 1 drawing #3 ..... A-4
Figure A-4. Panel 1 drawing #4 ..... A-5
Figure A-5. Panel 1 drawing #5 ..... A-6
Figure A-6. Panel 1 drawing #6. ..... A-7
Figure A-7. Panel 1 drawing #7 ..... A-8
Figure A-8. Panel 1 drawing #8 ..... A-9
Figure A-9. Panel 1 drawing #9 ..... A-10
Figure A-10. Panel 1 drawing #10 ..... A-11
Figure A-11. Panel 1 drawing #11 ..... A-12
Figure A-12. Panel 1 drawing #12 ..... A-13
Figure A- 13. Panel 1 drawing #13 ..... A-14
Figure A-14. Panel 1 drawing #14 ..... A-15
Figure A-15. Panel 1 drawing #15 ..... A-16
Figure A-16. Panel 1 drawing #16 ..... A-17
Figure A-17. Panel 1 drawing #17 ..... A-18
Figure A-18. Panel 1 drawing #18 (note this detail was changed during the circumferential crack test to repair cracking at the ends of the frame) A-19

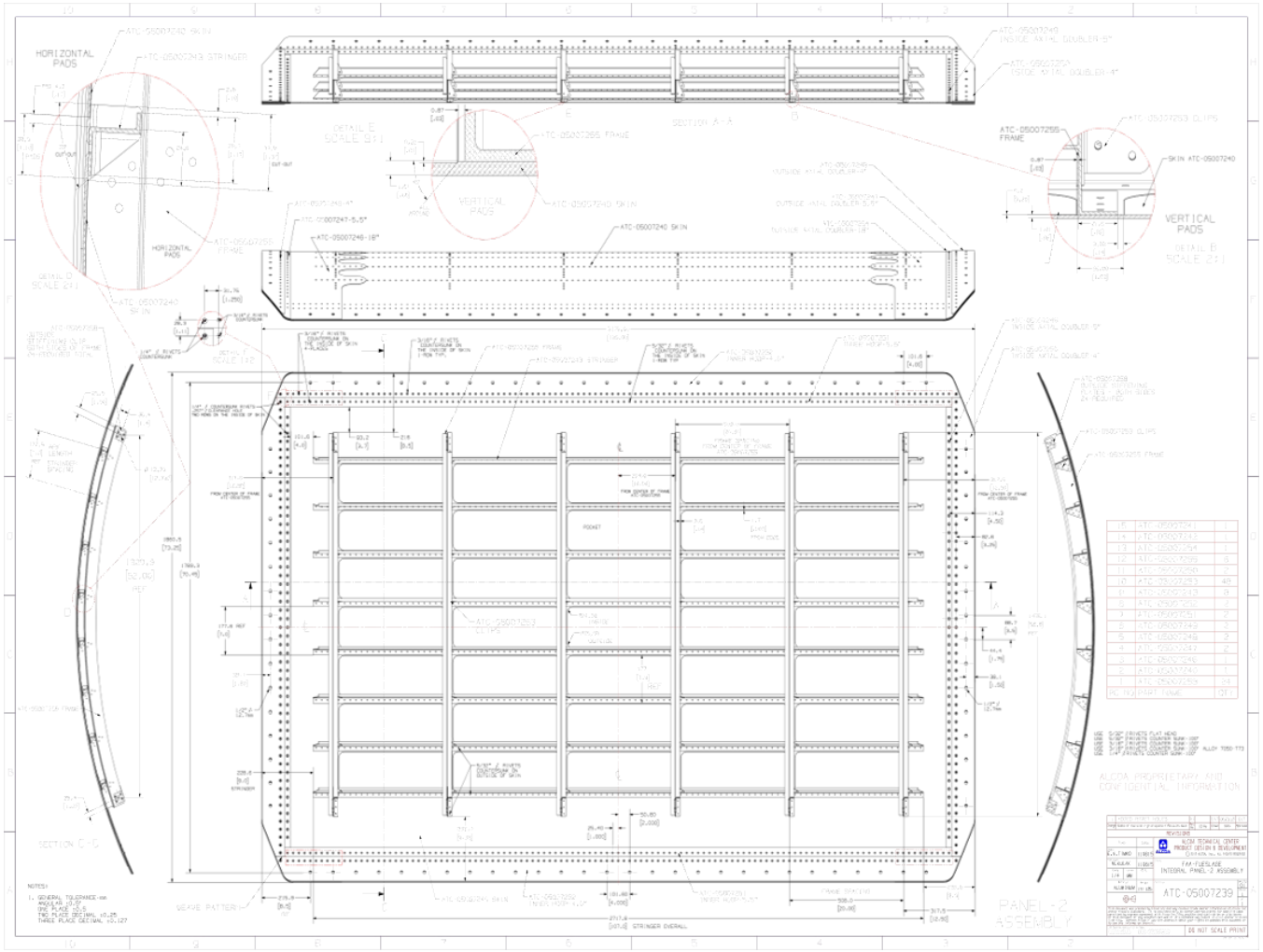

Figure A-1. Panel 1 drawing #1

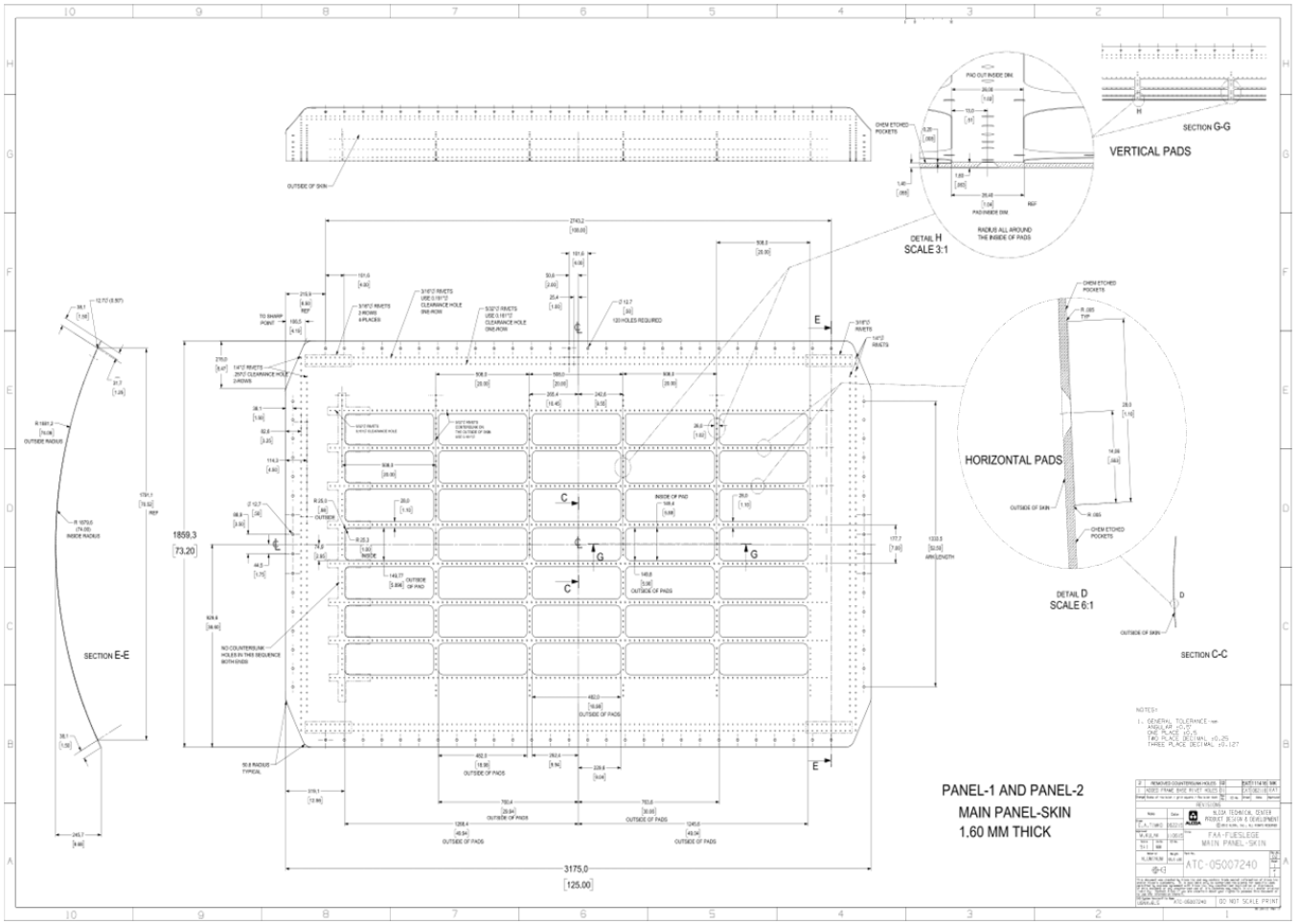

Figure A-2. Panel 1 drawing #2

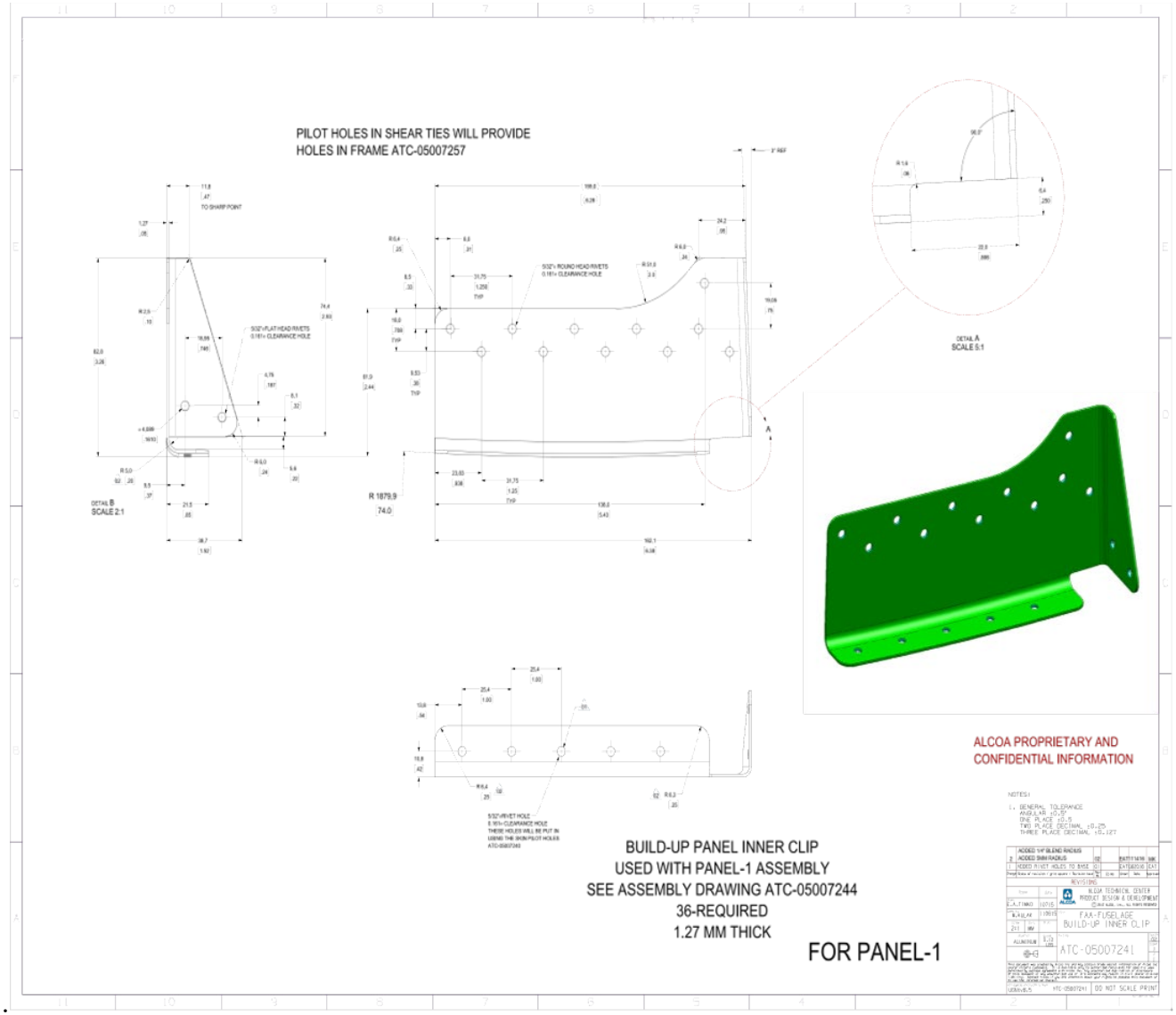

Figure A-3.Panel 1 drawing #3

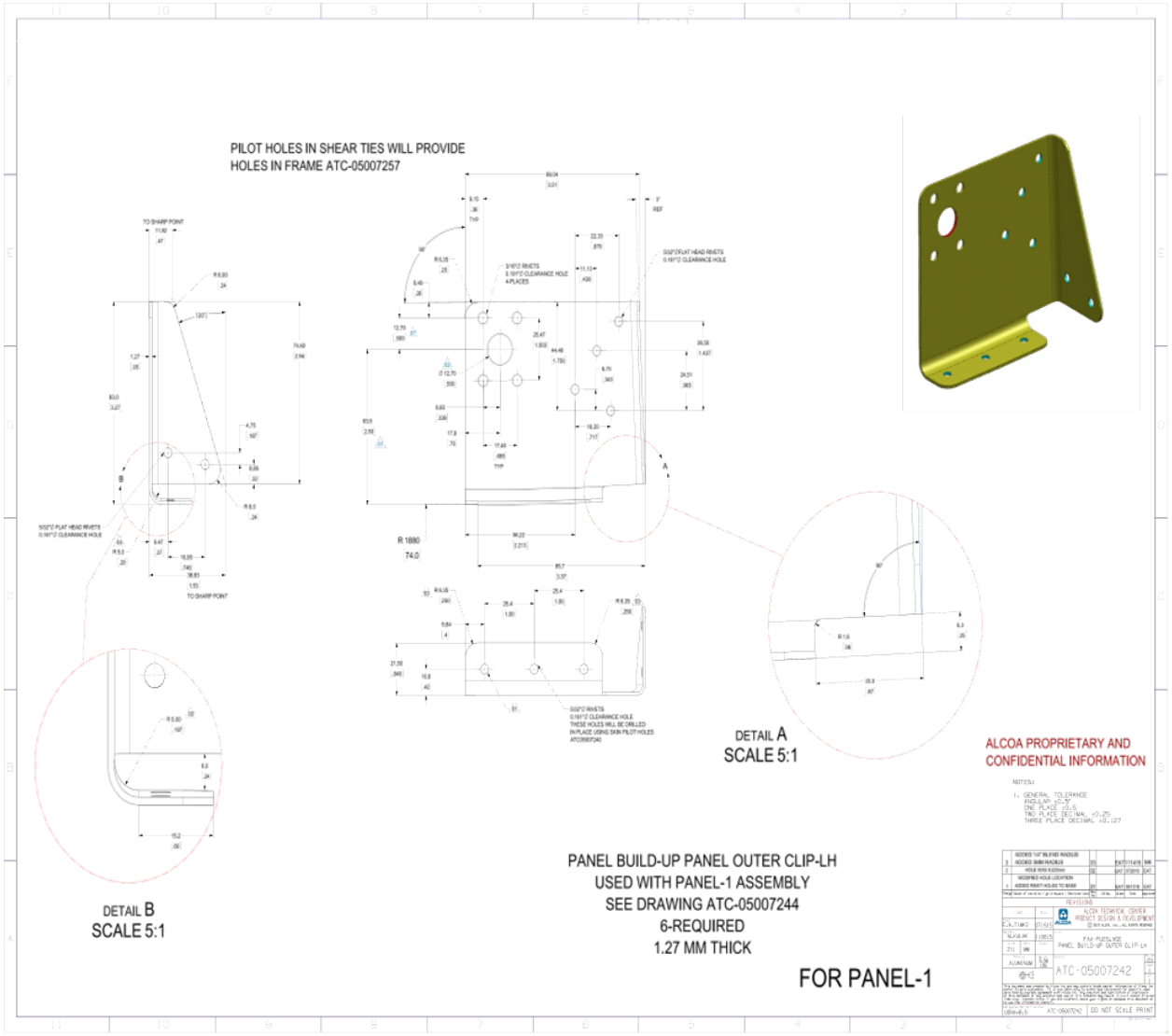

Figure A-4. Panel 1 drawing #4

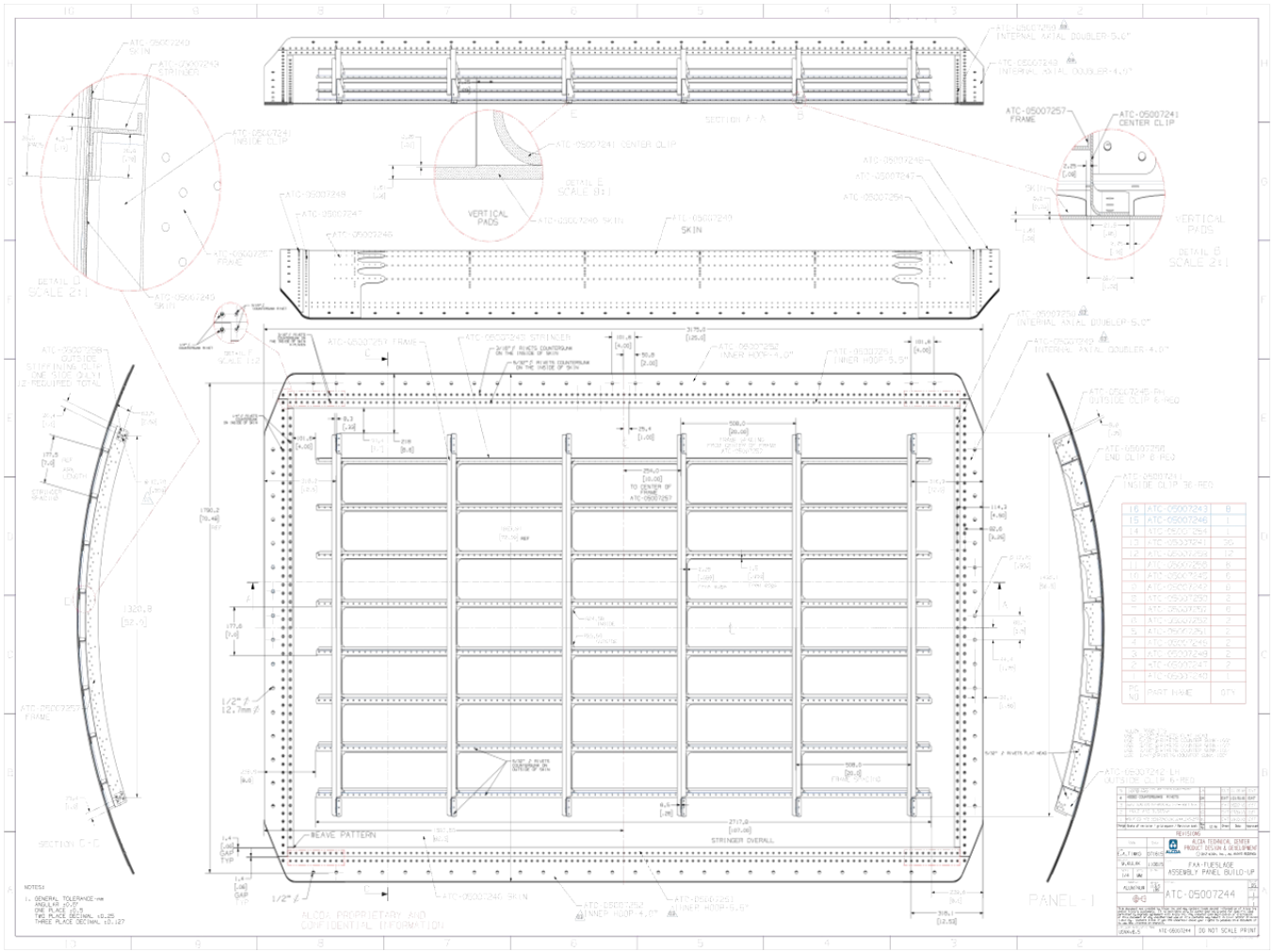

Figure A-5. Panel 1 drawing #5

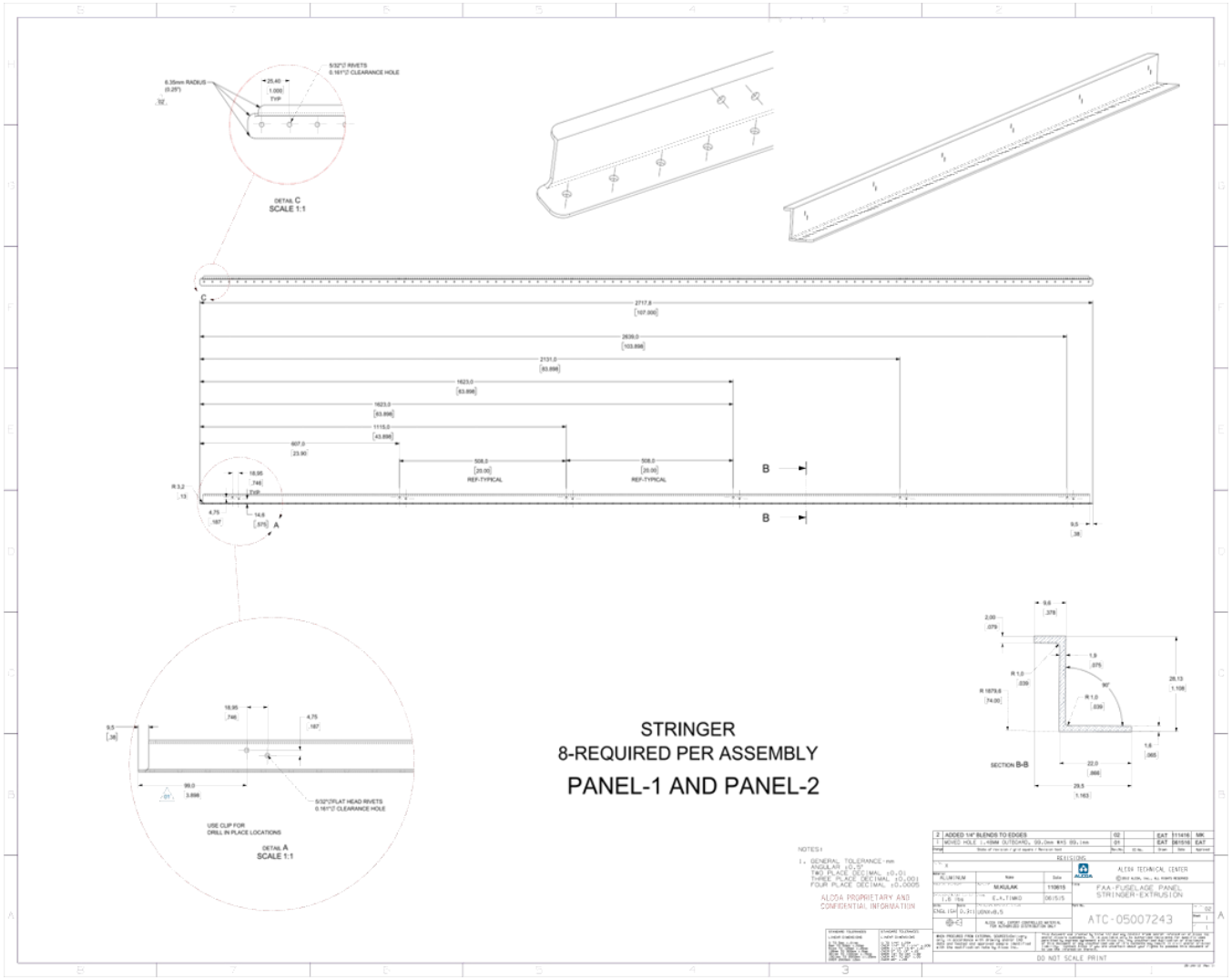

Figure A-6. Panel 1 drawing #6.

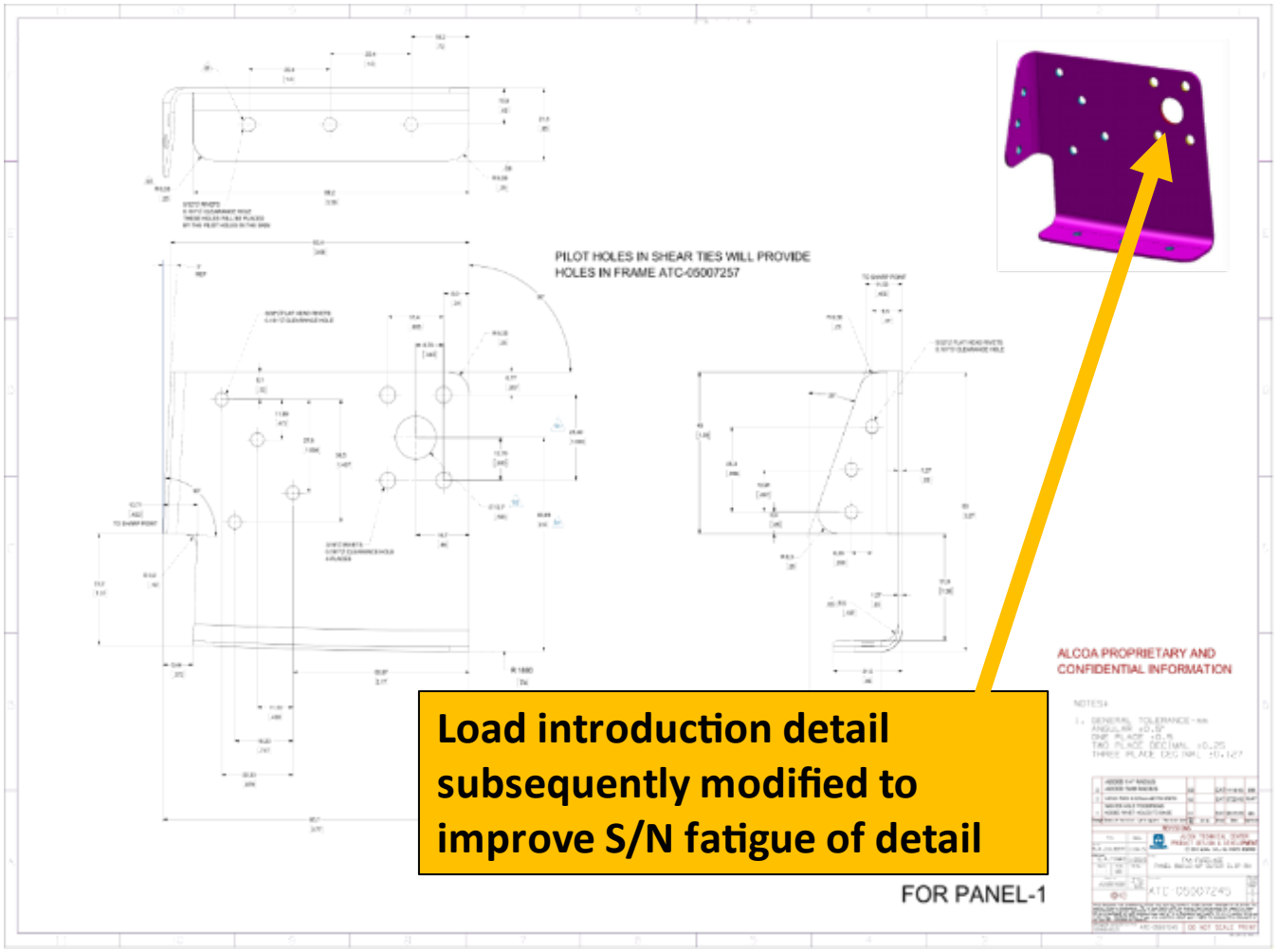

Figure A-7. Panel 1 drawing #7

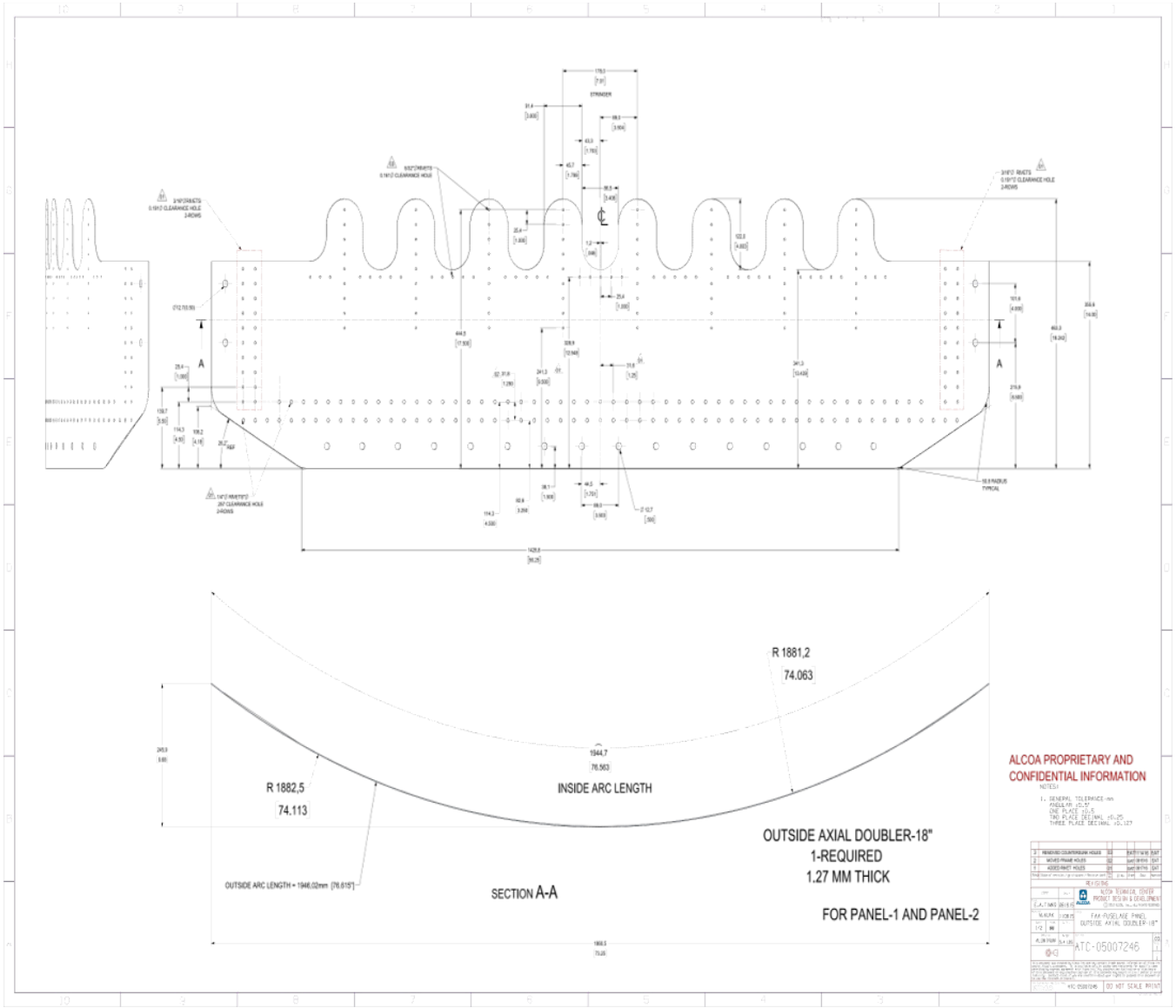

Figure A-8. Panel 1 drawing #8

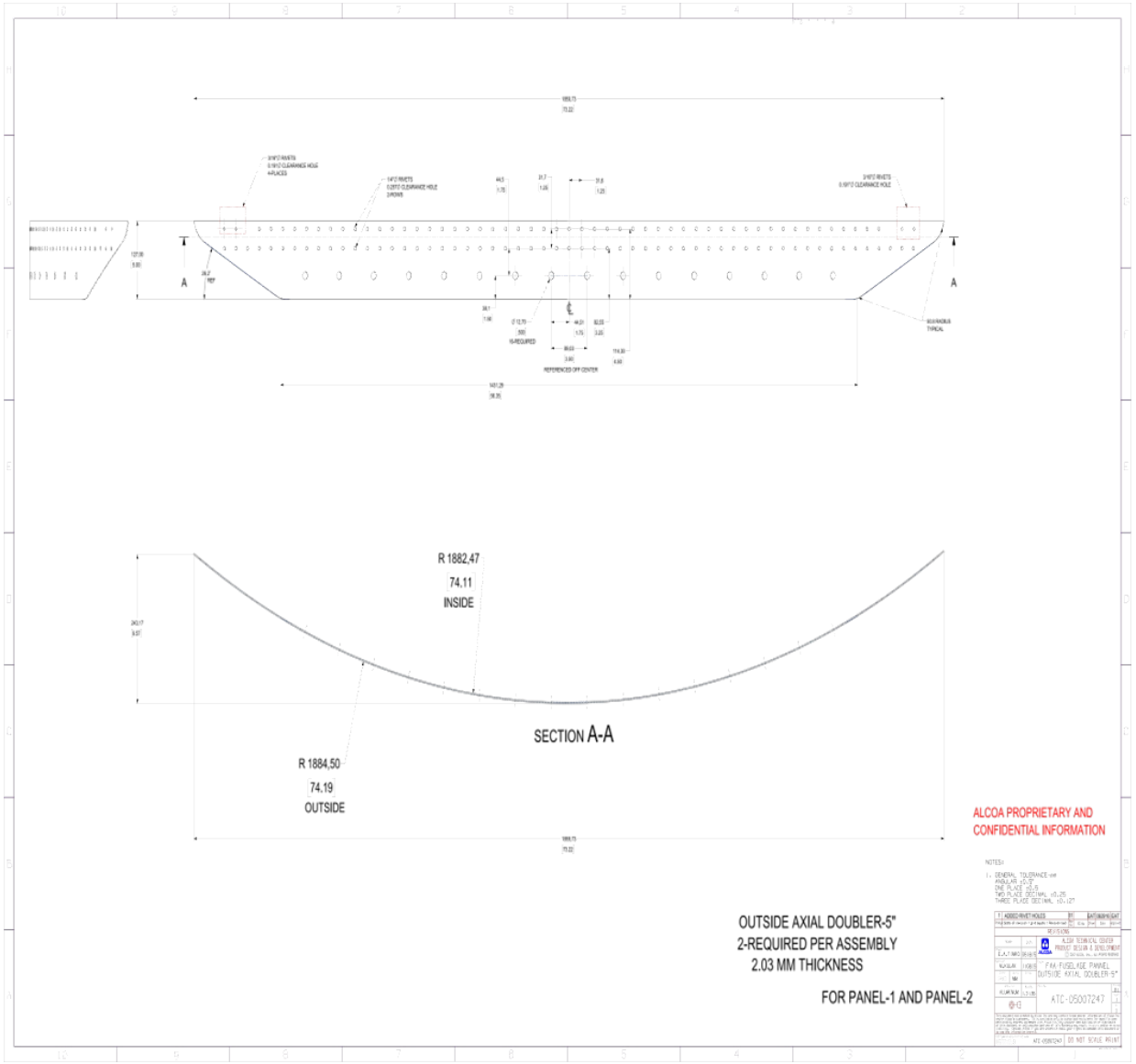

Figure A-9. Panel 1 drawing #9

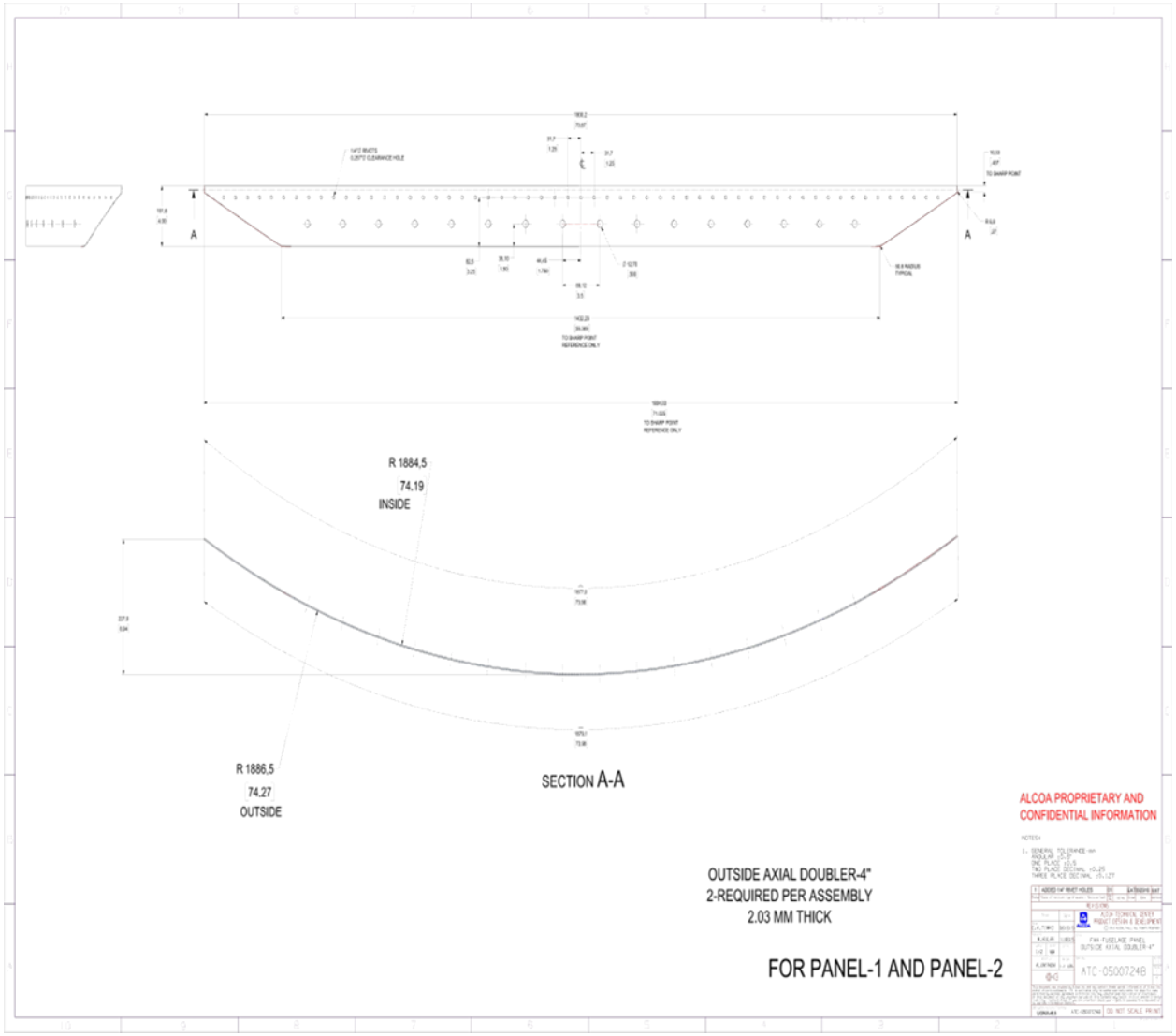

Figure A-10. Panel 1 drawing #10

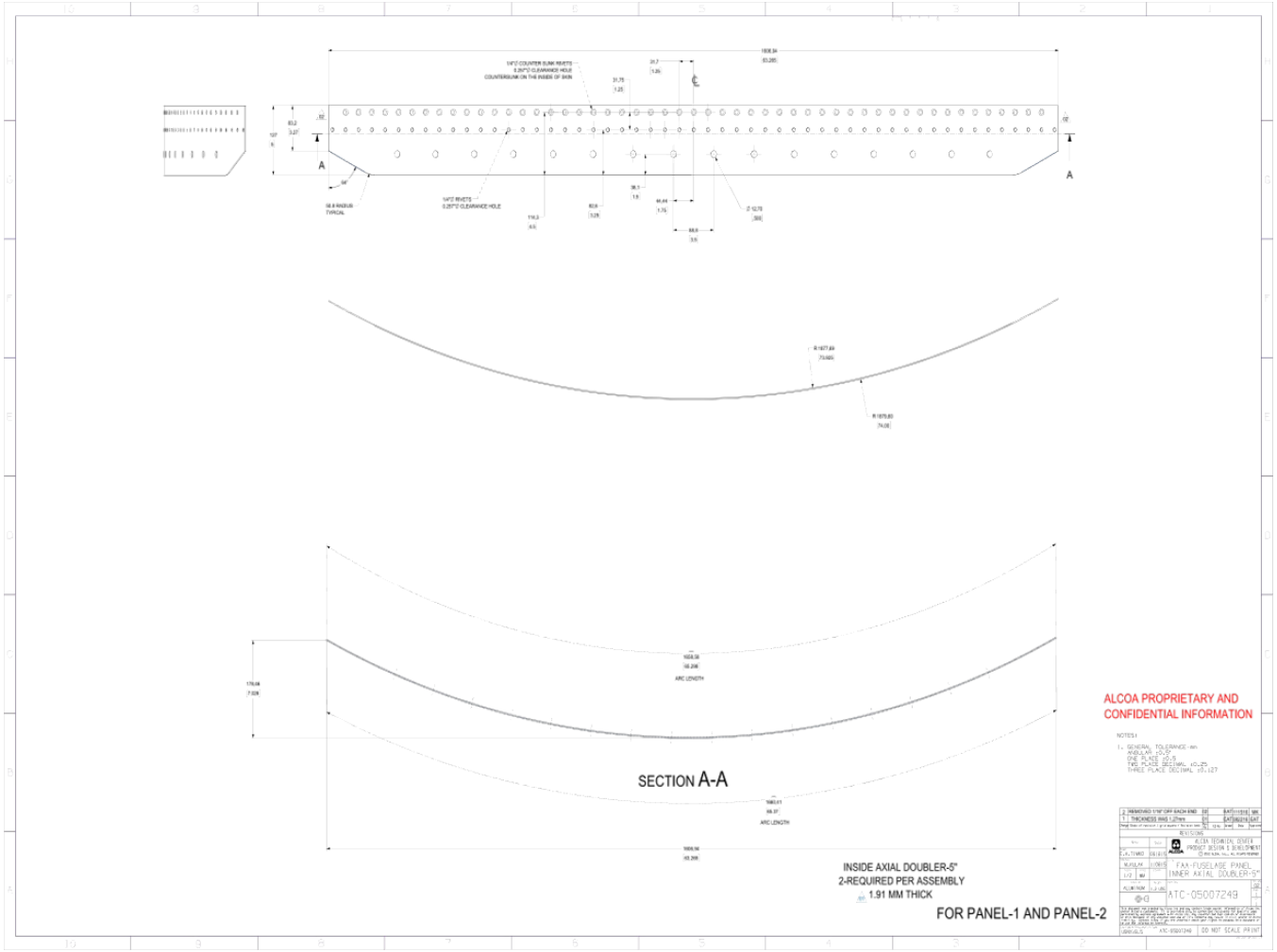

Figure A-11. Panel 1 drawing #11

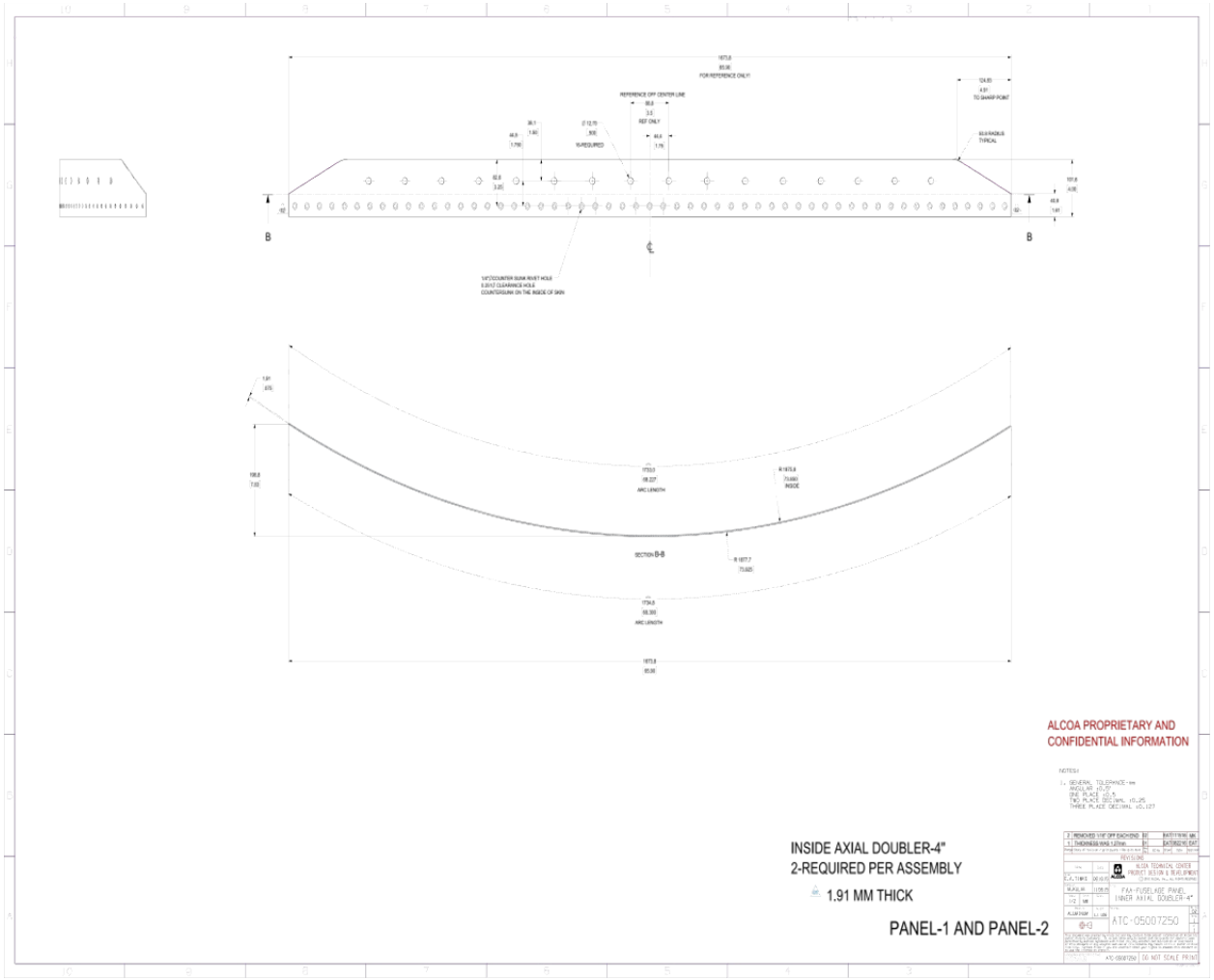

Figure A-12. Panel 1 drawing #12

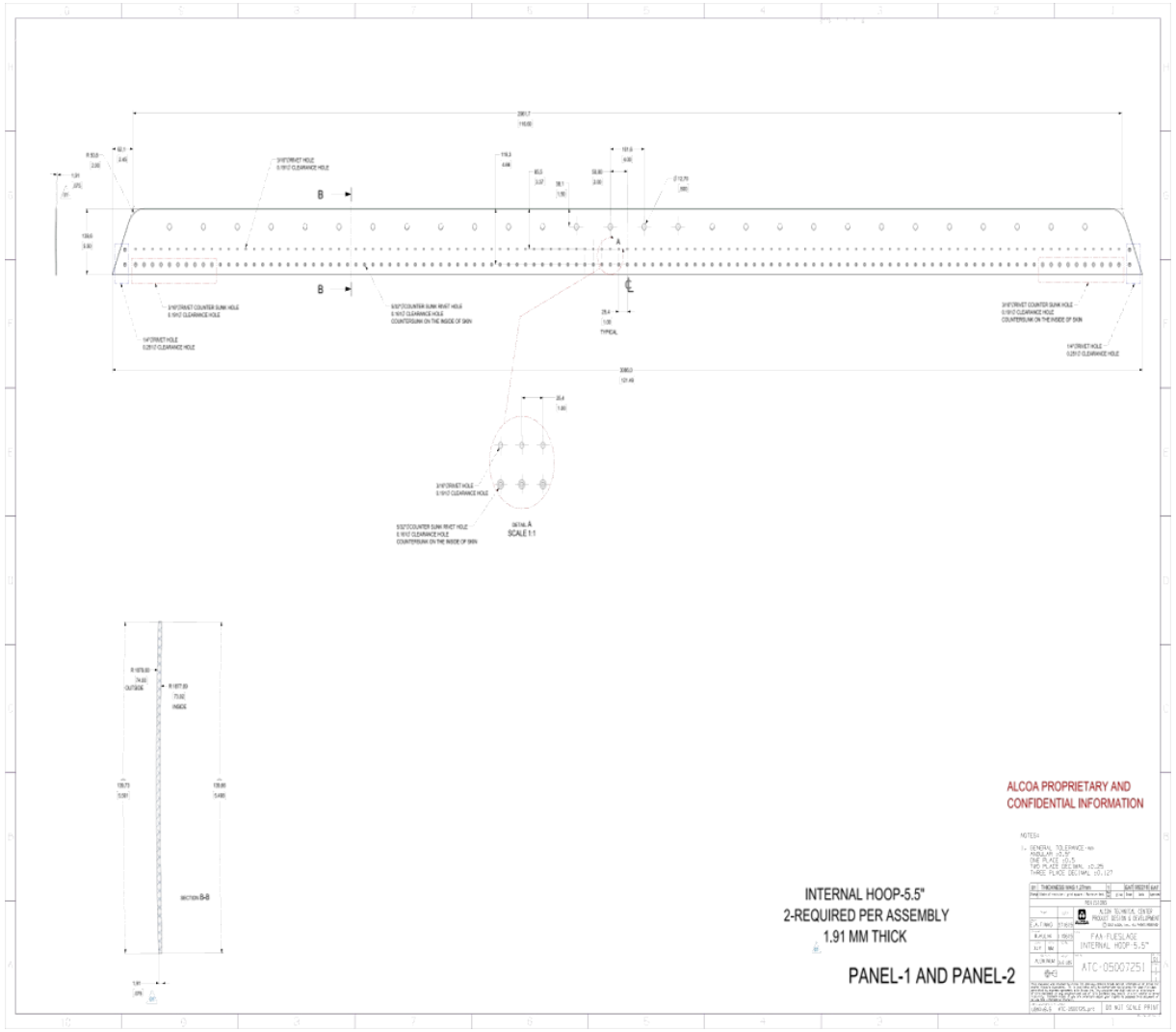

Figure A- 13. Panel 1 drawing #13

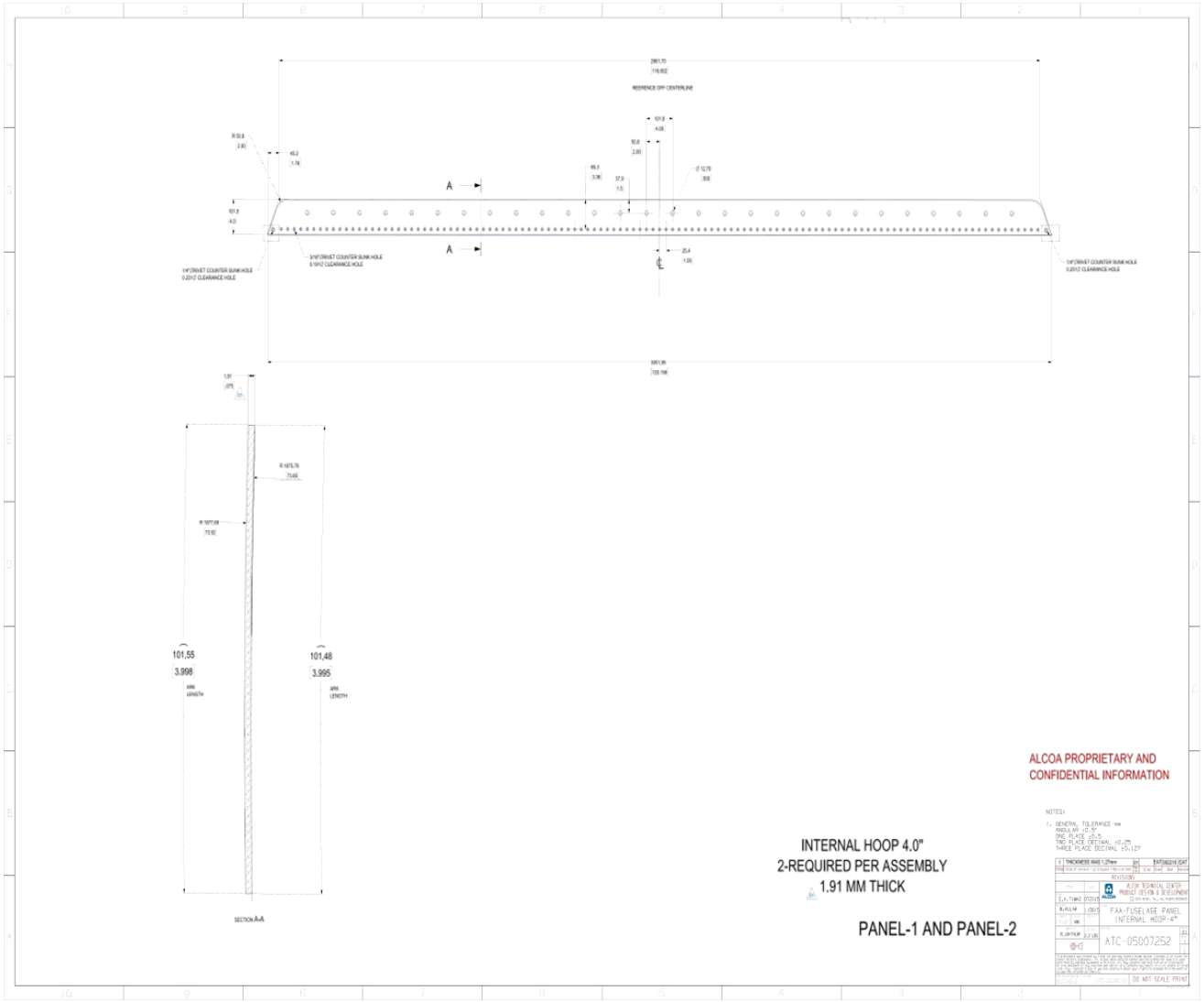

Figure A-14. Panel 1 drawing #14

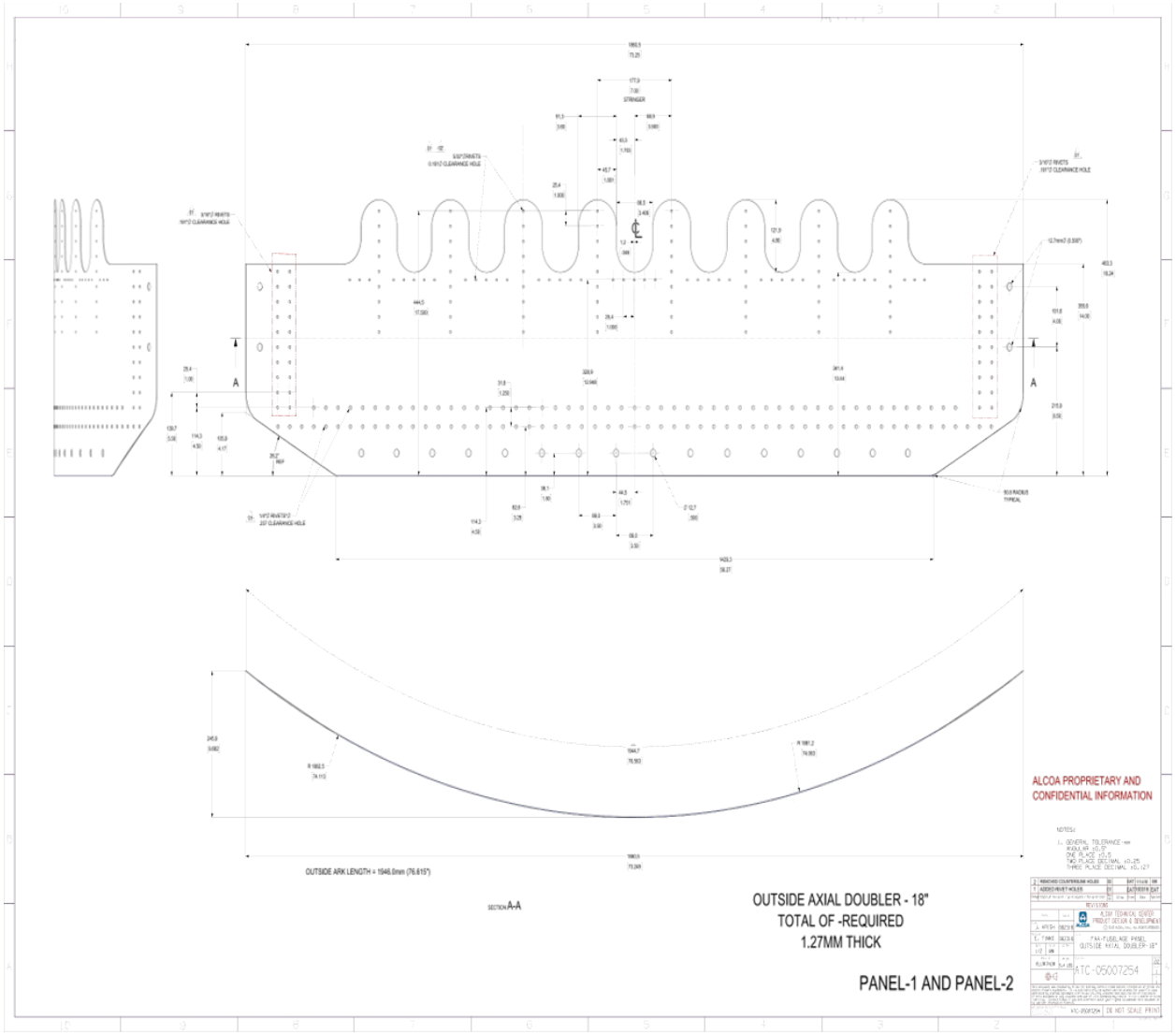

Figure A-15. Panel 1 drawing #15

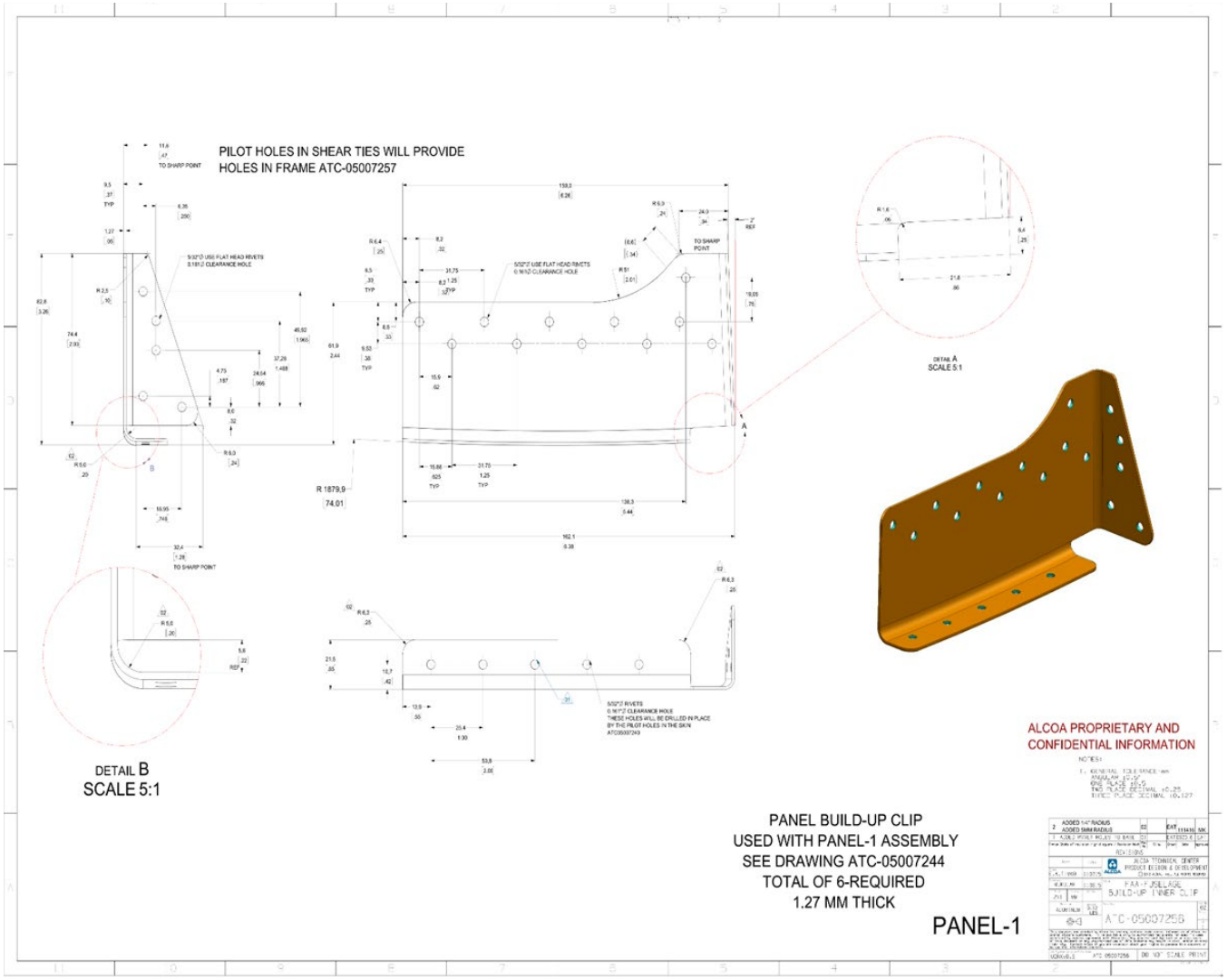

Figure A-16. Panel 1 drawing #16

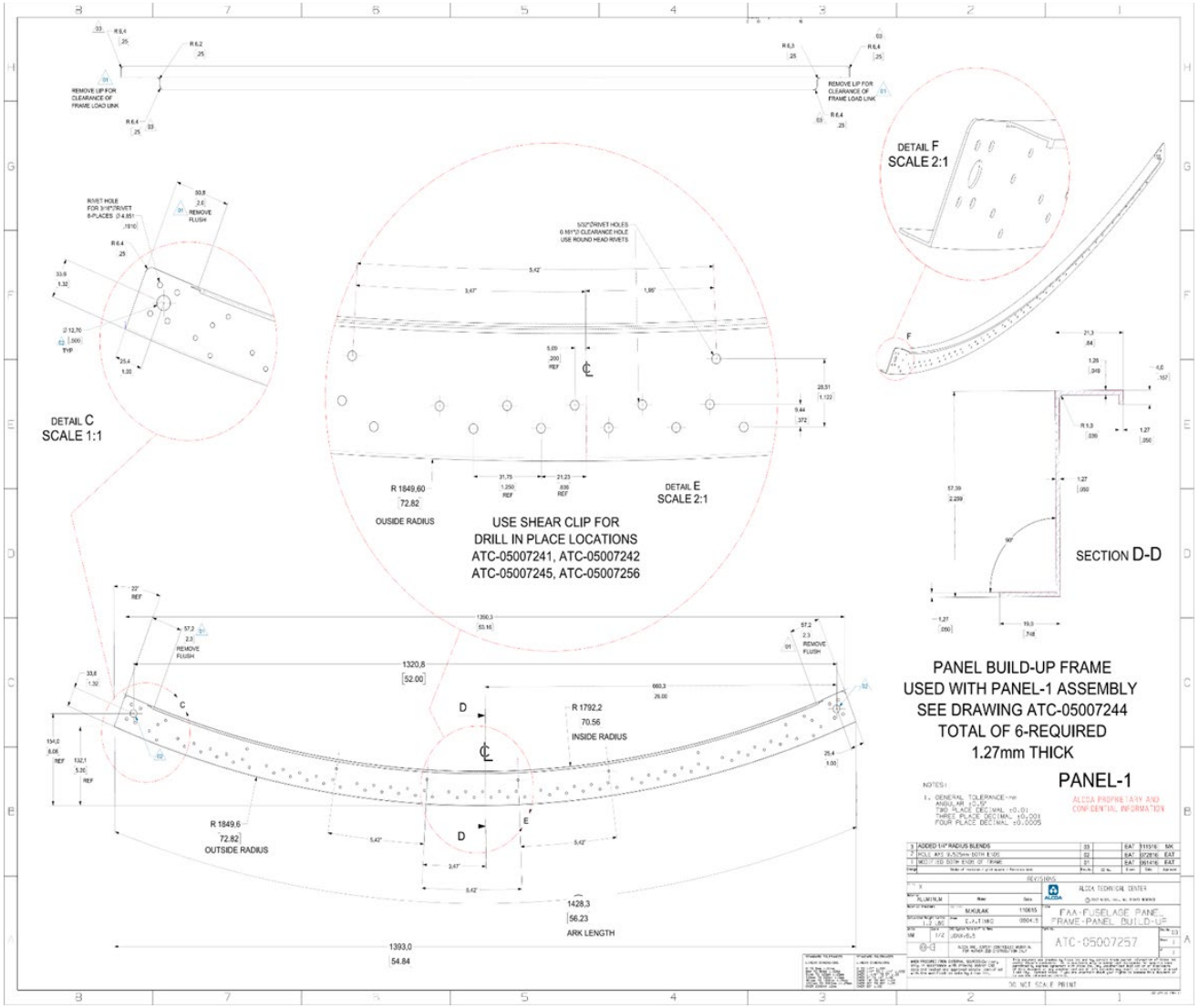

Figure A-17. Panel 1 drawing #17

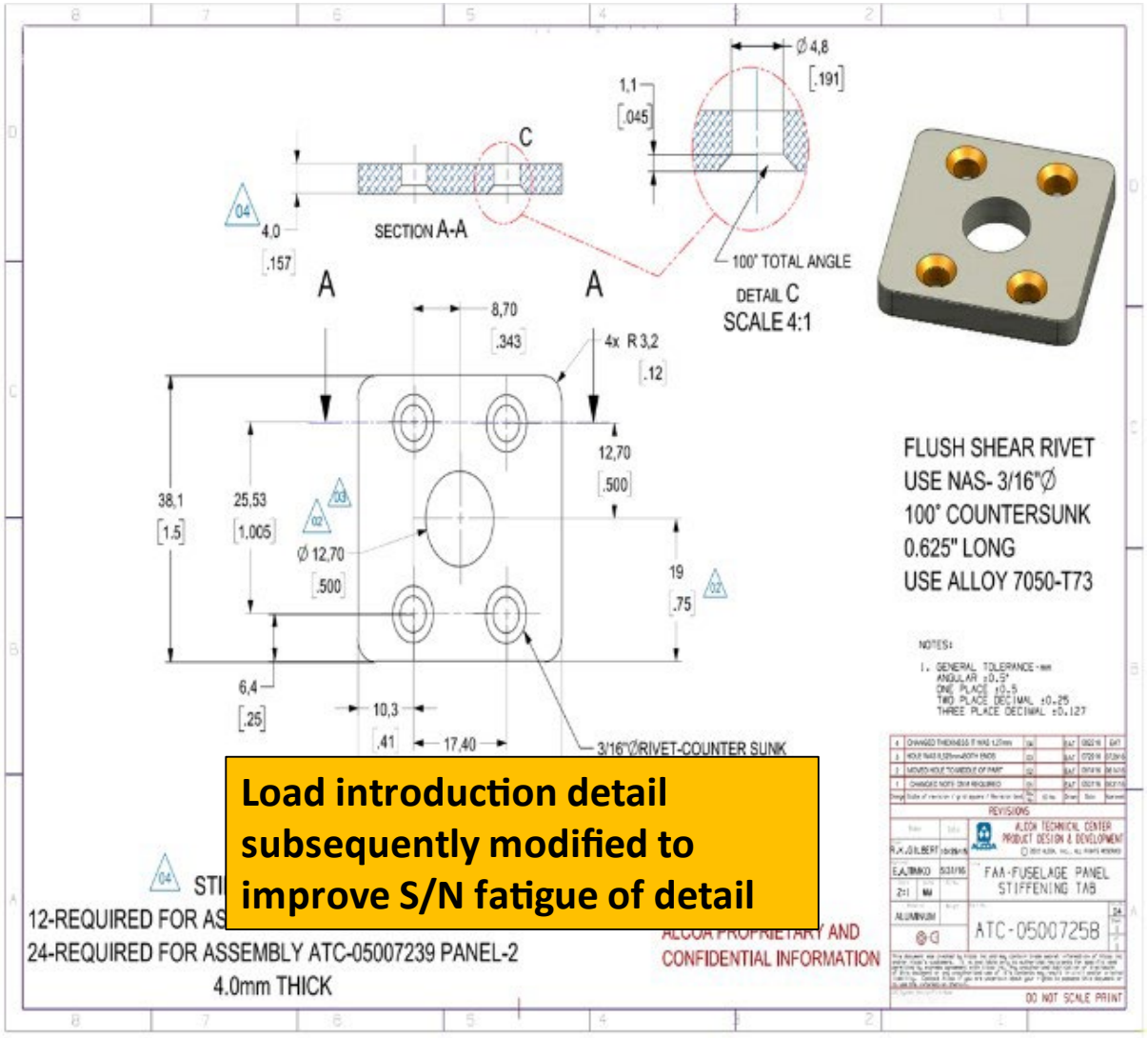

Figure A-18. Panel 1 drawing #18 (note this detail was changed during the circumferential crack test to improve S/N cracking resistance)

B Characterization

Figures

Figure B-1. Arconic characterization test matrix B-2
Figure B-2. Selected test results B-3
Figure B-3. Material stress strain curves B-4
Figure B-4. Material R-curves B-5
Figure B-5. 2524-T3 L-T crack growth rate curves B-6
Figure B-6. 2524-T3 T-L crack growth rate curves B-7
Figure B-7. 2524-T3 lot release tests used for panel manufacturing B-8
Figure B- 8. 7075-T62 extrusion property targets B-9
Figure B-9. 7150-T77511 stringer extrusion properties B-10
Figure B-10. 7075-T6 sheet properties used for Panel 1 load introduction doublers B-11

Characterization Matrix

Supporting Property Data for FAA Large Panel Tests

			Tensile		R-Curve		Full ΔK R = 0.05		Full ΔK R = 0.10		Full ΔK R = 0.10		Mini-Twist M(T) Tests Level III Truncation		M(T) Tests Constant Load	
	Lot	Specimen	Value	Stress-Strain Data	Plot	Data	Plot	Data	Plot	Data	Plot	Data	Plot	Data	Plot	Data
2524-T3	601363	918564	X	X	X	X	X	X	X	X	X	X	X	X	X	X
	601363	918564	X	X	X	X	X	X	X	X	X	X	X	X	X	X
2029-T8 (C51R)		918565	X	X	X	X			X	X	X	X	X	X	X	X
		918565	X	X	X	X	X	X	X	X	X	X	X	X	X	X
2060-T8	494712	921837	X	X	X	X	X	X					X	X	X	X
	494712	921837	X	X	X	X	X	X					X	X		
2029-T3	777344	925611							X	X			X	X	X	X
	777344	925611														

Figure B-1. Arconic characterization test matrix

Static Results

Uniaxial Tensile Properties for Tested Materials

Alloy-Temper	Lot No.	S No.	Plate Thickness (in.)	Tension Modulus (msi) L	Tension Modulus (msi) LT	Longitudinal Yield Strength (ksi)	Longitudinal Tensile Strength (ksi)	Longitudinal % Elong.	Long-Transverse[R] Yield Strength (ksi)	Long-Transverse[R] Tensile Strength (ksi)	Long-Transverse[R] % Elong.
2524-T3	601363	918564	0.090	10.19	10.58	48.0	66.1	20.0	41.6	62.9	26.0
	601363	918564	0.090	10.10	10.52	47.9	66.2	19.5	41.7	62.9	26.0
2029-T8 (C51R)		918565	0.095	9.80	9.92	59.4	62.9	11.5	59.1	63.1	13.0
		918565	0.095	9.72	10.13	59.1	62.6	11.0	59.2	63.3	12.5
2060-T8	494712	921837	0.071	10.90	10.96	72.3	77.3	10.5	68.7	78.4	11.5
	494712	921837	0.071	10.97	11.13	72.7	77.5	10.5	68.3	77.8	11.5

Figure B-2. Selected test results

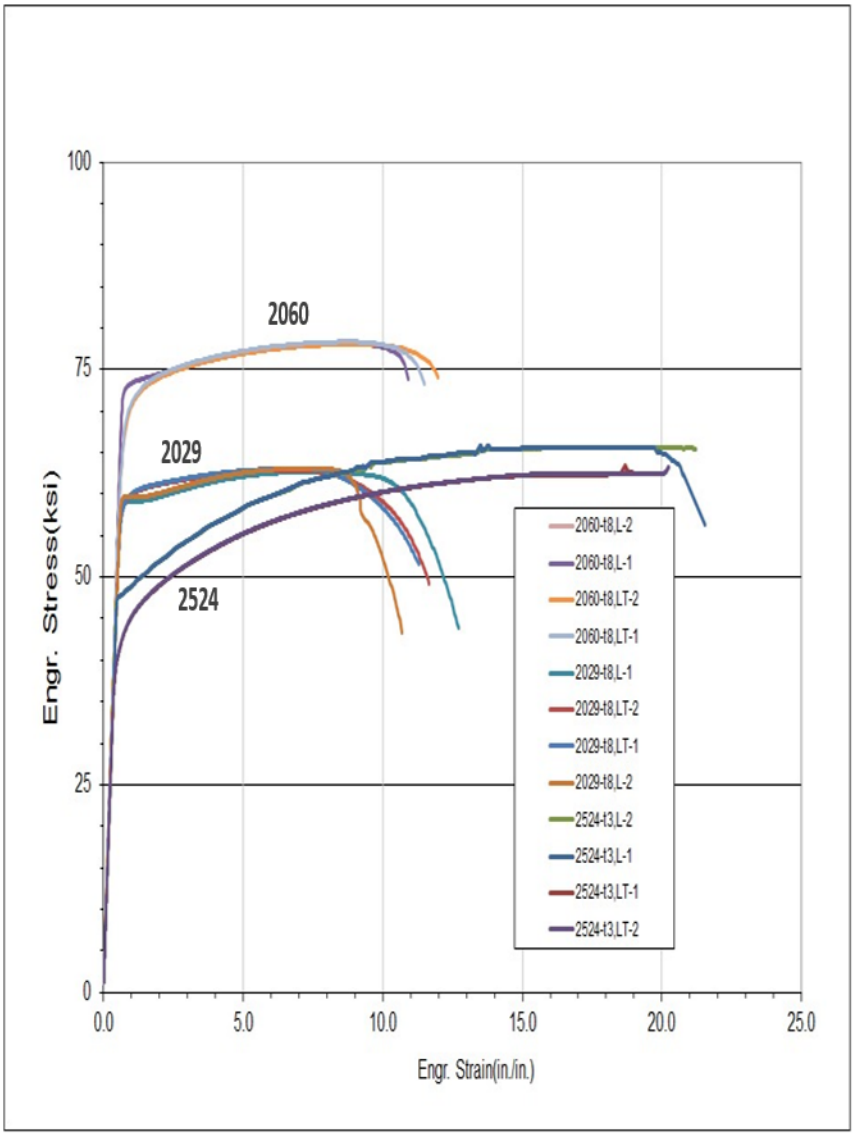

Figure B-3. Material stress strain curves

R-Curves

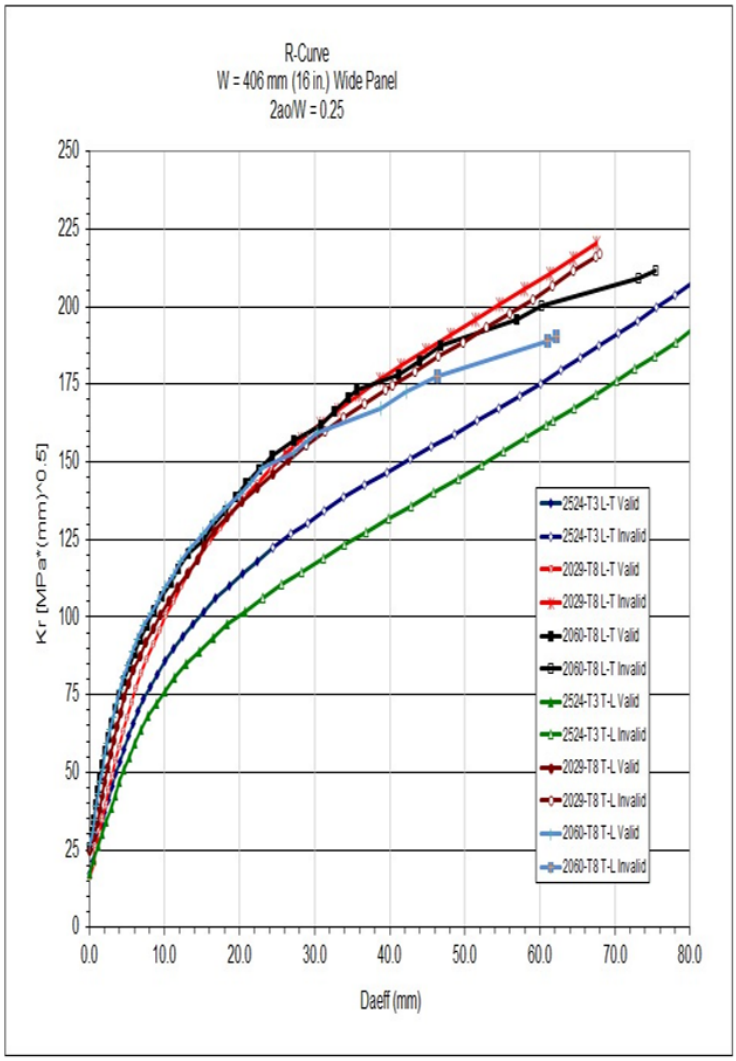

Figure B-4. Material R-curves

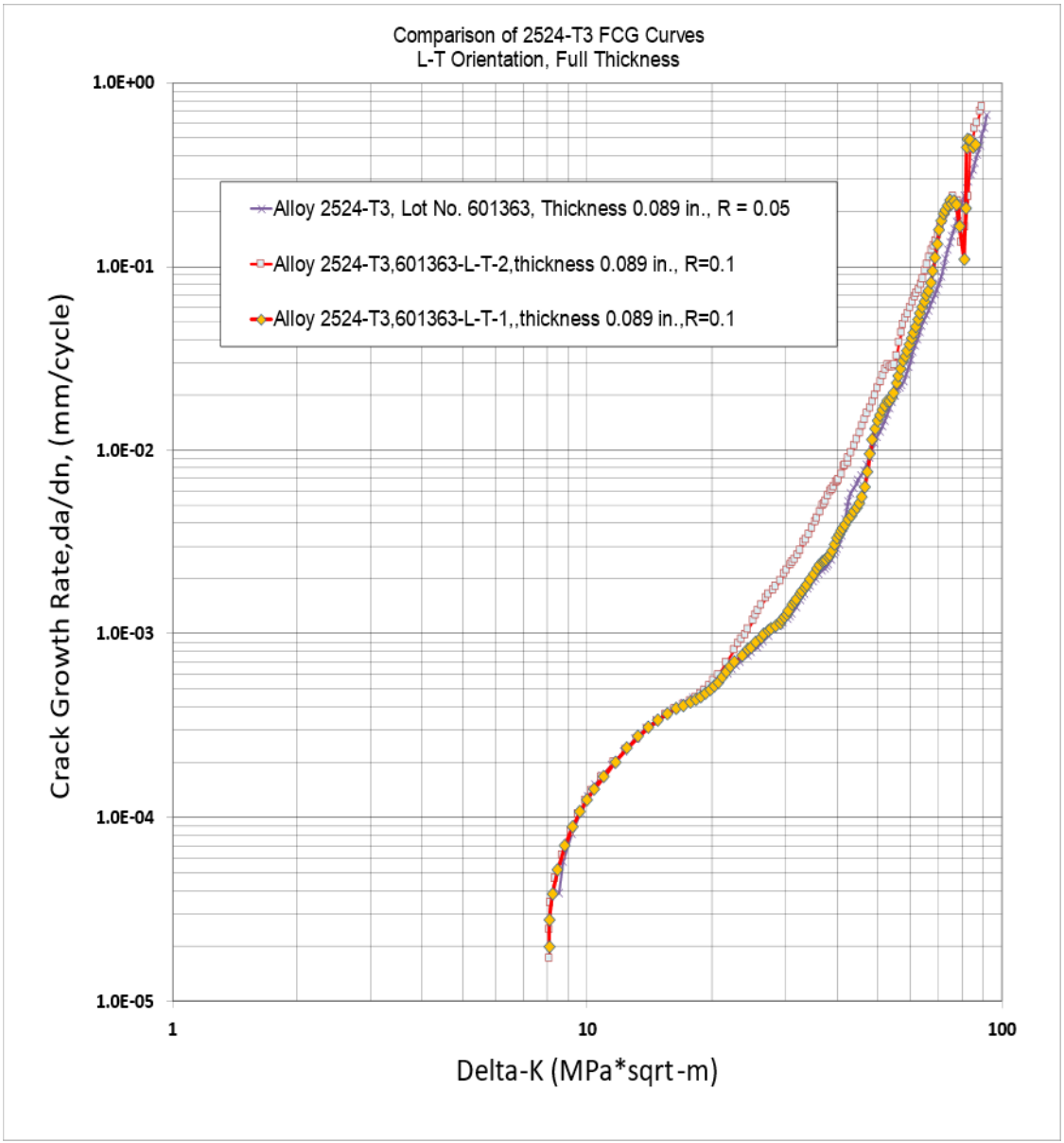

Figure B-5. 2524-T3 L-T crack growth rate curves

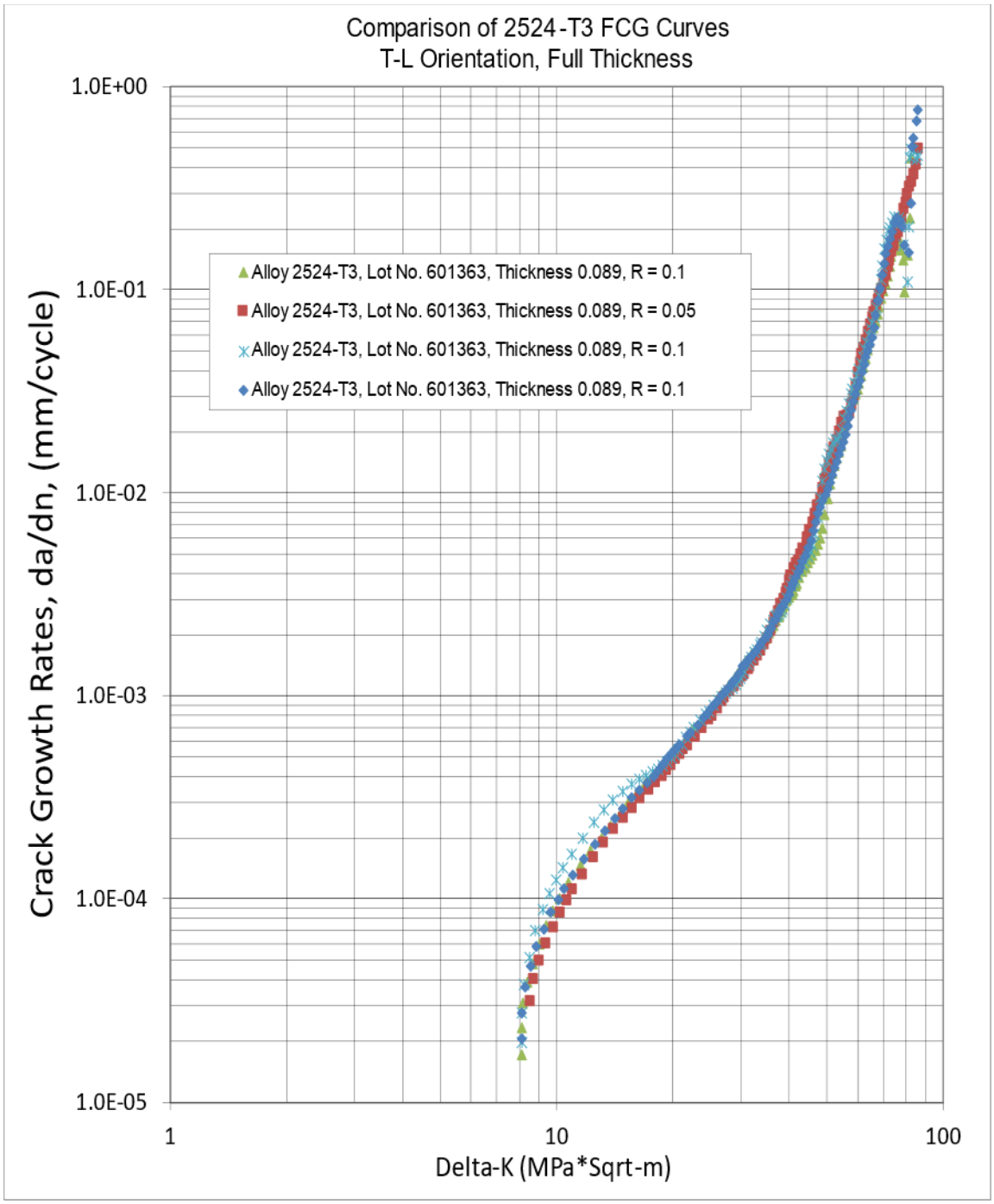

Figure B-6. 2524-T3 T-L crack growth rate curves

Static 2524-T3 Skin Properties for Panel Manufacturing

Uniaxial Tensile Properties for Tested Materials

Alloy-Temper	Lot No.	S No.	Plate Thickness (in.)	Tension Modulus (msi) L	Tension Modulus (msi) LT	Longitudinal Yield Strength (ksi)	Longitudinal Tensile Strength (ksi)	Longitudinal % Elong.	Long-Transverse® Yield Strength (ksi)	Long-Transverse® Tensile Strength (ksi)	Long-Transverse® % Elong.
2524-T3	601363	918564	0.090	10.19	10.58	48.0	66.1	20.0	41.6	62.9	26.0
	601363	918564	0.090	10.10	10.52	47.9	66.2	19.5	41.7	62.9	26.0

Test Results from Lot To Be Used for Panel Manufacturing

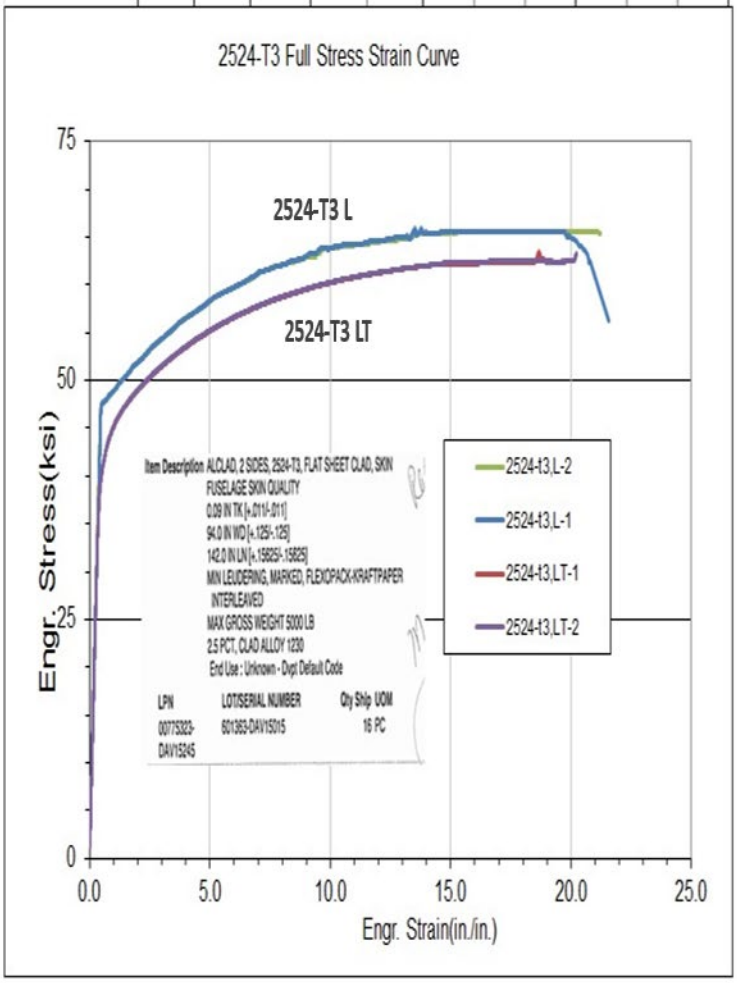

Figure B-7. 2524-T3 lot release tests used for panel manufacturing

7075-T62 Extrusion Frame Final Temper Target

Table 3.7.4.0(g_1). Design Mechanical and Physical Properties of 7075 Aluminum Alloy Extrusion

Specification	QQ-A-200/11														
Form	Extrusion (rod, bar, and shapes)														
Temper	T6, T6510, T6511, and T62[a]														
Cross-Sectional Area, in.[2]	≤20												>20, ≤32	≤32	
Thickness, in.[b]	≤0.249		0.250-0.499		0.500-0.749		0.750-1.499		1.500-2.999		3.000-4.499			4.500-5.000	
Basis	A	B	A	B	A	B	A	B	A	B	A	B	S	A	B
Mechanical Properties:															
F_{tu}, ksi:															
L	78	82	83	85	81	85	81	85	81	85	81	84	78	78	
LT	75	79	78	82	77	81	75	79	71	75	67	69	64	63	
ST	...	...	...	...	...	...	...	...	67[c]	71[c]	67[c]	69[c]	64[c]	63[c]	
F_{ty}, ksi:															
L	70	74	73	77	72	76	72	76	72	76	71	74	70	68	
LT	66	70	69	72	67	71	65	69	61	65	56	59	55	52	
ST	...	...	...	...	...	...	...	...	56[c]	59[c]	55[c]	58[c]	55[c]	52[c]	
F_{cy}, ksi:															
L	70	74	73	77	72	76	72	76	72	76	71	74	70	68	
LT	72	76	74	78	73	77	71	75	67	71	62	64	61	57	
ST	...	...	...	...	...	...	...	...	62	66	62	64	61	57	
F_{su}, ksi	41	44	43	45	43	45	43	45	42	44	40	42	39	38	
F_{bru}[d], ksi:															
(e/D = 1.5)	111	117	115	121	115	120	113	119	110	115	106	110	102	101	1
(e/D = 2.0)	140	148	146	153	145	152	144	151	141	148	137	142	132	131	1
F_{bry}[d], ksi:															
(e/D = 1.5)	92	97	96	101	96	99	93	98	89	94	84	88	83	79	
(e/D = 2.0)	108	114	113	119	111	117	110	116	106	112	101	105	100	95	1
e, percent (S-basis):															
L	7	...	7	...	7	...	7	...	7	...	7	...	6	6	
E, 10^3 ksi	10.4														
E_c, 10^3 ksi	10.7														
G, 10^3 ksi	4.0														
μ	0.33														
Physical Properties:															
ω, lb/in.[3]	0.101														
C, K, and α	See Figure 3.7.4.0														

a Design allowables were based upon data obtained from testing T6, T6510, and T6511 temper extrusions and from testing samples of extrusion supplied in the O or F temper, w
were heat treated to T62 temper to demonstrate response to heat treatment by suppliers. Properties obtained by the user may be lower than those listed if the material has been
formed or otherwise cold worked, particularly in the annealed temper, prior to solution heat treatment.
b The mechanical properties are to be based upon the thickness at the time of quench.
b Caution: This specific alloy, temper, and product form exhibits poor stress-corrosion cracking resistance in this grain direction. It corresponds to an SCC resistance rating of I
indicated in Table 3.1.2.3.1(a).
d Bearing values are "dry pin" values per Section 1.4.7.1.

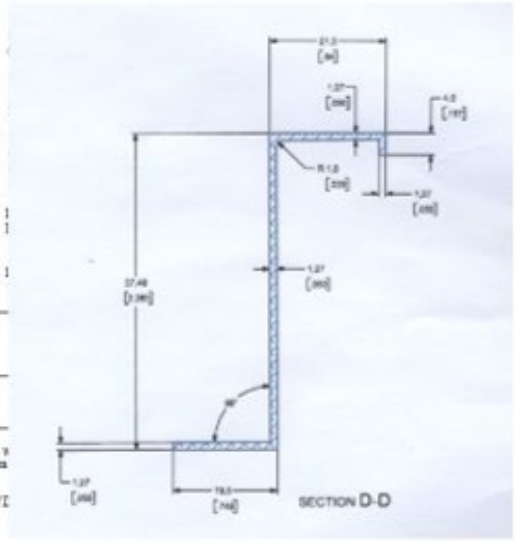

MIL-HDBK-5H
1 December 1998

Figure B- 8. 7075-T62 extrusion property targets

7150-T77511 Extrusion for Stringers

Table 3.7.5.0(c$_1$). Design Mechanical and Physical Properties of 7150 Aluminum Alloy Extrusion

Specification	AMS 4307					
Form	Extrusion					
Temper	T61511					
Thickness or diameter,[b] in.	0.250-0.499	0.500-0.749	0.750-0.999	1.000-1.499		1.500-2.000
Basis	S	S	S	A	B	S
Mechanical Properties:						
F_{tu}, ksi:						
L	87	88	89	89	94	89
LT	80	79	79	85	86	74
F_{ty}, ksi:						
L	82	83	84	83	88	84
LT	73	73	73	77	78	68
F_{cy}, ksi:						
L	80	81	82	82	87	84
LT	80	80	80	77	81	75
F_{su}, ksi	44	45	45	44	46	42
F_{bru}[a], ksi:						
(e/D = 1.5)	119	120	120	118	125	116
(e/D = 2.0)	152	153	154	152	161	150
F_{bry}[a], ksi:						
(e/D = 1.5)	100	100	100	96	102	94
(e/D = 2.0)	118	120	120	117	124	117
e, percent (S-basis):						
L	8	9	8	8	...	8
E, 10^3 ksi	10.4					
E_c, 10^3 ksi	11.0					
G, 10^3 ksi	4.0					
μ	0.33					
Physical Properties:						
ω, lb/in.^{3}	0.102					
C, K, and σ	...					

a. Bearing values are "dry pin" values per Section 1.4.7.1.
b. The mechanical properties are to be based upon the thickness at the time of quench.

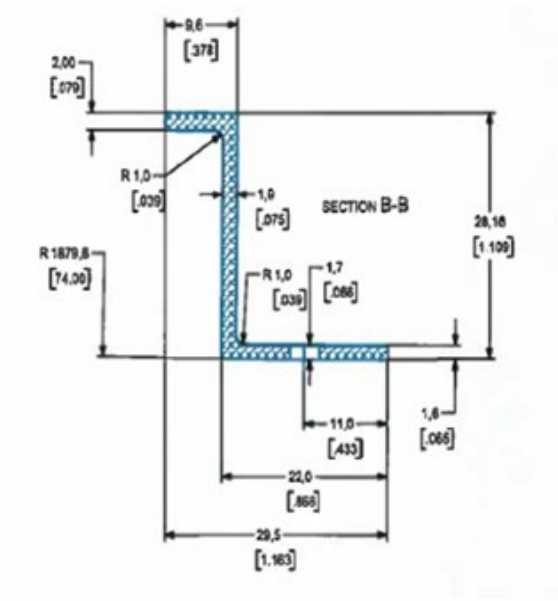

7150-T77511 (piece 1F) stringer	85.5 ksi	91.2 ksi	9.4 in/.in.

Figure B-9. 7150-T77511 stringer extrusion properties

7075-T6 Sheet For All Doublers

Table 3.7.4.0(b$_1$). Design Mechanical and Physical Properties of 7075 Aluminum Alloy Sheet and Plate

Specification	AMS 4045 and AMS-QQ-A-250/12																				
Form	Sheet							Plate													
Temper	T6 and T62[a]							T651													
Thickness, in.	0.008-0.011	0.012-0.039		0.040-0.125		0.126-0.249		0.250-0.499		0.500-1.000		1.001-2.000		2.001-2.500		2.501-3.000		3.001-3.500		3.501-4.000	
Basis	S	A	B	A	B	A	B	A	B	A	B	A	B	A	B	A	B	A	B	A	B
Mechanical Properties:																					
F_{tu}, ksi:																					
L	...	76	78	78	80	78	80	77	79	77	79	76	78	75	77	71	73	70	72	66	68
LT	74	76	78	78	80	78	80	78	80	78	80	77	79	76	78	72	74	71	73	67	69
ST	...	...	...	...	...	...	...	...	...	...	...	...	...	70[b]	71[b]	66[b]	68[b]	65[b]	67[b]	61[b]	63[b]
F_{ty}, ksi:																					
L	...	69	72	70	72	71	73	69	71	70	72	69	71	66	68	63	65	60	62	56	58
LT	63	67	70	68	70	69	71	67	69	68	70	67	69	64	66	61	63	58	60	54	56
ST	...	...	...	...	...	...	...	...	...	...	...	...	...	59[b]	61[b]	56[b]	58[b]	54[b]	55[b]	50[b]	52[b]
F_{cy}, ksi:																					
L	...	68	71	69	71	70	72	67	69	68	70	66	68	62	64	58	60	55	57	51	52
LT	...	71	74	72	74	73	75	71	73	72	74	71	73	68	70	65	67	61	64	57	59
ST	...	...	...	...	...	...	...	...	...	...	...	...	...	67	70	64	66	61	63	57	59
F_{su}, ksi	...	46	47	47	48	47	48	43	44	44	45	44	45	44	45	42	43	42	43	39	41
f^{bru},[c] ksi:																					
(e/D = 1.5)	...	118	121	121	124	121	124	117	120	117	120	116	119	114	117	108	111	107	110	101	104
(e/D = 2.0)	...	152	156	156	160	156	160	145	148	145	148	143	147	141	145	134	137	132	135	124	128
f^{bry},[c] ksi:																					
(e/D = 1.5)	...	100	105	102	105	103	106	97	100	100	103	100	103	98	101	94	97	89	93	84	87
(e/D = 2.0)	...	117	122	119	122	121	124	114	118	117	120	117	120	113	117	109	112	104	108	98	103
e, percent (S-basis):																					
LT	5	7	...	8	...	8	...	9	...	7	...	6	...	5	...	5	...	5	...	3	...
E, 10^3 ksi	10.3							10.3													
E_c, 10^3 ksi	10.5							10.6													
G, 10^3 ksi	3.9							3.9													
μ	0.33							0.33													
Physical Properties:																					
ω, lb/in.^{3}	0.101																				
C, K, and α	See Figure 3.7.4.0																				

a Design allowables were based upon data obtained from testing T6 temper sheet and from testing samples of sheet, supplied in the O or F temper, which were heat treated to demonstrate response to heat treatment by suppliers. Properties obtained by the user may be lower than those listed if the material has been formed or otherwise cold worked, particularly in the annealed temper, prior to solution heat treatment.

b Caution: This specific alloy, temper, and product form exhibits poor stress-corrosion cracking resistance in this grain direction. It corresponds to an SCC resistance rating of D, as indicated in Table 3.1.2.5.1(a).

c Bearing values are "dry pin" values per Section 1.4.7.1. See Table 3.1.2.1.1.

Figure B-10. 7075-T6 sheet properties used for Panel 1 load introduction doublers

C Spectrum development

Figures

Figure C-1. FASTER load development for circumferential crack repeat inspection interval testing C-2
Figure C-2. Mini-TWIST spectrum definition table from Steadman C-3
Figure C-3. Parameter input page for generating the FTA spectrum file for the modified mini-TWIST fuselage spectrum C-5
Figure C-4. First 20 lines of an FTA spectrum endpoint file C-6

A fuselage spectrum was developed following the approach in Steadman (2007). This spectrum was based on flight recorded accelerometer data on B737 and B727 single-aisle aircraft. It was observed that the mini-TWIST exceedance data matched the flight recorded data reasonably well when the mini-TWIST acceleration excursions were reduced by 50%, as shown in Figure C-1.

However, the 50% reduction in acceleration amplitudes was not conservative in the high exceedance regime. The authors modified the number of cycles in amplitude levels IX and X for all flight types as shown in Figure C-2 to make the modified mini-TWIST spectrum conservative relative to the flight measured data. Both spectrums represent 4000 flights, but the mini-TWIST spectrum contains 58,422 flight cycles (plus 4000 landing loads) while the spectrum in the FAA report contains 91,496 cycles.

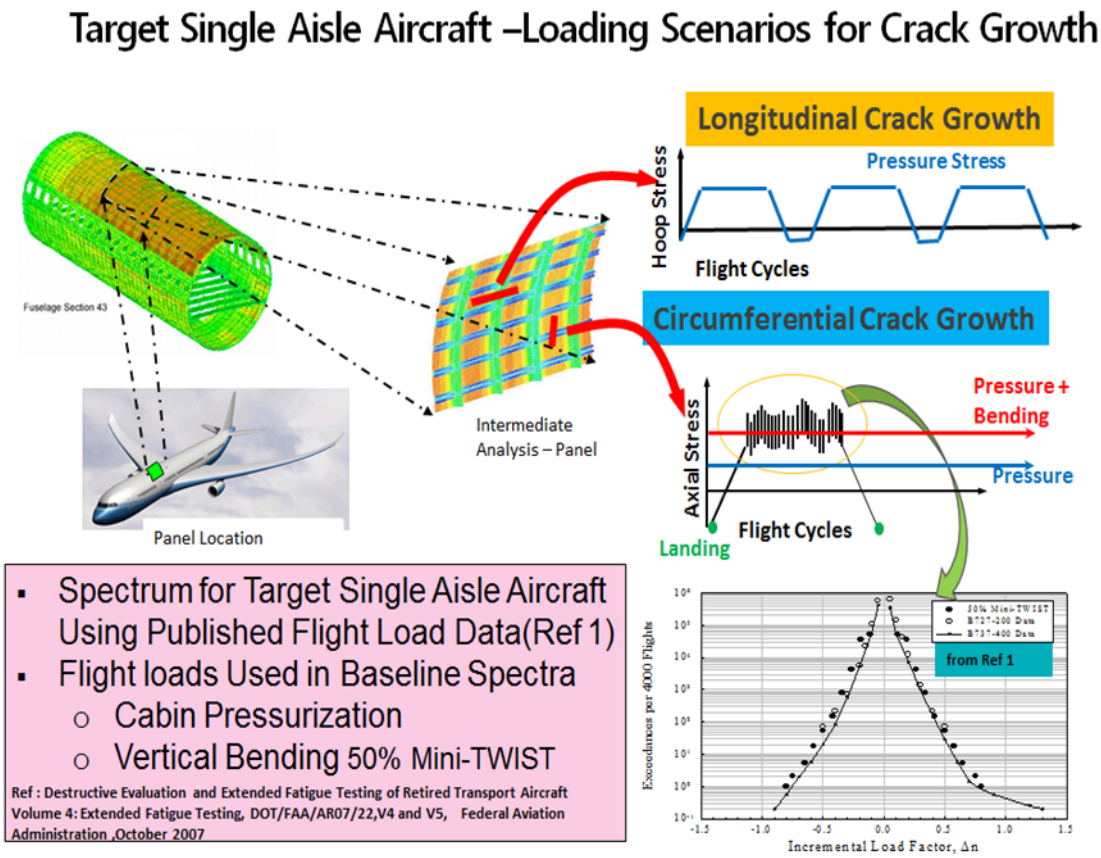

Figure C-1. FASTER load development for circumferential crack repeat inspection interval testing

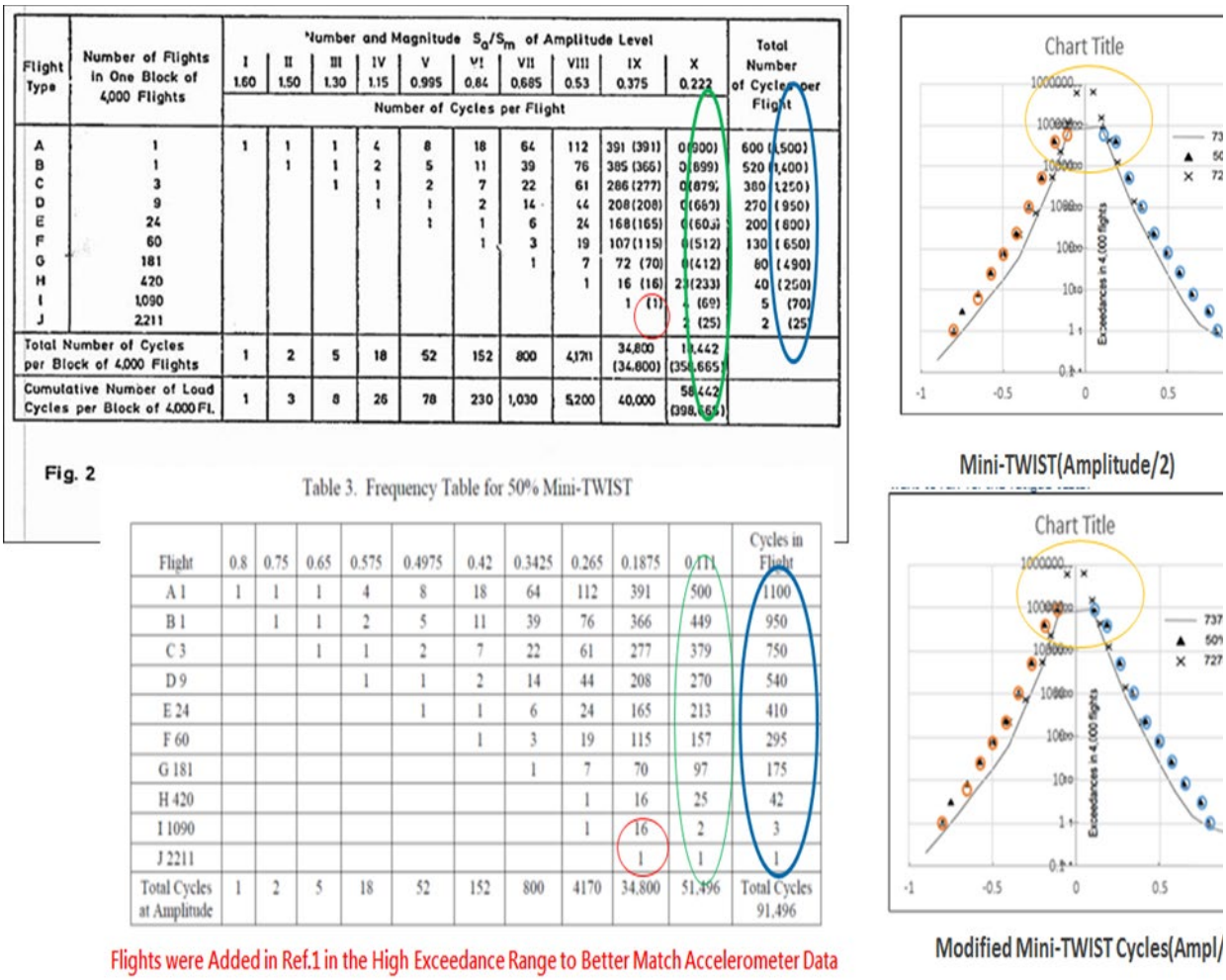

Flight Type	Number of Flights in One Block of 4,000 Flights	Number and Magnitude S_a/S_m of Amplitude Level: I 1.60	II 1.50	III 1.30	IV 1.15	V 0.995	VI 0.84	VII 0.685	VIII 0.53	IX 0.375	X 0.222	Total Number of Cycles per Flight
		Number of Cycles per Flight										
A	1	1	1	1	4	8	18	64	112	391 (391)	0 (900)	600 (1,500)
B	1		1	1	2	5	11	39	76	385 (366)	0 (899)	520 (1,400)
C	3			1	1	2	7	22	61	286 (277)	0 (879)	380 (1,250)
D	9				1	1	2	14	44	208 (208)	0 (665)	270 (950)
E	24					1	1	6	24	168 (165)	0 (603)	200 (800)
F	60						1	3	19	107 (115)	0 (512)	130 (650)
G	181							1	7	72 (70)	0 (412)	80 (490)
H	420								1	16 (16)	24 (233)	40 (250)
I	1,090									1 (1)	4 (69)	5 (70)
J	2,211										2 (25)	2 (25)
Total Number of Cycles per Block of 4,000 Flights		1	2	5	18	52	152	800	4,171	34,800 (34,800)	16,442 (356,665)	
Cumulative Number of Load Cycles per Block of 4,000 Fl.		1	3	8	26	78	230	1,030	5,200	40,000	56,442 (398,665)	

Fig. 2

Mini-TWIST(Amplitude/2)

Table 3. Frequency Table for 50% Mini-TWIST

Flight	0.8	0.75	0.65	0.575	0.4975	0.42	0.3425	0.265	0.1875	0.171	Cycles in Flight
A 1	1	1	1	4	8	18	64	112	391	500	1100
B 1		1	1	2	5	11	39	76	366	449	950
C 3			1	1	2	7	22	61	277	379	750
D 9				1	1	2	14	44	208	270	540
E 24					1	1	6	24	165	213	410
F 60						1	3	19	115	157	295
G 181							1	7	70	97	175
H 420								1	16	25	42
I 1090								1	16	2	3
J 2211									1	1	1
Total Cycles at Amplitude	1	2	5	18	52	152	800	4170	34,800	51,496	Total Cycles 91,496

Flights were Added in Ref.1 in the High Exceedance Range to Better Match Accelerometer Data

Modified Mini-TWIST Cycles(Ampl/

Figure C-2. Mini-TWIST spectrum definition table from Steadman

The TWIST paper (deJonge & et al., 1973) includes landing load exceedance data, but neither this paper nor the mini-TWIST software (Lowak, et al., 1979) explicitly includes landing loads. Landing loads make up the largest overall loading cycle per flight (the ground-air-ground cycle, GAG). Arconic modified the original mini-TWIST software to insert a constant compression landing load at the end of every flight.

The spectrum in deJonge, et. al (1973) was a static normalized spectrum, meaning that the only variable that needs to be chosen for a particular test is the mean flight load (or stress). All the normalized spectrum values were multiplied by the mean flight stress to give the spectrum endpoint load values. This original Mini-TWIST software was applicable to bending-only situations like wing spectra. This approach was modified by Arconic to add a constant pressure component to the bending component in the modified mini-TWIST spectrum. This modification

followed the approach and used the software described in Lowak, et al. (1979). The input array Table relating flight type and number of cycles at amplitude levels IX and X was updated in the software to reflect the changes shown Figure C-2. If the reader wishes to write their own modified spectrum software, it should be noted that in Lowak, et al. (1979), a standardized sequence was used. The authors embedded a random number generator to establish flight type sequencing. Also, a different random number generator is used to generate the sequence of loads within a flight type. These random number generators were written to be initialized internally in the code such they generate the exact same random number sequences each time the code is run. Thus, the same order of flight types and flight sequence is produced every time the code is run.

To facilitate the use of the software to produce the modified mini-TWIST for fuselage, three parameters are input: the 1G stress, the pressure stress, and a parameter to specify the landing stress. To generate the loading spectrum, the normalized spectrum values from the modified mini-TWIST exceedance diagram are multiplied by the 1G bending stress and then added to the pressure stress. All flight loads are generated the same way. The inter-flight landing load is specified by a parameter α, which is multiplied by the 1G load to generate the single landing load between flights.

To use the spectrum with the FTA control system (Donald, 1990) for crack growth testing, all the spectrum values are normalized to the composite mean flight stress, which was defined to be the 1G stress plus the pressure stress. These normalized values are written to a text file with the header line containing the spectrum scale factor, which is equal to the maximum normalized value in the spectrum. In the FTA software, this scale factor is associated with the maximum load that will be applied to the specimen.

An Excel spreadsheet and Excel macro were developed, which use the modified mini-TWIST sequence of flights to generate a new sequence. This sequence includes the input values provided in Figure C-3. The inputs are:

- 1-g stress: S_{1g}
- Pressure stress: S_{press}
- Landing stress parameter: α

Enter these values into the spreadsheet and click the “generate FTA spectrum file” button.

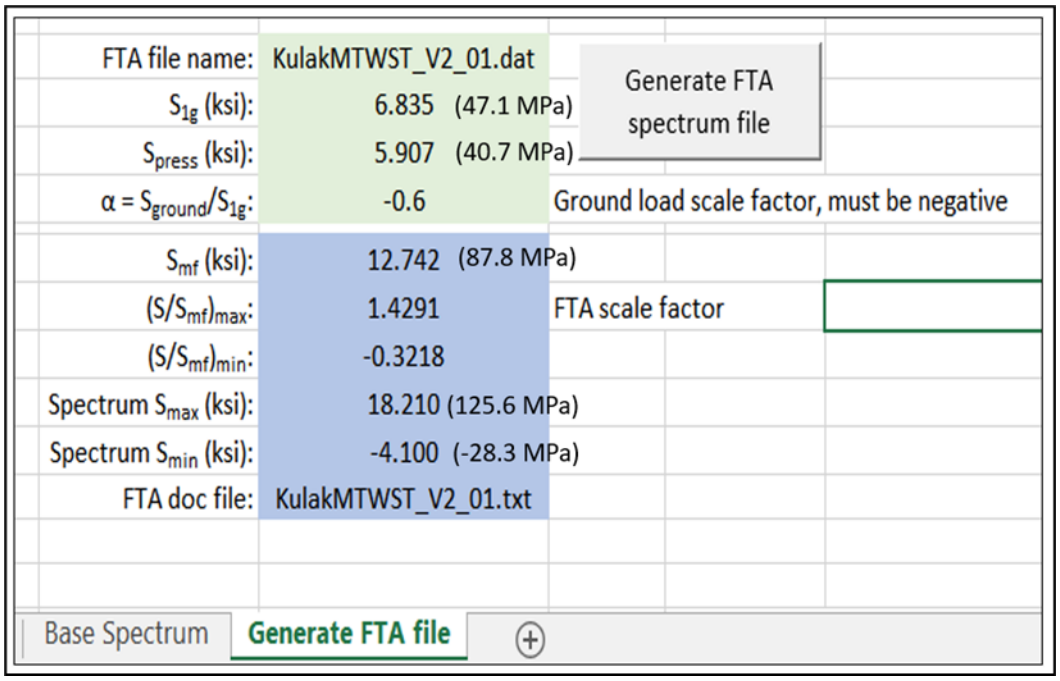

Figure C-3. Parameter input page for generating the FTA spectrum file for the modified mini-TWIST fuselage spectrum

The following parameters are calculated and displayed:

- S_{1g} is the axial bending stress in the skin at 1G.
- S_{press} is the axial pressure skin stress (Flugge smeared axial skin stress used in this study at the characteristic stress location, defined in Section 5).
- S_{mfs} is the mean flight stress in the skin defined by $S_{mfs} = S_{1g} + S_{press}$.
- S_{max} is the skin maximum stress in the spectrum.
- α is input as the ratio of the landing stress to the 1G bending.

One other parameter that needs to be calculated to properly operate the FTA system is F_{max}. This depends on the specimen cross-sectional area, so it is determined at the time of the test once the specimen size has been chosen. F_{max} is the maximum load to be applied to the specimen as defined by $F_{max} = S_{max}$*Area. F_{max} needs to be entered into the FTA software as the "Maximum Load" parameter to properly scale the normalized spectrum values from the endpoint file into force values to be applied to the specimen.

The first few lines of an FTA endpoint file are shown in Figure C-4. The first value written to that file is the FTA header, which is shown below:

header = 0, FSF,0

F_{SF} is the FTA scale factor, which is the largest value in the normalized endpoints and equal to $F_{sf}=(S/S_{mf})_{max}$. In the case of this modified mini-TWIST spectrum, it is equal to $(1.8*S_{1g} + S_{press})/S_{mf}$, because the largest value of S/S_{1g} in the base spectrum is 1.8. The other two parameters are always zero for this type of spectrum file. All values are rounded to four decimal places before being written to the endpoint file.

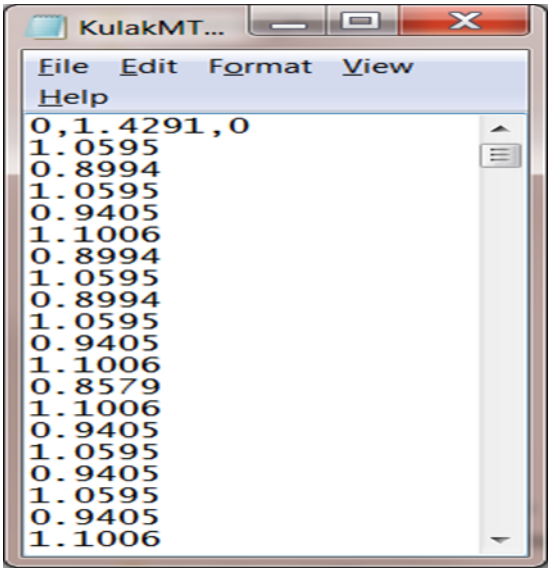

Figure C-4. First 20 lines of an FTA spectrum endpoint file

Because the FTA endpoint file can contain no comments, a document file is also generated when the endpoint file is written. The document file shows the parameters S_{1g}, S_{press}, and α used to generate the endpoint file. The time and date that the data file is generated provides documentation to go along with the FTA spectrum endpoint file.

The highest compressive stress will be $(S/S_{mf})_{min} \times S_{mf} = -0.3218 \times 12.742 = -4.100$ ksi. This was used to check for specimen buckling.